



UNIVERSITY OF TRENTO - Italy

International Doctoral School in Biomolecular Sciences

XXV Cycle

**Design, Chemical Synthesis and Biological
Evaluation of Potential New Antiviral Agents**

Tutor

Prof. Ines MANCINI

University of Trento, Italy

Ph.D. Thesis of

Andrea DEFANT

University of Trento, Italy

to my parents

Contents

List of Abbreviations	v
List of Figures	ix
List of Schemes	xii
List of Tables	xv
Abstract	1
1. INTRODUCTION	3
1.1. Structure of HIV virion	4
1.2. HIV life cycle	6
1.3. Possible targets for anti-HIV agents and clinically used therapeutic agents	7
1.4. Reverse transcriptase enzyme	17
1.5. HIV-1 Non-Nucleoside Reverse Transcriptase Inhibitors (NNRTIs)	19
1.6. Drug design of new potential NNRTI molecules	25
2. MATERIAL AND METHODS	37
2.1. Computational approach	37
2.2. Chemistry	37
2.2.1 General	38
2.2.2 Instruments	38
2.2.3 Chemical procedures of synthesis	
2.3. Biological assays	39
2.3.1. ELISA enzymatic assay	39
2.3.2. <i>In vitro</i> anti-HIV activity	39
2.3.3. <i>In vitro</i> antiviral activity	39
2.3.4. Antibacterial activity	40
3. RESULTS	43
3.1. Drug design	43
3.1.1. Docking calculation	45
3.1.1.1. Proteins preparation	45
3.1.1.2. Preparation of ligands	46
3.1.1.3. Molecular docking	47
3.1.1.4 ADME and drug-like properties prediction	50

3.2. Chemical synthesis and structural characterization of the new molecules	55
3.2.1. Precursors 29, 30 and 35	58
3.2.2. Tosylate precursors	59
3.2.2.1. General procedure of synthesis	59
3.2.2.2. Spectroscopic and mass spectrometric data	60
3.2.3. New amino-pyrones 1-6 and 22-23	61
3.2.3.1. General procedure of synthesis	61
3.2.3.2. Spectroscopic and mass spectrometric data	62
3.2.4. New dichloroketo-amino compounds	66
3.2.4.1. General procedure of synthesis	66
3.2.4.2. Spectroscopic and mass spectrometric data	67
3.2.5. New amides 8-10	69
3.2.5.1. General procedure of synthesis	70
3.2.5.2. Spectroscopic and mass spectrometric data	70
3.2.6. New thioethers 14, 16, 25 and 32	71
3.2.6.1. General procedure of synthesis	71
3.2.6.2. Spectroscopic and mass spectrometric data	72
3.2.7. New sulfones 15, 17, 21 and 26	74
3.2.7.1. General procedure of synthesis	74
3.2.7.2. Spectroscopic and mass spectrometric data	74
3.2.8. New ethers 18-20 and 23	76
3.2.8.1. General procedure of synthesis	76
3.2.8.2. Spectroscopic and mass spectrometric data	77
3.2.9. Synthesis and structural characterization of 4-bromo-6-methyl-2 <i>H</i> -pyran-2-one (37)	80
3.2.10. Study of the selectivity in <i>N, C</i> -acylation of 4-benzylamino-pyrone	80
3.2.10.1. Synthesis and structural characterization of compounds 38-43	81
3.2.10.2. Spectroscopic and mass spectrometric data	82
3.2.10.3. Study of selectivity in enamino-ester 45 as a model compound	85
3.2.11. Isolation and purification of drug nevirapine (NVP) from Viramune [®] tablets	86
3.3. Biological evaluation	89
3.3.1. ELISA enzymatic assay	89
3.3.1.1. Validation of ELISA assay	90
3.3.1.2. Results of the assay	92
3.3.2. Anti-HIV activity assay	92
3.3.3. Antiviral activity	94
3.3.4. Cytostatic activity	102
3.3.5. Antibacterial activity	103

4. DISCUSSION	107
4.1. Drug design	107
4.1.1. Docking validation	109
4.1.2. Docking evaluation	111
4.1.3. ADME and drug-like properties prediction	112
4.2. Chemical synthesis and structural characterization of the new molecules	112
4.3. Study of the selectivity in N,C-acylation of 4-benzylamino-pyrone	120
4.3.1. Regioselectivity in a model enamino-ester	127
4.4. Biological evaluation	128
4.4.1. ELISA enzymatic assay	128
4.4.2. Anti-HIV activity	129
4.4.3. Antiviral activity	131
4.4.4. Cytostatic activity of some molecules	131
4.4.5. Antibacterial activity of some molecules	133
5. CONCLUSION	135
6. REFERENCES	137
Acknowledgments	147
Appendix A: Table I. Results from docking calculations on a theoretical library of molecules	I
Appendix B: Presentation of preliminary results at XIII International Workshop on Complex Systems	VIII
Appendix C: Contribution at the 16 th International Electronic Conference on Synthetic Organic Chemistry	X
Appendix D: Additional research activity	XII
Appendix E: <i>Curriculum vitae</i>	XVII

List of Abbreviations

ABTS	2,2'-azino-bis(3-ethylbenzothiazoline-6-sulphonic acid)
ADME	Absorption, Distribution, Metabolism, Excretion
AIDS	Acquired Immuno Deficiency Syndrome
α -APA	2-((2-acetyl-5-methylphenyl)amino)-2-(2,6-dichlorophenyl)acetamide
ATCC	American Type Culture Collection
AZT	3'-azido-2',3'-dideoxythymidine
CAN	cerium(IV) ammonium nitrate
CC ₅₀	Cytotoxic Concentration required to reduce cell growth by 50%.
CCID ₅₀	Virus Dose to Infect 50% of the Cell Cultures
CCR5	C-C Chemokine Receptor type 5
CDC	Centers for Disease Control and Prevention
CrFK	Crandell-Rees Feline Kidney
CXCR4	C-X-C chemokine receptor type 4
DABCO	1,4-diazabicyclo[2.2.2]octane
DBU	1,8-diazabicyclo[5.4.0]undec-7-ene
DFT	Density Functional Theory
DIG-POD	digoxigenin-peroxidase
DIPEA	<i>N,N</i> -diisopropylethylamine
DMAP	4-dimethylaminopyridine
DMSO	dimethyl sulfoxide
dNTP	desoxyribonucleotides triphosphate
DS-5000	dextran sulfate with molecular weight 5000
EC ₅₀	Half Maximal Effective Concentration

EI-MS	Electron Impact Mass Spectrometry
ELISA	Enzyme-Linked ImmunoSorbant Assay
ESI-MS	ElectroSpray Ionization Mass Spectrometry
FC	Flash Chromatography
FIPV	Feline Corona Virus
FPR	False Positive Rate
GA	Genetic Algorithm
HAART	Highly Active Anti-Retroviral Therapy
HBY	(S)-4-isopropoxycarbonyl-6-methoxy-3-methylthiomethyl-3,4-dihydroquinoxalin-2(1H)-thione
HHA	carbohydrate-binding <i>Hippeastrum hybrid</i>
HIA	Human Intestinal Absorption
HIV	Human immunodeficiency Virus
HMBC	Heteronuclear Multiple Quantum Correlation
HR(EI)MS	High Resolution Electron Impact ionization Mass Spectrometry
HSQC	Heteronuclear Single Quantum Correlation
HSV	Herpes Simplex Virus
IC ₅₀	50 % Inhibitory Concentration ($\mu\text{mol L}^{-1}$) required to inhibit tumor cell proliferation by 50 %.
Log P	Partition Coefficient
LS	Local Search
MDCK	Madin Darby Canine Kidney
MIC	Minimum Inhibitory Concentration
MTP	MicroTitre Plate
MRSA	Methicillin-Resistant <i>Staphylococcus aureus</i>
MRX	5-bromo-3-(pyrrolidin-1-ylsulfonyl)-1H-indole- 2-carboxamide
NCI	National Cancer Institute
NMR	Nuclear Magnetic Resonance

NNIBP	Non-Nucleoside Inhibitors Binding Pocket
NNRTI	Non-Nucleoside Reverse Transcriptase Inhibitor
NVP	Nevirapine
OD	Optical Density
PFU	Plaque-Forming Units
Ph	phenyl
PPB	Plasma Proteins Binding
PZ2	3-[2-bromo-4-(1H-pyrazolo[3,4-c]pyridazin-3-ylmethyl)phenoxy]-5-methylbenzotrile
RMS	Root Mean Square
RMSD	Root-Mean-Square Deviation
ROC	Receiver Operating Characteristic Curve
RT	Reverse Transcriptase
SD	Standard Deviation
(S)-DHPA	(S)-3-(6-Amino-purin-9-yl)-propane-1,2-diol
SI	Selectivity Index
THF	tetrahydrofuran
TLC	Thin Layer Chromatography
TMDM	<i>N,N,N',N'</i> -tetramethyldiamino-methane
TMED	<i>N,N,N',N'</i> -tetramethyl-ethylendiamine
Topo-I	Topoisomerase-I
TPR	True Positive Rate
TsCl	<i>p</i> -toluensulfonyl chloride
UDA	carbohydrate-binding <i>Urtica dioica</i>
UHP	Hydrogen peroxide–Urea adduct
VZV	varicella-Zoster Virus
WHO	World Health Organization

List of Figures

Figure 1.1. Adults and children estimated to be living with HIV in 2010 in the world. (from UNAIDS, WHO Report)

Figure 1.2. Genome structure of HIV-1 (Montagner, 2010)

Figure 1.3. Schematic diagram of HIV virion structure

Figure 1.4. HIV viral entry (Chinen, 2002)

Figure 1.5. HIV life cycle (Tibotec archive)

Figure 1.6. Molecular structure of FDA approved CCR5 inhibitor

Figure 1.7. Molecular structure and primary sequence of enfuvirtide

Figure 1.8. Molecular structures of FDA approved HIV-1 protease inhibitors

Figure 1.9. Molecular structure of the integrase inhibitor raltegravir

Figure 1.10. Mechanism of action of zidovudine (AZT). Following phosphorylation to its triphosphate form (AZT-TP), AZT acts as a competitive inhibitor/alternative substrate with respect to dTTP in the reverse transcriptase reaction. (De Clercq, 2009)

Figure 1.11. Molecular structure of nucleoside reverse transcriptase inhibitors(NRTIs)

Figure 1.12. Molecular structure of the pro-drug tenofovir disoproxil fumarate

Figure 1.13. Mechanism of action of tenofovir. Following phosphorylation of tenofovir to its diphosphate, the latter one acts as an obligate chain terminator in the reverse transcriptase reaction (De Clercq, 2009)

Figure 1.14. Molecular structure of commercial non-nucleoside reverse transcriptase inhibitors

Figure 1.15. Theoretically possible drug combinations for the treatment of AIDS patients (adapted from De Clercq, 2009)

Figure 1.16. 3D-Structure of HIV-1 reverse transcriptase in the complex with DNA (PDB code: 3KJV)

Figure 1.17. Diagram of HIV reverse transcription mediated by the DNA polymerase, RNase H and strand transfer activities of RT

Figure 1.18. HIV-1 RT with binding site for NRTIs/NtRTIs and the binding site NNRTIs (Sluis-Cremer, 2008)

Figure 1.19. Schematic HIV life-cycle showing points of action of NNRTI (in red) (Sluis-Cremer, 2008)

Figure 1.20. (a) Chemical structure of TIBO, (b) 3D-model of the NNRTI proposed by Schäfer

Figure 1.21. Schematic representation of NNRTI pharmacophoric distance map (Zhan, 2011)

Figure 1.22. Schematic representation showing how a flexible inhibitor can adapt to changes in the binding pocket of RT due to mutations. A rigid inhibitor (left panel), although binding strongly to the unmutated target, fails to bind strongly to the mutated pockets. A flexible inhibitor (right panel) can adapt to those changes in the pocket by its torsional changes and repositioning (Das, 2005)

Figure 1.23. Schematic 2D representation of commone mode of binding in butterfly-like (9-Cl-TIBO) and horseshoe-like (TMC125, etravirine) shapes in the NNIBP (Zhan, 2011).

Figure 1.24. General approach for the rational design of inhibitors

Figure 1.25. Schematic outline for structure-based lead discovery (adapted from Jorgensen, 2009)

Figure 1.26. The most used docking software (Sousa, 2006)

Figure 1.27. a) Best pose with reference to crystallographic pose, b) Top ten poses with reference to crystallographic pose, c) Ligand rotatable bonds in relation to docking accuracy, d) % of hydrogen bonding in terms of docking accuracy (Chikhi, 2008)

Figure 1.28. Thermodynamic cycle for the binding of an enzyme (E) and an inhibitor (I) in both the solvated phase and in *vacuo*. (<http://www.scripps.edu/pub/olsonweb/doc/autodock/>)

Figure 1.29. Genotypic and phenotypic search by Darwinian(right-hand side) and Lamarckian(left-hand side) search. $f(x)$ is the fitness function. With sufficient iterations, the local search arrive at a local minimum, and an inverse mapping function is used to convert

from its phenotype to its corresponding genotype. In the case of molecular docking, however, local search is performed by continuously converting from the genotype to the phenotype, so inverse mapping is not required. The genotype of the parent is replaced by the resulting genotype, however, in accordance with Lamarckian principles. (adapted from Morris, 1998)

Figure 1.30. Example of main feature of grid map (<http://www.scripps.edu/pub/olson-web/doc/autodock/>)

Figure 1.31. (a) Comparison of the distribution of binding energies for known inhibitors and NCI Diversity Set compounds.(b) ROC curve showing a sensitivity/specificity tradeoff for threshold values from -8 to -6 kcal/mol. (adapted from Chang, 2007)

Figure 3.1. Drug design of new potential NNRTIs by molecular hybridization method

Figure 3.2. General structure of designed new molecules as potential NNRTIs

Figure 3.3. Structure of inhibitors in complex with downloaded RT

Figure 3.4. Visual inspection of some results obtained by docking validation test. In green are reported the original ligand position in X-ray crystallographic structure, in red are reported the docked molecules. a) rilpivirine (pdb code:2ZD1), b) efavirenz (pdb code: 1FK9), c) delavirdine (pdb code:1KLM), d) nevirapine (pdb code:1VRT), e) compound PZ2 (pdb code:3E01), f) compound MRX (pdb code: 2RF2)

Figure 3.5. Amino acid residues in Rasmol colours of NNIBP surrounding the *in vitro* resulted most active molecules **23** (in red)

Figure 3.6. Cluster analysis of compound **23**

Figure 3.7. Overlapped structures in the RT binding site (pdb code 1FK9) of compound **23** (in red), calanolide A (in blue) and α -APA (in green) deriving from AutoDock calculation

Figure 3.8. Visual inspection of overlapped molecules of compound **23** (in red), calanolide A (in blue) and α -APA (in green) obtained using a superimposing genetic algorithm that considers shape, electrostatic potential, lipophilicity and molecular refractivity

Figure 3.9. Imino-enamino tautomeric equilibrium for pyrone **1**

Figure 3.10. ^1H -NMR (400MHz) spectrum in CDCl_3 of the isolated nevirapine

Figure 3.11. ^1H , ^{13}C NMR (HSQC) spectrum of nevirapine in CDCl_3

Figure 3.12. Long range ^1H , ^{13}C NMR (HMBC) spectrum of nevirapine in CDCl_3

Figure 3.13. Schematic representation of working method for RT ELISA.

Figure 3.14. Comparison of percentage inhibition with different RT enzyme in the presence of nevirapine ($200\mu\text{M}$)

Figure 3.15. Comparison between Roche and Pierce RT inhibition after a cycle of freezing/thawing

Figure 4.1. Drug design process to select the series of new molecules

Figure 4.2. Success and failures of docking calculation of rigid and flexible ligands in different family of enzymes. Red arrow indicates the HIV-RT family; (a) rigid ligand (RGD), (b) flexible ligand (FLX). The left y-axis shows protein family and size and the right y-axis shows average number of ligand rotatable bonds (#RB). (c) (orange bars) shows difference in scoring - sampling failures for FLX (adapted from Mukherjee, 2010)

Figure 4.3. ESI(-)-MS/MS spectrum of $[\text{M}-\text{H}]^-$ ion at m/z 310 of the by-product from aminolyses of tosylate **28**. M is the by-product of aminolysis

Figure 4.4. ^1H -NMR spectrum (400 MHz, in CDCl_3) and chemical structure of the by-product deriving from aminolysis of tosylate **28** with 1-naphthylmethanamine

Figure 4.5. ^1H -NMR of compound **23** (400MHz, in CDCl_3)

Figure 4.6. HSQC spectrum of compound **23** (400MHz, in CDCl_3)

Figure 4.7. Relevant $^1\text{H}/^{13}\text{C}$ long-range correlations deduced by HMBC experiment in CDCl_3 for the compound **23**

Figure 4.8. Long-range ^1H , ^{13}C NMR spectrum by HMBC experiment in CDCl_3 for **23**

Figure 4.9. EI-MS spectrum of compound **23** with indication of the fragmentation pattern

Figure 4.10. Energy minimized structure of compound **7** by DFT calculation (top); experimental (centre) and calculated (bottom) infrared spectra of compound **7**

Figure 4.11. Energy minimized structure of compound **38** by DFT calculation (top); experimental (centre) and calculated (bottom) infrared spectra of compound **38**

Figure 4.12. Two resonance forms of aminopyrone **1**

List of Schemes

Scheme 3.1. Chemical synthesis of compounds **1-13**. *Reagents and conditions:* a) TsCl (1.1 eq)/ Et₃N(1.5 eq)/CH₂Cl₂ 0°C→r.t., 24h, 90% yield; b) suitable (aryl)alkyl amine (1.1 eq), Et₃N(1.5eq.) EtOH r.t., 60h, 50-55% yield; c) acyl chloride (1.2 eq)/ Py (2 eq)/ CH₂Cl₂ 0°C→r.t., 24h 85-95% yield; d) acyl chloride (1.2 eq)/ (2 Et₃N eq)/ CH₂Cl₂ 0°C→r.t., 24h, 25-84% yield

Scheme 3.2. Chemical synthesis of compounds **14-21**. *Reagents and conditions:* a) NaSH in EtOH r.t., 2h, suitable (aryl)alkyl bromide (1 eq), DBU (1.5eq.) C₆H₆ r.t., 18 h, 40-86% yield; b) UHP / HCOOH 85% r.t., 4h, 100% yield; c) suitable (aryl)alkyl bromide (1.1 eq), K₂CO₃, KI, acetone reflux 20h, 40-60% yield; d) I₂/AgNO₃/MeOH under N₂ at r.t. in the dark for 5h, 85% yield; e) Br₂ /CH₂Cl₂ 3h, 66% yield; f) TsCl (1.1 eq)/ Et₃N(1.5 eq)/CH₂Cl₂ 0°C→r.t. 24h, 90% yield)

Scheme 3.3. Chemical synthesis of compounds **22-26**. *Reagents and conditions:* a) TsCl (1.1 eq)/ Et₃N(1.5 eq)/CH₂Cl₂ 0°C→r.t., 24h, 90% yield; b) naphthalen-1-ylmethanamine (1.1 eq), Et₃N(1.5eq.) EtOH r.t. 60h, 55 % yield; c) Et₃SiH/LiClO₄/CF₃COOH r.t. 60 h 90 % yield; d) 1-(bromomethyl)naphthalene (1.1 eq), K₂CO₃, KI, acetone reflux 20h, 60% yield; e) NaSH in EtOH r.t. 2h, 1-(bromomethyl)naphthalene (1.2 eq), DBU (1.5eq.) C₆H₆ r.t., 18 h, 80 % yield; f) UHP / HCOOH 85% r.t. 5h, 100% yield

Scheme 3.4. Base effect on the selectivity of *N, C*-acylation of benzylpyrone **1**. *Reagents and conditions:* a) base (2.5 eq.) suitable acyl chloride (2.0 eq.), CH₂Cl₂, 0 °C →r.t., 18h, 78-90% yield

Scheme 3.5. Acylation of enaminoester **45**. *Reagents and conditions:* a) different base (2.5 eq.) dichloroacetyl chloride (2.0 eq.), CH₂Cl₂, 0°C →r.t., 18h, 78-90% yield

Scheme 4.1. Synthesis of 4-bromo-6-methyl-2*H*-pyran-2-one. *Reagents and conditions:* a) *n*Bu₄N⁺Br⁻/P₂O₅/ toluene, 100°C 1h, 82% yield; b) 1-naphthylmethanamine (1.5 eq)/ EtOH/ reflux 20h, 50% yield or c) 1-naphthylmethanamine (1.5 eq), MW, 100°C, 2h, 55% yield

Scheme 4.2. *N, C*-acylation of benzylpyrone **1**. *Reagents and conditions:* a) Et₃N (2.5 eq.) dichloroacetyl chloride (2.0 eq.), CH₂Cl₂, 0 °C →r.t., 18h, 88 % yield

Scheme 4.3. Base effect on the selectivity of *N, C*-acylation of enaminoester **45**. *Reagents and conditions:* a) different base (2.5 eq.) dichloroacetyl chloride (2.0 eq.), CH₂Cl₂, 0°C →r.t., 18h, 78-90% yield

List of Tables

Table 1.1. Summary of potential HIV target and potential drugs

Table 1.2. Approved antiretroviral drugs. Adapted from: *Drugs Used in the Treatment of HIV Infection, U.S. FDA*, <http://www.fda.gov/oashi/aids/virals.html>

Table 1.3. Interactions involved in binding of NNRTIs to HIV Reverse Transcriptase (Zhan, 2011)

Table 3.1. Details of RT X-Ray crystal structure

Table 3.2. Calculated binding energy by docking validation of different X-ray RT structures. The values in red are the energy corresponding to re-docked of ligand in the same original RT

Table 3.3. Docking and ADME parameters for the synthesized molecules

Table 3.4. Validation of ELISA enzymatic test (Roche)

Table 3.5. Results of HIV-RT Kit Assay

Table 3.6. Anti-HIV activity, cytotoxicity in CEM cells

Table 3.7. Anti-herpes simplex, vaccinia and vesicular stomatitis virus activity in HEL cell line cultures

Table 3.8. Anti-varicella-zoster virus activity in HEL cell line cultures

Table 3.9. Anti-vesicular stomatitis, Coxsackie and respiratory syncytial viruses activity in HeLa cell line cultures

Table 3.10. Anti-parainfluenza, reovirus-1, Sindbis, Coxsackie and Punta Toro viruses activity in VERO cell line cultures

Table 3.11. Anti-feline corona virus and feline herpes virus activity in CRFK cell cultures

Table 3.12. Anti-influenza A and B activity in MDCK cell cultures

Table 3.13. Anti- Cytomegalovirus activity in HEL cell cultures

Table 3.14. Cytostatic activity on murine leukemia, human T-lymphocyte and human cervix carcinoma activity

Table 3.15. Antibacterial activity on *E. coli* (ATCC 25922), *S. aureus* (ATCC 25923) *MRSA* (ATCC 43300) and *P. aeruginosa* (ATCC 27853) strains

Table 3.16. Minimal Inhibitory Concentration on *S. aureus* (ATCC 25923), *MRSA* (ATCC 43300) and *P. aeruginosa* (ATCC 27853) strains

Table 4.1. Selectivity in *N, C*- dichloroacetylation of aminopyrone **1** by changing the base (in CH₂Cl₂ at 0°C for 18 hours, yield 89%), see scheme 3.4

Table 4.2. Calculated values for proton affinity of some bases used in the acylation reaction

Table 4.3. Selectivity in *N, C*- dichloroacetylation of aminopyrone **1** using pyridine or DBU by changing the solvent (at 0°C for 18 hours, yield 89%)

Table 4.4. Selectivity in *N, C*- acylation of aminopyrone **1** using pyridine or DBU by changing the acyl halide (in CH₂Cl₂ at 0°C for 18 hours, yields 78-90%)

Table 4.5. Selectivity in *N, C*- dichloroacetylation of enaminoester **45** by changing the base (in CH₂Cl₂ at 0°C for 18 hours, yield 85%), see scheme 3.5

Table 4.6. Anti-HIV activity, cytotoxicity and selectivity index in CEM cells

Table 4.7. Cytostatic activity on murine leukemia, human T-lymphocyte and human cervix carcinoma activity

Table in Appendix A. Results from docking calculations on a theoretical library of molecules

Abstract

Acquired Immunodeficiency Syndrome (AIDS) is a disease caused by the Human Immunodeficiency Virus (HIV). Since its discovery in 1981, more than 25 million people died due to this disease. To date, an effective HIV-1 vaccine usable in prophylaxis or in the therapy of humans has not yet been identified. The failures and limited success of HIV vaccines have reinforced the role of chemotherapy and therefore research on the development of effective drugs. Non-nucleoside reverse transcriptase inhibitors (NNRTIs) were the early agents introduced in the therapy and currently they are the most used, based on their concurrent high activity against the virus and low toxicity against human cells. In addition, the rapid development of virus resistance against these types of drugs, needs to find new molecules able to overcome this drawback.

My thesis work started from the design of a small library of new molecules, with hybrid structures based on a template deriving from the natural product (+)-calanolide A and the synthetic molecule α -APA, both showing a potent and selective activity against reverse transcriptase. Docking calculation has allowed to select molecules having the best values of interaction energy with the viral enzyme. Chemical synthesis was carried out together with structural characterization by extensive spectroscopic analysis including NMR technique and mass spectrometry.

In particular, the synthesis of the amide group present in the structure of some amino-pyrone compounds using the standard method, resulted in the expected *N*-acylation, but with a *C*-acyl byproduct. This result has suggested to look further into the study of *N,C*-acylation selectivity for the ambidentate amino-pyrone moiety, whose reactivity is poorly known. Regioselectivity was investigated under different conditions (organic bases, solvent, acylating agent), also for an enamino-ester taken as a model compound. Experimental procedures were optimized in order to synthesize selectively pure *N*- and *C*-acylated compounds.

A preliminary enzymatic assay indicated a good activity in the early prepared compounds of the series, promising for the following *in vitro* tests on HIV infected cells of each molecule in the whole series. In addition, these compounds were tested against other common viruses for human infective pathologies. With the aim of identifying molecules with potential therapeutic applications, the antiviral activity must be related to cytostatic effect, in order to select the ones with a favored selectivity index. Unfortunately, the

molecules showed paragonable values in antiviral and cytostatic effects, the latter one not easily predictable neither by the chemical structure, nor by a computational approach.

If the drug design by molecular docking has failed in selecting a new scaffold for NNRTIs, the study has driven the interest towards new potential antitumoral molecules showing activity at sub-micromolar concentration against leukemic cell lines.

Due to the structural similarity with recently studied antibacterial natural pyrones, the synthetic molecules showing the lowest values of cytotoxicity were investigated in the inhibition of bacterial strains. Some tested compounds have shown a good activity and selectivity against Gram(+) bacteria.

1. Introduction

Acquired Immunodeficiency Syndrome (AIDS) is a disease caused by the Human Immunodeficiency Virus (HIV) (Sepkowitz, 2001; Weiss, 1993). The first cases of AIDS were reported in 1981 when the Centers for Disease Control and Prevention (CDC) observed a cluster of *Pneumocystis carinii* pneumonia in five homosexual men in Los Angeles. In 1982 CDC gave the name AIDS at this illness. The major factors in the diffusion of AIDS pandemic are sexual transmission and vertical transmission from mother to child at the birth and through breast milk (Kallings, 2008). It is estimated that 34.0 million (range 31.6 million–35.2 million) people lived with HIV in 2010 (Figure 1.1), including 3.4 million (range 3.0 million–3.8 million) children. An estimated 2.7 million (range 2.4 million–2.9 million) people were newly infected in 2010, including 390,000 children. A total of 1.8 million (range 1.6 million–1.9 million) of people died due to AIDS in 2010 (UNAIDS, WHO 2011).

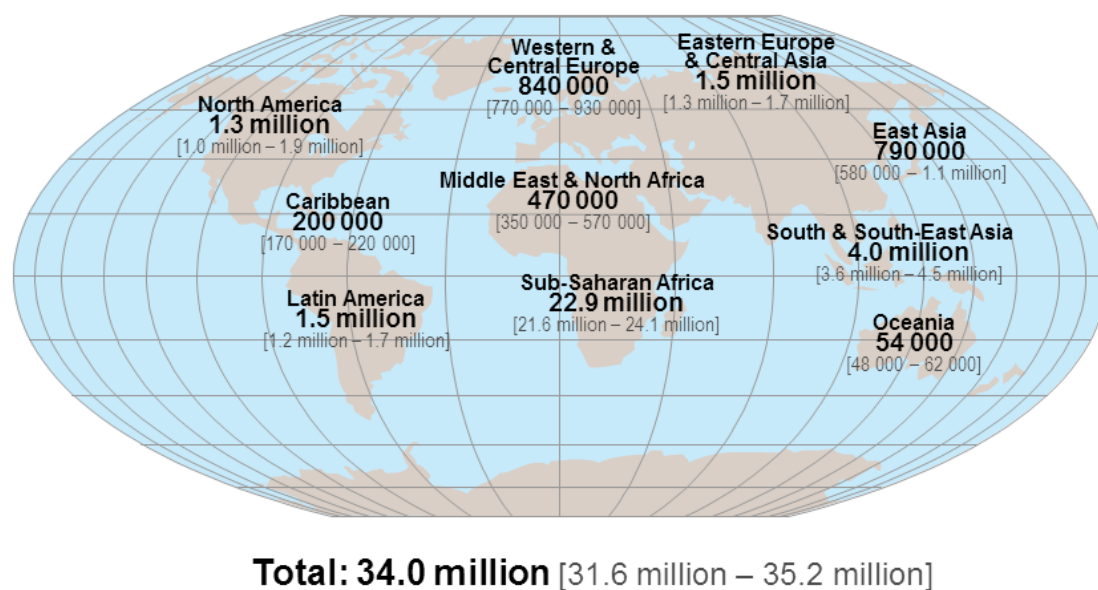


Figure 1.1. Adults and children estimated to be living with HIV in 2010 in the world (from UNAIDS, WHO Report)

Two HIV types infect humans: HIV-1 and HIV-2, both discovered by Luc Montagnier and colleagues in 1983 and 1986 respectively (Barre-Sinoussi, 1983; Clavel, 1986). HIV-1 virus probably came from the Congo in 1959 and 1960, although genetic studies indicate that

it passed into the human population from chimpanzees around fifty years earlier (Worobey, 2008). A recent study shows that a strain of HIV-1 probably moved from Africa to Haiti and then entered the United States around 1969 (Gilbert, 2007), whereas HIV-2 may have originated from the sooty mangabey (*Cercocebus atys*), and is largely confined to West Africa (Reevers, 2002).

HIV-1 is more virulent in comparison with HIV-2, is more easily transmitted and is globally the most present in the HIV infected people (Reeves, 2002). HIV infects human host cells, in particular cells of immune system, as T lymphocytes (CD4+ T cells), macrophages and dendritic cells. The result of this infection is the destruction and functional impairment of the immune system, leading a drop of levels in CD4 + T cells through three main mechanisms: direct viral killing of infected cells, increase of the apoptosis rates in infected cells and finally the killing of infected CD4 + T cells by CD8 cytotoxic lymphocytes, that are able to recognize infected cells. In the plasma of a healthy uninfected people are usually present between 800 and 1,200 CD4 + T cells/mm³. The progress of HIV infection decreases the number of CD4+ T cells and when it arrives to be lower than 200/mm³, the patients become particularly susceptible to tumors (e.g. Kaposi's sarcoma and lymphomas) and to opportunistic infections caused by microorganisms, that usually do not infect people with a working immune system.

1.1. Structure of HIV virion

HIV is a member of genus *lentivirus*, family of *Retroviridae*, which has a relatively small genome consisting of a single-strand positive sense ribonucleic acid (RNA). The viral genome contains three main genes (*gag*, *pol* and *env*), as well as regulatory (*tat* and *rev*) and accessory (*vif*, *nev*, *vpr* and *vpu*) genes (Figure 1.2; Montagnier, 2010).

Human immunodeficiency virus is a spherical retrovirus with a diameter of ~100–150 nm (Liu, 2010). The viral structure contains a bilayer lipidic membrane deriving from the host cell in which two viral glycoproteins called gp120 and gp 41 are present. Both they derive from the cleavage by a viral enzyme (protease) of a larger protein (gp160) encoded by *env* gene. The HIV core contains three structural proteins (p24, p16 and p9). The protein p24 envelops two RNA single-stand chains and the viral enzymes Reverse Transcriptase (RT) Integrase (IN) and Protease (PR). The protein p16 is a matrix protein and it is anchored to

the internal face of nucleocapsid, whereas the protein p9 is non-covalently linked to viral RNA (Figure 1.3) (Chinen, 2002). The virulence and transmissibility of HIV depend from the viral subtypes, in particular they are classified in three groups: M (majority), O (outliers) and N (non-M/non-O). Each group can be classified in further different subtypes, which can be also associated to geographic location (Hu, 1999).

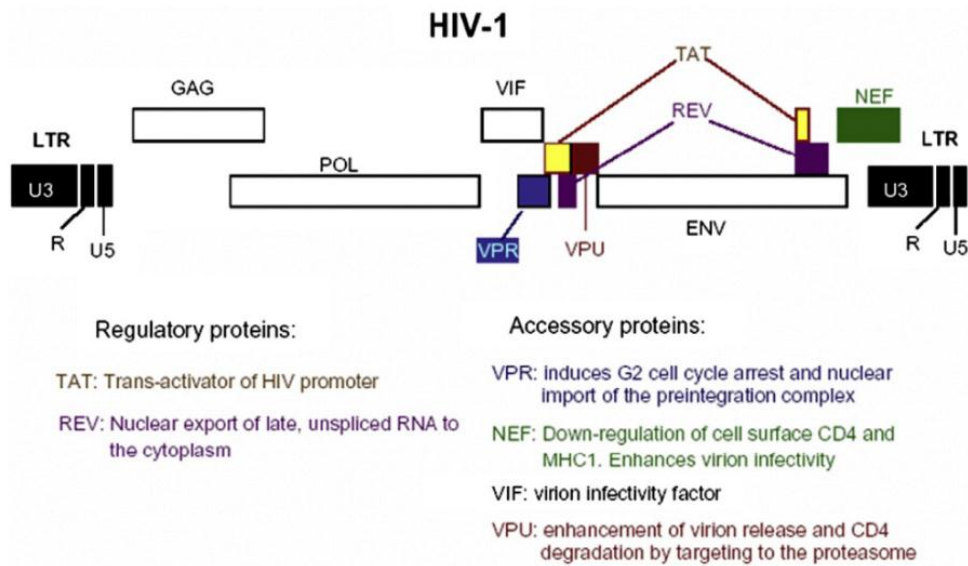


Figure 1.2. Genome structure of HIV-1 (Montagnier 2010)

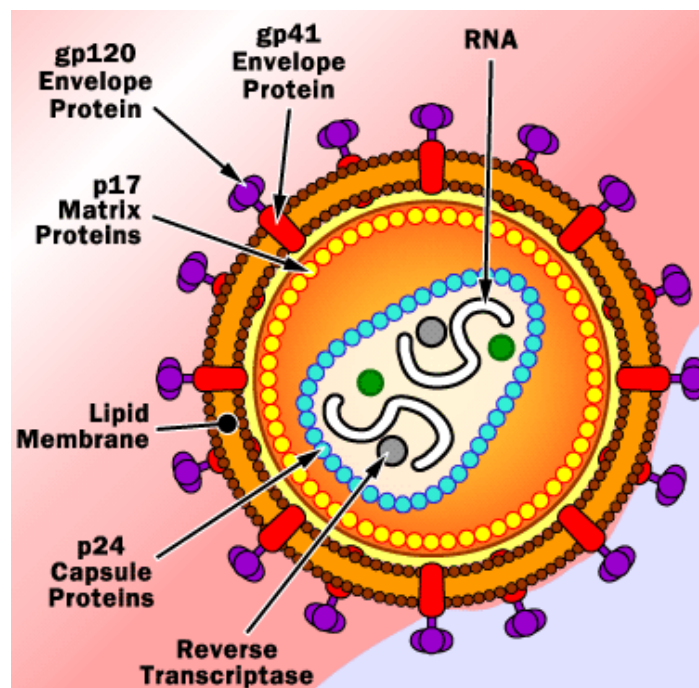


Figure 1.3. Schematic diagram of HIV virion structure

1.2. HIV life cycle

HIV begins its life cycle when the HIV surface protein gp 120 binds to CD4 receptor. A conformational change in this protein allows to interact with one of two chemokine co-receptors (CCR5 or CXCR4) present on the membrane of CD4+ T- lymphocyte or macrophages. The result of this interaction gives a conformational rearrangement of the hydrophobic domain in gp 41, triggering the fusion of viral envelope with the cell membrane and the release of the nucleocapsid into the cytoplasm (Figure 1.4).

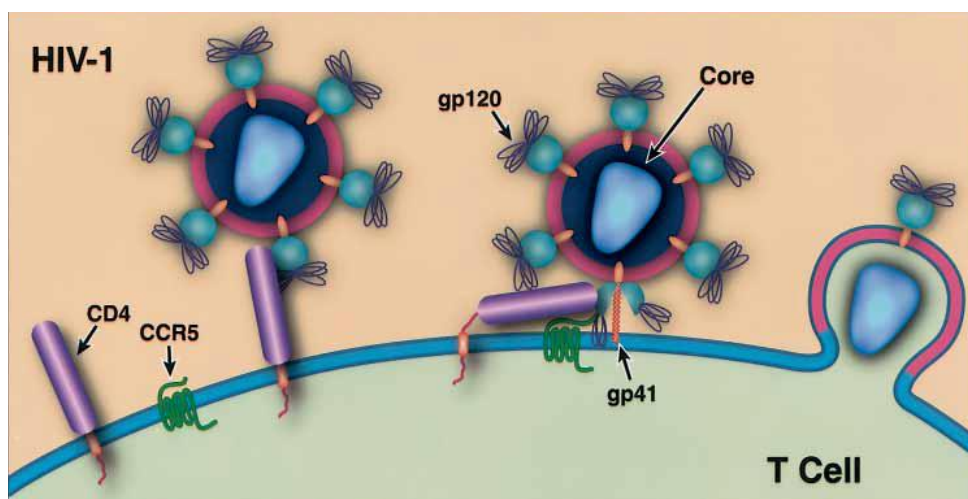


Figure 1.4. HIV viral entry (Chinen, 2002)

Reverse transcriptase (RT) converts the single-stranded HIV RNA to double stranded HIV cDNA through a hybrid RNA-DNA molecule. The newly formed HIV cDNA is transported into the host cell's nucleus by the help of the two HIV proteins Vpr and Vif. The integrase, a HIV enzyme, "hides" as provirus the HIV cDNA within the host cell's own DNA. After integration, the viral gene transcription is activated by cellular transcription factors, producing low levels of mRNA transcripts. They encode for the regulatory proteins Tat, Rev, and Nef. The effect of these regulatory proteins is the activation or inhibition in the replication of viral DNA.

The viral DNA (provirus) may be transcribed into viral messenger RNA (mRNA), which is transported to the cytoplasm, where is translated into viral proteins by the cell's machinery.

These proteins together with copies of HIV's RNA give a new virus particle. The newly assembled virus pushes out ("buds") from the host cell. During budding, the new virus steals part of the cell's outer envelope. This envelope, which acts as a covering, is studded with HIV glycoproteins, which are necessary to the virus for binding CD4 and co-receptors. The new copies of HIV can infect other cells (Figure 1.5).

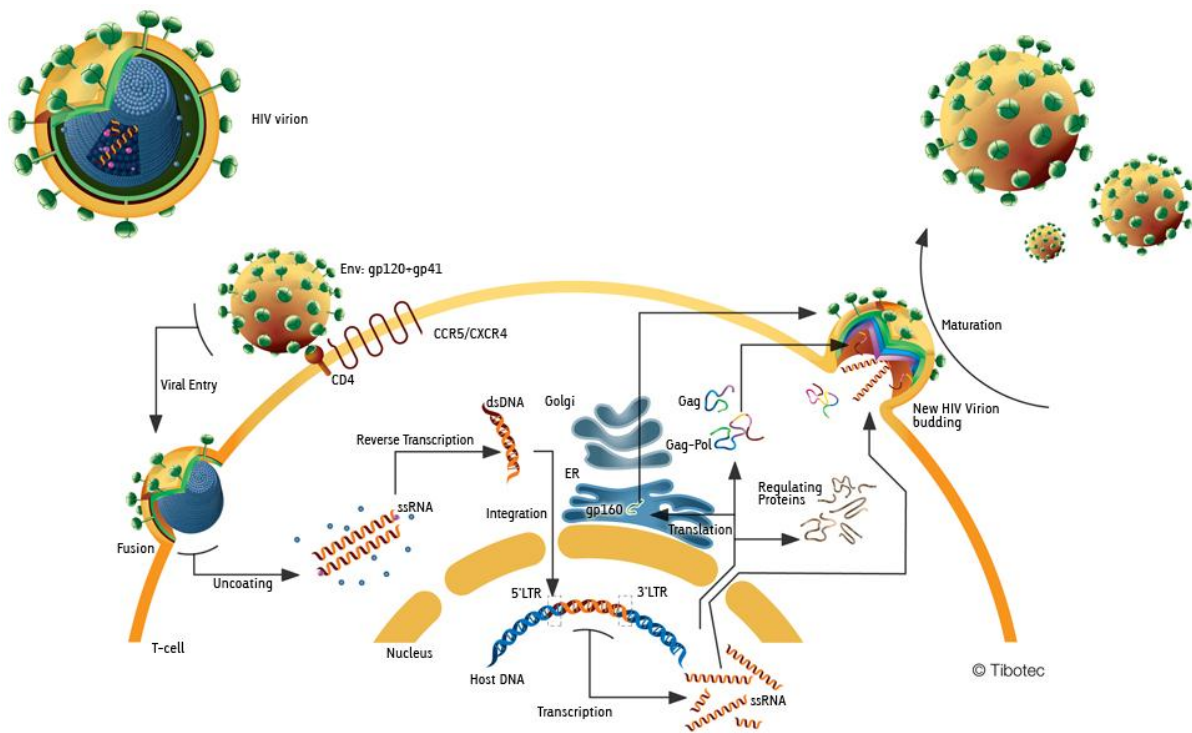


Figure 1.5. HIV Life Cycle (Tibotec archive)

1.3. Possible targets for anti-HIV and clinically used therapeutic agents

To date, an effective HIV-1 vaccine usable in prophylaxis or in therapy of humans has not yet been identified, although many HIV-1 vaccines have been developed in the last thirty years (Wijesundara, 2011; Estè, 2010). The failures and limited successes of HIV-1 vaccines have driven the research on the development of effective drugs for AIDS (Montagnier, 2010) and the knowledge of replicative cycle of HIV has allowed to identify potential targets for drug discovery, as reported in Table 1.1.

Since the discovery of HIV as agent causing AIDS, many drugs have been introduced in clinical use (Mehellou, 2010).

Table 1.1. Summary of potential HIV target and potential drugs

Stage of HIV life cycle	Potential drugs
Binding to target cell	Antibodies to the virus or cell receptor
Early entry to target cell	Drug that block fusion or interfere with retroviral uncoating
Trascription of RNA to DNA by reverse transcriptase	Reverse transcriptase inhibitors
Degradation of viral RNA in the RNA-DNA hybrid	Inhibitors of RNase H activity
Integration of viral cDNA in the host genome	Integrase inhibitors
Expression of viral genes	Inhibitors of regulatory proteins as tat or vif
Viral component production and assembly	Myristoylation, glycosidation and protease inhibitors
Budding of virus	Interferons

They can be divided into seven main types of inhibitors:

- Virus adsorption inhibitors (co-receptor inhibitors (CRIs))
- Virus-cell fusion inhibitors (FIs)
- Protease inhibitors (PIs)
- Integrase inhibitors (INIs)
- Nucleoside Reverse Transcriptase inhibitors (NRTIs)
- Nucleotide Reverse Transcriptase inhibitors (NtRTIs)
- Non-Nucleoside Reverse Transcriptase inhibitors (NNRTIs)

Currently Food and Drug Administration (FDA) has approved only maraviroc as co-receptor inhibitor CCR5 (Figure 1.6) .

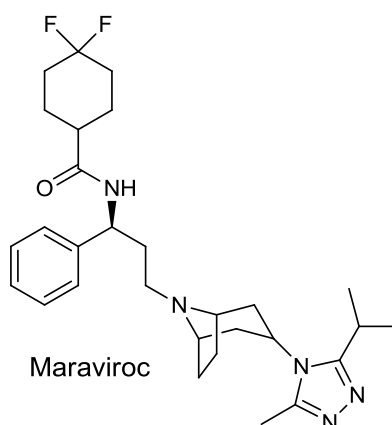
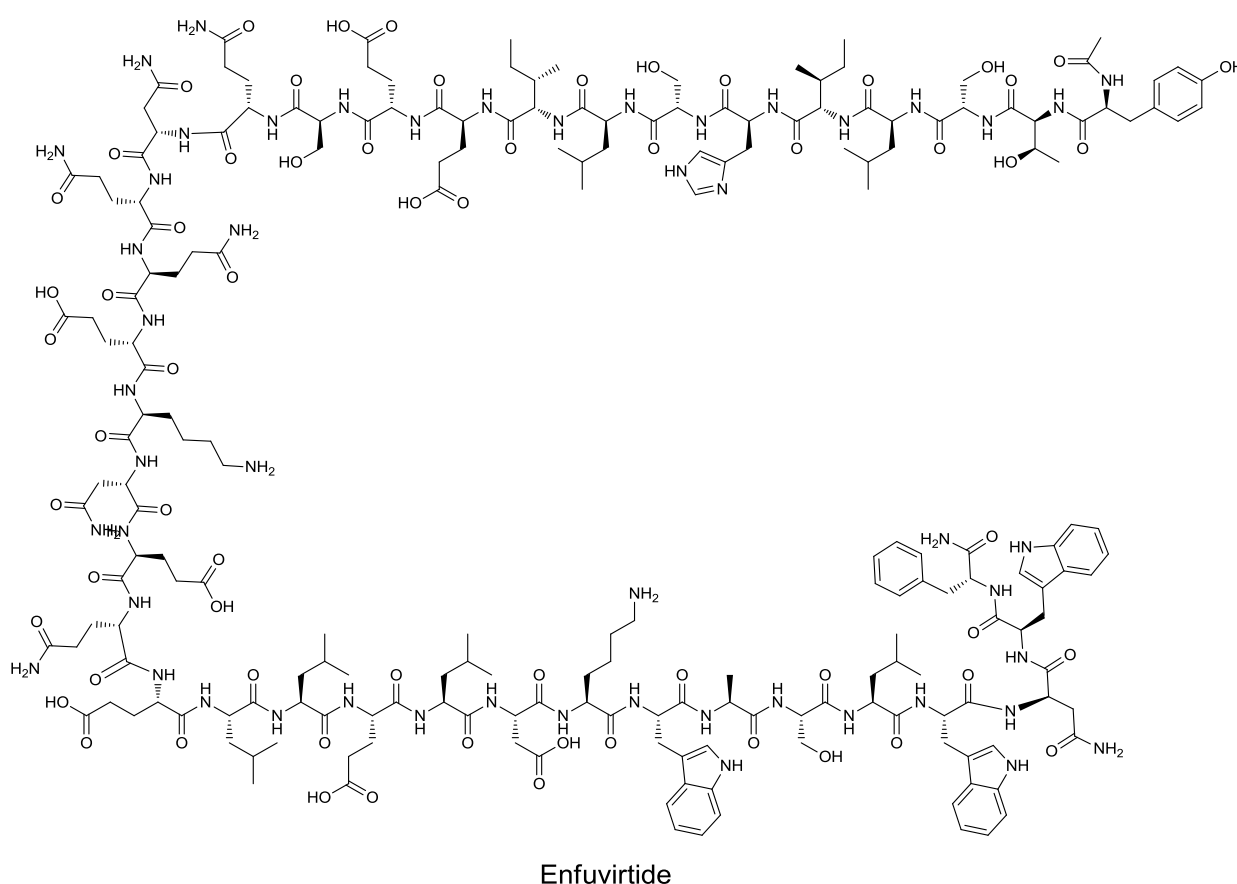


Figure 1.6. Molecular structure of FDA approved CCR5 inhibitor

It has shown a very good activity both *in vitro* and *in vivo* and it is able to suppress the viral load at very low level after ten days of therapy at 100 mg twice a day.

During the study of potential immunogenic peptides, to be used as vaccine and deriving from gp41, it was observed that a peptide of 38 amino acids showed an appreciable antiviral activity. A little chemical modification produced a 36-amino acid peptide called enfuvirtide (Figure 1.7), that has become the first and the only drug approved as HIV-1 fusion inhibitor. It is able to reduce plasma HIV RNA of two fold in 15 days after administration twice a day by subcutaneous injection. As disadvantages it has the formation of erythema in the site of injection and the high production cost.



Ac-Tyr-Thr-Ser-Leu-Ile-His-Ser-Leu-Ile-Glu-Glu-Ser-Gln-Asn-Gln-Gln-Glu-Lys-Asn-Glu-Gln-Glu-Leu-Leu-Glu-Leu-Asp-Lys-Trp-Ala-Ser-Leu-Trp-Asn-Trp-Phe-NH₂

Figure 1.7. Molecular structure and primary sequence of enfuvirtide.

At present, ten protease inhibitors have been approved by FDA. They are : saquinavir, ritonavir, darunavir, indinavir, tipranavir, fosamprenavir, nelfinavir, atazanavir,

lopinavir/ritonavir and aprenavir (Figure 1.8). Protease inhibitors interfere with the late stage of virus replication, preventing the formation of infective viral particles. With exception of tripanavir, they act as peptidomimetic non-hydrolysable transition-state analogues. The bioavailability is poor due to the peptidic feature of these compounds; in addition, the problem of resistance and the toxicity make protease inhibitors not useful as single drug therapy, but as a part of the Highly Active Anti-Retroviral Therapies (HAART).

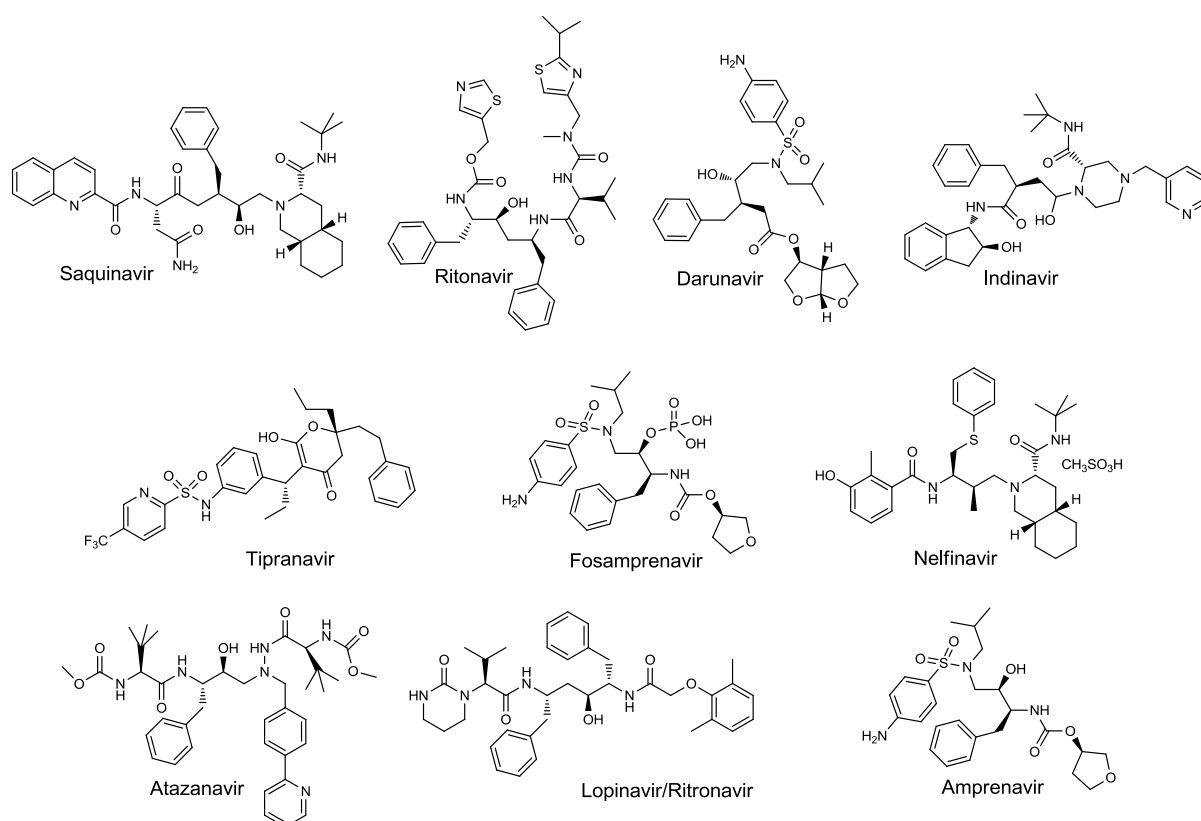


Figure 1.8. Molecular structures of FDA approved HIV-1 protease inhibitors

The integration of viral cDNA into the host cell is a crucial step of HIV replication and it is done by the viral enzyme integrase. Due to the absence of integrase-like enzyme in humans, it was an attractive target for the AIDS therapy. Integrase is a highly conserved 32 kDa protein which uses two divalent metal ions (Mg^{2+} or Mn^{2+}) as cofactor for its activity. Recently FDA has approved only raltegravir as integrase inhibitor (Figure 1.9). It acts as chelating agent of Mg^{2+} in the active site of integrase.

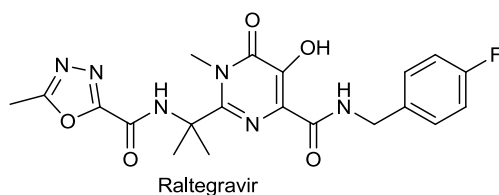


Figure 1.9. Molecular structure of the integrase inhibitor raltegravir

Reverse transcriptase inhibitors have been the early drugs to be introduced in the therapy. The first anti-HIV agent was 3'-azido-2',3'-dideoxythymidine (Zidovudine, AZT), which is a nucleoside analogue blocking the synthesis of viral DNA after triphosphorilation by cellular enzymes (kinases) (Figure 1.10). Zidovudine interacts with the active site of reverse transcriptase (De Clercq, 2009).

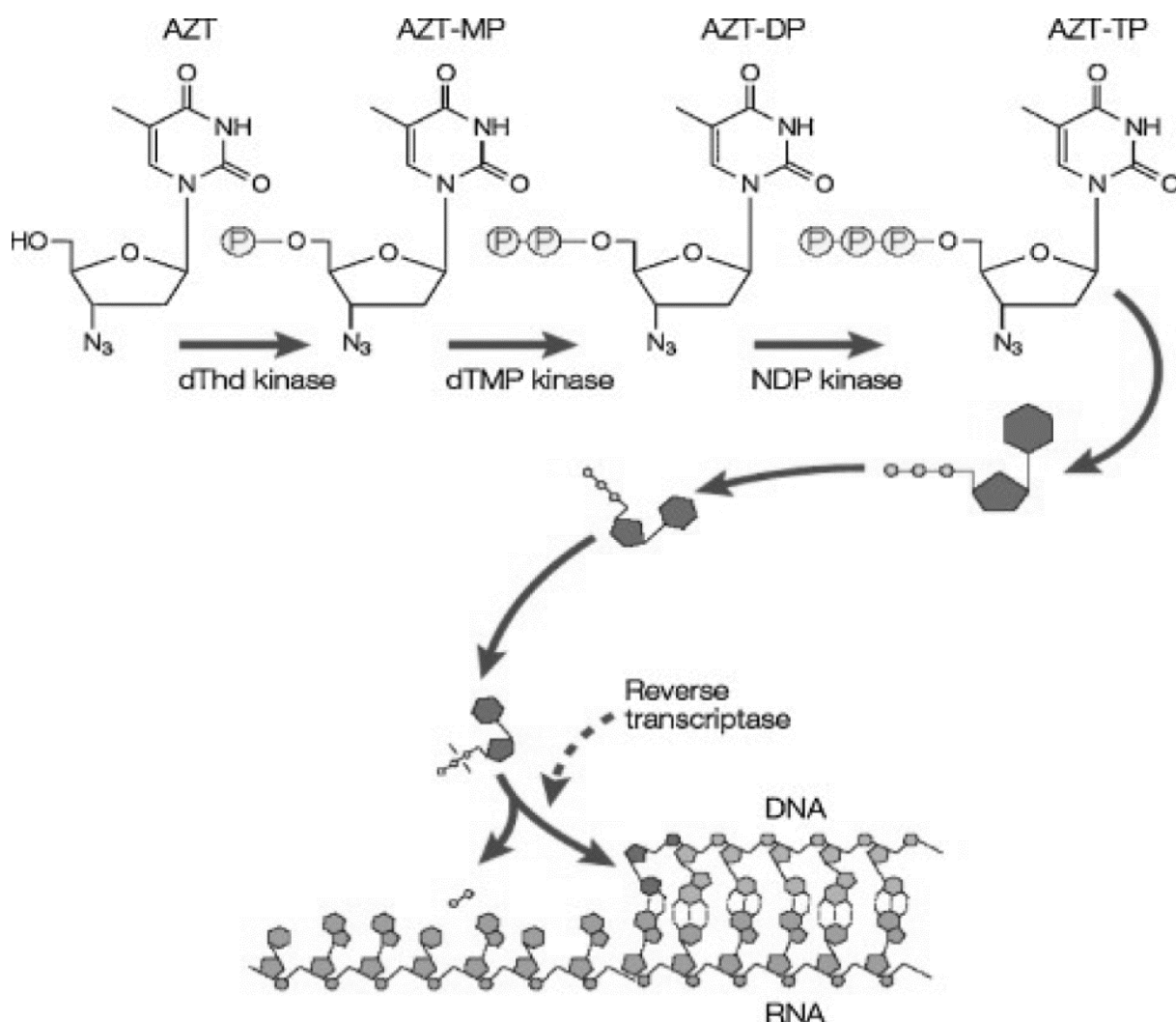


Figure 1.10. Mechanism of action of zidovudine (AZT). Following phosphorylation to its triphosphate form (AZT-TP), AZT acts as a competitive inhibitor/alternative substrate with respect to dTTP in the reverse transcriptase reaction (De Clercq 2009)

In subsequent years other nucleoside analogues have been approved as NRTIs (Figure 1.11).

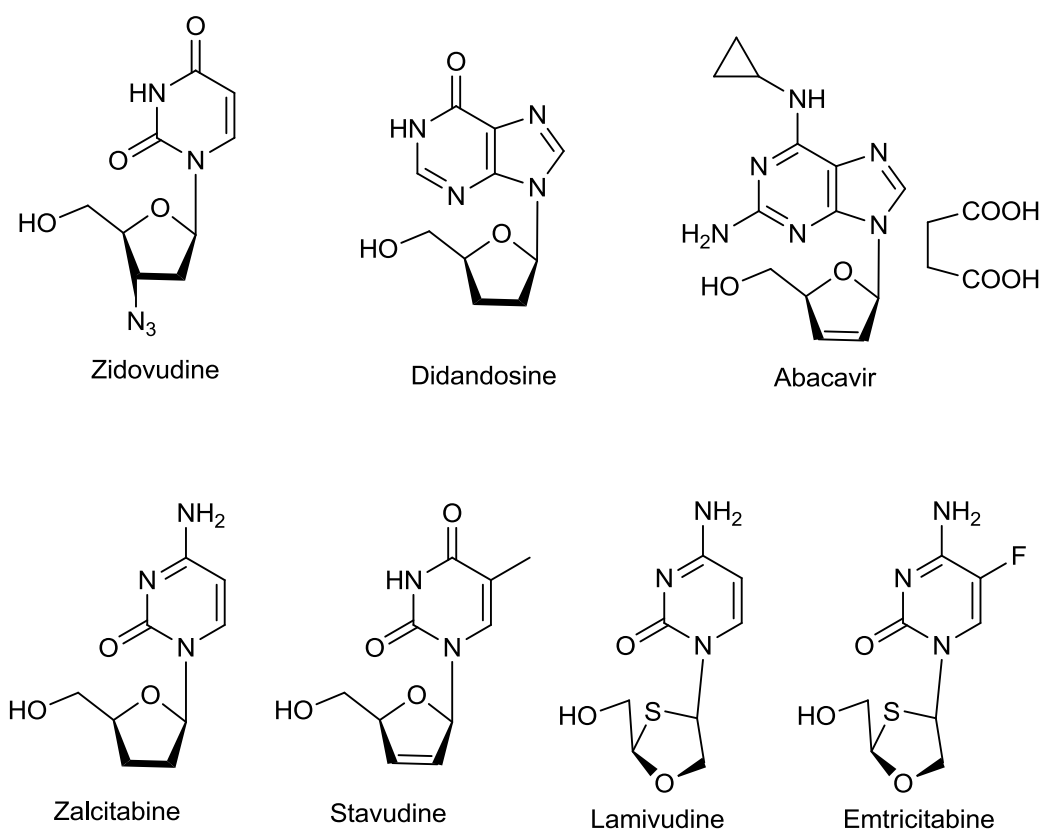


Figure 1.11. Molecular structure of nucleoside reverse transcriptase inhibitors (NRTIs)

Later, the nucleotide analogue tenofovir disoproxil fumarate (Figure 1.12), a prodrug of tenofovir previously reported in 1993 has been introduced in the therapeutic armamentarium.

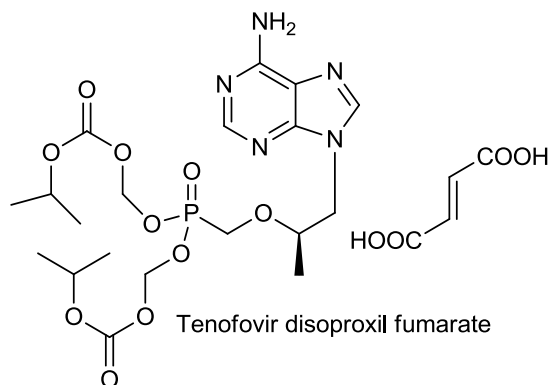


Figure 1.12. Molecular structure of the pro-drug tenofovir disoproxil fumarate

The advantage of this drug is that it does not need to be phosphorylated in three steps but only in two steps (Figure 1.13). Its good activity has made it one of the most frequently prescribed drug in AIDS treatment (De Clercq, 2009).

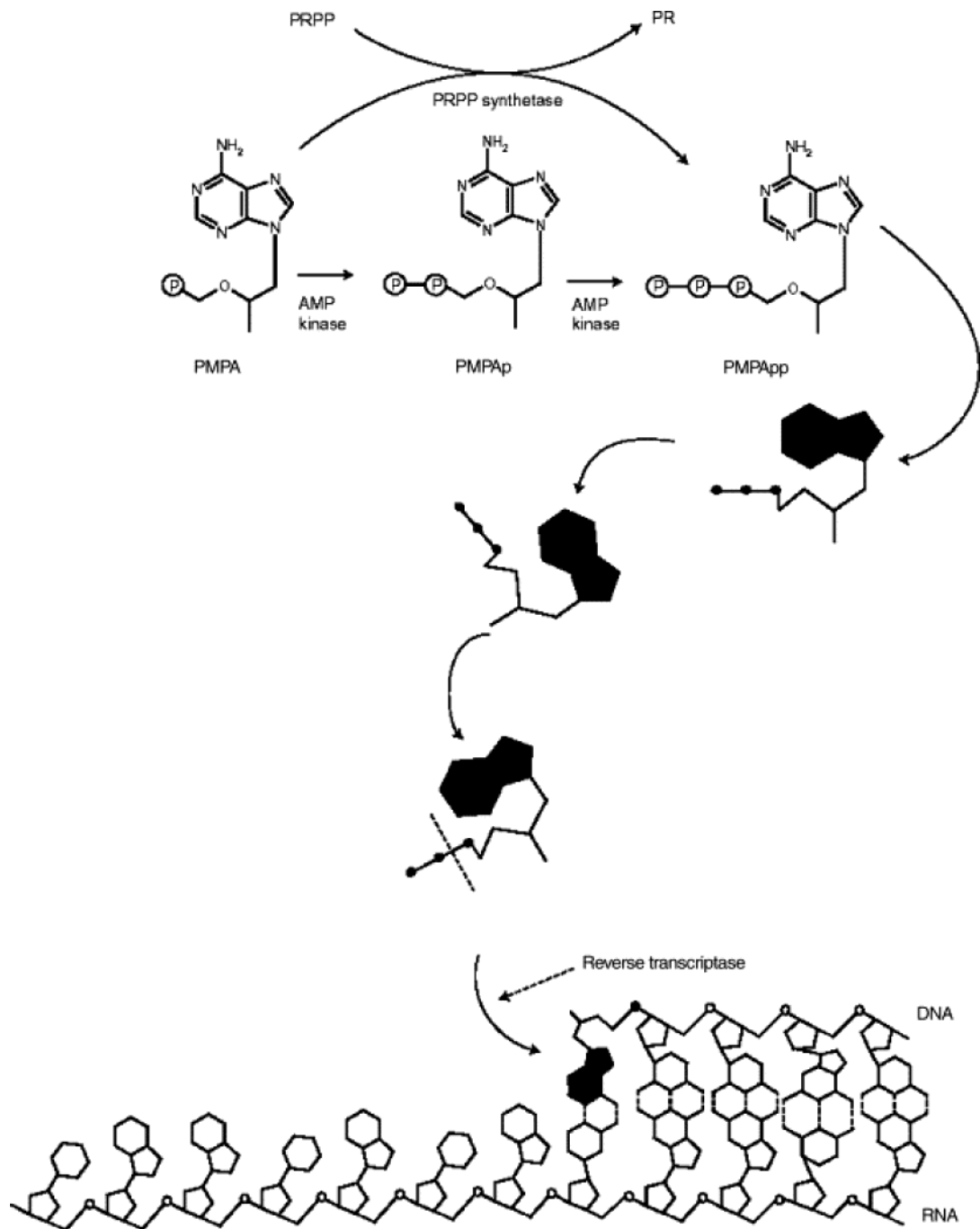


Figure 1.13. Mechanism of action of tenofovir. Following phosphorylation of tenofovir to its diphosphate, the latter one acts as an obligate chain terminator in the reverse transcriptase reaction (De Clercq 2009).

The previous types of reverse transcriptase inhibitors interact with the active site of the RT enzyme, whereas the non-nucleoside reverse transcriptase inhibitors (NNRTIs) are

allosteric inhibitors and they bind in a non-covalent mode to a lipophilic pocket of RT enzyme. The first drug introduced in therapy was nevirapine followed by delavirdine and efavirenz (Figure 1.14). Recently etravirine and rilpivirine (De Clercq, 2009) were introduced, they are able to overcome the drug resistance due to the possibility to adapt themselves better to the allosteric site of RT.

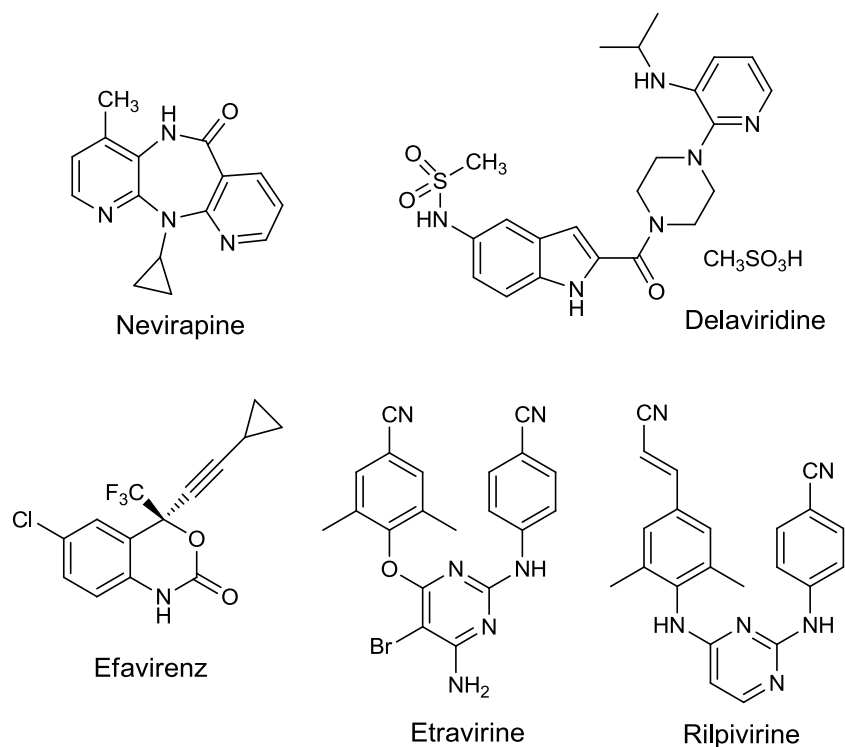


Figure 1.14. Molecular structure of commercial non-nucleoside reverse transcriptase inhibitors.

Since 1996 the introduction of drug combinations as therapeutic approach (HAART) for the control of HIV replication, in order to avoid the progression of latent HIV infection to AIDS, has shown to be a pivotal protocol in HIV infected patients. The best results are obtained by a combination of three drugs, which allows to decrease the single drug dosage and consequently their toxicity and the side effects. Currently, physicians have approximately 30 antiretroviral products, formulated either singly or in combination, to treat HIV infected patients (Broder, 2010; Table 1.2). The potential number of possible drug combinations is high (Figure 1.15), although some of the 25 compounds approved and put on the market are no longer used due to the viral resistance or too high toxicity.

Table 1.2. Approved antiretroviral drugs. Adapted from: *Drugs Used in the Treatment of HIV Infection, U.S. FDA*, <http://www.fda.gov/oashi/aids/virals.html>

Brand Name	Generic Name	Manufacturer Name	Approval Date	Time to Approval (months)
<i>Nucleoside Reverse Transcriptase Inhibitors (NRTIs)</i>				
Combivir	lamivudine and zidovudine	GlaxoSmithKline	27-Sep-97	3.9
Emtriva	emtricitabine, FTC	Gilead Sciences	02-Jul-03	10
Epivir	lamivudine, 3TC	GlaxoSmithKline	17-Nov-95	4.4
Epzicom	abacavir and lamivudine	GlaxoSmithKline	02-Aug-04	10
Hivid	zalcitabine, dideoxycytidine, ddC (no longer marketed as of December 2006)	Hoffmann-La Roche	19-Jun-92	7.6
Retrovir	zidovudine, azidothymidine, AZT, ZDV	GlaxoSmithKline	19-Mar-87	3.5
Trizivir	abacavir, zidovudine, and lamivudine	GlaxoSmithKline	14-Nov-00	10.9
Truvada	tenofovir disoproxil fumarate and emtricitabine	Gilead Sciences, Inc.	02-Aug-04	5
Videx EC	enteric coated didanosine, ddi EC	Bristol Myers-Squibb	31-Oct-00	9
Videx	didanosine, dideoxyinosine, ddi	Bristol Myers-Squibb	9-Oct-91	6
Viread	tenofovir disoproxil fumarate, TDF	Gilead	26-Oct-01	5.9
Zerit	stavudine, d4T	Bristol Myers-Squibb	24-Jun-94	5.9
Ziagen	abacavir sulfate, ABC	GlaxoSmithKline	17-Dec-98	5.8
<i>Non-nucleoside Reverse Transcriptase Inhibitors (NNRTIs)</i>				
Edurant	rilpivirine	Tibotec Therapeutics	20-May-11	10
Intelence	etravirine	Tibotec Therapeutics	18-Jan-08	6
Rescriptor	delavirdine, DLV	Pfizer	04-Apr-97	8.7
Sustiva	efavirenz, EFV	Bristol Myers-Squibb	17-Sep-98	3.2
Viramune	nevirapine, NVP	Boehringer Ingelheim	21-Jun-96	3.9
Viramune XR	nevirapine, NVP	Boehringer Ingelheim	25-Mar-11	9.9
<i>Protease Inhibitors (PIs)</i>				
Agenerase	amprenavir, APV	GlaxoSmithKline	15-Apr-99	6
Aptivus	tipranavir, TPV	Boehringer Ingelheim	22-Jun-05	6
Crixivan	indinavir, IDV,	Merck	13-Mar-96	1.4
Fortovase	saquinavir (no longer marketed)	Hoffmann-La Roche	07-Nov-97	5.9
Invirase	saquinavir mesylate, SQV	Hoffmann-La Roche	6-Dec-95	3.2
Kaletra	lopinavir and ritonavir, LPV/RTV	Abbott Laboratories	15-Sep-00	3.5
Lexiva	Fosamprenavir Calcium, FOS-APV	GlaxoSmithKline	20-Oct-03	10
Norvir	ritonavir, RTV	Abbott Laboratories	01-Mar-96	2.3
Prezista	darunavir	Tibotec, Inc.	23-Jun-06	6
Reyataz	atazanavir sulfate, ATV	Bristol-Myers Squibb	20-Jun-03	6
<i>Fusion Inhibitors (FIs)</i>				
Fuzeon	enfuvirtide, T-20	Hoffmann-La Roche & Trimeris	13-Mar-03	6
<i>Entry Inhibitors - CCR5 co-receptor antagonist (CRIs)</i>				
Selzentry	maraviroc	Pfizer	06-Aug-07	8
<i>HIV integrase strand transfer inhibitors (INIs)</i>				
Isentress	raltegravir	Merck & Co., Inc.	12-Oct-07	6
<i>Multi-class Combination Products</i>				
Atripla	efavirenz, emtricitabine and tenofovir disoproxil fumarate	Bristol-Myers Squibb and Gilead Sciences	12-Jul-06	2.5
Complera	emtricitabine, rilpivirine, and tenofovir disoproxil fumarate	Gilead Sciences	10-Aug-11	6

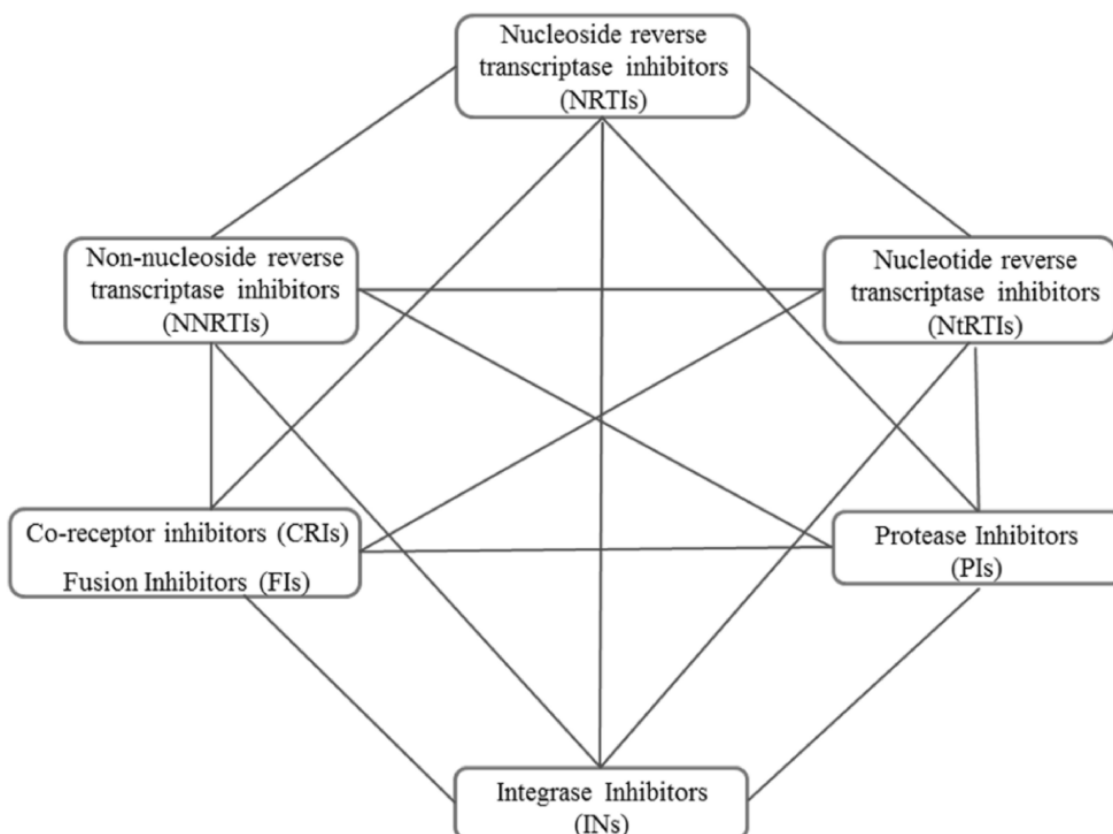


Figure 1.15. Theoretically possible drug combinations for the treatment of AIDS patients (adapted from De Clercq, 2009)

After about 30 years of research, there is not yet an effective vaccine or a definitive cure for AIDS (Montagnier, 2010), so it is important to study new potential molecules with anti-HIV activity.

The research activity of my thesis is inserted in this scenario. Its purposes are: *i*) the design by a molecular docking approach of new molecules, deriving from hybridization of known non-nucleoside reverse transcriptase inhibitors, *ii*) the selection of the molecules giving the highest values in energy and the best interactions with reverse transcriptase, as compounds to be synthesized, *iii*) the planning of the synthetic sequences, possibly by a convergent approach and common precursors, *iv*) the production of these molecules, their purification and structural characterization, *v*) biological evaluation, including preliminary test by ELISA method, before sending the compounds to be subjected to the evaluation on HIV infected cells.

1.4. Reverse transcriptase enzyme

Reverse Transcriptase (RT) is an flexible, multifunctional essential enzyme present in all the members of *Retroviridae* family. HIV-1 RT catalyses three reactions necessary to transcribe a single stranded viral RNA into a double stranded DNA. Its activities are: RNA-dependent DNA polymerase, DNA-dependent DNA polymerase and ribonuclease H (RNase H) (Goff, 1990). Although it has three enzymatic activities, the enzyme has only two active sites.

The RT form found in the virion is a stable heterodimer composed by two subunits, p66 and p51 containing 560 and 440/441 residues respectively (Figure 1.16; Di Marzo, 1986). They are very similar, although the smaller unit p51 is lacking of RNase H domain (p15), due to the cleavage of C-terminal end of p66 by HIV protease (Lowe, 1988). Despite the same primary amino-acidic sequence, the polymerase domains p66 and p51 have a different topology (Kohlstaedt, 1992).

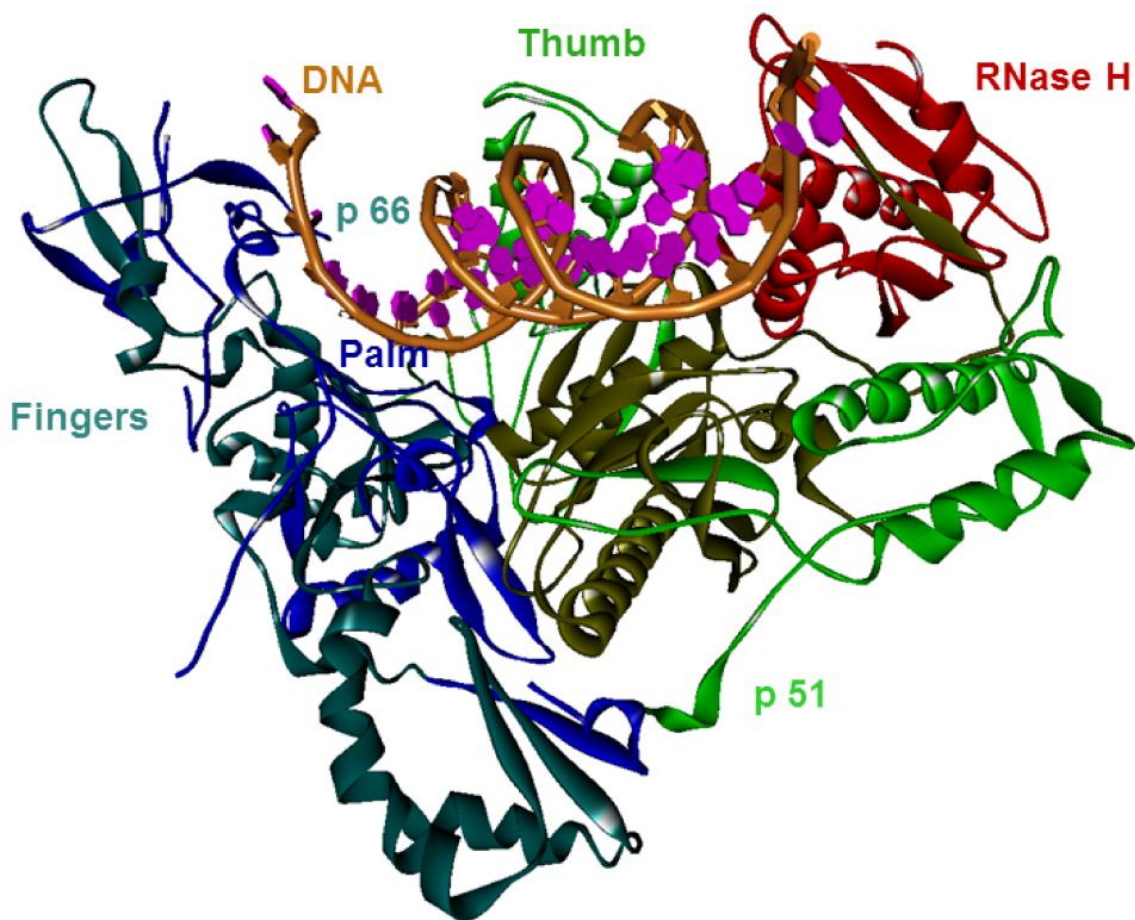


Figure 1.16. 3D-Structure of HIV-1 reverse transcriptase in the complex with DNA (PDB code: 3KJV)

Globally the enzyme resembles as a right hand, because it has four subdomains called fingers, palm, thumb and connection, and shows a classical polymerase structure. All the three enzymatic activities are present only in the p66 subunit, whereas the role of p51 subunit is a structural support and may have a role in binding the tRNA_{Lys3} required for priming the RT reaction (Mishima, 1995). The monomeric forms of p66 and p51 are enzymatically inactive.

The mechanism of cDNA synthesis from the viral RNA starts when RT binds a specific transfer RNA (tRNA) that is used as the primer for the RNA-dependent DNA polymerase reaction. In both HIV-1 and HIV-2 the primer is tRNA_{Lys3}, made by 18 bases complementary to the primer-binding site in HIV genome. Only in this step RNA acts both as template and primer, giving the formation of the hybrid RNA/DNA. RNA is degraded through the endonuclease activity of RNase H domain of RT, and later a new complementary DNA strand is synthesized. At the end of this process the proviral double-strand cDNA is obtained (Figure 1.17).

The huge importance of RT for the virus replication and its absence in the mammals have made this enzyme an ideal target for a therapeutic approach, as previously reported.

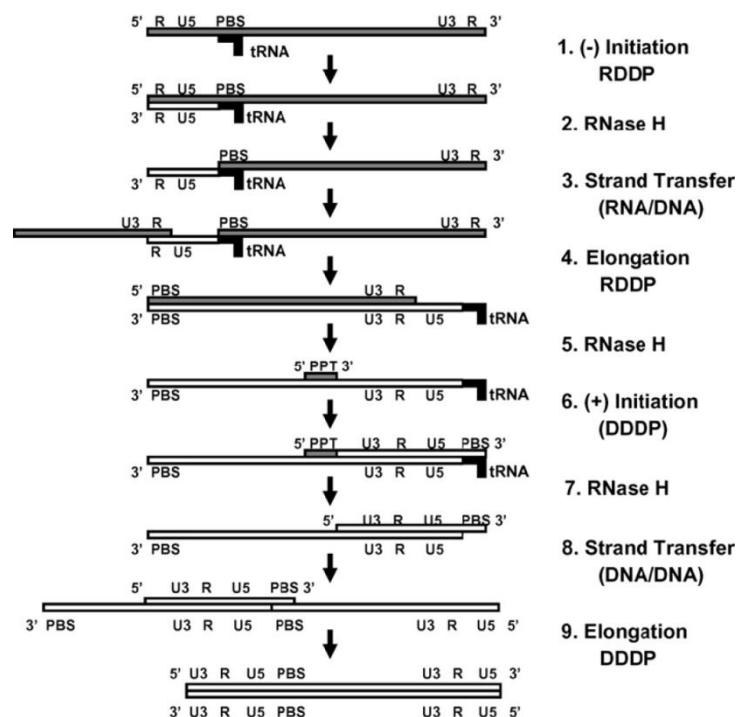


Figure 1.17. Diagram of HIV reverse transcription mediated by the DNA polymerase, RNase H and strand transfer activities of RT

1.5. HIV-1 Non-Nucleoside Reverse Transcriptase Inhibitors (NNRTIs)

NNRTI molecules bind specifically at an allosteric site (NNIBP) situated about 10 Å far from the polymerase catalytic site (Figure 1.18).

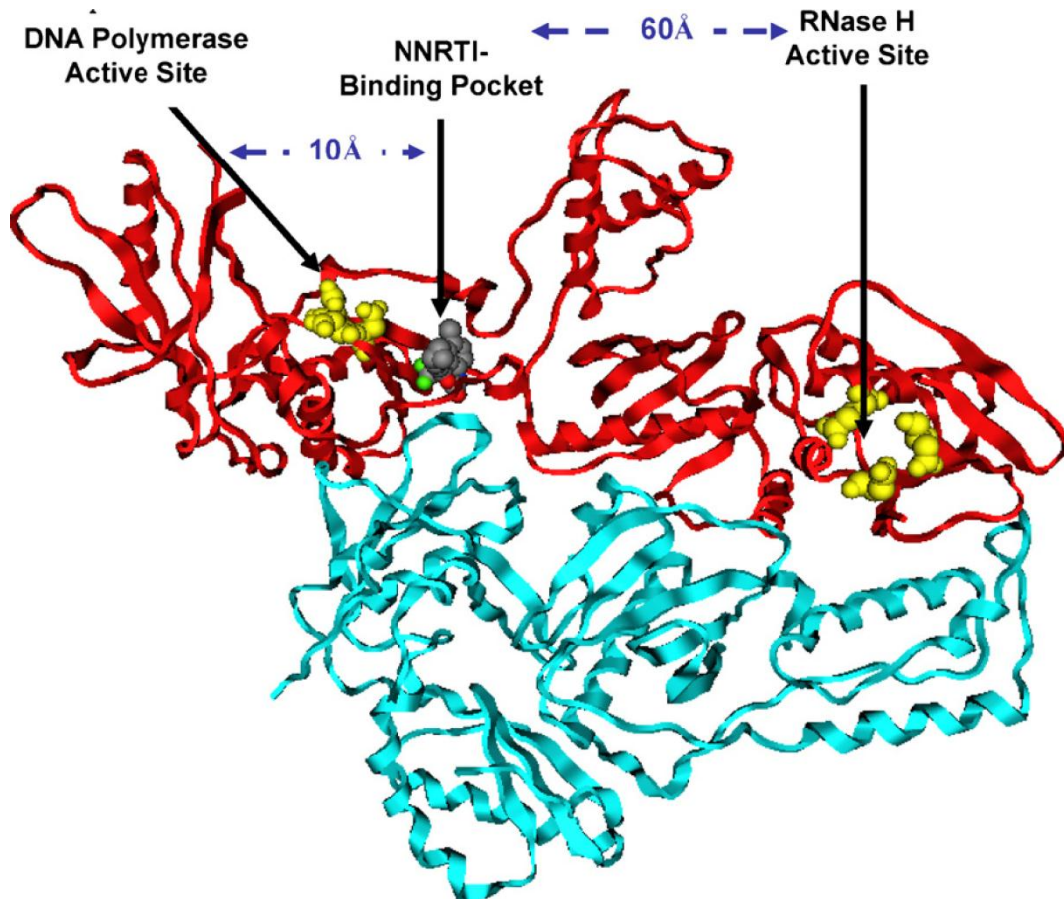


Figure 1.18. HIV-1 RT with binding site for NRTIs/NtRTIs and the binding site NNRTIs (Sluis-Cremer, 2008)

The allosteric site is an especially flexible pocket rich in hydrophobic amino-acids and in some polar amino-acids. The ones present in NNIBP of HIV-1 wild type (WT) that can interact with non-nucleoside reverse transcriptase inhibitors are : P95, L100, V106, K101, K103, Q138, V179, Y181, Y188, F227, W229, L234 and P236. In particular P95 represents the "mouth" which allows the entry of the inhibitors molecules into the pocket.

When a NNRTI molecule binds to the allosteric pocket, it induces several conformational changes in reverse transcriptase, causing in particular a distortion of an aspartic acid unit in the catalytic site. This event restricts the relative subdomain movements required to complete the catalytic cycle of the enzyme and it blocks the incorporation of deoxyribonucleotides triphosphate (dNTP) in the growing DNA chain (Esnouf, 1995; Hsiou, 1996). In detail, a NNRTI binding causes a change in the thumb subdomain, which adopts a more open

conformation in comparison with the closed conformation of native reverse transcriptase (Kohlstaedt, 1992; Rodgers, 1995). This rearrangement, imaginatively called as ‘molecular arthritis’, does not allow the correct interaction between RT and template/primer. This is the crucial mechanism of action of NNRTIs (Figure 1.19, step 3), but recently for efavirenz and etravirine it has been reported a further inhibitory activity at the late stages of HIV-1 replication, by interfering with HIV-1 Gag-Pol polyprotein processing (Figure 1.19, step 7). In the case of IQP-0410 (=1-(3-cyclopenten-1-yl)methyl-6-(3,5-dimethylbenzoyl)-5-ethyl-2,4-pyrimidinedione) the block of viral entry and reverse transcriptase inhibition has been observed (Figure 1.19, step 2; Sluis-Cremer, 2008).

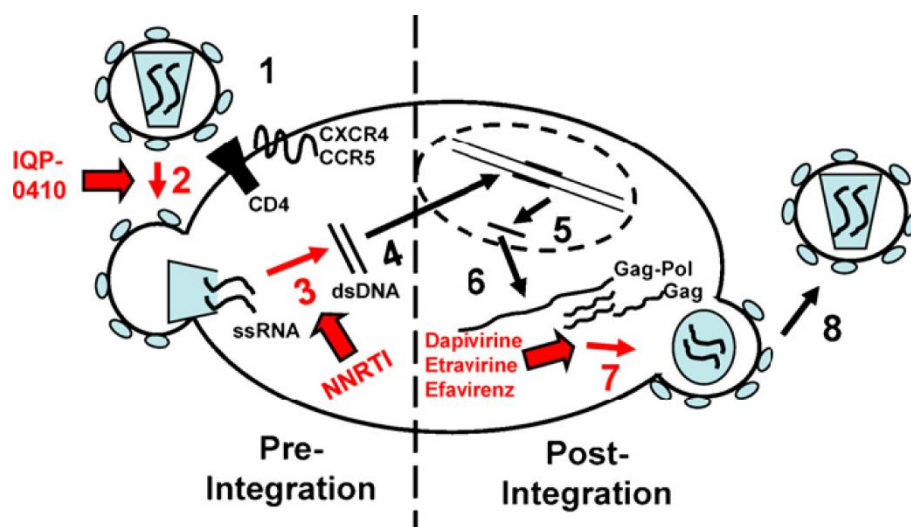


Figure 1.19. Schematic HIV life-cycle showing points of action of a NNRTI (in red) (Sluis-Cremer, 2008)

By steady-state kinetic analysis it was demonstrated that NNRTIs acted as non-competitive or uncompetitive inhibitors of HIV-1 RT DNA polymerization reactions (De Clercq, 1998). In this case the kinetic constants for inhibition (IC_{50} or K_i) depend on the template/primer substrate length used in the polymerase assay. In addition, recent studies have demonstrated that NNRTIs may preferentially target specific steps during reverse transcription (Quan 1998 and 1999). The RT transcription process initially requires the strand transfer reaction as essential step (Figure 1.17) and it needs the coordination of both the DNA polymerase and RNaseH activities. Although the NNRTI-binding pocket in RT is around 60 Å far from the RNase H active site of RT (Figure 1.18), several studies have demonstrated that NNRTIs can either partially inhibit or accelerate this activity depending on the mode of RNase H activity (Shaw-Reid,2005; Hang, 2007; Radzio, 2008).

In addition, the power of NNRTIs in strand transfer may depend on the efficiencies against DNA polymerase and RNase H inhibition. The inhibition of plus-strand initiation has been studied, demonstrating that NNRTIs potently inhibit *in vitro* plus-strand initiation under conditions in which a little or no inhibition of minus-strand DNA synthesis was observed, showing that NNRTIs completely abolish the dNTP binding to RT associated with RNA primer/DNA template substrate (Grobler, 2007).

Steady-state kinetic analysis is not able to resolve kinetic steps which are masked by the rate-limiting step of a reaction, so that this approach does not explain in detail the interactions of the drug with RT in the polymerase active site (Kati, 1992). An approach based on the pre-steady-state kinetic study provides detailed mechanistic insights into the catalytic events that occur directly at the enzyme's active site. These studies have shown that NNRTI-RT-template/primer complexes display a metal-dependent increase in dNTP binding affinity (K_d). An in-depth understanding of the multiple mechanisms by which NNRTIs inhibit reverse transcription is essential for the development of novel drugs overcoming the resistance.

Both HIV reverse transcriptase and host RNA-dependent DNA polymerase are not able to have error correction capabilities, so the error rate in the nucleotide introduction is in the range $10^{-4} \div 10^{-5}$ in a single cycle of HIV replication (Das, 2005). In this manner HIV combines a high rate of replication and a high mutation rate resulting in the production of a large pool of viral mutants, making the HIV a "quasispecies" (Coffin, 1995). Many mutant viruses maintain the capability to replicate in the presence of a drug, which kills the wild type, and so the mutants can dominate in the viral population (Ho, 1995). The most important mutations affecting a single amino acid in the NNIBP are Y188C, Y181C, K103N, L100I and the double mutated K103N/Y181C. When one or two mutations are present in the enzyme a high-level resistance is involved against the clinically used drugs (Zhan, 2011).

Initially the first generation of NNRTIs has been found accidentally. X-ray crystallographic study on the complex between RT and nevirapine (Figure 1.14) and (*S*)-8-methyl-7-(3-methylbut-2-en-1-yl)-6,7,8,9-tetrahydro-2,7,9a-triaza-benzo-[*cd*]azulen-1(2H)-one (TIBO), (Figure 1.20a) showed a closed contact between the drug (also called small molecule or ligand) and the amino acids present in the NNIBP, allowing Schäfer and coauthors to propose a three-dimensional model called "butterfly-like", in which to a central lipophilic domain ("body") are linked two π -extended hydrophobic units ("wings") (Figure 1.18b, Schäfer 1993).

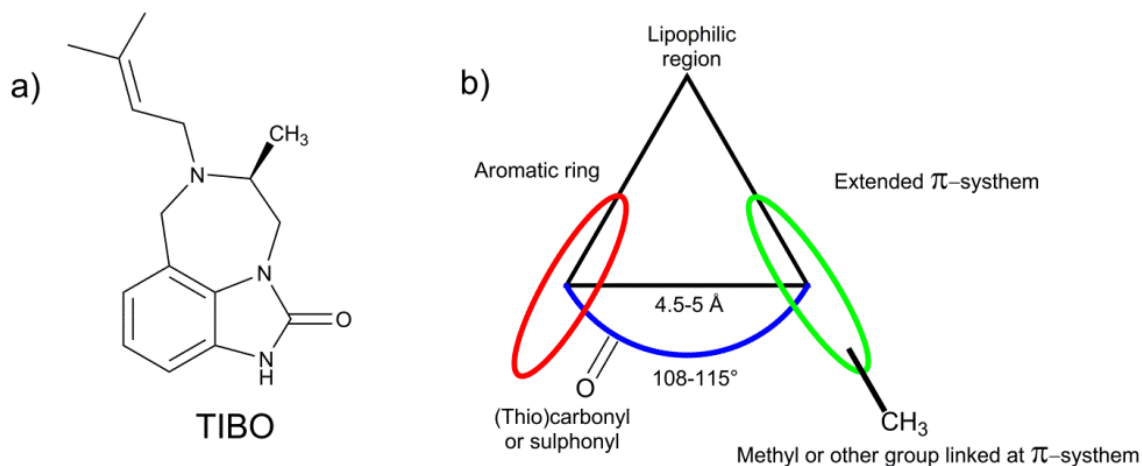


Figure 1.20. (a) Chemical structure of TIBO, (b) 3D-model of the NNRTI proposed by Schäfer

Currently more than 50 structurally different classes of molecules have been identified, showing specific inhibition of reverse transcriptase by interaction with NNIBP and able to suppress *in vitro* HIV-1 replication. It is possible to classify the compounds on the base of chemical structure principally into: multicyclic scaffold, benzo-fused heterocyclic scaffold, six-membered heterocyclic core scaffolds, five-membered heterocyclic core scaffolds, (thio)amide linker containing scaffolds, diphenyl scaffold.

A better pharmacophore can be obtained taking into account the topology of all the molecules having a butterfly-like geometry with the lower conformational energy. The geometric map of this new pharmacophore is reported in Figure 1.21.

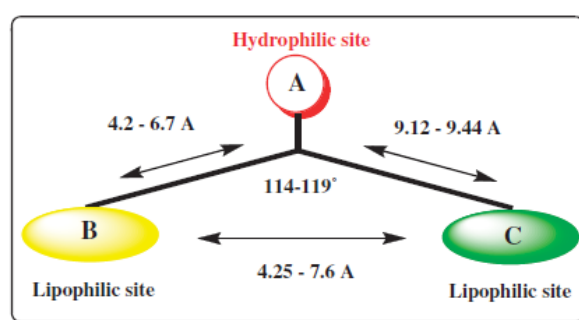


Figure 1.21. Schematic representation of NNRTI pharmacophoric distance map (Zhan, 2011).

On the contrary, in the inhibitors of second generation, as etravirine or rilpivirine (Figure 1.14), the conformation resembles a “U” or “horseshoe”. This model has a greater flexibility and the molecule can adapt better to the flexible NNIBP, increasing the therapeutic potency in

comparison with the drug of the first generation adopting a butterfly-like conformation with a lower degree of freedom and consequently a more rigid structure (Figure 1.22; Das, 2005). In addition, the better adaptability of the molecules having a horseshoe structure overcomes the drug resistance, both in single and double mutated HIV strains (Meréndez-Arias, 2010). The comparison of X-ray crystallographic analysis of different HIV reverse transcriptase and NNRTI complexes supported by computational calculation has shown that the "butterfly-like" or "horseshoe" NNRTIs share the common binding mode with NNIBP (Table 1.3 and Figure 1.23).

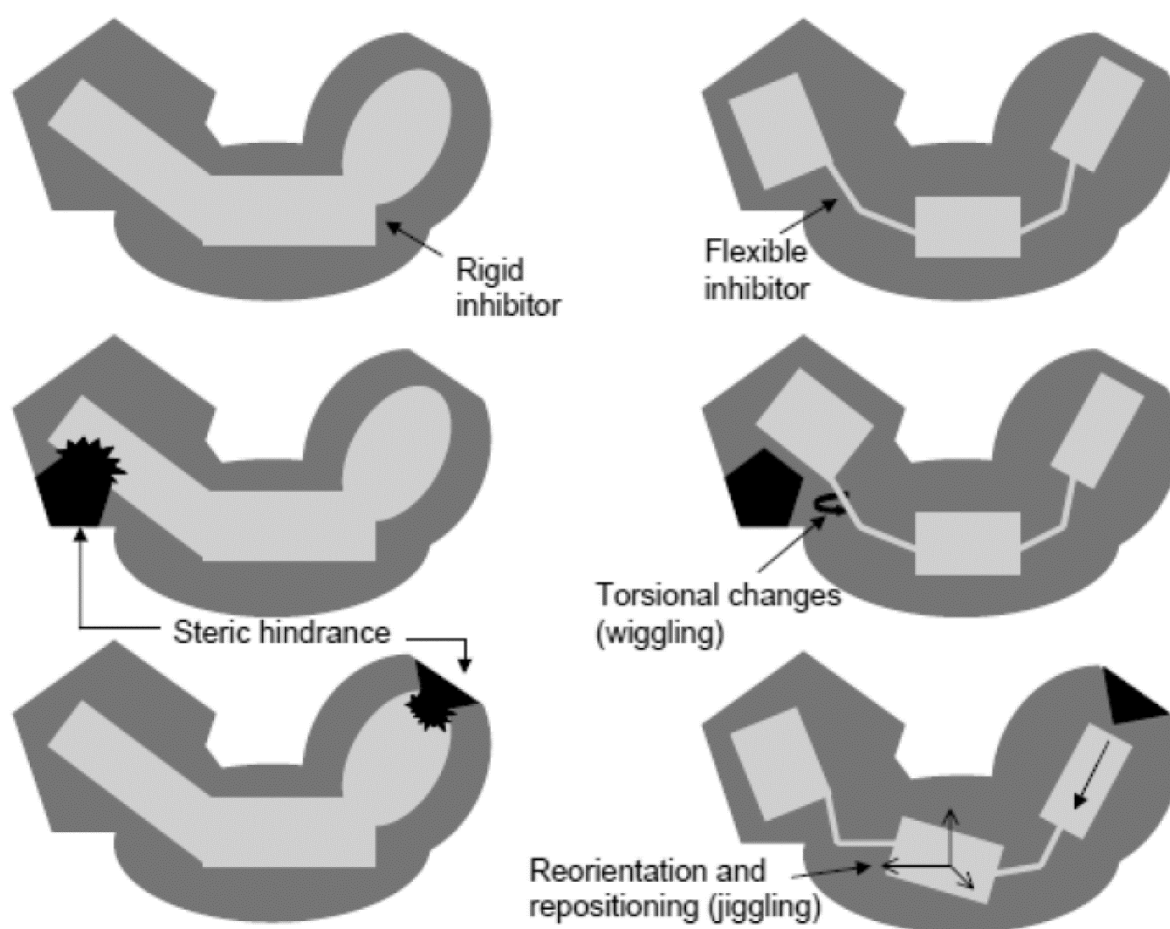


Figure 1.22. Schematic representation showing how a flexible inhibitor can adapt to changes in the binding pocket of RT due to mutations. A rigid inhibitor (left panel), although binding strongly to the unmutated target, fails to bind strongly to the mutated pockets. A flexible inhibitor (right panel) can adapt to those changes in the pocket by its torsional changes and repositioning (Das, 2005)

Table 1.3. Interactions involved in binding of NNRTIs to HIV Reverse Transcriptase (Zhan, 2011)

Pharmacophore points	Groups	Interaction
Hydrogen bond donors	O–H, S–H, N–H	Donor to K103 (1EP4, 1KLM) or K101
Hydrogen bond acceptors	(Thio)carbonyl, ester, sulfone O in ether, Pyridine N atom, N, O in aromatic, 5/6-membered rings	Acceptor to K103 (1EP4, 1KLM) or K101
Hydrophobic domains	Aliphatic or aromatic rings, Double and triple C–C bonds, CF ₃ , Aliphatic chains	Hydrophobic interaction with Y188, Y181, W229, F227, L100, L234, V106, Y318

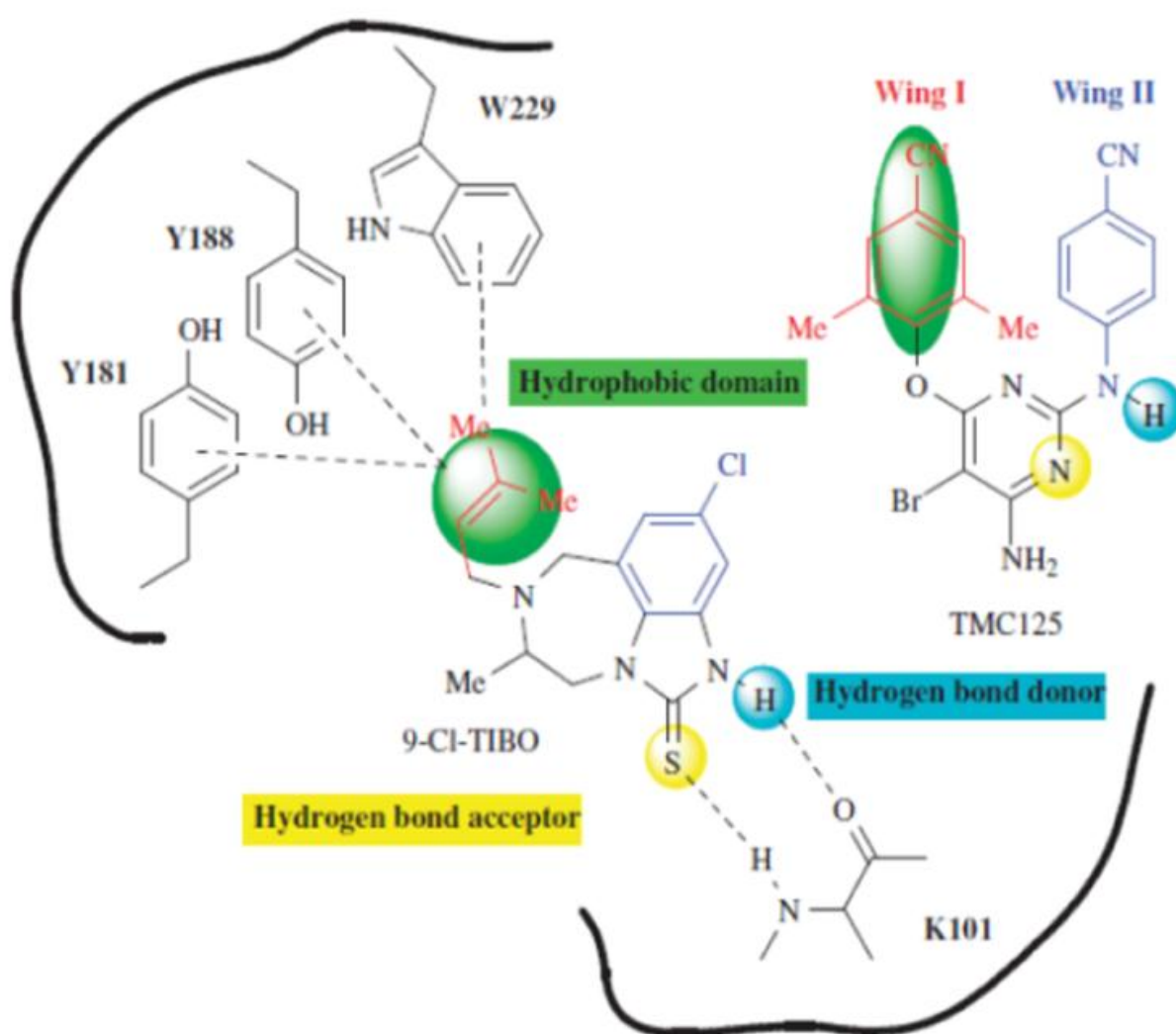


Figure 1.23. Schematic 2D representation of common mode of binding in butterfly-like (9-Cl-TIBO) and horseshoe-like (TMC125, etravirine) shapes in the NNIBP (Zhan, 2011)

1.6. Drug design of new potential NNRTI molecules

1.6.1. General

The past search of new potential drugs has followed a process of trial and error, whereas nowadays it has been substituted by a rational drug design, often using sophisticated procedures including several computer-based approaches.

Drug design is a long, multidisciplinary iterative process of finding new potential drugs based on the knowledge of the biological target. It involves small molecules that are complementary in shape and charge distribution to the bio-molecular target (protein or DNA) with which they interact and therefore will bind. For this purpose, it is necessary to have the X-ray or NMR three-dimensional structure of the target molecule in the complex with a known inhibitor (Figure 1.24).

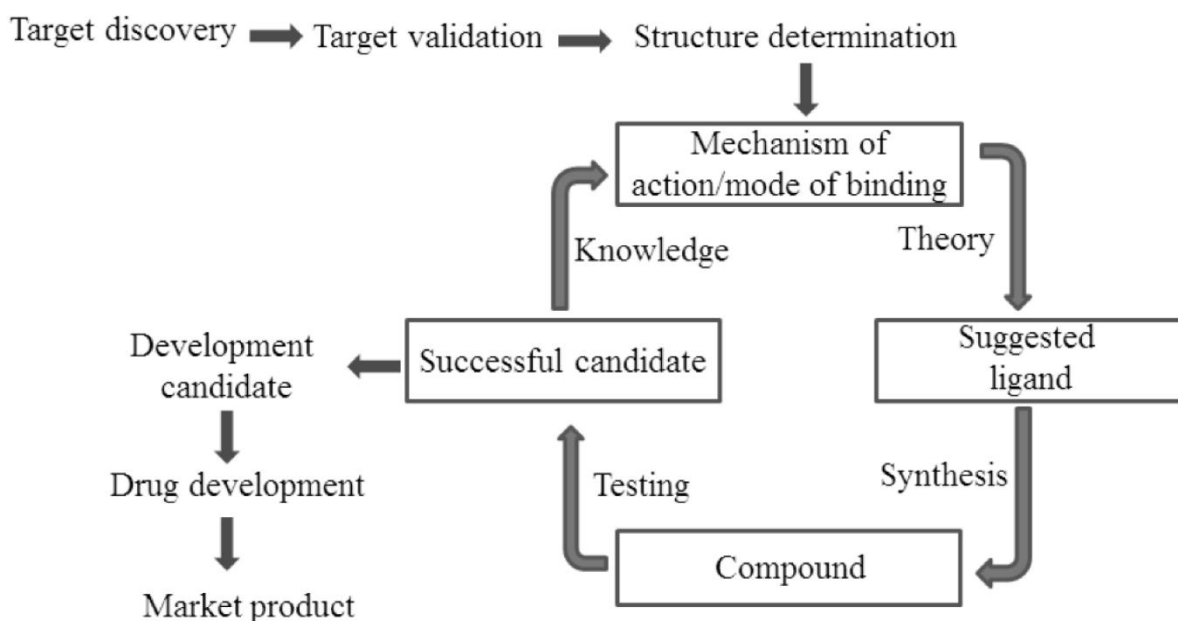


Figure 1.24. General approach for the rational design of inhibitors

The three most used approaches in new lead discovery include *de novo* design, *fragment based* design and virtual screening, as summarized in Figure 1.25.

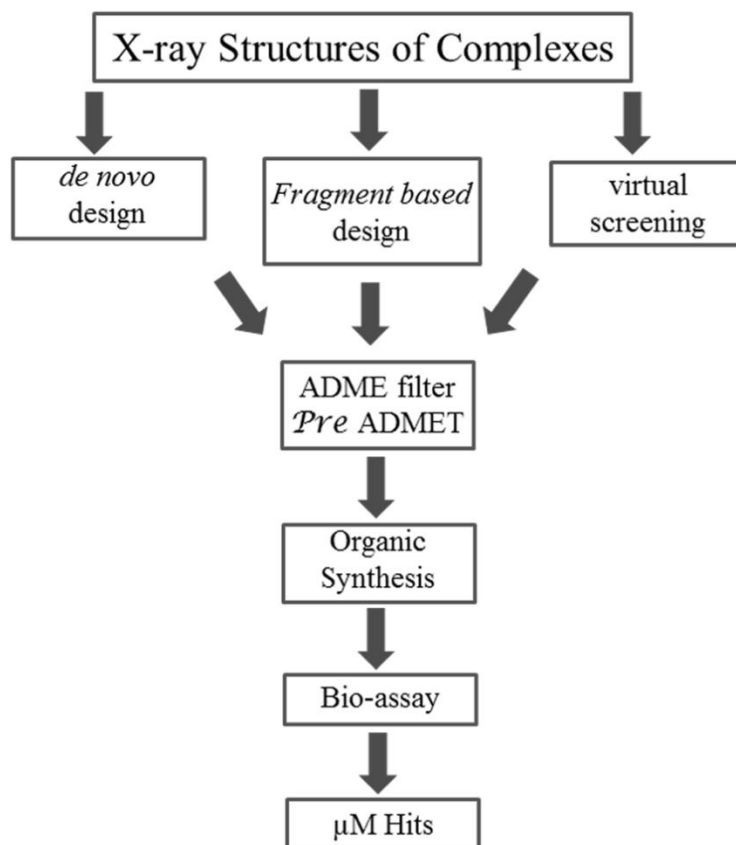


Figure 1.25. Schematic outline for structure-based lead discovery (adapted from Jorgensen, 2009).

In *de novo* design a program is used to add various substituents by replacing hydrogen atoms of a core structure placed in the binding site, in order to obtain a "template". The core structure can be a simple molecule as benzene or adamantane. In this manner a combinatorial library is obtained, in which the user selects the templates with the lowest energy to be submitted to docking calculation. An alternative to *de novo* design is the virtual screening design, using docking calculation on a database of chemicals (Jorgensen, 2009).

In the *fragment based* design a library of bioactive compounds is decomposed in order to furnish a pool of fragments that can be recombined to obtain a subset of new compounds. The *molecular hybridization* approach can be incorporate into *fragment based* design. The new built molecules are based on the combination of specific pharmacophoric moieties present in different bioactive substances to produce hybrid compounds (Viegas-Junior, 2007). These compounds are submitted to flexible docking calculations and ranked according to their binding energy (Huang, 2009).

Another filter in the "rational drug design" is the prediction of drug-likes of the newly designed molecules. This step is important in order to select the synthesized molecules having a good oral bioavailability and in general good properties in adsorption, distribution,

metabolism and excretion (ADME). Predicting human intestinal absorption (HIA) of drugs is very important to identify potential drug candidates. A number of software is able to predict percent human intestinal absorption (% HIA). Human intestinal absorption data are the sum of bioavailability and absorption evaluated from the ratio of excretion or cumulative excretion in urine, bile and feces (Beresford, 2002). Compounds can be classified in poorly adsorbed (with HIA is between 0 and 20%), moderately adsorbed (from 20 to 70%) and well adsorbed (from 70 to 100%) (Zhao, 2001; Yee, 1997).

Another relevant calculated parameter is Plasma Protein Binding (PPB). Only the unbound drug is generally available for diffusion or transport across cell membranes, and also for interactions with a pharmacological target. As a result, a degree of plasma protein binding of a drug affects not only the drug's action, but also its disposition and efficacy. A compound is strongly bound if the entity (expressed in percentage) is major than 90 whereas if it is lower than 90% the compound is regarded weakly bound.

Some chemical-physical properties are also correlated to the drug-like activity. In particular "the rule of five" proposed by Lipinski has given a good index to establish if a molecule is a candidate as drug. A molecule follows this rule if Log P is lower than five, its molecular weight is less than 500 Da and the number of H-bond donors is less than five, as well as the number of H-bond acceptors is less than ten (Lipinsky, 2000 and 2001).

Potency and respect of this rule are not the only parameters to be considered in drug design. In fact a general observation to be taken into account in the process of a lead development, is the growth of molecular weight, to which the potency is strongly correlated. In addition is useful to convert the binding energy into a new parameter called ligand efficiency (Δg), as proposed by Kuntz and shown in Eq.1.1, in order to compare the calculated values of binding energy in a chemical series (Kuntz, 1999).

$$\Delta g = \Delta G/N \quad \text{Eq 1.1}$$

where ΔG =calculated binding free energy, N =number of non-hydrogen atoms (heavy atoms)

Based on the equation 1.1, Hoptkins and coauthors have suggested a ligand efficiency cutoff equal to 0.29 for a drug-like molecule with nanomolar binding affinity, Reynolds has concluded that the maximum of ligand efficiency can be observed in molecules containing between 10 and 25 heavy atoms, whereas molecules with a number of heavy atoms higher than 25 the ligand efficiency essentially plateaued (Reynolds, 2007).

1.6.2. Molecular docking

The pioneering studies involving the docking of small molecules to protein binding sites started during the early 1980s' (Kuntz, 1982). The increased availability of three-dimensional structures of bio-macromolecules obtained by X-ray or NMR analyses, as well as the involvement of computer programs has made molecular docking one of the most used techniques in virtual screening of potential bioactive compounds. Docking promise is that the structure of the target will provide a template for the discovery of novel ligands, dissimilar to those previously known (Shoichet, 2002).

Molecular docking is an optimization problem in which the best orientation of a small molecule (ligand) binds the protein of interest. The protein could be seen as a "lock" and the ligand as a "key" searching the right orientation after insertion in the key hole in order to "open" the lock (best-fit ligand), but both the protein and the ligand are flexible so that the system is more similar to a "hand-in-glove". Modeling the interaction of a ligand with a protein is a complex problem. The intermolecular forces involved in the protein- ligand complex include hydrophobic, van der Waals, hydrogen bonding and electrostatic non-covalent interactions. Although hydrophobic interactions are much more involved in the binding, hydrogen bonds and electrostatic ones are responsible for the specificity in the molecular recognizing. The major problem in handling the intermolecular interactions is the presence of many degrees of freedom and the lacking knowledge of the solvation effect (Gohlke, 2002).

Currently, computation of molecular docking uses models with a flexible ligand and a rigid target, although it is possible the treatment of chain flexibility in the amino acids involved in the binding by using some software. In the vast landscape of software for docking calculation (over 70 in 2010) a comparison among them is difficult mainly due to different set of proteins that have been used in each software for benchmark it (Cole, 2005). One of the most used software is AutoDock (Figure 1.26; Sousa, 2006). Recently, a comparison of AutoDock with other two molecular docking software (FlexX and Arguslab) has shown that it outperforms the two other programs (Chikhi, 2008). The best ranking poses, predicted by the three programs and their root mean square deviation (RMSD) values from the original crystallographic pose, are reported in Figure 1.27a, whereas figure 1.27 b shows the evaluation of docking algorithms for their sampling accuracy. Additional parameters to be taken into account in accuracy of docking calculation are given by the degrees of freedom in

the ligand (Figure 1.27c) and by the chemical nature of protein-ligand interactions that are correlated with binding energy (Figure 1.27d).

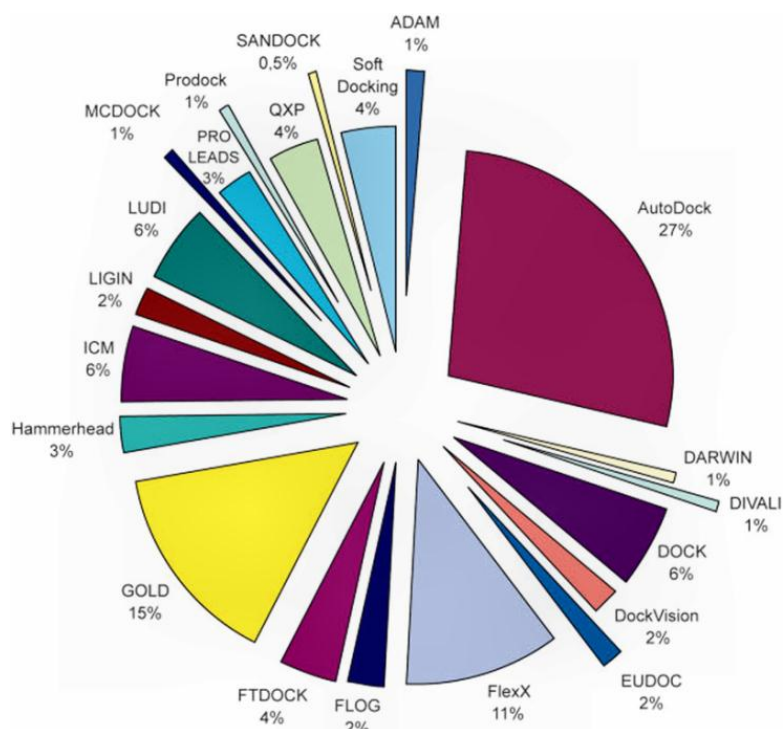


Figure 1.26. The most used docking software (Sousa, 2006)

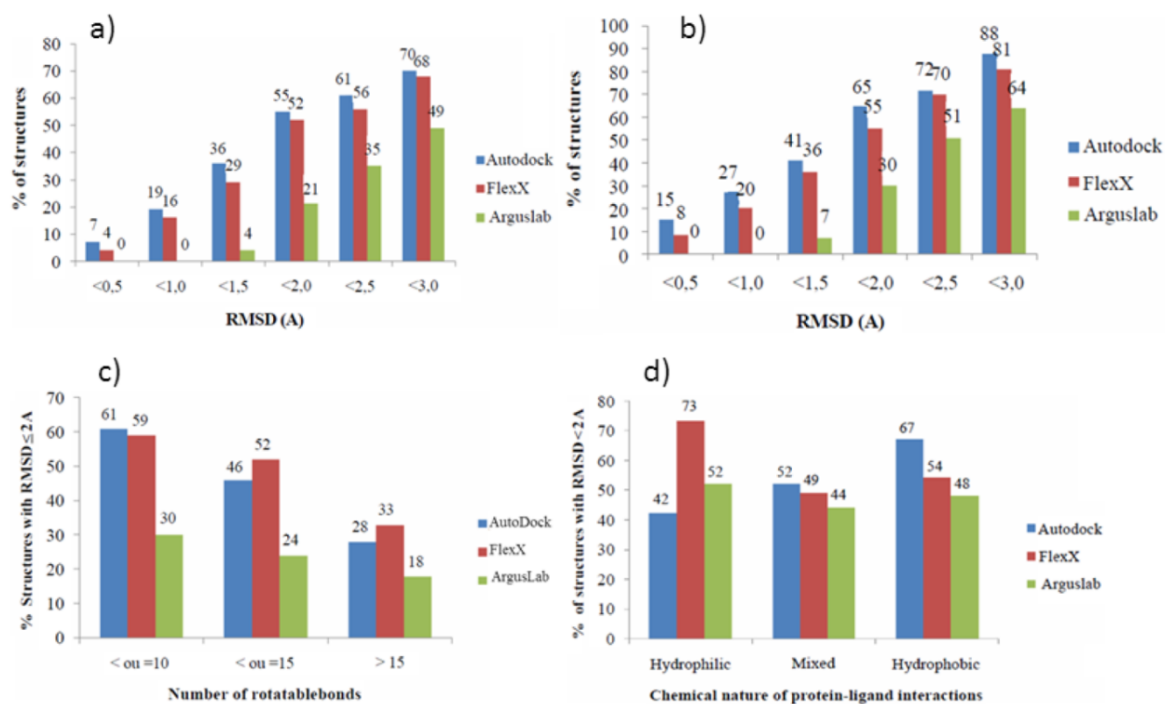


Figure 1.27. a) Best pose with reference to crystallographic pose, b) Top ten poses with reference to crystallographic pose, c) Ligand rotatable bonds in relation to docking accuracy, d) % of hydrogen bonding in terms of docking accuracy (Chikhi, 2008)

AutoDock uses a scoring function to rank the ligand conformations in order to evaluate the binding free energy (ΔG) and consequently the binding constant (K_i) according to the equation 1.2:

$$\Delta G = RT \ln K_i \quad \text{Eq. 1.2}$$

where R is the gas constant, $1.987 \text{ cal K}^{-1} \text{ mol}^{-1}$, and T is the absolute temperature, assumed to be room temperature 298.15 K . It is noteworthy that a minus sign lacks in the equation, because the inhibition constant is defined for the dissociation reaction, $EI \rightleftharpoons E+I$ whereas ΔG refers to the opposite process of binding, $E+I \rightleftharpoons EI$, where E is the enzyme and I is the inhibitor.

In the classical structure-based scoring functions, the traditional force fields are implemented with empirical free energy functions so that to reproduce observed binding constants. In order to achieve this purpose an expanded "master equation" is used, which allows to model the free energy of binding, adding entropic terms to the molecular mechanics as shown in equations 1.3:

$$\Delta G = \Delta G_{\text{vdw}} + \Delta G_{\text{hbond}} + \Delta G_{\text{elec}} + \Delta G_{\text{conform}} + \Delta G_{\text{tor}} + \Delta G_{\text{sol}} \quad \text{Eq. 1.3}$$

where the first four terms are the typical molecular mechanics terms for dispersion/repulsion, hydrogen bonding, electrostatics, and deviations from covalent geometry respectively, whereas ΔG_{tor} models the restriction of internal rotors and global rotation and translation and ΔG_{sol} models desolvation upon binding plus the hydrophobic effect because the solvent entropy changes at solute-solvent interfaces (Morris, 1998).

Applying Hess' law to the change in free energy between the states in solution and *in vacuo* the equation 1.4 can be written:

$$\Delta G_{\text{binding,solution}} = \Delta G_{\text{binding,vacuo}} + \Delta G_{\text{solvation}(EI)} - \Delta G_{\text{solvation}(E+I)} \quad \text{Eq. 1.4}$$

After calculation of $\Delta G_{\text{binding,vacuo}}$ from docking simulation, the free energy change can be estimated upon solvation for the separate molecules E and I , and for the complex, EI , $\Delta G_{\text{solvation}(EI)}$ and $\Delta G_{\text{solvation}(E+I)}$ respectively. From these values it is also possible to calculate

the free energy change upon binding of the inhibitor to the enzyme in solution, $\Delta G_{binding,solv}$ and to estimate the inhibition constant, K_i , for the inhibitor, I (Figure 1.28).

The current version of AutoDock uses a genetic algorithm (GA) for global searching and a local search (LS) method to perform energy minimization, or a combination of both. In order to facilitate the torsional space search, the local search method is based on Solis and Wets approach (Solis, 1981), which require no gradient information about the local energy landscape and removes any steric clashes in the crystallographic complexes. In addition, the local search method is adaptive, because it adjusts the step size depending upon the recent history of energies: a user-defined number of consecutive failures, or increases in energy, causes the step size to be doubled conversely; a user-defined number of consecutive successes, or decreases in energy, causes the step size to be halved.

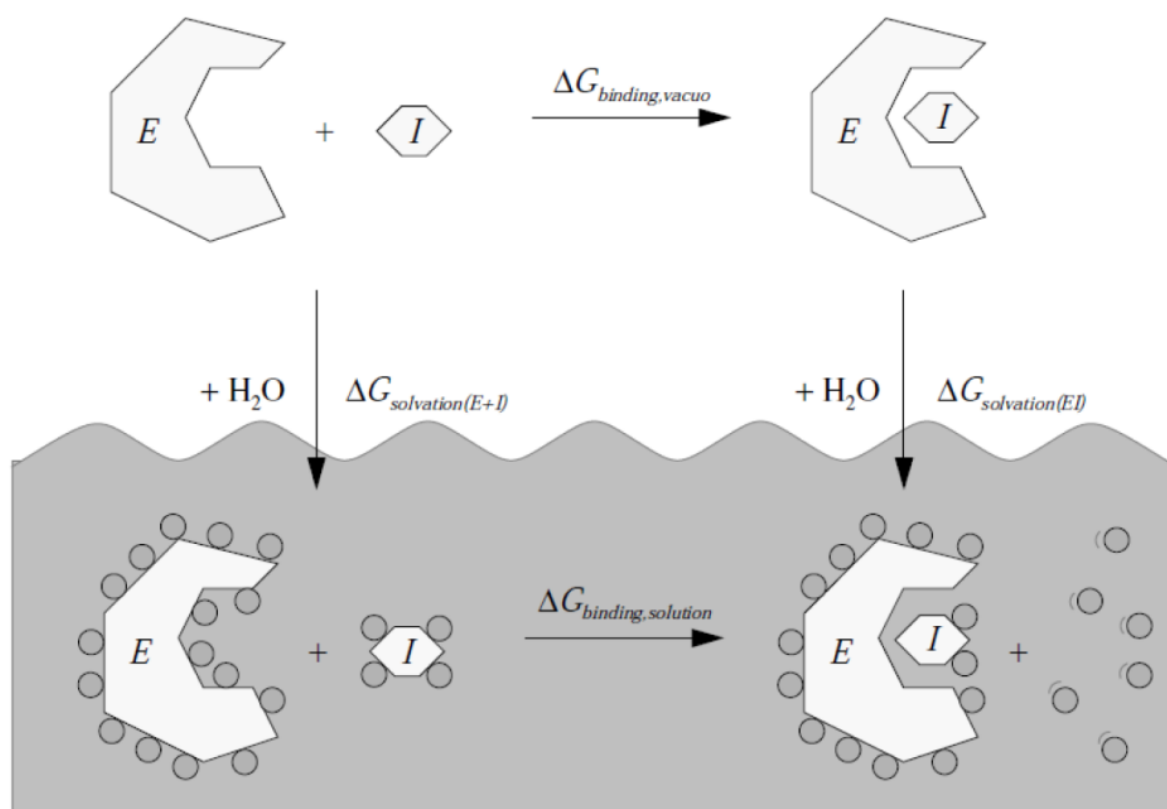


Figure 1.28. Thermodynamic cycle for the binding of an enzyme (E) and an inhibitor (I) in both the solvated phase and in *vacuo*. (<http://www.scripps.edu/pub/olsonweb/doc/autodock/>)

The hybrid between GA and the adaptive LS methods forms the so-called *Lamarckian genetic algorithm* (LGA), which has enhanced performance in comparison with simulated annealing (a little used algorithm in AutoDock) and a classical genetic algorithm. The latter one follows the scheme of Darwinian evolution and it applies Mendelian genetics

(Figure 1.29, right-hand side); this means that the information is transferred only unidirectionally from the genotype to the phenotype. In agreement with Jean Batiste de Lamarck's assertion, in which phenotypic characteristics acquired during the lifetime of an individual can become heritable, in Lamarckian genetic algorithm an inverse mapping function exists and one individual yields a genotype from a given phenotype. At this point it is possible to finish a local search by replacing the individual with the result of the local search (Figure 1.29, left-hand side).

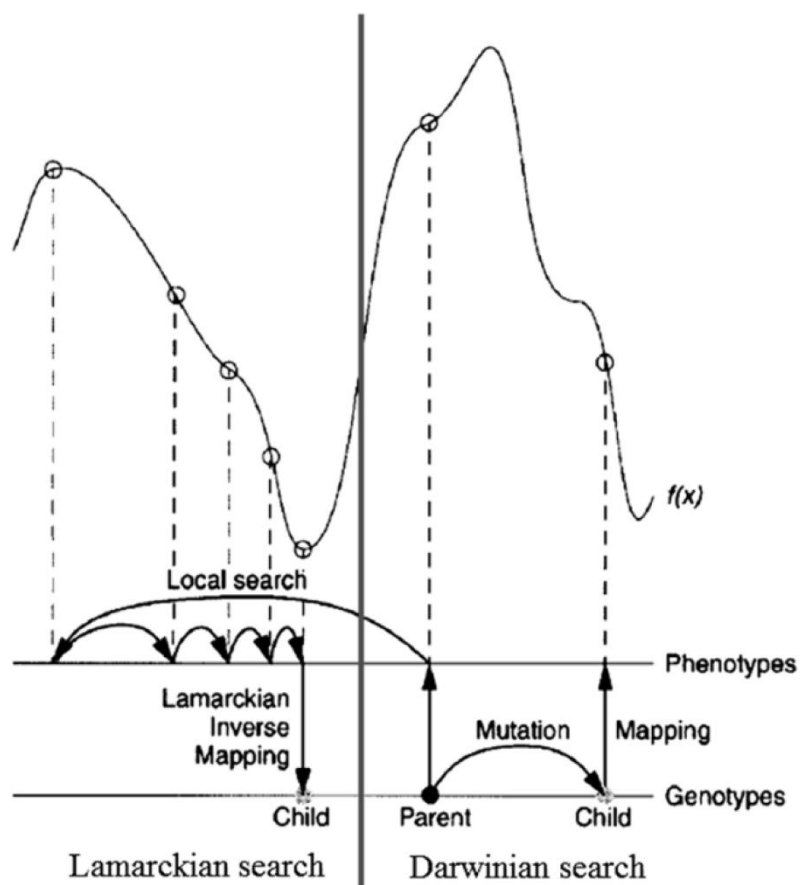


Figure 1.29. Genotypic and phenotypic search by Darwinian (right-hand side) and Lamarckian (left-hand side) search. $f(x)$ is the fitness function. With sufficient iterations, the local search arrive at a local minimum, and an inverse mapping function is used to convert from its phenotype to its corresponding genotype. In the case of molecular docking, however, local search is performed by continuously converting from the genotype to the phenotype, so inverse mapping is not required. The genotype of the parent is replaced by the resulting genotype, however, in accordance with Lamarckian principles. (adapted from Morris, 1998)

From a computational point of view pre-calculated grid maps for each type of atom present in the ligand are used to speed up the docking calculation in AutoDock.

A grid map consists of a three dimensional lattice of regularly spaced points, surrounded and centered on the region of interest of the macromolecule under study. Each point within the

grid map stores the potential energy of a 'probe' atom or functional group that is due to all the atoms in the macromolecule (Figure 1.30).

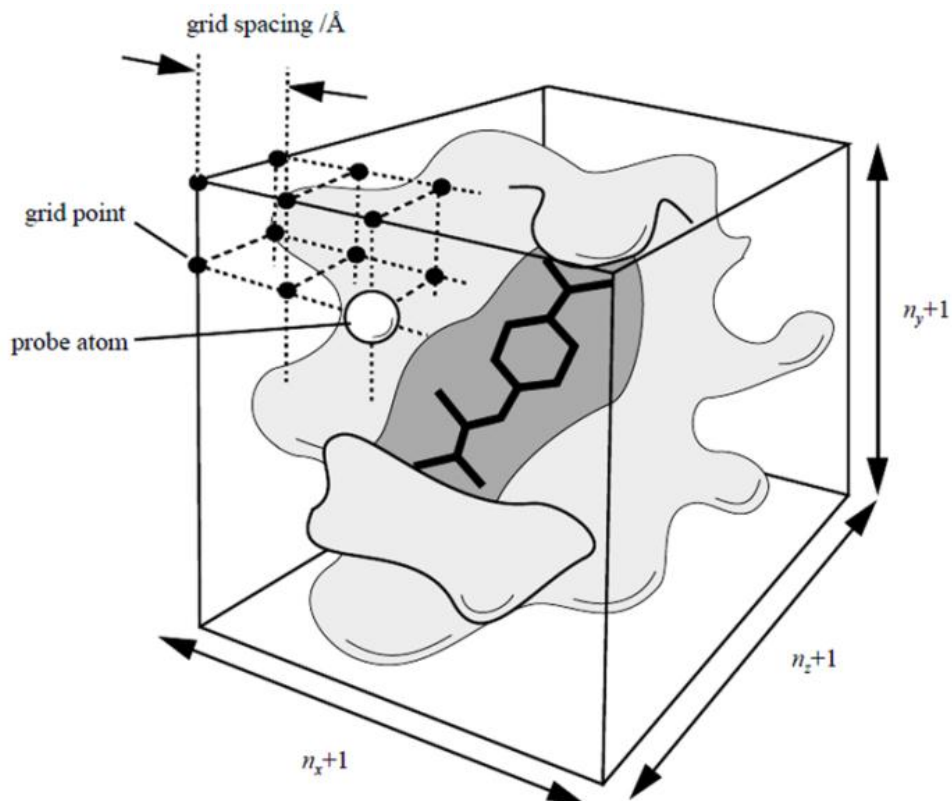


Figure 1.30. Example of the main feature of grid map (<http://www.scripps.edu/pub/olson-web/doc/autodock/>)

The boundaries of the interacting site must be selected neither too small (because the accuracy of docking prediction will be poor due to the limited motion of ligand into the grid box), nor too large (because the success rate decreases depending to its size). A grid map with 60x60x60 points and a grid-point spacing of 0.375 Å are straightforward parameters to be used in grid calculations.

By AutoDock software the parameters commonly used for docking calculation can be summarized as following reported:

- 100 independent runs starting from a population size of random individuals of 150
- a maximum number of 1.5×10^6 energy evaluations with
- a maximum number of 27,000 generations
- a step sizes of 0.2 Å for translations and 5° for orientations and torsions in the initial population

- an elitism value of 1, which is the number of top individuals that automatically survive into the next generation
- a mutation rate of 0.02, which is the probability that a gene would undergo a random change
- a crossover rate of 0.80, which is the probability that two individuals would undergo crossover
- in the analysis of the docked conformations, the clustering tolerance for the root-mean-square positional deviation is imposed 2.0 Å

At least, but not less important, the X-ray crystallographic resolution of the protein is a parameter to take into account in docking, in order to have realistic results. A threshold of 2.5 Å of nominal resolution appears to be optimal for the representation of protein conformations (Bottegoni, 2011).

Another aspect is given by the discrimination between specific and nonspecific interactions. Chang and coauthors have analyzed the results of binding energy obtained from AutoDock calculations for a known HIV protease inhibitors series with compounds from the National Cancer Institute (NCI) Diversity Set. From this analysis it is resulted that all compounds from NCI diversity set exhibit weak or moderate binding energies when compared with the known inhibitors. Figure 1.31 illustrates the comparison of the distribution of binding energies for known inhibitors and compounds randomly selected in NCI database (a). Receiver operating characteristic curve (ROC), obtained by plotting the fraction of true positives out of the positives (TPR = true positive rate) *versus* the fraction of false positives out of the negatives (FPR = false positive rate) at various threshold settings, provides to select the optimal threshold value in docking calculation (b).

For quantifying the comparison of the binding energies between the compounds acting as specific protease inhibitors and random compounds taken from the NCI Diversity Set, a threshold of -7.0 kcal/mol works well to discriminate between putative specific and nonspecific binding with HIV protease. This cutoff is specific for AutoDock and the protease system, but it is broadly applicable as a general approach to other systems (Chang, 2007).

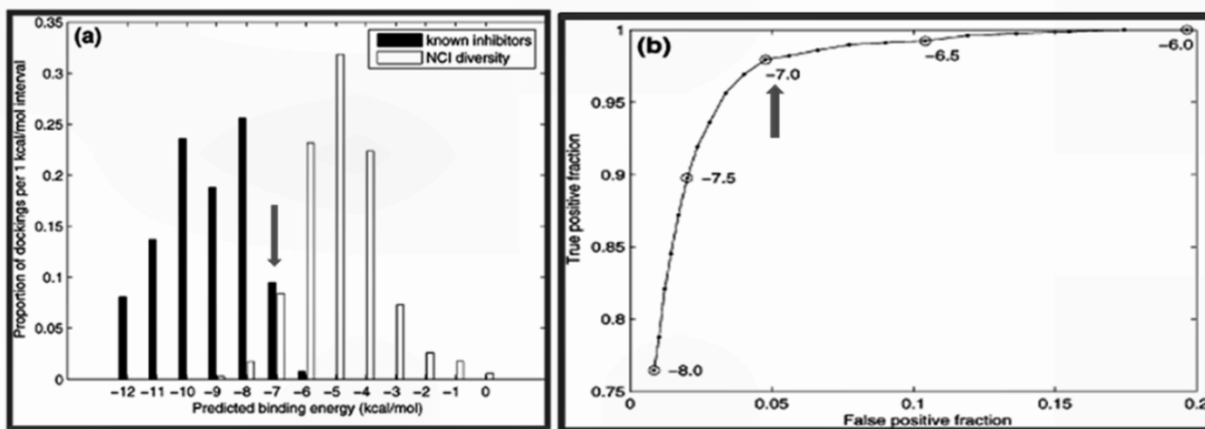


Figure 1.31. (a) Comparison of the distribution of binding energies for known inhibitors and NCI Diversity Set compounds. (b) ROC curve showing a sensitivity/specificity tradeoff for threshold values from -8 to -6 kcal/mol. (adapted from Chang, 2007)

2. Material and Methods

2.1. Computational approach

I carried out all computational studies using a single machine running on a 3.4 GHz on an Intel i7 2600 quad core processor with 8GB RAM and 1 TB hard disk with Windows 7 Home Premium 64-bit SP1 as an operating system. I built the ligands using PCModel version 8.0 (Serena Software, Bloomington, IN 47402-3076). For geometry optimization I used Gaussian 03W revision E.01 program set with graphical interface Gaussview 4.0. I employed AutoDock Tools (ADT) package version 1.5.6rc3 to generate the docking input files and to analyze docking results whereas AutoGrid 4.0 and AutoDock4.0 were taken on for grids and docking calculation respectively. The detailed parameters that I used in this thesis for the geometry calculations and docking evaluations will be reported in Results (Chapter 3).

ADME and drug-like properties prediction

I calculated *in silico* ADME data predictions using the freely available web-based application PreADMET (<http://preadmet.bmdrc.org/>); I calculated partition coefficient (LogP) of all compounds with ALOGPS 2.1 program (<http://www.vcclab.org/>) that uses an average of nine Log P methods.

2.2 Chemistry

2.2.1 General

All evaporations were carried out at reduced pressure at room temperature. Yields are given on the reacted compounds. Solvents and reagents were purchased from Sigma Aldrich Europe (Milan, Italy) and from Alfa Aesar and were used without purification. Thin layer chromatography (TLC) was carried out on Merck Kieselgel 60 PF254 and flash chromatography (FC) was carried on Merck silica gel (Si-60, 15 ± 25 µm). Preparative TLC was realized on 20 × 20 cm Merck Kieselgel 60 F254 0.5 mm plates. All the reaction

products were characterized by ^1H -NMR and mass spectrometry analysis to confirm the structure and the purity. Compounds used in biological assays have been fully characterized by extensive NMR analysis, and high resolution electron impact mass spectrometry.

2.2.2. Instruments

Melting points were determined on Reichert Thermovapor microscope (Reichert, Austria) and the data are uncorrected. Ultrasound bath Badelin Sonorex RK510, 35 KHz, 160W were used for the synthesis of compound **45**. IR spectra were acquired by FTIR Equinox 55 Bruker[®], equipped with ATR device in zinc selenide. NMR spectra were recorded by an Avance 400 Bruker spectrometer: ^1H at 400 MHz and ^{13}C at 100 MHz in CDCl_3 or CD_3OD on the base of sample solubility. δ values are reported in ppm relative to the solvent residual-signals $\delta_{\text{H}} = 7.25$ and $\delta_{\text{C}} = 77.00$ ppm for CDCl_3 and $\delta_{\text{H}} = 3.31$ and $\delta_{\text{C}} = 49.00$ for CD_3OD , where the solvent residual-signals are relative to SiMe_4 ($=0$ ppm); J values are given in Hertz. ^{13}C -NMR assignments come from heteronuclear single quantum-correlation (HSQC) and heteronuclear multiple bond correlation (HMBC) experiments. For Numbering adopted for NMR assignments is for convenience. Electron impact (EI) mass spectra (m/z ; rel.%) and high resolution EI data were taken by a Kratos-MS80-mass spectrometer with a home-built computerized acquisition-software. Electrospray ionization (ESI)-MS mass spectra and tandem fragmentation spectra (MS/MS) were recorded by a Bruker Esquire-LC[®] spectrometer with an electrospray ion source used in positive or negative ion mode by direct infusion of a methanolic solution of the sample, under the following conditions: source temperature 300°C , drying gas N_2 , 4 L/min, positive ion mode, ISV 4 kV, OV 38.3 V, scan range m/z 100–1,000. For the determination of optical activity of compounds **3**, **4**, **11** and **12** I used a single wavelength polarimeter ADP440 (Bellingham + Stanley Ltd).

2.2.3 Chemical procedures of synthesis

The details of chemical synthesis have been reported in chapter 3; a detailed discussion on the chosen methods and their optimizations has been inserted in chapter 4.

2.3 Biological assays

2.3.1. ELISA enzymatic assay

I performed the HIV-RT inhibition assay by using the Roche Reverse Transcriptase Assay, Colorimetric kit (Mannheim, Germany: Roche Diagnostics GmbH, Roche Applied Science). The procedure for assaying RT inhibition was performed as described in the kit protocol and it is reported in detail in chapter 3. Additional reverse transcriptase was obtained from Pierce Biotechnology (USA) and before using it, I compared the activity with the original one present in the Roche kit. Experimental details has been described in § 3.3.1.1.

2.3.2. *In vitro* anti-HIV activity

Inhibition of HIV-1(IIIB) and HIV-2(ROD)-induced cytopathicity in CEM cell cultures performed by the Prof. Balzarini's staff (Rega Institute, University of Leuven Belgium), was measured in microtiter 96-well plates containing $\sim 3 \times 10^5$ CEM cells/mL, infected with 100 CCID₅₀ of HIV per mL and containing appropriate dilutions of the test compounds. After 4–5 days of incubation at 37 °C in a CO₂-controlled humidified atmosphere, CEM giant (syncytium) cell formation was examined microscopically. The EC₅₀ (50% effective concentration) was defined as the compound concentration required to inhibit HIV-induced giant cell formation by 50%.

2.3.3. *In vitro* antiviral activity

The antiviral assays, performed in the laboratory of Prof. Snoeck and Prof. Andrei (Rega Institute, University of Leuven Belgium), were based on the inhibition of virus-induced cytopathicity in HEL cell cultures for herpes simplex virus type 1 (HSV-1), HSV-2(G), vaccinia virus, vesicular stomatitis virus (Table 3.7) and varicella-zoster virus (VZV) (Table 3.8); in Vero cell cultures for parainfluenza- 3, reovirus-1, Sindbis, Coxsackie B4 and Punta Toro virus (Table 3.10); in HeLa cell cultures for vesicular stomatitis virus, Coxsackie virus B4 and respiratory syncytial virus (Table 3.9); in MDCK (Madin Darby canine kidney) cell cultures for influenza A (H1N1 and H3N1) and influenza B virus (Table 3.12) and in CrFK (Crandell-Rees Feline Kidney) cell cultures for feline herpes virus and feline corona virus (FIPV) (Table 3.11). Confluent cell cultures in microtiter 96-well plates were inoculated with

100 cell culture inhibitory dose-50 (CCID₅₀) of virus (1 CCID₅₀ being the virus dose to infect 50% of the cell cultures) in the presence of varying concentrations of the test compounds. Viral cytopathicity was recorded as soon as it reached completion in the control virus infected cell cultures that were not treated with the test compounds.

For the anti-cytomegalovirus assay, confluent human embryonic lung (HEL) fibroblast cultures were grown in 96-well microtiter plates and infected with the human cytomegalovirus (HCMV) strains AD-169 and Davis at 100 PFU per well. After a 2-h incubation period, residual virus was removed and the infected cells were further incubated with medium containing different concentrations of the test compounds (in duplicate). After incubation for 7 days at 37 °C, virus-induced cytopathogenicity was monitored microscopically after ethanol fixation and staining with Giemsa. Antiviral activity was expressed as the EC₅₀ or compound concentration required to reduce virus-induced cytopathogenicity by 50%. EC₅₀'s were calculated from graphic plots of the percentage of cytopathogenicity as a function of concentration of the compounds (Table 3.13).

2.3.4. Antibacterial activity

The antibacterial tests were performed at the University A. Mira of Bejaia, Algeria, following the procedures reported below.

Agar diffusion assay

Well agar diffusion assays were performed to determine antibacterial activity. The pure compounds were dissolved in DMSO (1 mg/mL), assay plates were prepared by inoculating Mueller - Hinton agar medium with 24 hours old culture containing test organisms (10⁷ CFU/mL). A solution of dissolved compounds (100 µl) was added to separate wells (6 mm diameter). The plates were placed at 4°C for 2h; zones of inhibition were recorded after 24 hours of incubation at 37 °C. In all cases, for the controls containing only the respective amount of solvent, no growth inhibition was observed. Antimicrobial activities were assayed in triplicate.

Determination of the minimum inhibitory concentrations (MIC) for antibacterial activity

The isolated pure compound was dissolved in DMSO at 1 mg/mL concentration and diluted further to give required concentrations such as 2, 4, 8, 16 and 32 ($\mu\text{g/mL}$). The diluted solutions (2 mL) were added to Müller- Hinton plates (18 mL). An inoculum of 10 μL (10^7 CFU/mL) from culture of each test human pathogens, *MRSA ATCC 43300*, *Staphylococcus aureus ATCC 25923* and *P aeruginosa ATCC 27853*, were inoculated in each concentration plate. The plate's cultures were incubated for 24 hour at 37 °C. The MIC was defined as the lowest concentration of the purified compound showing no visible growth after overnight incubation. Vancomycin was used as positive control for MRSA and DMSO was used as negative control. Replicates were maintained for each test bacteria.

3. Results

3.1 Drug design

In medicinal chemistry the molecular simplification is a common paradigm in order to obtain a minimal structure with potential bioactivity. By reducing the complexity of an active natural product and introducing structural modifications, it is possible to achieve a library of novel compounds, easier to be prepared than the natural molecule itself. The design of these molecules can be allowed by molecular hybridization using different fragments present in known molecules interacting with the macromolecule of interest (Viegas-Junior, 2007). In this thesis I designed a small library of new molecules using this approach.

The scaffold present in the series of the new molecules derives from the disconnection of (+)-calanolide A, a natural product isolated from the Malaysian tree *Calophyllum lanigerum*, showing a potent anti-HIV activity (Currens, 1996; Xu, 2000) and from the disconnection of α -APA (=2-((2-acetyl-5-methylphenyl)amino)-2-(2,6-dichlorophenyl)-acetamide), a synthetic NNRTI (Ding, 1995, Figure 3.1). In particular (+)-calanolide A is unique among NNRTIs because it is able to bind two distinct sites in reverse transcriptase (Currens, 1996). This natural product exhibits a 10-fold enhanced activity against drug-resistant viruses, which show the most prevalent NNRTI resistance mutations such as the Y181C mutation (Auverx, 2005), probable due to the particular feature of binding of this molecule. Potent antiviral agents as etravirine or rilpivirine (Figure 1.14.) have been obtained by extensive modifications introduced in α -APA structure, so it represents a good starting molecule to be inserted in the hybridization method with the aim to find new active molecules.

Based on this idea, the study by docking calculation of a series of molecules has been planned with the aim of introducing changes in the (aryl)-alkyl unit, in the linking group X, as well as in the substituent R on the pyranone moiety, as reported in the general structure (Figure 3.2).

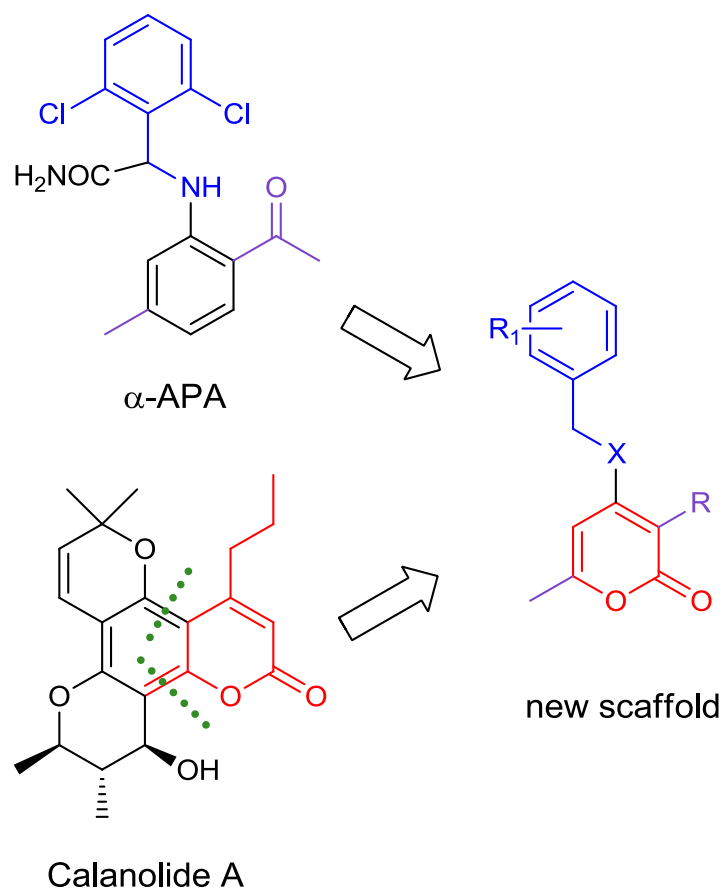


Figure 3.1. Drug design of new potential NNRTIs by molecular hybridization method

This is in line with a drug design using a fragment based strategy associated to molecular hybridization (§ 1.6.1), a more ambitious approach than the one based on the introduction of small structural modifications in known drug molecules.

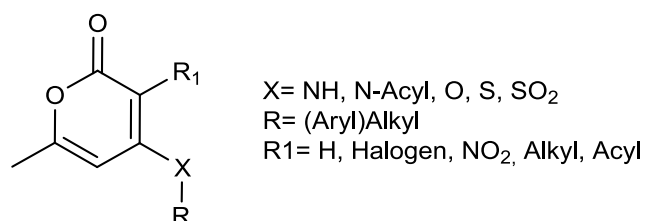


Figure 3.2. General structure of designed new molecules as potential NNRTIs

In fact the latter methodology can give easier successes, as reported in the case of nevirapine modification by adding a short chain on the aromatic ring present in dipyrindodiazepinone (Nisachon, 2009), or in the case of the drug rilpivirine, where a small modification on the atom linker between the pyrimidine unit and the aromatic ring bearing the acrylonitrile moiety gave new compounds showing the same activity as the starting drug (Mordant, 2007). In

literature other examples are also reported where small structural modifications decrease the bioactivity: for the drug efavirenz, the replacing of the chlorine atom on the aromatic ring (with NO₂, NH₂ or F), (Patel, 1999) or changing the side chain (Cocuzza, 2001), drastically reduce the antiviral activity. Anyway, it is the way to be followed up in order to find novel compounds overcoming the problem of resistance.

3.1.1. Docking calculation

3.1.1.1. Protein preparation

The X-ray crystallographic structure (resolution = 2.5 Å, R-factor¹ 0.214 space group P2₁P2₁P2₁, PDB accession code 1FK9) of RT in the complex with the clinically used efavirenz as ligand, was downloaded from PDB Database (<http://www.rcsb.org/pdb/home/home.do>). The PDB structure of RT presents a good resolution, although a residue of S-sulfino-cysteine was present instead of C279 residue in the chain A. It was manually substituted with a cysteine. All the water molecules of crystallization were removed, as well as the ligand and the cleaned protein structure was saved with pdb extension. In order to validate the docking method, other RT protein structures complexed with known allosteric inhibitors were downloaded from PDB Database, as reported in table 3.1 and submitted at the same procedure adopted for the protein 1FK9.

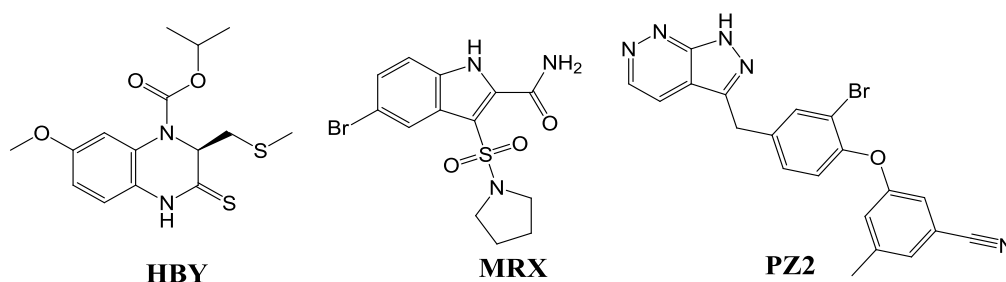


Figure 3.3. Structure of inhibitors present in a complex with downloaded RT

¹ **R-factor**: In crystallography, the **R-factor** is a measure of the agreement between the crystallographic model and the experimental X-ray diffraction data and it describes the quality of a model. It is defined by the following equation:

$$R = \frac{\sum ||F_{obs}| - |F_{calc}||}{\sum |F_{obs}|}$$

where F is the so called structure factor and the sum extends over all the reflections measured and their calculated counterparts respectively. The structure factor F is closely related to the intensity of the reflection it describes: $I_{hkl} \propto |F(hkl)|^2$. For large molecules, R-factor usually ranges between 0.6 (when comparing a random set of reflections with a given model) and 0.2 (for example for a well refined macromolecular model at a resolution of 2.5 Ångström).

Table 3.1. Details of RT X-Ray crystal structure.

PDB Code	Inhibitor	Resolution (Å)	R-Factor	Space group
1FK9	efavirenz	2.50	0.214	P ₂ ₁ P ₂ ₁ P ₂ ₁
2ZD1	rilpivirine	1.80	0.220	C2
3BGR (K103N/Y181C mutant)	rilpivirine	2.10	0.228	C2
2IC3 (K103N/Y181C mutant)	HBV	3.00	0.257	C2
2RF2	MRX	2.40	0.189	C222 ₁
3E01	PZ2	2.95	0.235	C222 ₁
1VRT	nevirapine	2.20	0.186	P ₂ ₁ P ₂ ₁ P ₂ ₁
1KLM	delavirdine	2.65	0.237	P ₂ ₁ P ₂ ₁ P ₂ ₁
1MU2 (HIV-2 RT)	-	2.35	0.192	P ₂ ₁ P ₂ ₁ P ₂ ₁

3.1.1.2. Preparation of ligands

All the new molecules were built with PCModel using the default molecular mechanics force field MMX. The geometry of each minimized molecules was furtherly optimized using the quantum-chemical software Gaussian 03W (Frisch, 2004). Restricted Density Functional Theory (DFT) was used invoking gradient geometry optimization. The basis set of choice resulted 6-31G(d,p) for all the atoms. The gradient-corrected DFT with the three-parameter hybrid functional (B3) (Becke 1993) for the exchange part and the Lee–Yang–Parr (LYP) correlation function (Lee, 1988) were utilized. The optimized structural parameters were employed in the vibrational energy calculations at the DFT levels to characterize all stationary points as minima. No imaginary wavenumber modes were obtained for each optimized structure, proving that a local minimum on the potential energy surface was actually found. The minimized molecules were saved with pdb extension.

3.1.1.3. Molecular docking

Employing AutoDock Tools (ADT), all the hydrogen atoms were added to reverse transcriptase structure and Gasteiger-Marsili charge were calculated saving the file with extension pdbqt.

Rotatable bonds were defined for each ligand molecule, previously minimized, after the addition of Gasteiger-Marsili charge, and the obtained file saved as pdbqt. For the grids calculation a grid box of 60x60x60 points in x,y,z directions was created, spacing of 0.375 Å and centered on the NNBP. Energy grid maps for all possible ligand atom types were generated with Autogrid 4.0 before performing docking.

Lamarckian genetic algorithm was used to search the conformational and orientational space of the ligands. A default protocol was applied with initial population of 150 randomly placed individuals, a maximum number of 2.5×10^5 energy evaluation and a maximum number of 2.7×10^4 generations. A mutation rate of 0.02 and a crossover rate of 0.8 were used. Hundred independent docking runs were performed and then the 100 solutions were clustered into groups with RMS deviation lower than 0.5 Å. The lowest energy conformation in the most populated cluster was chosen (Hu, 2009). Before starting the calculations with the new molecules, the method has been cross-validated using different X-ray structures bonded with various inhibitors, which were removed from the reverse transcriptase and a docking calculation was carried out for each inhibitor docked with each RT (Table 3.2).

Later the compounds selected to be synthesized were also submitted to further docking calculations using the software Molegro virtual docker (demo version) in order to compare the results obtained with Autodock. The calculations were carried out with default parameters: the used scoring function was MolDock Score with a grid resolution of 0.30 Å centered on the original ligand position and with a radius of 12 Å.

The search algorithm was MolDock Optimizer (a genetic-algorithm) using 10 independent runs starting from a random generated population of 50 individuals with a maximum number of 2000 iterations, a scaling factor of 0.50 with a crossover rate of 0.90. The end of calculation was based on variance-based method. A post-docking energy and H-bond optimization were applied, whereas a clusterization of similar poses for the generated structures has been performed with a RMSD threshold of 1.00 Å. The docking calculation

results for the selected molecules to be assayed *in vitro* are reported in table 3.3, whereas all the other calculated structures are reported in appendix A.

Table 3.2. Calculated binding energy by docking validation of different X-ray RT structures. The values in red are the energy corresponding to re-docked of ligand in the same original RT.

PDB code	Efavirenz	Rilpivirine	HBY	MRX	PZ2	NVP	Delavirdine
1FK9 (Efavirenz)	-8.61	-10.39	-8.89	-9.82	-10.50	-8.25	-9.21
2ZD1 (Rilpivirine)	-7.98	-12.99	-8.90	-8.68	-10.29	-8.17	-11.08
3BGR (Rilpivirine)	-6.57	12.81	n.c.	n.c.	n.c.	-7.81	-10.45
2IC3 (HBY)	n.c.	-9.30	-7.76	n.c.	n.c.	n.c.	n.c.
2RF2 (MRX)	n.c.	-8.37	n.c.	-9.62	n.c.	n.c.	n.c.
3E01 (PZ2)	n.c.	-11.69	n.c.	n.c.	-12.58	n.c.	n.c.
1VRT (NVP)	-7.73	-10.59	n.c.	n.c.	n.c.	-8.50	-10.07
1KLM (Delavirdine)	-7.93	-10.70	n.c.	n.c.	n.c.	-8.30	-10.05
1MU2 (HIV-2 RT)	-5.58	-7.41	n.c.	n.c.	n.c.	-5.65	-8.86

n.c. = not calculated

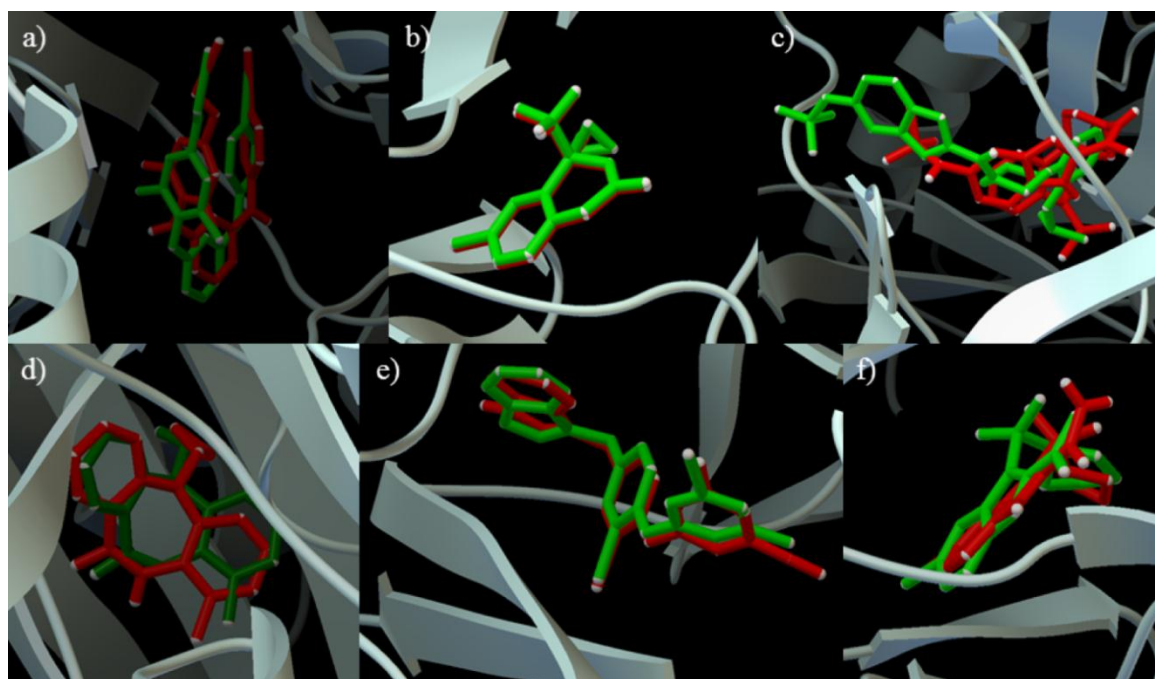


Figure 3.4. Visual inspection of some results obtained by docking validation test. In green are reported the original ligand position in X-ray crystallographic structure, in red are reported the docked molecules. a) rilpivirine (pdb code:2ZD1), b) efavirenz (pdb code: 1FK9), c) delavirdine (pdb code:1KLM), d) nevirapine (pdb code:1VRT), e) compound PZ2 (pdb code:3E01), f) compound MRX (pdb code: 2RF2).

In figure 3.5 the visualization of compound **23** is reported (in red lines) surrounded by the amino acids present in NNIBP of RT (pdb code 1FK9). Compound **23** has been chosen because it resulted one of the most promising molecule. It is also reported as an example the cluster histogram of binding energy clustered at rms 0.5Å, by docking calculation it is also reported as an example (Figure 3.6).

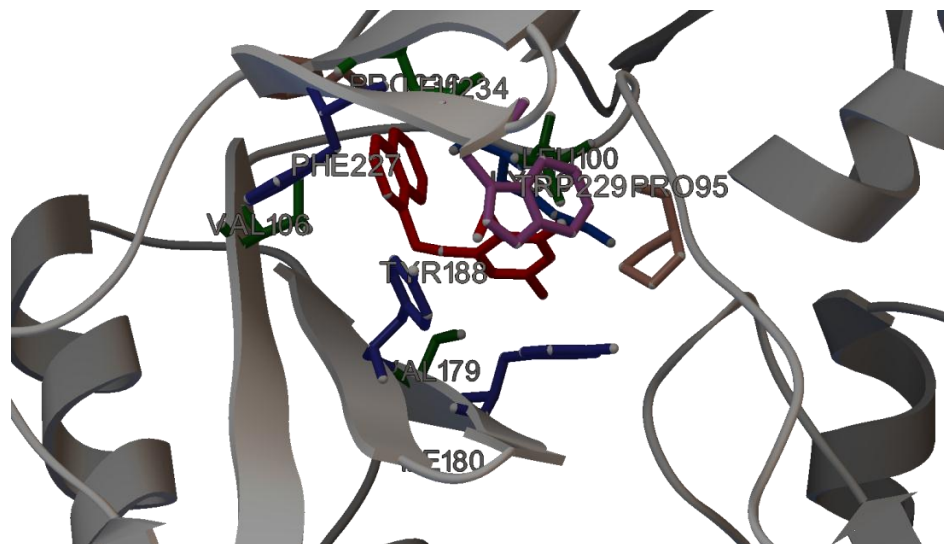


Figure 3.5. Amino acid residues in Rasmol colours of NNIBP surrounding the *in vitro* resulted most active molecules **23** (in red)

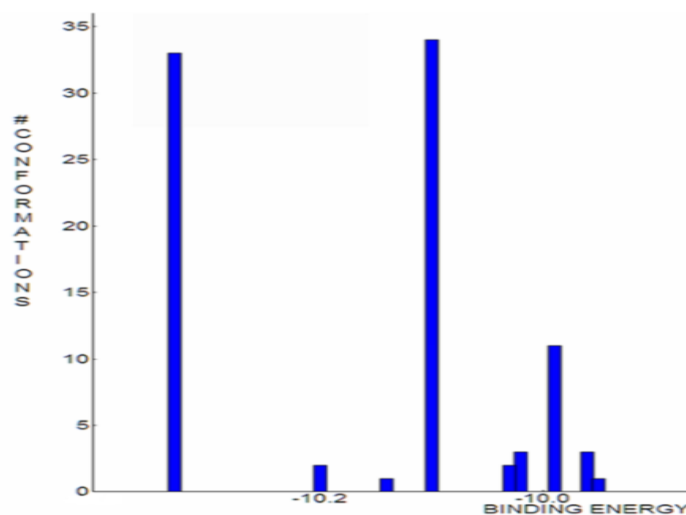


Figure 3.6. Cluster analysis of compound **23**

The figure 3.7 shows the overlap among compound **23**, the natural product calanolide A and the synthetic NNRTI α -APA in the same binding site. Although the molecules show a little bit different arrangement in the pocket, all the atoms are superimposable.

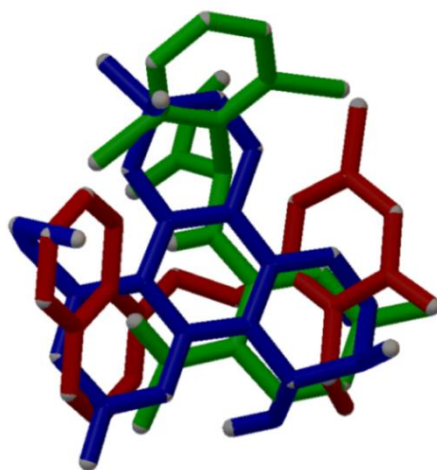


Figure 3.7. Overlapped structures in the RT binding site (pdb code 1FK9) of compound **23** (in red), calanolide A (in blue) and α -APA (in green) deriving from AutoDock calculation

In order to search the best overlap among the three molecules previously docked by AutoDock, a superimpose procedure using the software MOE was applied. It takes into account shape, electrostatic potential, lipophilicity and molecular refractivity and the visual results are reported in figure 3.8.

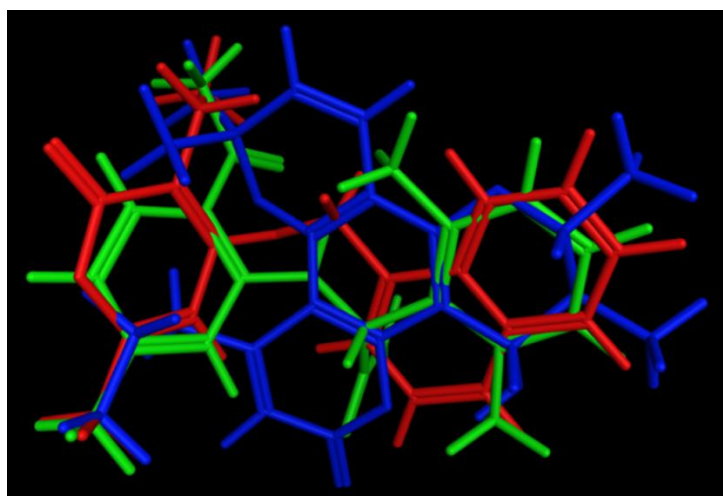
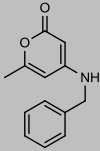
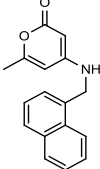
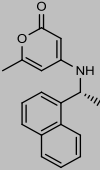
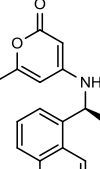
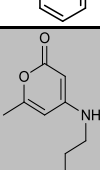
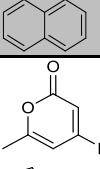
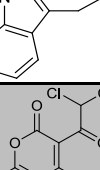
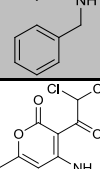
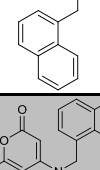


Figure 3.8. Visual inspection of overlapped molecules of compound **23** (in red), calanolide A (in blue) and α -APA (in green) obtained using a superimposing genetic algorithm that considers shape, electrostatic potential, lipophilicity and molecular refractivity.

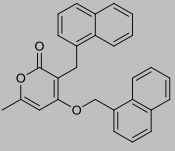
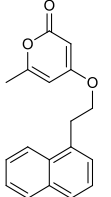
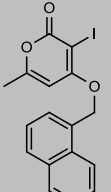
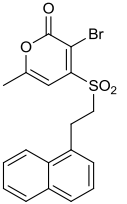
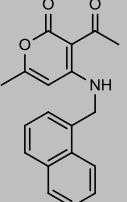
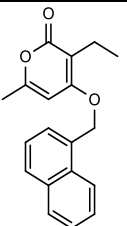
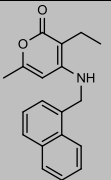
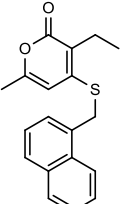
3.1.1.4 ADME and drug-like properties prediction

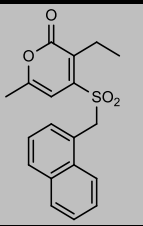
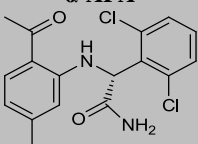
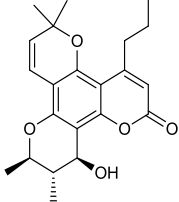
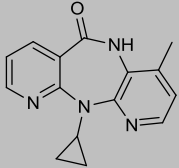
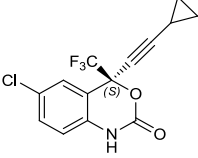
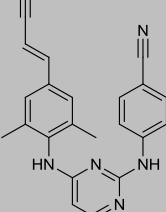
Each pdb file of the new molecules was subjected to the different web-based program and the results are summarized in table 3.3.

Table 3.3. Docking and ADME parameters for the synthesized molecules

Entry	Chemical Structure	Molecular Formula M.W.	E_{Docking} AutoDock (Kcal/mol)	Ligand Efficiency	E_{Docking} Molegro Score (Rerankin)	Calculated Log P	ADME Prediction	
							HIA (%)	<i>In vitro</i> PPB (%)
1		C ₁₃ H ₁₃ NO ₂ 215.25	-7.04	0.44	-97 (-82)	1.8±0.6	95	100
2		C ₁₇ H ₁₅ NO ₂ 265.35	-8.78	0.44	-119 (-97)	3.0±0.6	96	100
3		C ₁₈ H ₁₇ NO ₂ 279.33	-9.39	0.44	-123 (-101)	3.4±0.7	96	100
4		C ₁₈ H ₁₇ NO ₂ 279.33	-9.47	0.45	-127 (-104)	3.4±0.7	96	100
5		C ₁₈ H ₁₇ NO ₂ 279.33	-9.26	0.44	-131 (-103)	3.3 ±0.6	96	100
6		C ₁₆ H ₁₆ N ₂ O ₂ 268.31	-8.40	0.35	-137 (-108)	2.7±0.7	91	88
7		C ₁₅ H ₁₃ Cl ₂ NO ₃ 326.20	-7.47	0.36	-119 (-93)	2.6±1.0	96	94
8a		C ₁₉ H ₁₅ Cl ₂ NO ₃ 376.26	-9.41	0.38	-141 (-117)	3.7±1.0	97	96
8b		C ₁₉ H ₁₅ Cl ₂ NO ₃ 376.23	-10.89	0.44	-145 (-97)	3.8±0.5	98	92

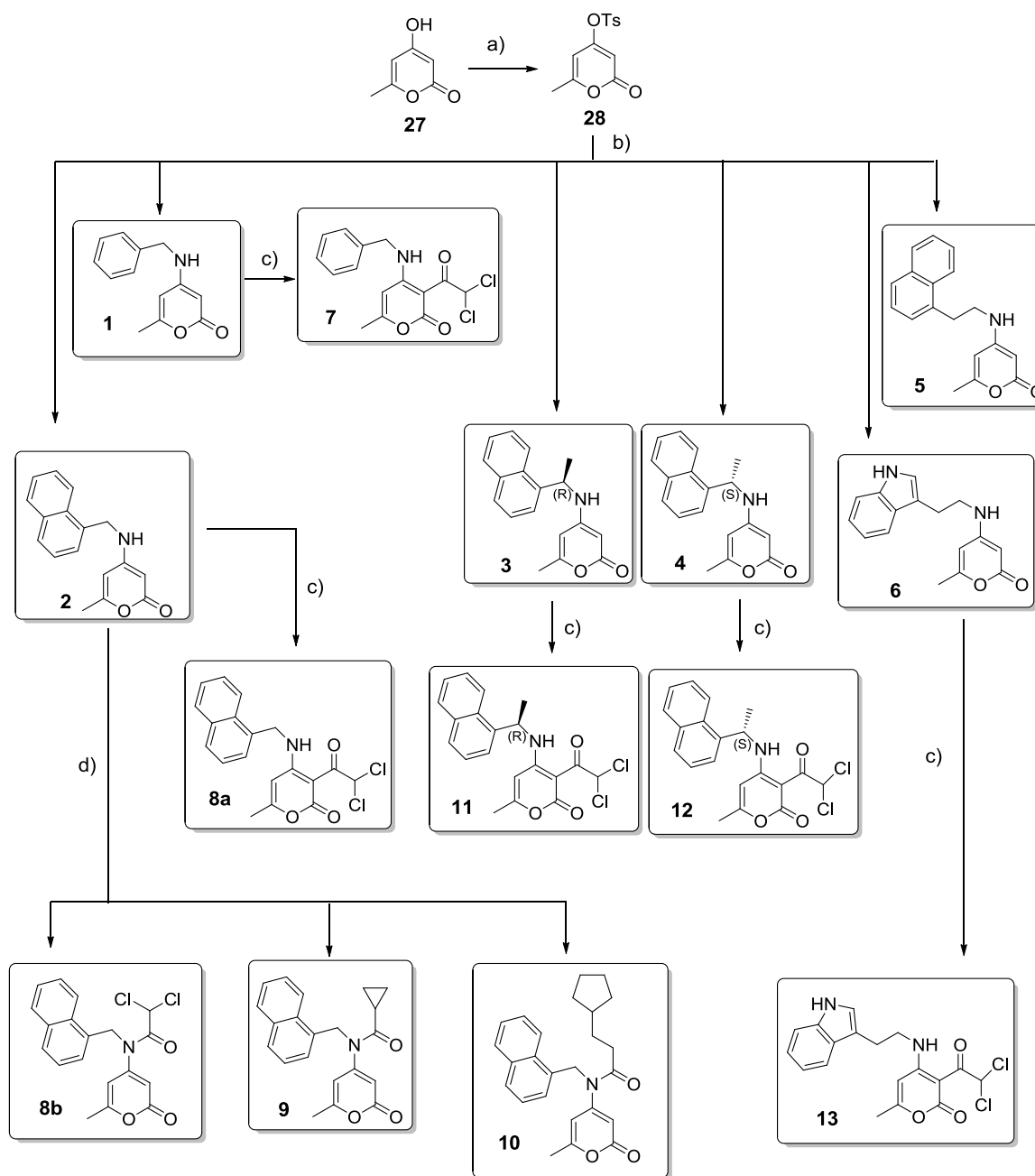
Entry	Chemical Structure	Molecular Formula M.W.	E _{Docking} AutoDock (Kcal/mol)	Ligand Efficiency	E _{Docking} Molegro Score (Rerankin)	Calculated Log P	ADME Prediction	
							HIA (%)	In vitro PPB (%)
9		C ₁₉ H ₁₅ Cl ₂ NO ₃ 376.23	-8.27	0.33	-145 (-107)	3.4±0.4	97	92
10		C ₂₅ H ₂₇ NO ₃ 389.53	-12.29	0.42	-168 (-100)	5.2±0.6	97	92
11		C ₂₀ H ₁₇ Cl ₂ NO ₃ 390.29	-9.20	0.35	-140 (-107)	4.2±1.1	97	93
12		C ₂₀ H ₁₇ Cl ₂ NO ₃ 390.29	-9.33	0.36	-147 (-111)	4.2±1.1	97	93
13		C ₁₈ H ₁₆ Cl ₂ N ₂ O ₃ 308.33	-8.72	0.35	-139 (-115)	3.0±1.0	85	80
14		C ₁₇ H ₁₄ O ₂ S 282.36	-9.37	0.47	-124 (-102)	4.0±0.4	97	92
15		C ₁₇ H ₁₄ O ₄ S 314.36	-9.91	0.45	-133 (-105)	2.3±0.8	98	99
17		C ₁₈ H ₁₆ O ₄ S 328.38	-10.12	0.44	-145 (-102)	2.6±0.9	98	98
18		C ₁₇ H ₁₄ O ₃ 266.29	-8.76	0.44	-124 (-102)	3.4±0.5	99	100

Entry	Chemical Structure	Molecular Formula M.W.	E _{Docking} AutoDock (Kcal/mol)	Ligand Efficiency	E _{Docking} Molegro Score (Rerankin)	Calculated Log P	ADME Prediction	
							HIA (%)	<i>In vitro</i> PPB (%)
18a		C ₂₈ H ₂₂ O ₃ 406.46	-13.32	0.43	-167 (-116)	6.3±0.6	99	96
19		C ₁₈ H ₁₆ O ₃ 280.32	-9.44	0.45	-129 (-103)	3.6±0.4	99	96
20		C ₁₇ H ₁₃ IO ₃ 392.19	-9.76	0.46	-133 (-106)	3.9±0.8	99	95
21		C ₁₈ H ₁₅ BrO ₄ S 407.28	-10.92	0.46	-143 (-98)	3.1±1.2	98	98
22		C ₁₉ H ₁₇ NO ₃ 307.34	-9.75	0.42	-130 (-104)	2.8±0.9	96	100
23		C ₁₉ H ₁₈ O ₃ 294.34	-10.33	0.44	-130 (-109)	4.1±0.5	99	95
24		C ₁₉ H ₁₉ NO ₂ 293.36	-10.12	0.46	-122 (-102)	3.8±0.5	97	100
25		C ₁₉ H ₁₈ O ₂ S 310.41	-10.08	0.46	-136 (-110)	4.9±0.5	97	96

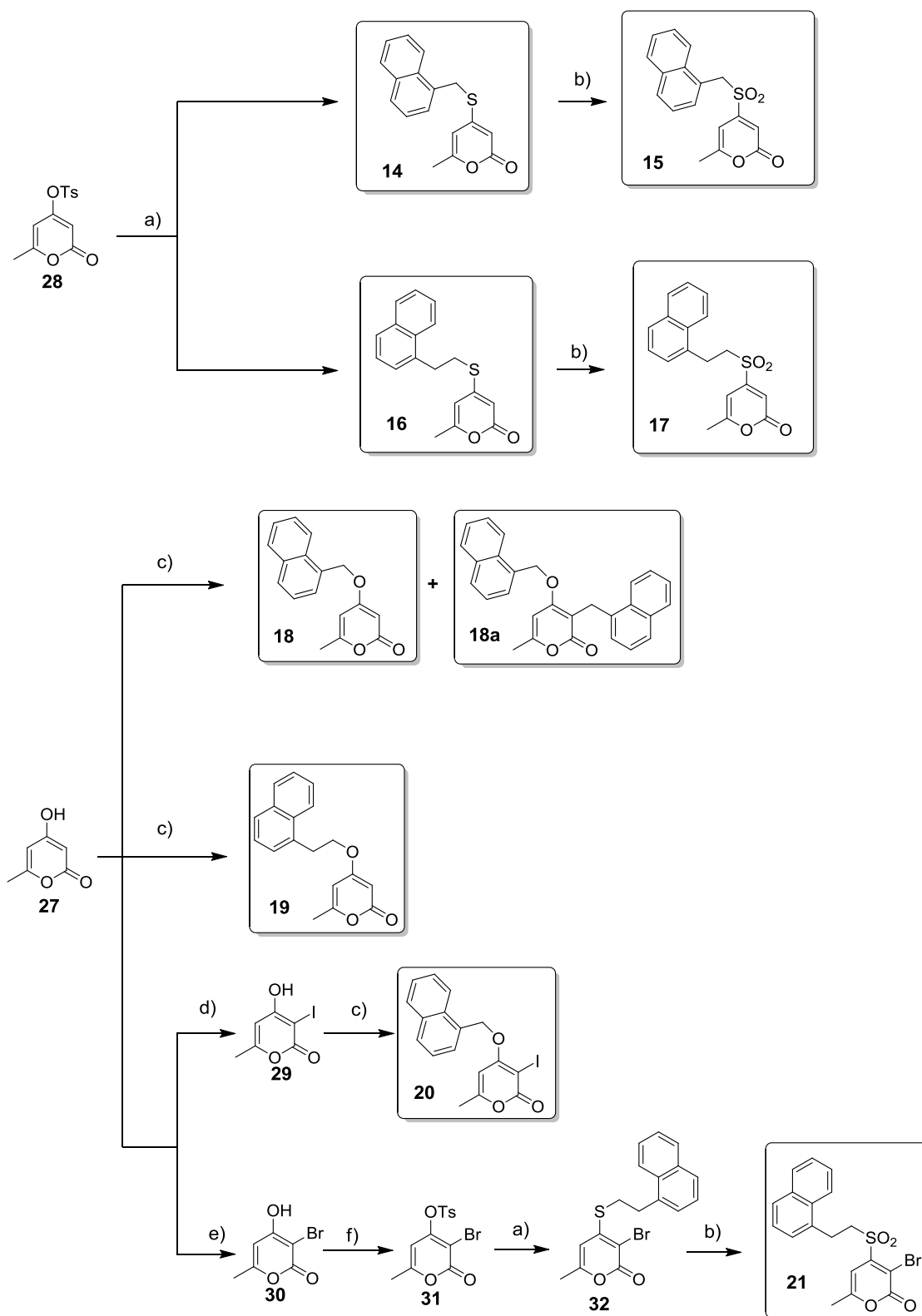
Entry	Chemical Structure	Molecular Formula M.W.	E_{Docking} AutoDock (Kcal/mol)	Ligand Efficiency	E_{Docking} Molegro Score (Rerankin)	Calculated Log P	ADME Prediction	
							HIA (%)	<i>In vitro</i> PPB (%)
26		C ₁₉ H ₁₈ O ₄ S 342.41	-10.63	0.44	-143 (-114)	3.1±0.7	98	96
Reference Compounds								
	α-APA 	C ₁₇ H ₁₆ Cl ₂ N ₂ O ₂ 351.23	-8.93	0.39	-132 (-104)	3.8±0.5	95	86
	Calanolide A 	C ₂₂ H ₂₆ O ₅ 370.48	-10.29	0.38	-121 (-66)	4.2±0.4	98	95
	Nevirapine 	C ₁₅ H ₁₄ N ₄ O 266.30	-8.25	0.41	-104 (-80)	1.7±0.6	96	66
	Efavirenz 	C ₁₄ H ₉ ClF ₃ NO ₂ 315.67	-8.61	0.41	-139 (-119)	4.0±0.8	96	95
	Etravirine 	C ₂₂ H ₁₈ N ₆ 366.42	-10.39	0.37	-151 (-74)	4.4±1.0	95	95

3.2. Chemical synthesis and structural characterization of the new molecules

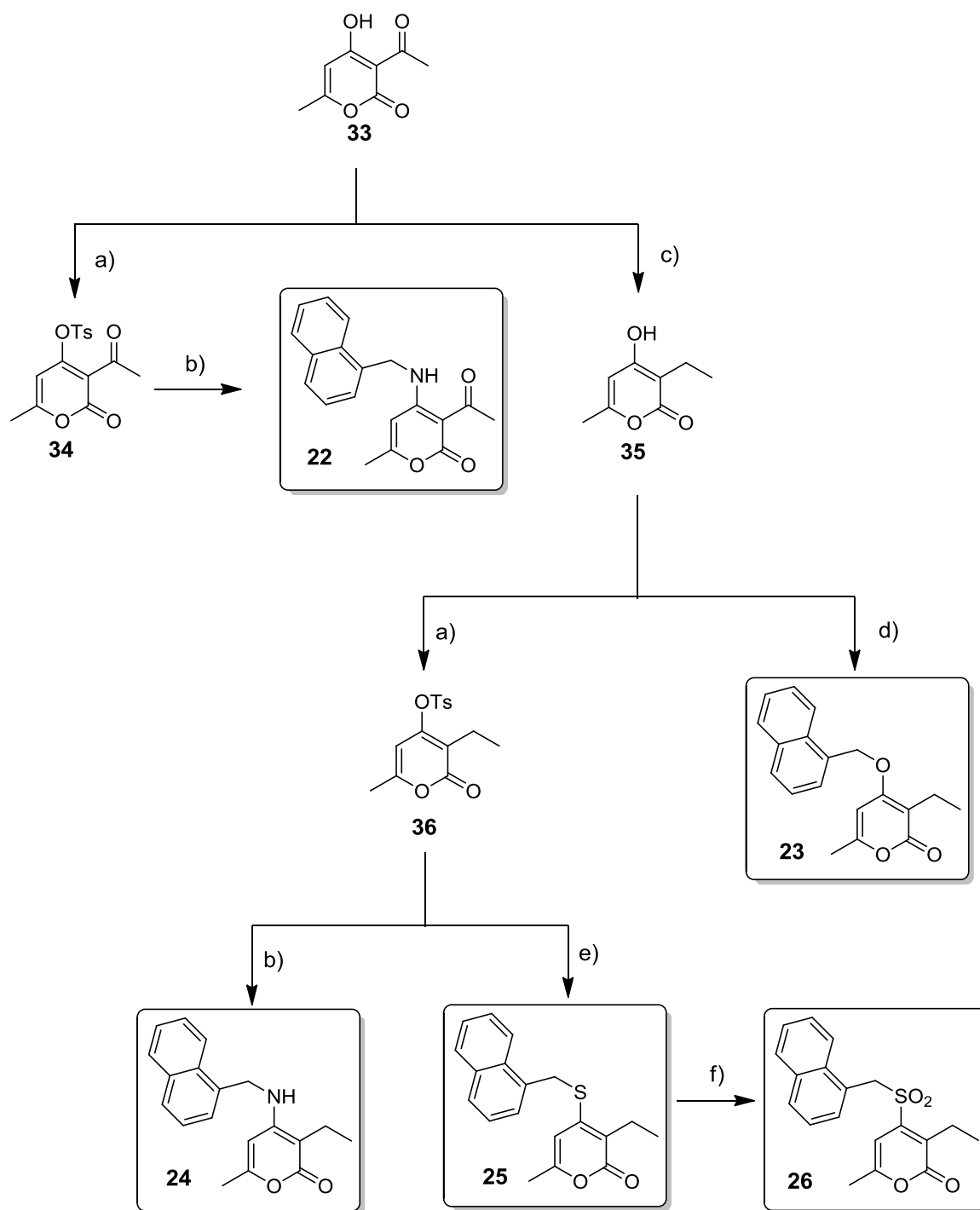
Compounds **1-13** and **28** with general structure as in figure 3.2 were synthesized as reported in scheme 3.1, **14-21** according to scheme 3.2 and **22-26** as illustrated in scheme 3.3.



Scheme 3.1. Chemical synthesis of compounds **1-13**. *Reagents and conditions:* a) TsCl (1.1 eq)/ Et₃N(1.5 eq)/CH₂Cl₂ 0°C→r.t., 24h, 90% yield; b) suitable (aryl)alkyl amine (1.1 eq), Et₃N(1.5eq.) EtOH r.t., 60h, 50-55% yield; c) acyl chloride (1.2 eq)/ Py (2 eq)/ CH₂Cl₂ 0°C→r.t., 24h 85-95% yield; d) acyl chloride (1.2 eq)/ (2 Et₃N eq)/ CH₂Cl₂ 0°C→r.t., 24h, 25-84% yield.



Scheme 3.2. Chemical synthesis of compounds **14-21**. *Reagents and conditions:* a) NaSH in EtOH r.t., 2h, suitable (aryl)alkyl bromide (1 eq), DBU (1.5eq.) C₆H₆ r.t., 18 h, 40-86% yield; b) UHP / HCOOH 85% r.t., 4h, 100% yield; c) suitable (aryl)alkyl bromide (1.1 eq), K₂CO₃, KI, acetone reflux 20h, 40-60% yield; d) I₂/AgNO₃/MeOH under N₂ at r.t. in the dark for 5h, 85% yield; e) Br₂ /CH₂Cl₂ 3h, 66% yield; f) TsCl (1.1 eq)/ Et₃N(1.5 eq)/CH₂Cl₂ 0°C→r.t. 24h, 90% yield).

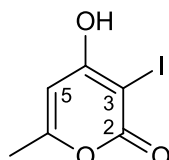


Scheme 3.3. Chemical synthesis of compounds **22-26**. *Reagents and conditions:* a) TsCl (1.1 eq)/ Et₃N (1.5 eq)/ CH₂Cl₂ 0°C → r.t., 24h, 90% yield; b) naphthalen-1-ylmethanamine (1.1 eq), Et₃N (1.5 eq.) EtOH r.t. 60h, 55% yield; c) Et₃SiH/LiClO₄/CF₃COOH r.t. 60 h 90% yield; d) 1-(bromomethyl)naphthalene (1.1 eq), K₂CO₃, KI, acetone reflux 20h, 60% yield; e) NaSH in EtOH r.t. 2h, 1-(bromomethyl)naphthalene (1.2 eq), DBU (1.5 eq.) C₆H₆ r.t., 18 h, 80% yield; f) UHP / HCOOH 85% r.t. 5h, 100% yield.

3.2.1. Precursors **29**, **30** and **35**

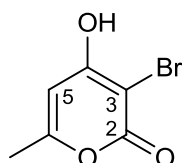
Compounds **29** and **30** (Scheme 3.2) and **35** (Scheme 3.3) were prepared and characterized as described below.

Synthesis and structural characterization of 4-hydroxy-3-iodo-6-methyl-2H-pyran-2-one (**29**)



A mixture of 4-hydroxy-6-methyl-2H-pyran-2-one (**27**, Scheme 3.1), (1.26 g, 10 mmol) silver nitrate (1.71 g, 10 mmol), and iodine (2.80 g, 11 mmol) in methanol (65 mL) was stirred overnight at room temperature under nitrogen atmosphere. The formed yellow precipitate of silver iodide was filtered off and washed with methanol. The methanol was removed *in vacuo*; the solid residue was suspended in chloroform (30 mL) for several minutes to remove the iodine in excess and then filtered. The yellow solid corresponds to the product **29** (2.15 g, 85 % yield). M.p. 203-204°C. ¹H NMR (400 MHz, CD₃OD) δ(ppm): 6.04 (s, 1H, H-5), 2.25 (s, 3H, CH₃). EI-MS *m/z* (%): 252 ([M⁺], 100), 224 (38), 168 (46); HR(EI)MS: 251.92807±0.0030 (C₆H₅IO₃, calcd. 251.92835).

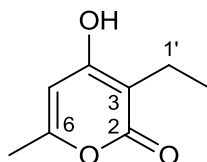
Synthesis and structural characterization of 4-hydroxy-3-bromo-6-methyl-2H-pyran-2-one (**30**)



To a solution of 4-hydroxy-6-methyl-2H-pyran-2-one (**27**), (1.26 g, 10 mmol) in CH₂Cl₂ (60 mL) a solution of bromine (600μL, 11 mmol) in CH₂Cl₂ (6 mL) was added slowly. The mixture was stirred at room temperature in the dark for 3 hours monitoring by TLC (ethyl acetate 100%). Dichloromethane was removed *in vacuo* and the residue was recrystallized from ethanol to give pure **30** (1.9 g, 93% yield) as pale yellow crystals. M.p. 214-215 (Lit. 214-217; De March, 1985). ¹H NMR (400 MHz, CD₃OD) δ(ppm): 6.09 (s, 1H, H-5), 2.25 (s,

3H, CH₃). ESI-MS (positive mode): m/z 205 ([M+ H]⁺), 229 ([M + Na]⁺). The data are consistent with the ones reported by De March, 1985.

Synthesis and structural characterization of 3-ethyl-4-hydroxy-6-methyl-2H-pyran-2-one (35)



Dehydroacetic acid (**33**, Scheme 3.3), (2.0 g, 12 mmol), triethylsilane (7.6 mL, 48 mmol) and LiClO₄ (13 mg, 0.12 mmol) were dissolved in trifluoroacetic acid (35 mL) and stirred at room temperature for 60 hours monitoring by TLC (hexane/ethyl acetate= 1:1). The solvent was evaporated *in vacuo* and the two phase-residue was put into a separating funnel to separate the lower phase, which was treated with methanol to give a white precipitate. After filtration, it was dried to give **35** which was used without further purification (1.6 g, 86% yield). M.p. 186°C (Lit.: 187°C; Lokot, 1999). ¹H NMR (400 MHz, CD₃OD) δ(ppm): 6.00 (s, 1H, H-5), 2.41 (q, $J=7.4$ Hz, 2H, H-1'), 2.22 (s, 3H, CH₃), 1.05 (t, $J=7.4$ Hz, 3H, H-2'). ¹³C NMR (100 MHz, CD₃OD) δ (ppm): 167.24 (C-4), 165.98 (C-2), 160.26 (C-6), 103.44 (C-3), 100.16 (C-5), 17.91 (CH₃), 15.46 (C-1'), 11.19 (C-2'). EI-MS m/z (%): 154 ([M⁺], 100); HR(EI)MS: 154.06280±0.0030 (C₈H₁₀O₃, calcd. 154.06299). The data are consistent with the ones reported by Lokot, 1999.

3.2.2. Tosylate precursors

Compounds **28**, **31** and **36**, later used in the synthetic sequences reported in schemes 3.1, 3.2 and 3.3, were prepared and characterized as described below.

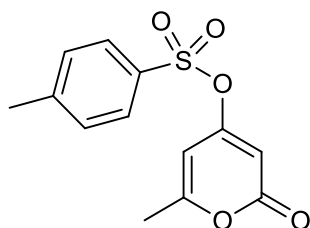
3.2.2.1. General procedure of synthesis

4-Hydroxy-6-methyl-2H-pyran-2-one(**27**), or 3-ethyl-4-hydroxy-6-methyl-2H-pyran-2-one (**26**), or 3-bromo-4-hydroxy-6-methyl-2H-pyran-2-one (**31**) (10 mmol) and tosyl chloride (2.10g, 11 mmol) were dissolved in CH₂Cl₂ (75 mL) at 0°C. Et₃N (4.20 mL, 30 mmol) was added and the reaction mixture was left under stirring at room temperature for 24 hours

monitoring by TLC (hexane/ ethyl acetate = 1:1 for **28**, or 6:4 for **31**, or 7:3 for **36**). CH₂Cl₂ (125 mL) was added and the organic phase was washed with water (70 mL) and brine (70 mL). The organic phase was dried over anhydrous Na₂SO₄. After concentration *in vacuo*, the crude products were purified by recrystallization or liquid chromatography on SiO₂ column.

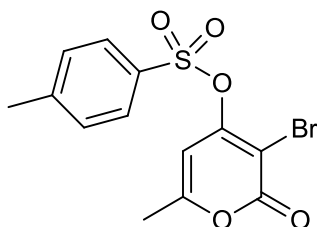
3.2.2.2. Spectroscopic and mass spectrometric data

6-Methyl-2-oxo-2H-pyran-4-yl 4-tosylate (**28**)



Yield 90 %. Pale pink crystals (from EtOH), m.p. 101-102 °C (Lit.: 101.2 – 102.0 °C; Djakovitch, 2004). ¹H NMR (400 MHz, CDCl₃) δ (ppm): 8.04 (d, *J* = 8.4Hz, 2H), 7.38 (d, *J* = 8.4 Hz, 2H), 5.99 (s, 1H), 5.80 (s, 1H), 2.47 (s, 3H), 2.23 (s, 3H). ¹³C NMR (100 MHz, CDCl₃) δ (ppm): 164.4, 163.0, 162.1, 146.8, 131.8, 130.4(2C), 128.5(2C), 100.9, 100.8, 21.9, 20.3. EI-MS: *m/z* (%) 280 ([M⁺], 6), 155 (43), 132 (23), 91(100); HR(EI)MS: 280.0403±0.0030 (C₁₃H₁₂O₅S, calcd. 280.0406). The data are consistent with the ones reported by Djakovitch, 2004.

3-Bromo-6-methyl-2-oxo-2H-pyran-4-yl 4-tosylate (**31**)

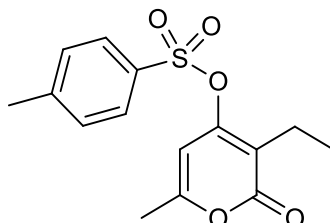


Yield 95%. Pale yellow crystals (from EtOH), m.p. 165-166°C (Lit. 165-166°C; Lei, 2011). ¹H NMR (400 MHz, CDCl₃) δ(ppm): 7.86 (d, *J* = 8.0 Hz, 2H), 7.38 (d, *J* = 8.0 Hz, 2H), 6.43 (s, 1H), 2.46 (s, 3H), 2.28 (s, 3H). ¹³C NMR (100 MHz, CDCl₃) δ (ppm): 162.2, 161.9, 159.0,

147.2, 130.6, 130.4, 128.7, 101.6, 99.7, 22.3, 20.2. ESI-MS (positive mode): m/z 358 ($[M+H]^+$), 380 ($[M+Na]^+$).

The data are consistent with the ones reported by Lei, 2011.

3-Ethyl-6-methyl-2-oxo-2H-pyran-4-yl-tosylate (36)



Yield 92%. White solid. 1H NMR (400 MHz, $CDCl_3$) δ (ppm): 7.82 (d, $J = 8.3$ Hz, 2H), 7.38 (d, $J = 8.3$ Hz, 2H), 6.22 (s, 1H), 2.46 (s, 3H), 2.23 (s, 3H), 2.17 (q, $J = 7.5$ Hz, 2H), 0.89 (t, $J = 7.5$ Hz, 3H). ESI-MS (positive mode): m/z 309 ($[M+H]^+$), 331 ($[M+Na]^+$); MS/MS (309): m/z 155 ($[M+H-C_8H_9O_3]^+$).

3.2.3. New amino-pyrones 1-6 and 22-23

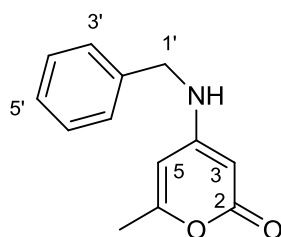
Compounds **1-6** and **22-23** (Schemes 3.1 and 3.3 respectively) were prepared and characterized as described below.

3.2.3.1. General procedure of synthesis

A mixture containing 6-methyl-2-oxo-2H-pyran-4-yl 4-tosylate (**28**) or 3-acetyl-6-methyl-2-oxo-2H-pyran-4-yl 4-tosylate (**34**), or 3-ethyl-6-methyl-2-oxo-2H-pyran-4-yl 4-tosylate (**36**) (1 mmol), the suitable (aryl)alkyl amine (1.1 mmol) and Et_3N (210 μL , 1.5 mmol) in absolute ethanol (60 mL) was stirred at room temperature for 60 hours monitoring by TLC (hexane/ethyl acetate/ $Et_3N = 20:79:1$). After concentration *in vacuo*, the crude residues were purified by column chromatography using hexane/ethyl acetate by gradient elution.

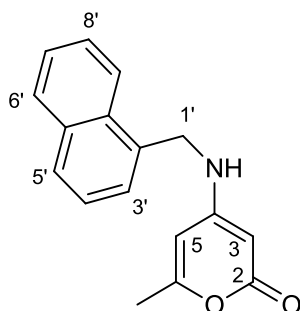
3.2.3.2. Spectroscopic and mass spectrometric data

4-(Benzylamino)-6-methyl-2H-pyran-2-one (1)



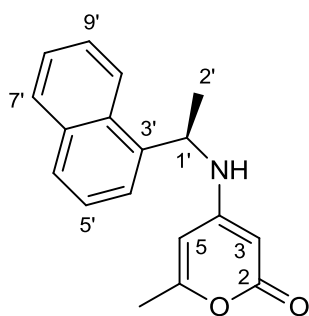
Yield 55%. Viscous transparent oil. ^1H NMR (400 MHz, CDCl_3) δ (ppm): 7.47 – 7.14 (m, 5H, C_6H_5 -), 5.57 (s, 1H, H-3), 5.16 (br s, 1H, NH), 4.99 (s, 1H, H-5), 4.27 (d, $J = 5.2$ Hz, 2H, H-1'), 2.12 (s, 3H, CH_3 -C(6)). ^{13}C NMR (100 MHz, CDCl_3) δ (ppm): 165.55 (C-4), 161.31 (C-2 and C-6), 136.72 (C-2'), 129.00 (C-4' and C-6'), 127.92 (C-3' and C-7'), 127.53 (C-5'), 99.22 (C-5), 81.11 (C-3), 46.80 (C-1'), 19.91 (CH_3 -C(6)). EI-MS m/z (%): 215 ($[\text{M}^+]$, 40), 187 (30), 106(22); HR(EI)MS: 215.09448 \pm 0.0030 ($\text{C}_{13}\text{H}_{13}\text{NO}_2$, calcd. 215.09463). The data are consistent with the ones reported by McLaughlin, 2002.

6-Methyl-4-((naphthalen-1-ylmethyl)amino)-2H-pyran-2-one (2)



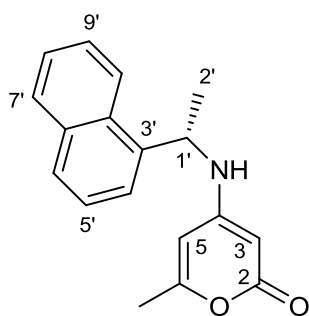
Yield 55%. Light yellow viscous oil. ^1H NMR (400 MHz, CDCl_3) δ (ppm): 7.84 (dd, $J = 9.4$, 2.1 Hz, 2H, H-6' and H-9'), 7.77 (t, $J = 5.0$ Hz, 1H, H-5'), 7.49 (d quint, $J = 7.6$, 1.5 Hz, 2H, H-7' and H-8'), 7.38 (dd, $J = 7.0$, 5.7 Hz, 2H, H-3' and H-4'), 5.59 (br s, 1H, NH), 5.58 (s, 1H, H-5), 4.96 (s, 2H, H-3), 4.60 (d, $J = 4.9$ Hz, 2H, H-1'), 2.04 (s, 3H, CH_3 -C(6)). ^{13}C NMR (100 MHz, CDCl_3) δ (ppm): 165.58 (C-4) 161.37 (C-2 and C-6), 133.64 (C-5'a and C-9'a), 131.47 (C-2') 129.10 (C-9'), 128.55 (C-5'), 126.17 (C-7' and C8'), 125.67 (C-3' and C4'), 98.92 (C-5), 81.05 (C-3), 44.63 (C-1'), 20.03 (CH_3 -C(6)). EI-MS m/z (%): 265 ($[\text{M}^+]$) (34), 237 (9), 141(100); HR(EI)MS: 265.11007 \pm 0.0030 ($\text{C}_{17}\text{H}_{15}\text{NO}_2$, calcd. 265.11028).

(R)-6-Methyl-4-((1-(naphthalen-1-yl)ethyl)amino)-2H-pyran-2-one (3)



Yield 50%. White solid (from hexane/ ethyl acetate), m.p. 240-241°C. $[\alpha]_D^{20} = -121^\circ$ (c 0.15, MeOH) $^1\text{H NMR}$ (400 MHz, CDCl_3) δ (ppm): 7.94 (dd, $J = 8.3, 1.4$ Hz, 1H, H-7'), 7.89 (dd, $J = 8.3, 1.4$ Hz, 1H, H-10'), 7.79 (d, $J = 8.4$ Hz, 1H, H-6'), 7.53 (m, = 2H, H-8' and H-9'), 7.44 (m, 2H, H-4' and H-5'), 5.52 (s, 1H, H-5), 5.29 (quint. $J = 5.1$ Hz, 1H, H-1') 4.87 (s, 1H, H-3), 4.79 (br s, 1H, NH), 2.12 (s, 3H, $\text{CH}_3\text{-C}(6)$), 1.68 (d, $J = 5.1$ Hz, 3H, H-2'). $^{13}\text{C NMR}$ (100 MHz, CDCl_3) δ (ppm): 165.55 (C-4) 161.35 (C-6), 161.23 (C-2), 137.10 (C-3'), 133.38 (C-10'a), 130.27 (C-6'a), 128.80 (C-10'), 128.60 (C-6'), 126.14 (C-8' and C9'), 125.34 and 122.07 (C4' and C5'), 121.87 (C-7'), 98.61 (C-5), 81.92 (C-3), 48.63 (C-1'), 21.85 (C-2'), 19.51 ($\text{CH}_3\text{-C}(6)$). ESI-MS (positive mode): m/z 280 ($[\text{M} + \text{H}]^+$), 302 ($[\text{M} + \text{Na}]^+$); MS/MS (280): m/z 155 ($[\text{M} + \text{H} - \text{C}_6\text{H}_7\text{NO}_2]^+$), 126 ($[\text{M} + \text{H} - \text{C}_{12}\text{H}_{11}]^+$). EI-MS m/z (%): 279 ($[\text{M}^+]$, 26), 155(100); HR(EI)MS: 279.12630 \pm 0.0030 ($\text{C}_{18}\text{H}_{17}\text{NO}_2$, calcd. 279.12593).

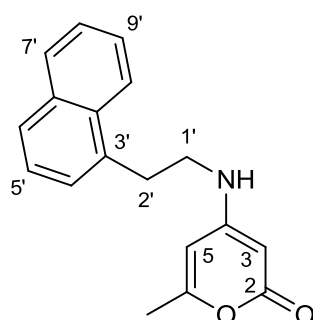
(S)-6-Methyl-4-((1-(naphthalen-1-yl)ethyl)amino)-2H-pyran-2-one (4)



Yield 50%. White solid (from hexane/ethyl acetate), m.p. 240-241°C. $[\alpha]_D^{20} = +120^\circ$ (c 0.14, MeOH), $^1\text{H NMR}$ (400 MHz, CDCl_3) δ (ppm): 7.94 (dd, $J = 8.3, 1.4$ Hz, 1H, H-7'), 7.89 (dd, $J = 8.3, 1.4$ Hz, 1H, H-10'), 7.79 (d, $J = 8.4$ Hz, 1H, H-6'), 7.53 (m, 2H, H-8' and H-9'), 7.44 (m, 2H, H-4' and H-5'), 5.52 (s, 1H, H-5), 5.29 (quint. $J = 5.1$ Hz, 1H, H-1') 4.87 (s, 1H, H-3), 4.79 (br s, 1H, NH), 2.12 (s, 3H, $\text{CH}_3\text{-C}(6)$), 1.68 (d, $J = 5.1$ Hz, 3H, H-2'). $^{13}\text{C NMR}$ (100 MHz, CDCl_3) δ (ppm): 165.55 (C-4) 161.35 (C-6), 161.23 (C-2), 137.10 (C-3'), 133.38

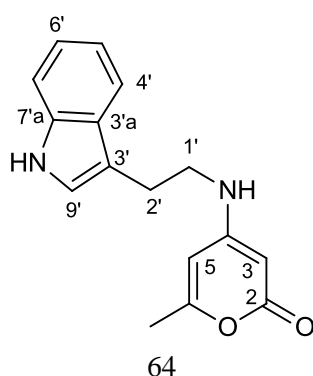
(C-10'a), 130.27 (C-6'a), 128.80 (C-10'), 128.60 (C-6'), 126.14 (C-8' and C9'), 125.34 and 122.07 (C4' and C5'), 121.87 (C-7'), 98.61 (C-5), 81.92 (C-3), 48.63 (C-1'), 21.85 (C-2'), 19.51 (CH₃-C-6). ESI-MS (positive mode): m/z 280 ([M+ H]⁺), 302 ([M + Na]⁺); MS/MS (280): m/z 155 ([M + H -C₆H₇NO₂]⁺), 126 ([M + H -C₁₂H₁₁]⁺). EI-MS m/z (%): 279 ([M⁺], 14), 155(59); HR(EI)MS: 279.12623 ±0.0030 (C₁₈H₁₇NO₂, calcd. 279.12593).

6-Methyl-4-((2-(naphthalen-1-yl)ethyl)amino)-2H-pyran-2-one (5)



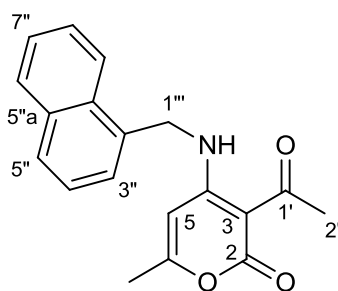
Yield 53 %. White solid (from hexane/ethyl acetate), m.p. 60-63°C. ¹H NMR (400 MHz, CDCl₃) δ(ppm): 7.97 (d, J = 7.9, 1H, H-10'), 7.87 (dd, J = 7.4, 1.8 Hz, 1H, H-10'), 7.77 (d, J = 8.2 Hz, 1H, H-6'), 7.53 (d quint, J = 7.6, 1.8 Hz, 2H, H-8' and H-9'), 7.41 (t, J = 7.1 Hz, 1H, H-5'), 7.30 (d, J = 7.1 Hz, 1H, H-4') 5.40 (s, 1H, H-5), 5.05 (s, 1H, H-3), 4.64 (br s, 1H, NH), 3.52 (q, J = 6.8 Hz, 2H, H-2'), 3.36 (t, J = 6.8 Hz, 2H, H-1') 2.10 (s, 3H, CH₃-C(6)). ¹³C NMR (100 MHz, CDCl₃) δ (ppm): 165.21 (C-4) 161.28 (C-6 and C-2), 134.22 (C-3'), 131.74 (C-10'a), 129.06 (C-7'), 128.96 (C-6'a), 127.58 (C-6'), 126.57 (C-4') 126.02 (C-8' and C9'), 125.48 (C5'), 122.99 (C-10'), 98.68 (C-5), 80.71 (C-3), 50.51 (C-1'), 42.36 (C-2'), 19.81 (CH₃-C(6)). ESI-MS (positive mode): m/z 280 ([M+ H]⁺), 302 ([M + Na]⁺); MS/MS (280): m/z 155 ([M + H -C₆H₇NO₂]⁺), 126 ([M + H -C₁₂H₁₁]⁺). EI-MS m/z (%): 279 ([M⁺], 19), 154(76); HR(EI)MS: 279.12584 ±0.0030 (C₁₈H₁₇NO₂, calcd. 279.12593).

4-((2-(1H-indol-3-yl)ethyl)amino)-6-methyl-2H-pyran-2-one (6)



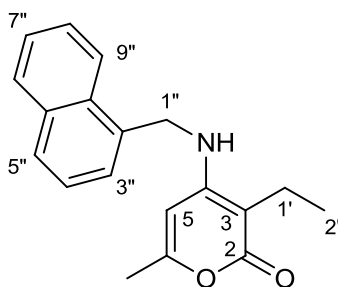
Yield 52 %. White solid (from hexane/ethyl acetate), m.p. 252-153°C. ¹H NMR (400 MHz, CDCl₃) δ(ppm): 8.10 (br s, 1H, indole NH) 7.55 (d, *J* = 7.9, 1H, H-4'), 7.38 (d, *J* = 8.1, 1H, H-7'), 7.21 (t, *J* = 7.5 Hz, 1H, H-6'), 7.12 (t, *J* = 7.3 Hz, 1H, H-5'), 7.02 (s, 1H, H-9'), 5.38 (s, 1H, H-5), 5.02 (s, 1H, H-3), 4.64 (br s, 1H, NH), 3.43 (q, *J* = 6.8 Hz, 2H, H-2'), 3.05 (t, *J* = 6.8 Hz, 2H, H-1') 2.08 (s, 3H, CH₃-C(6)). ¹³C NMR (100 MHz, CDCl₃) δ (ppm): 165.20 (C-4), 161.28 (C-6 and C-2), 136.44 (C-7'a), 126.74 (C-3'a), 122.64 (C-9'), 122.45 (C-6'), 120.04 (C-5'), 118.35 (C-4'), 111.85 (C-7'), 111.54 (C-3'), 98.70 (C-5), 80.69 (C-3), 43.61 (C-1'), 25.01 (C-2'), 19.90 (CH₃-C(6)). EI-MS *m/z* (%): 279 ([M⁺], 6), 130(43); HR(EI)MS: 268.12074 ±0.0030 (C₁₆H₁₆N₂O₂, calcd. 268.12118).

3-Acetyl-6-methyl-4-((naphthalen-1-ylmethyl)amino)-2H-pyran-2-one (22)



Yield 50%. White solid (from hexane/ethyl acetate), m.p. 199-200°C. ¹H NMR (400 MHz, CDCl₃) δ(ppm): 11.96 (br s, 1H, NH), 7.90 (t, *J* = 8.1 Hz, 2H, H-6'' and H-9''), 7.84 (d, *J* = 8.2 Hz, 1H, H-5''), 7.57 (m, 2H, H-7'' and H-8''), 7.44 (t, *J* = 7.5 Hz, 1H, H-4''), 7.35 (d, *J* = 7.5 Hz, 1H, H-3''), 5.85 (s, 1H, H-5), 4.95 (d, *J* = 5.7 Hz, 2H, H-1''), 2.62 (s, 3H, CH₃-C(6)), 2.14 (s, 3H, H-2'). ¹³C NMR (100 MHz, CDCl₃) δ (ppm): 165.49 (C-4), 162.46 (C-2 and C-6), 133.86 (C-5''a), 131.06 (C-2''), 130.61 (C-9''a), 129.12 (C-5''), 128.82 (C-6''), 126.22 (C-7'' and C-8''), 125.46 (C-4''), 124.90 (C-3''), 122.20 (C-9''), 94.44 (C-3 and C-5), 44.88 (C-1''), 32.47 (C-2'), 20.90 (CH₃-C(6)). EI-MS *m/z* (%): 307 ([M⁺], 61), 292 (12), 264 (22), 180 (21), 160 (20), 141 (100); HR(EI)MS: 307.12042 ±0.0030 (C₁₉H₁₇NO₃, calcd. 307.12084).

3-Ethyl-6-methyl-4-((naphthalen-1-ylmethyl)amino)-2H-pyran-2-one (24)



Yield 50 %. White solid (from hexane/ethyl acetate), m.p. 204-205 . ^1H NMR (400 MHz, CDCl_3) δ (ppm): 7.92 (br d, $J = 7.0$ Hz, 2H, H-6'' and H-9''), 7.85 (d, $J = 8.1$ Hz, 1H, H-5''), 7.56 (m, 2H, H-7'' and H-8''), 7.46 (t, $J = 7.2$ Hz, 1H, H-4''), 7.40 (d, $J = 6.8$ Hz, 1H, H-3''), 5.83 (s, 1H, H-5), 4.83 (d, $J = 5.3$ Hz, 2H, H-1''), 4.73 (br s, 1H, NH), 2.36 (q, $J = 7.5$ Hz, 2H, H-1'), 2.15 (s, 3H, $\text{CH}_3\text{-C}(6)$), 1.02 (t, $J = 7.5$ Hz, 3H, H-2'). ^{13}C NMR (100 MHz, CDCl_3) δ (ppm): 164.62 (C-4), 160.69 (C-2 and C-6), 133.85 (C-9''a) 132.27 (C-2''), 130.77(C-5''a), 129.22 (C-6''), 128.75 (C-5''), 126.19 (C-7'' and C-8''), 125.28 (C-3'' and C-4''), 122.54 (C-9''), 96.63 (C-3), 95.06 (C-5), 44.77 (C-1''), 16.73 (C-1'), 20.21 ($\text{CH}_3\text{-C}(6)$), 12.39 (C-2'). EI-MS m/z (%): 293 ($[\text{M}^+]$, 20), 141(100); HR(EI)MS: 293.14176 \pm 0.0030 ($\text{C}_{19}\text{H}_{19}\text{NO}_2$, calcd. 293.14158).

3.2.4. New dichloroketo-amino compounds

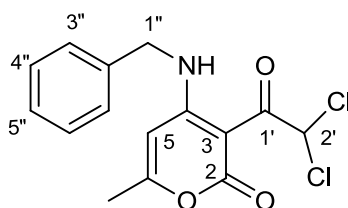
Compounds **7**, **8a**, **11-13** (Scheme 3.1) were prepared and characterized as described below.

3.2.4.1. General procedure of synthesis

To a solution of compound **1-6** (0.2 mmol) dissolved in anhydrous CH_2Cl_2 (5 mL) anhydrous pyridine (90 μL , 1 mmol) was added and the solution cooled at 0°C for 30 minutes. Dichloroacetyl chloride (30 μL , 0.3 mmol) was slowly added at this temperature. The mixture was stirred at room temperature for 24 hours monitoring by TLC (hexane / ethyl acetate = 6:4). After concentration *in vacuo*, each crude product was purified by preparative TLC (PLC) using hexane/ethyl acetate = 6:4 as eluent.

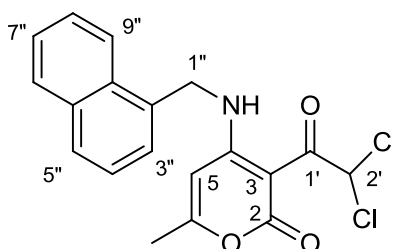
3.2.4.2. Spectroscopic and mass spectrometric data

4-(Benzylamino)-3-(2,2-dichloroacetyl)-6-methyl-2H-pyran-2-one (7)



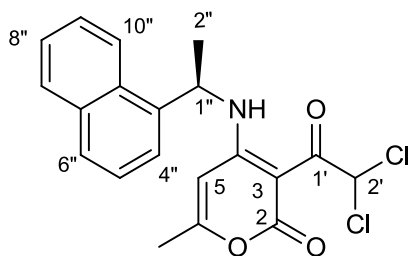
Yield 89%. White solid (from hexane/ ethyl acetate), m.p. 94-95 °C. ^1H NMR (400 MHz, CDCl_3) δ (ppm): 11.43 (br s, 1H, NH), 7.67 (s, 1H, H-2'), 7.38 (m, 3H, H-4'', H-5'' and H-6''), 7.26 (m, 2H, H-3'' and H-7''), 5.93 (s, 1H, H-5), 4.57 (d, $J = 5.6$ Hz, 2H, H-1''), 2.21 (s, 3H, $\text{CH}_3\text{-C}(6)$). ^{13}C NMR (100 MHz, CDCl_3) δ (ppm): 188.44 (C-1'), 166.86 (C-2 and C-6), 163.25 (C-4), 135.20 (C-2''), 129.15 (C-4'', C-5'' and C-6''), 126.97 (C-3'' and C-7''), 95.31 (C-5), 90.41 (C-3) 69.81 (C-2'), 47.02 (C-1''), 20.62 ($\text{CH}_3\text{-C}(6)$). EI-MS m/z (%): 325 ($[\text{M}^+]$, 4), 290 (16), 254 (23), 242 (86); HR(EI)MS: 325.02575 \pm 0.0030 ($\text{C}_{15}\text{H}_{13}\text{Cl}_2\text{NO}_3$, calcd. 325.02725).

3-(2,2-Dichloroacetyl)-6-methyl-4-((naphthalen-1-ylmethyl)amino)-2H-pyran-2-one (8a)



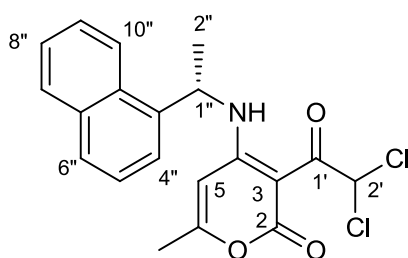
Yield 92%. White solid (from chloroform), m.p. 201-202 °C. ^1H NMR (400 MHz, CDCl_3) δ (ppm): 11.47 (br s, 1H, NH), 7.93 (d, $J = 7.4$ Hz, 1H) and 7.87 (d, $J = 8.1$ Hz, 2H) [H-5'', H-6'' and H-9''], 7.66 (s, 1H, H-2'), 7.58 (d quint, $J = 7.6, 1.8$ Hz, 2H, H-7'' and H-8''), 7.46 (t, $J = 7.4$ Hz, 1H, H-4''), 7.37 (d, $J = 6.9$ Hz, 1H, H-3''), 6.00 (s, 1H, H-5), 5.00 (d, $J = 5.5$ Hz, 2H, H-1''), 2.23 (s, 3H, $\text{CH}_3\text{-C}(6)$). ^{13}C NMR (100 MHz, CDCl_3) δ (ppm): 188.41 (C-1'), 166.62 (C-6), 162.92 (C-4), 161.12 (C-2), 134.77 (C-2''), 131.00 (C-5''a), 130.23 (C-9''a), 129.33, 121.82 (C-5'', C-6'' and C-9''), 126.50 (C-7'' and C-8''), 125.46 (C-3'' and C-4''), 94.86 (C-3 and C-5), 69.59 (C-2'), 45.47 (C-1''), 20.68 ($\text{CH}_3\text{-C}(6)$). EI-MS m/z (%): 375 ($[\text{M}^+]$, 8), 264 (6), 141 (100); HR(EI)MS: 375.04267 \pm 0.0030 ($\text{C}_{19}\text{H}_{15}\text{Cl}_2\text{NO}_3$, calcd. 375.04290).

(R)-3-(2,2-Dichloroacetyl)-6-methyl-4-((1-(68aphthalene-1-yl)ethyl)amino)-2H-pyran-2-one (11)



Yield 95%. White solid (from hexane/ ethyl acetate), m.p. 74-75°C. $[\alpha]_D^{20} = -376^\circ$ (c 0.16, MeOH) $^1\text{H NMR}$ (400 MHz, CDCl_3) δ (ppm): 11.47 (br s, 1H, NH), 7.99 (d, $J = 8.4$ Hz, 1H, H-10''), 7.94 (d, $J = 7.8$ Hz, 1H, H-7''), 7.82 (d, $J = 8.2$ Hz, 1H, H-6''), 7.71 (s, 1H, H-2'), 7.59 (m, 2H, H-8'' and H-9''), 7.46 (t, $J = 7.9$ Hz, 1H, H-5''), 7.37 (d, $J = 6.9$ Hz 1H, H-4''), 5.58 (s, 1H, H-5), 5.51 (q, $J = 6.6$ Hz, 1H, H-1''), 2.01 (s, 3H, $\text{CH}_3\text{-C}(6)$), 1.79 (d, $J = 6.6$ Hz, 3H, H-2''). $^{13}\text{C NMR}$ (100 MHz, CDCl_3) δ (ppm): 188.21 (C-1'), 166.72 (C-2 and C-6), 162.67 (C-4), 137.30 (C-3''), 134.10 (C-6''a and C-10''a), 129.38 (C-7''), 128.60 (C-6''), 126.49 (C-8'' and C-9''), 125.80 (C-5''), 122.37 (C-4''), 121.31 (C-10''), 95.43 (C-5), 90.53 (C-3), 69.70 (C-2'), 50.14 (C-1''), 23.01 (C-2''), 20.29 ($\text{CH}_3\text{-C}(6)$). EI-MS m/z (%): 389 ($[\text{M}^+]$, 2), 318 (68), 155 (100); HR(EI)MS: 389.05804 ± 0.0030 ($\text{C}_{20}\text{H}_{17}\text{Cl}_2\text{NO}_3$, calcd. 389.05855).

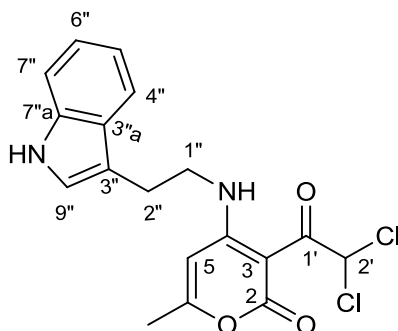
(S)-3-(2,2-Dichloroacetyl)-6-methyl-4-((1-(68aphthalene-1-yl)ethyl)amino)-2H-pyran-2-one (12)



Yield 93 %. White solid (from hexane/ ethyl acetate), m.p. 74-75°C. $[\alpha]_D^{20} = +400^\circ$ (c 0.14, MeOH). $^1\text{H NMR}$ (400 MHz, CDCl_3) δ (ppm): 11.47 (br s, 1H, NH), 7.99 (d, $J = 8.4$ Hz, 1H, H-10''), 7.94 (d, $J = 7.8$ Hz, 1H, H-7''), 7.82 (d, $J = 8.2$ Hz, 1H, H-6''), 7.71 (s, 1H, H-2'), 7.59 (m, 2H, H-8'' and H-9''), 7.46 (t, $J = 7.9$ Hz, 1H, H-5''), 7.37 (d, $J = 6.9$ Hz 1H, H-4''), 5.58 (s, 1H, H-5), 5.51 (q, $J = 6.6$ Hz, 1H, H-1''), 2.01 (s, 3H, $\text{CH}_3\text{-C}(6)$), 1.79 (d, $J = 6.6$ Hz, 3H, H-2''). $^{13}\text{C NMR}$ (100 MHz, CDCl_3) δ (ppm): 188.21 (C-1'), 166.72 (C-2 and C-6), 162.67 (C-4), 137.30 (C-3''), 134.10 (C-6''a and C-10''a), 129.38 (C-7''), 128.60 (C-6''), 126.49 (C-8'' and C-9''), 125.80 (C-5''), 122.37 (C-4''), 121.31 (C-10''), 95.43 (C-5), 90.53 (C-3), 69.70

(C-2'), 50.14 (C-1''), 23.01(C-2''), 20.29 (CH₃-C(6)). EI-MS *m/z* (%): 389 ([M⁺], 2), 318 (60), 155 (100); HR(EI)MS: 389.05819±0.0030 (C₂₀H₁₇Cl₂NO₃, calcd.389.05855).

4-((2-(1H-indol-3-yl)ethyl)amino)-3-(2,2-dichloroacetyl)-6-methyl-2H-pyran-2-one (13)



Yield 88 %. White solid. ¹H NMR (400 MHz, CDCl₃) δ(ppm): 11.17 (br s, 1H, NH), 8.11 (br s, 1H, indole NH), 7.65 (s, H-2'), 7.56 (d, *J* = 7.7 Hz, 1H, H-4''), 7.38 (d, *J* = 8.1 Hz, 1H, H-9''), 7.22 (t, *J* = 7.7 Hz, 1H, H-7''), 7.13 (m, 2H, H-5'' and 6''), 5.62 (s, 1H, H-5), 3.66 (q, *J* = 6.6 Hz, 2H, H-1''), 3.15 (t, *J* = 6.6 Hz, 2H, H-2''), 2.02 (s, 3H, CH₃-C(6)). ¹³C NMR (100 MHz, CDCl₃) δ (ppm): 188.70 (C-1'), 165.92 (C-6 and C-2), 162.91 (C-4), 136.39 (C-7''a), 126.67 (C-3''a), 123.12 (C-6''), 122.49 (C-7''), 119.54 (C-5''), 117.78 (C-4''), 111.33 (C-9''), 110.93 (C-3''), 94.95 (C-5), 90.17 (C-3), 69.30 (C-2'), 43.60 (C-1''), 25.08 (C-2''), 20.05 (CH₃-C(6)). EI-MS *m/z* (%): 378 ([M⁺], 6), 265 (14); HR(ESI)MS: 378.05292 ±0.0030 (C₁₈H₁₆Cl₂N₂O₃, calcd. 378.05380).

3.2.5. New amides 8b-10

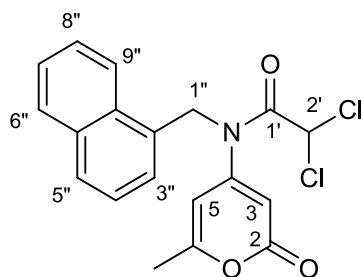
Compounds **8b**, **9** and **10** (Scheme 3.1) were prepared and characterized as described below.

3.2.5.1. General procedure of synthesis

To a solution of compound **1-6** (0.2 mmol) dissolved in anhydrous CH₂Cl₂ (5 mL) anhydrous DBU (1 mmol, 150 μL) was added and the mixture was cooled at 0°C for 30 minutes. Dichloroacetyl chloride (0.3 mmol, 30 μL) was slowly added at this temperature. The mixture was stirred at room temperature for 24 hours monitoring by TLC (hexane / ethyl acetate = 6:4). After concentration *in vacuo*, each crude product was purified by PLC using hexane/ethyl acetate = 6:4 as eluent.

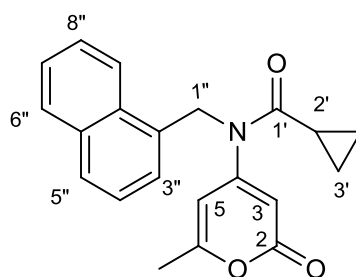
3.2.5.2. Spectroscopic and mass spectrometric data

2,2-Dichloro-*N*-(6-methyl-2-oxo-2H-pyran-4-yl)-*N*-(naphthalene-1-ylmethyl)- acetamide (8b)



Yield 70%. Viscous oil. ^1H NMR (400 MHz, CDCl_3) δ (ppm): 7.93 (d, $J=8.2$ Hz, 1H, H-9''), 7.89 (d, $J=7.7$ Hz, 1H, H-6''), 7.83 (d, $J=8.3$ Hz, 1H, H-5''), 7.56 (m, 2H, H-5'' and H-6''), 7.38 (t, $J=7.7$ Hz, 1H, H-4''), 7.22 (d, $J=7.1$ Hz, H-3''), 6.17 (s, 1H, H-2'), 5.78 and 5.81 (s, 1H respectively, H-3 and H-5), 2.19 (s, 3H, $\text{CH}_3\text{-C}(6)$). ^{13}C NMR (100 MHz, CDCl_3) δ (ppm): 164.07 (C-2 and C-6), 163.22 (C-4), 154.33 (C-1'), 133.78 (C-2'' and C-5''a), 130.35 (C-9''a), 129.92 (C-5''), 128.85 (C-6''), 126.46 (C-7'' and C-8''), 126.46 (C-3''), 124.93 (C-4''), 108.33 and 102.75 (C-3 and C5), 63.73 (C-2'), 50.54 (C-1''), 19.75 ($\text{CH}_3\text{-C}(6)$). EI-MS m/z (%): 375 ($[\text{M}^+]$, 6), 264 (5), 141(100); HR(EI)MS: 375.04189 \pm 0.0030 ($\text{C}_{19}\text{H}_{15}\text{Cl}_2\text{NO}_3$, calcd. 375.04290).

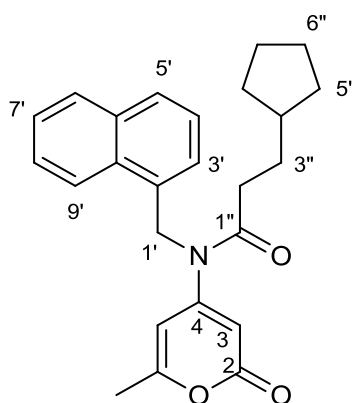
N-(6-Methyl-2-oxo-2H-pyran-4-yl)-*N*-(naphthalene-1-yl-methyl)cyclopropane carboxamide (9)



Yield 73%. Viscous oil. ^1H NMR (400 MHz, CDCl_3) δ (ppm): 7.94 (d, $J=7.8$ Hz, 1H, H-9''), 7.89 (d, $J=8.3$ Hz, 1H, H-6''), 7.79 (d, $J=8.2$ Hz, 1H, H-5''), 7.54 (m, 2H, H-7'' and H-8''), 7.40 (t, $J=7.6$ Hz, 1H, H-4''), 7.23 (d, $J=7.1$ Hz, 1H, H-3''), 6.16 (s, 1H, H-5), 5.85 (s, 1H, H-3), 5.45 (s, 2H, H-1''), 2.18 (s, 3H, $\text{CH}_3\text{-C}(6)$), 1.81 (m, 1H, H-2'), 1.19 and 0.88 (two m, 4H, H-3' and H-4'). ^{13}C NMR (100 MHz, CDCl_3) δ (ppm): 173.94 (C-4), 163.61 (C-2), 162.12 (C-6), 157.72 (C-1'), 133.80 (C-2''), 130.95 (C-5''a), 130.48 (C-9''a), 129.09, 128.58 (C-3'', C-6'', C-5'' and C-8''), 126.31, 126.07, 126.00 (C-4'', C-7'' and C-9''), 104.16

(C-3), 102.97 (C-5), 49.58 (C-1''), 20.05 (CH₃-C(6)), 14.26 (C-2'), 10.16(C-3' and C-4'). EI-MS *m/z* (%): 333 ([M⁺], 16), 264 (26), 141(100); HR(EI)MS: 333.13627±0.0030 (C₂₁H₁₉NO₃, calcd. 333.13649).

3-Cyclopentyl-N-(6-methyl-2-oxo-2H-pyran-4-yl)-N-(naphthalene-1-ylmethyl)propanamide (10)



Yield 25%. Waxy solid. ¹H NMR (400 MHz, CDCl₃) δ(ppm): 7.93 (d, *J* = 7.8 Hz, 1H, H-9'), 7.88 (d, *J* = 8.1 Hz, 1H, H-6'), 7.77 (d, *J* = 8.1 Hz, 1H, H-5'), 7.53 (m, 2H, H-8' and H-9'), 7.35 (t, *J* = 7.6, 1H, H-4'), 7.19 (d, *J* = 7.6 Hz, 1H, H-3'), 6.37 (s, 1H, H-5), 5.75 (s, 1H, H-3), 5.40 (s, 2H, H-1'), 2.37 (m, 2H, H-2''), 2.18 (s, 3H, CH₃-C(6)), 1.77 (m, 1H, H-4''), 1.64 (m, 2H, H-3''), 1.31 (m, 4H, H-5''), 1.53 and 1.45 (m, 4H, H-6''). ¹³C NMR (100 MHz, CDCl₃) δ (ppm): 171.63 (C-1''), 163.51 (C-2 and C-4), 161.45 (C-6), 133.72 (C-2' and C-5'a), 130.34 (C-9'a), 129.00 (C-6'), 128.10 (C-5'), 126.21 (C-7' and C-8'), 125.31 (C-4'), 124.68 (C-3'), 122.24 (C-9'), 102.43 (C-3), 101.80 (C-5), 49.29 (C-1'), 38.72 (C-4''), 32.76 (C-5''), 31.90 (C-3''), 30.96 (C-2''), 24.69 (C-6''), 20.05 (CH₃-C(6)). EI-MS *m/z* (%): 389 ([M⁺], 3), 388 ([M⁺-H], 11), 264 (12), 141(87); HR(EI)MS on [M⁺-H] : 388.1902±0.0030 (C₂₅H₂₆NO₃, calcd. 388.1913).

3.2.6. New thioethers 14, 16, 25 and 32

Compounds **14**, **16** and **32** (Scheme 3.2) and **25** (Scheme 3.3) were prepared and characterized as described below.

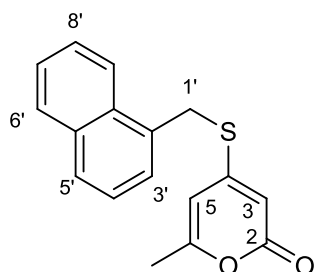
3.2.6.1. General procedure of synthesis

To a magnetically stirred solution of NaSH (230 mg, 4.0 mmol) in dry ethanol (5.0 mL), a solution of 6-methyl-4-tosyloxy-pyran-2-one (**28**) or 3-bromo-6-methyl-2-oxo-2H-pyran-4-yl

4-tosylate (**31**) or 3-ethyl-6-methyl-2-oxo-2H-pyran-4-yl 4-tosylate (1.0 mmol) in dry ethanol was added dropwise at room temperature under nitrogen atmosphere over a period of 30 minutes. Stirring was continued for additional 2 hours after the addition, then ethanol was removed *in vacuo* at room temperature. The residue was acidified with conc. HCl (2.0 mL), later extracted with benzene (4x2.5 mL, *CAUTION*). The organic solution was washed with water (2x2.0 mL) and dried (anhydrous Na₂SO₄). Attempts to evaporate benzene led to considerable decomposition of intermediate, therefore the solution was directly used for the following alkylation by adding DBU (224 μL, 1.5 mmol) and the suitable (aryl)alkyl bromide (1.0 mmol) under nitrogen. The mixture was stirred at room temperature overnight (TLC: hexane/ethyl acetate= 6:4). CH₂Cl₂ (50 mL) was added and the organic phase was washed with 2M HCl (60 mL) and successively with brine (70 mL). The organic phase was dried over anhydrous Na₂SO₄. After concentration *in vacuo* each crude product was purified by PLC using hexane/ethyl acetate = 6:4 as eluent (Schemes 3.2 and 3.3).

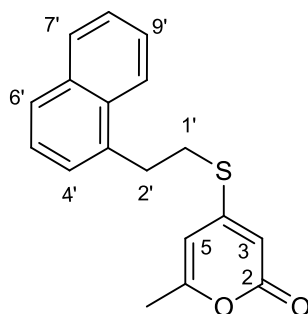
3.2.6.2. Spectroscopic and mass spectrometric data

6-Methyl-4-((naphthalen-1-ylmethyl)thio)-2H-pyran-2-one (**14**)



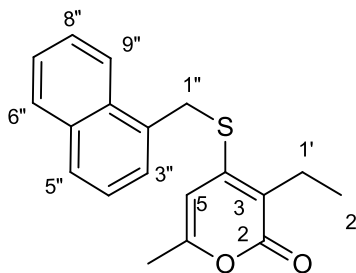
Yield 80%. Light yellow solid (from hexane/ ethyl acetate), m.p. 103-104°C. ¹H NMR (400 MHz, CDCl₃) δ(ppm): 8.00 (d, *J* = 8.3 Hz, 1H, H-9'), 7.89 (d, *J* = 7.7 Hz, 1H, H-6'), 7.83 (d, *J* = 8.3 Hz 1H, H-5'), 7.56 (m, 2H, H-7' and H-8'), 7.53 (d, *J* = 7.4 Hz, 1H, H-3'), 7.42 (t, *J* = 7.9 Hz, 1H, H-4'), 5.99 (s, 1H, H-5), 5.82 (s, 2H, H-3), 4.56 (s, 2H, H-1'), 2.04 (s, 3H, CH₃). ¹³C NMR (100 MHz, CDCl₃) δ (ppm): 161.99 (C-6), 160.38 (C-2), 159.35 (C-4), 133.93 (C-2'), 133.89 (C-5'a), 131.57 (C-10'a), 129.13 (C-7'), 128.90 (C-6'), 128.59 (C-4'), 126.62 (C-5'), 126.14 (C-3'), 123.17 (C-9'), 103.27 (C-3), 102.70 (C-5), 33.33 (C-1'), 19.69 (CH₃). EI-MS *m/z* (%): 282 ([M⁺], 2), 141(16), 115 (3); HR(EI)MS: 282.07155±0.0030 (C₁₇H₁₄O₂S, calcd. 282.07145).

6-Methyl-4-((2-(naphthalen-1-yl)ethyl)thio)-2H-pyran-2-one (16)



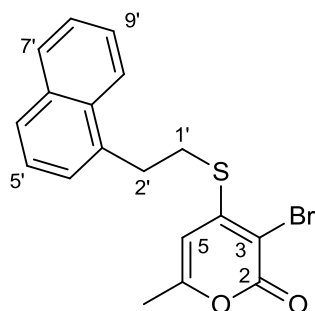
Yield 74 %. Ivory powder (from hexane/ethyl acetate), m.p. 68-69°C. ^1H NMR (400 MHz, CDCl_3) δ (ppm): 7.97 (d, $J = 8.4$ Hz, 1H, H-10'), 7.88 (d, $J = 8.4$ Hz, 1H, H-7'), 7.78 (d, $J = 8.1$ Hz, 1H, H-6'), 7.53 (m, 2H, H-8' and H-9'), 7.42 (t, $J = 7.1$ Hz, 1H, H-5'), 7.36 (d, $J = 6.7$ Hz, 1H, H-4'), 5.86 (s, 1H, H-5), 5.80 (s, 2H, H-3), 3.45 (t, $J = 7.2$ Hz, 2H, H-2'), 3.28 (t, $J = 7.2$ Hz, 2H, H-1'), 2.17 (s, 3H, CH_3). ^{13}C NMR (100 MHz, CDCl_3) δ (ppm): 161.31 (C-6), 160.01 (C-2), 159.16 (C-4), 135.02 (C-3'), 134.00 (C-6'a), 131.60 (C-10'a), 128.94 (C-7'), 127.69 (C-6'), 126.28 (C-4'), 126.62 (C-5'), 125.91 (C-8 and C-9'), 122.76 (C-10'), 103.41 (C-3), 102.35 (C-5), 31.20 (C-2'), 30.90 (C-1'), 19.27 (CH_3). EI-MS m/z (%): 296 ($[\text{M}^+]$, 3), 154(100); HR(EI)MS: 296.08698 \pm 0.0030 ($\text{C}_{18}\text{H}_{16}\text{O}_2\text{S}$, calcd. 296.08710).

3-Ethyl-6-methyl-4-((naphthalen-1-ylmethyl)thio)-2H-pyran-2-one (25)



Yield 60%. Light yellow solid (from hexane/ethyl acetate), m.p. 89-90°C. ^1H NMR (400 MHz, CDCl_3) δ (ppm): 8.07 (d, $J = 8.3$ Hz, 1H, H-9''), 7.89 (d, $J = 7.7$ Hz, 1H, H-6''), 7.83 (d, $J = 8.3$ Hz, 1H, H-5''), 7.56 (m, 3H, H-3'', H-7'' and H-8''), 7.43 (t, $J = 7.9$ Hz, 1H, H-4''), 6.12 (s, 1H, H-5), 4.59 (s, 2H, H-1''), 2.52 (q, $J = 7.5$ Hz, 2H, H-1'), 2.21 (s, 3H, CH_3), 1.03 (t, $J = 7.5$ Hz, 3H, H-2'). ^{13}C NMR (100 MHz, CDCl_3): δ (ppm) 161.76 (C-2), 158.39 (C-6), 152.54 (C-4), 133.93 (C-5''a), 131.26 (C-2''), 130.26 (C-9''a), 128.88 (C-6'' and C-5''), 128.60 (C-3''), 126.42 (C-7'' and C-8''), 125.45 (C-4''), 123.30 (C-9''), 120.50 (C-3), 101.33 (C-5), 33.65 (C-1''), 20.77 (C-1'), 19.62 (CH_3), 11.21 (C-2'). EI-MS m/z (%): 310 ($[\text{M}^+]$, 22), 141(100); HR(EI)MS: 310.10294 \pm 0.0030 ($\text{C}_{19}\text{H}_{18}\text{O}_2\text{S}$, calcd. 310.10275).

3-Bromo-6-methyl-4-((2-(naphthalen-1-yl)ethyl)thio)-2H-pyran-2-one (32)



Yield 40 %. Ivory powder . ^1H NMR (400 MHz, CDCl_3) δ (ppm): 7.99 (d, $J = 8.3$ Hz, 1H, H-10'), 7.89 (d, $J = 7.9$ Hz, 1H, H-7'), 7.77 (d, $J = 7.6$ Hz, 1H, H-6'), 7.55 (m, 2H, H-8' and H-9'), 7.39 (m, 2H, H-4' and H-5'), 5.65 (s, 1H, H-5), 3.47 (t, $J = 7.2$ Hz, 2H, H-2'), 3.31 (t, $J = 7.2$ Hz, 2H, H-1'), 2.01 (s, 3H, CH_3). ^{13}C NMR (100 MHz, CDCl_3) δ (ppm): 160.51 (C-2), 159.04 (C-6), 158.07 (C-4), 134.38 (C-3'), 133.83 (C-6'a), 131.44 (C-10'a), 128.87 (C-7'), 127.74 (C-6'), 127.02 (C-4'), 126.65 (C-5'), 126.02 (C-8' and C-9'), 122.67 (C-10'), 101.46 (C-3), 100.91 (C-5), 32.33 (C-2'), 32.09 (C-1'), 19.74 (CH_3). EI-MS m/z (%): 374 ($[\text{M}^+]$, 4), 295 (13), 154 (100); HR(EI)MS: 373.99687 ± 0.0030 ($\text{C}_{18}\text{H}_{15}\text{BrO}_2\text{S}$, calcd. 373.99761).

3.2.7. New sulfones 15, 17, 21 and 26

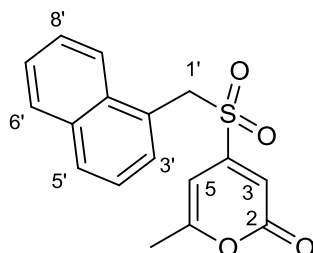
Compounds **15**, **17** and **21** (Scheme 3.2) and **26** (Scheme 3.3) were prepared and characterized as described below.

3.2.7.1. General procedure of synthesis

The suitable substrate **14**, **16**, **25** or **32** (0.1 mmol) is added to the solution of hydrogen peroxide–urea adduct (UHP) (40 mg, 0.4 mmol) in formic acid 85% (0.5 mL) at room temperature with stirring. A white precipitate is formed during the reaction. After 4 hours the reaction was complete as verified by TLC monitoring (hexane/ethyl acetate = 6:4). The mixture was partitioned between CH_2Cl_2 (10 mL) and water. The organic phase was washed with saturated solution of NaHCO_3 (10 mL) and successively with brine (10 mL), then dried over anhydrous Na_2SO_4 . After concentration *in vacuo*, each crude product was purified by PLC using hexane/ethyl acetate = 6:4 as eluent.

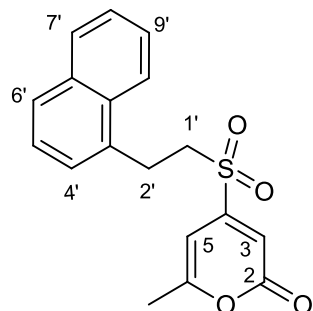
3.2.7.2. Spectroscopic and mass spectrometric data

6-Methyl-4-((naphthalen-1-ylmethyl)sulfonyl)-2H-pyran-2-one (15)



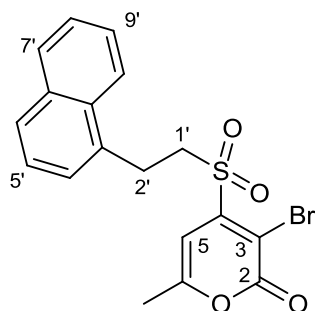
Yield 100%. White powder (from hexane/ethyl acetate), 175-176°C . ^1H NMR (400 MHz, CDCl_3) δ (ppm): 7.90 (m, 3H, H-5', H-6' and H-9'), 7.53 (m, 2H, H-7' and H-8'), 7.45 (m, 2H, H-3' and H-4'), 6.51 (s, 1H, H-5), 5.84 (s, 2H, H-3), 4.86 (s, 2H, H-1'), 2.08 (s, 3H, CH_3). EI-MS m/z (%): 314 ($[\text{M}^+]$, 3), 141(100); HR(EI)MS: 314.06122 \pm 0.0030 ($\text{C}_{17}\text{H}_{14}\text{O}_4\text{S}$, calcd. 314.06128).

6-Methyl-4-((2-(naphthalen-1-yl)ethyl)sulfonyl)-2H-pyran-2-one (17)



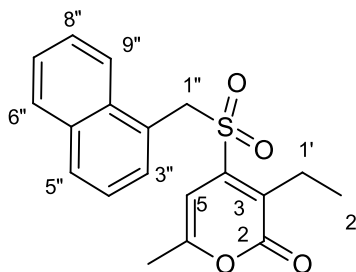
Yield 100 %. White powder (from dichloromethane), m.p. >300°C (dec.) . ^1H NMR (400 MHz, CDCl_3) δ (ppm): 7.88 (t, $J = 8.2$ Hz, 1H, H-7' and H-10'), 7.76 (d, $J = 8.2$ Hz, 1H, H-6'), 7.53 (m, 2H, H-8' and H-9'), 7.38 (t, $J = 7.2$ Hz, 1H, H-5'), 7.33 (d, $J = 6.7$ Hz, 1H, H-4'), 6.63 (s, 1H, H-5), 6.12 (s, 2H, H-3), 3.58 and 3.52 (two m, 4H, 2H-1' and 2H-2'), 2.21 (s, 3H, CH_3). EI-MS m/z (%): 328 ($[\text{M}^+]$, 14), 154(100); HR(EI)MS: 328.07686 \pm 0.0030 ($\text{C}_{18}\text{H}_{16}\text{O}_4\text{S}$, calcd. 328.07693).

3-Bromo-6-methyl-4-((2-(naphthalen-1-yl)ethyl)sulfonyl)-2H-pyran-2-one (21)



Yield 100 %. White powder (from dichloromethane), m.p. >300 °C (dec.) . ¹H NMR (400 MHz, CDCl₃) δ(ppm): 7.93 (d, *J* = 8.2 Hz, 1H, H-10'), 7.85 (d, *J* = 8.0 Hz, 1H, H-7'), 7.74 (t, *J* = 4.5 Hz, 1H, H-6'), 7.53 (m, 2H, H-8' and H-9'), 7.35 (d, *J* = 4.7 Hz, 2H, H-4' and H-5'), 6.35 (s, 1H, H-5), 3.92 (t, *J* = 7.3 Hz, 2H, H-1'), 3.58 (t, *J* = 7.3 Hz, 2H, H-2'), 2.18 (s, 3H, CH₃). EI-MS *m/z* (%): 406 ([M⁺], 1), 256 (19), 154 (48); HR(EI)MS: 405.98618±0.0030 (C₁₈H₁₅BrO₄S, calcd.405.98744).

3-Ethyl-6-methyl-4-((naphthalen-1-ylmethyl)sulfonyl)-2H-pyran-2-one (26)



Yield 95%. Light yellow solid (from hexane/ethyl acetate), m.p. 97-98°C. ¹H NMR (400 MHz, CDCl₃) δ(ppm): 7.94 (d, *J* = 7.3 Hz, 1H, H-9''), 7.87 (m, 2H, H-5'' and H-6''), 7.52 (m, 2H, H-7'' and H-8''), 7.42 (m, 2H, H-3'' and H-4''), 6.06 (s, 1H, H-5), 4.86 (s, 2H, H-1''), 2.56 (q, *J* = 7.3 Hz, 2H, H-1'), 2.08 (s, 3H, CH₃), 1.09 (t, *J* = 7.3 Hz, 3H, H-2'). EI-MS *m/z* (%): 342 ([M⁺], 5), 141(100); HR(EI)MS: 342.09282±0.0030 (C₁₉H₁₈O₄S, calcd.342.09258).

3.2.8. New ethers 18-20 and 23

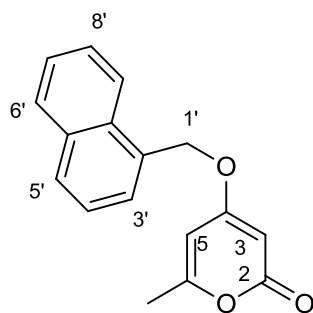
Compounds **18-20** (Scheme 3.2) and **23** (Scheme 3.3) were prepared and characterized as described below.

3.2.8.1. General procedure of synthesis

To a solution of 4-hydroxy-6-methyl-2H-pyran-2-one (**27**), or 4-hydroxy-3-iodo-6-methyl-2H-pyran-2-one (**29**), or 3-ethyl-4-hydroxy-6-methyl-2H-pyran-2-one (**35**) (1 mmol) and suitable (aryl)alkyl bromide (1.1 mmol) in anhydrous acetone (5 mL) was added KI (166 mg, 1 mmol) and anhydrous K_2CO_3 (345 mg, 2.5 mmol). The mixture was refluxed for 20 hours monitoring by TLC (hexane/ethyl acetate= 6:4). The filtered solution was evaporated *in vacuo* and each crude products was purified by PLC using hexane/ethyl acetate = 6:4 as eluent.

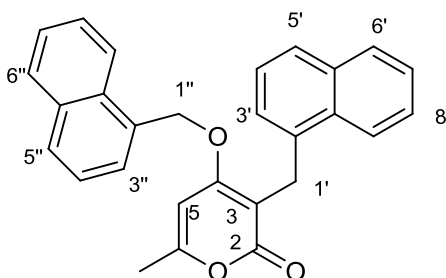
3.2.7.2. Spectroscopic and mass spectrometric data

6-Methyl-4-(naphthalen-1-ylmethoxy)-2H-pyran-2-one (**18**)



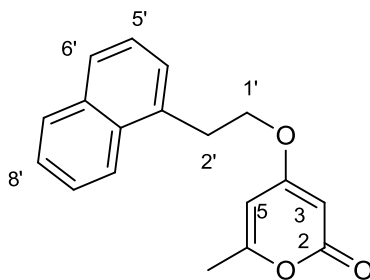
Yield 60%. White solid (from hexane/ethyl acetate), m.p. 118-119 °C. 1H NMR (400 MHz, $CDCl_3$) δ (ppm): 7.90 (m, 3H, H-5', H-6' and H-9'), 7.54 (m, 3H, H-3', H-7' and H-8'), 7.47 (t, $J = 8.2$ Hz, 1H, H-4'), 5.81 (s, 1H, H-5), 5.65 (s, 1H, H-3), 5.45 (s, 2H, H-1'), 2.18 (s, 3H, CH_3). ^{13}C NMR (100 MHz, $CDCl_3$) δ (ppm): 170.29 (C-4), 164.14 (C-2), 162.28 (C-6), 133.90 (C-5'a), 132.89 (C-2'), 131.25 (C-10'a), 129.13 (C-6'), 128.02 (C-5'), 126.90 (C-3'), 128.61 (C-4'), 125.89 (C-7' and C-8'), 123.04 (C-9'), 100.30 (C-5), 88.20 (C-3), 64.01 (C-1'), 20.03 (CH_3). EI-MS m/z (%): 266 ($[M^+]$, 2), 141 (100); HR(EI)MS: 266.09439 \pm 0.0030 ($C_{17}H_{14}O_3$, calcd. 266.09429).

6-Methyl-4-(naphthalen-1-ylmethoxy)-3-(naphthalen-1-ylmethyl)-2H-pyran-2-one (18a)



Yield 50%. White solid (from hexane/ethyl acetate), m.p. 106-107°C. ^1H NMR (400 MHz, CDCl_3) δ (ppm): 8.19 (d, $J = 8.6$ Hz, 1H), 7.87 (t, $J = 9.0$ Hz, 2H), 7.78 (t, $J = 8.8$ Hz, 2H), 7.60 (d, $J = 8.1$ Hz, 1H), 7.49 (t, $J = 7.0$ Hz, 1H), 7.38 (t, $J = 8.2$ Hz, 3H), 7.29 (t, $J = 6.8$ Hz, 2H), 7.20 (d, $J = 7.0$ Hz, 1H), 7.12 (t, $J = 8.0$ Hz, 1H), 6.14 (s, 1H, H-5), 5.50 (s, 2H, H-1''), 4.20 (s, 2H, H-1'), 2.24 (s, 3H, CH_3). ^{13}C NMR (100 MHz, CDCl_3) δ (ppm): 166.31 (C-4), 165.38 (C-2), 162.19 (C-6), 135.36, 133.61, 132.10, 132.05, 130.41, 129.07, 128.34, 126.32, 126.09, 126.06, 125.83, 125.53, 125.31, 124.23, 123.90 and 123.03 (naphthalene units), 104.38 (C-3), 95.80 (C-5), 69.16 (C-1''), 25.98 (C-1'), 20.30 (CH_3). EI-MS m/z (%): 406 ($[\text{M}^+]$, 6), 265 (30), 141 (100); HR(EI)MS: 406.15669 \pm 0.0030 ($\text{C}_{28}\text{H}_{22}\text{O}_3$, calcd. 406.15689).

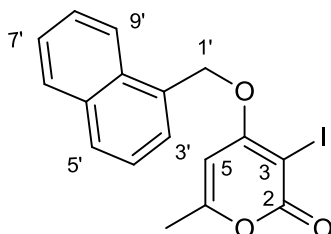
6-Methyl-4-(2-(naphthalen-1-yl)ethoxy)-2H-pyran-2-one (19)



Yield 40 %. White powder (from hexane/ethyl acetate), m.p. 65-66°C. ^1H NMR (400 MHz, CDCl_3) δ (ppm): 8.00 (d, $J = 8.2$ Hz, 1H, H-10'), 7.88 (d, $J = 8.1$ Hz, 1H, H-7'), 7.78 (d, $J = 8.1$ Hz, 1H, H-6'), 7.52 (m, 2H, H-8' and H-9'), 7.42 (t, $J = 7.5$ Hz, 1H, H-5'), 7.37 (d, $J = 6.8$ Hz, 1H, H-4'), 5.74 (s, 1H, H-5), 5.36 (s, 2H, H-3), 4.28 (t, $J = 7.0$ Hz, 2H, H-1'), 3.54 (t, $J = 7.0$ Hz, 2H, H-2'), 2.17 (s, 3H, CH_3). ^{13}C NMR (100 MHz, CDCl_3) δ (ppm) 170.28 (C-4), 164.73 (C-2), 162.23 (C-6), 133.94 (C-6'a), 132.90 (C-3'), 131.72 (C-10'a), 129.13 (C-7'), 127.63 (C-6'), 127.00 (C-4'), 126.42 (C-5'), 125.91 (C-8 and C-9'), 123.05 (C-10'), 100.35

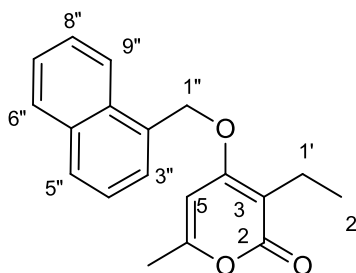
(C-5), 88.13 (C-3), 68.03 (C-1'), 31.82 (C-2'), 19.60 (CH₃). EI-MS *m/z* (%): 280 ([M⁺], 20), 155 (100); HR(EI)MS: 280.10991±0.0030 (C₁₈H₁₆O₃, calcd. 280.10994).

3-Iodo-6-methyl-4-(naphthalen-1-ylmethoxy)-2H-pyran-2-one (20)



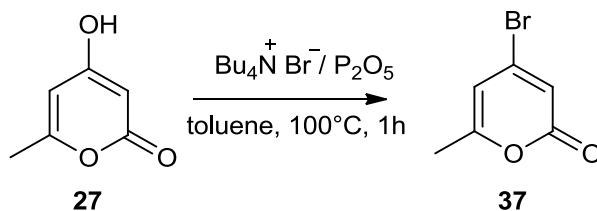
Yield 50%. Viscous oil. ¹H NMR (400 MHz, CDCl₃) δ(ppm): 8.00 (d, *J* = 8.6 Hz, 1H, H-9'), 7.91 (t, *J* = 9.1 Hz, 2H, H-5 and H-6'), 7.57 (m, 3H, H-3', H-7' and H-8'), 7.49 (t, *J* = 8.2 Hz, 1H, H-4'), 6.06 (s, 1H, H-5), 5.71 (s, 2H, H-1'), 2.24 (s, 3H, CH₃). ¹³C NMR (100 MHz, CDCl₃) δ (ppm): 169.75 (C-4), 164.14 (C-6), 163.98 (C-2), 133.72 (C-2' and C-5'a), 130.21 (C-10'a), 129.83 (C-6'), 128.90 (C-5'), 128.60 (C-4'), 126.80 (C-3'), 125.90 (C-7' and C-8'), 123.04 (C-9'), 70.14 (C-3), 95.48 (C-5), 63.25 (C-1'), 20.05 (CH₃). EI-MS *m/z* (%): 292 ([M⁺], 2), 310 (7), 294 (7), 141 (100); HR(EI)MS: 391.98828±0.0030 (C₁₇H₁₃IO₃, calcd. 391.99095).

3-Ethyl-6-methyl-4-(naphthalen-1-ylmethoxy)-2H-pyran-2-one (23)



Yield 60%. White solid. ¹H NMR (400 MHz, CDCl₃) δ(ppm): 7.91 (m, 3H, H-5'', H-6'' and H-9''), 7.56 (m, 2H, H-7'' and H-8''), 7.49 (m, 2H, H-3'' and H-4''), 6.12 (s, 1H, H-5), 5.56 (s, 2H, H-1''), 2.44 (q, *J* = 7.5, 2H, H-1'), 2.23 (s, 3H, CH₃), 1.00 (t, *J* = 7.5 Hz, 3H, H-2'). ¹³C NMR (100 MHz, CDCl₃) δ (ppm): 165.59 (C-2), 164.73 (C-4), 160.72 (C-6), 133.78 (C-5''a), 130.90 (C-2'' and C-9''a), 129.04 (C-6''), 126.21 (C-7'' and C-8''), 125.81 (C-3'' and C-4''), 122.75 (C-9''), 107.75 (C-3), 95.57 (C-5), 68.94 (C-1''), 20.25 (CH₃), 16.23 (C-1'), 11.74 (C-2'). EI-MS *m/z* (%): 294 ([M⁺], 5), 141(100); HR(EI)MS: 294.12587±0.0030 (C₁₉H₁₈O₂S, calcd. 294.12559).

3.2.9. Synthesis and structural characterization of 4-bromo -6-methyl-2H-pyran-2-one (37)



A mixture of 4-hydroxy-6-methyl-2H-pyran-2-one (**27**, 0.428g, 3.40 mmol), tetrabutylammonium bromide (1.350 mg, 4.2 mmol) and P_2O_5 (1.180 g, 8.31 mmol) in anhydrous toluene (8.0 mL) was heated at 100°C for 1 hour under stirring (TLC: hexane/ ethyl acetate = 1:1). After cooling, the toluene layer was separated. The gummy residual was extracted with toluene (4x8 mL). The combined organic layers were washed with a saturated solution of NaHCO_3 and brine, dried over anhydrous sodium sulfate and then evaporated *in vacuo*, giving pure compound **37** (0.54 g, 82% yield). Light-brown crystal, m.p. 88-90 (Lit. 87-89°C; Fairlamb, 2004). ^1H NMR (400 MHz, CDCl_3) δ (ppm): 6.44 (s, 1H), 6.18 (s, 1H), 2.23 (s, 3H). ^{13}C NMR (100 MHz, CDCl_3) δ (ppm): 162.0, 160.3, 140.9, 114.5, 108.2, 19.5.

3.2.10. Study of the selectivity in *N,C*-acylation of 4-benzylamino-pyrone

For 4-benzylamino-pyrone (**1**) a tautomeric equilibrium between the imino and enamino forms can be written (Figure 3.9). The geometry of the two forms have been optimized and the corresponding energy values have been calculated using the quantum-chemical software Gaussian 03W (Frisch, 2004). Restricted Density Functional Theory (DFT) using basis set 6-311++G(d,p) for all the atoms and hybrid functional B3LYP was applied (§ 3.1.1.2). The optimized structural parameters were employed in the vibrational energy calculations at the DFT levels to characterize all stationary points as minima. For each optimized structure, no imaginary wavenumber modes were obtained, proving that a local minimum on the potential energy surface was actually found. The computed wavenumbers were scaled by factor 0.9688, which is suggested for B3LYP/6-311++G(d,p) calculations (Merrick, 2007). The value of total energy is in the favor of enamino-form with a difference of -99.5 KJ/mol if compared with the value for imino-form (Figure 3.9).

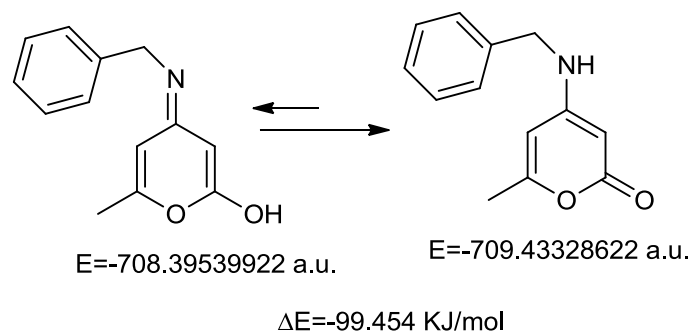


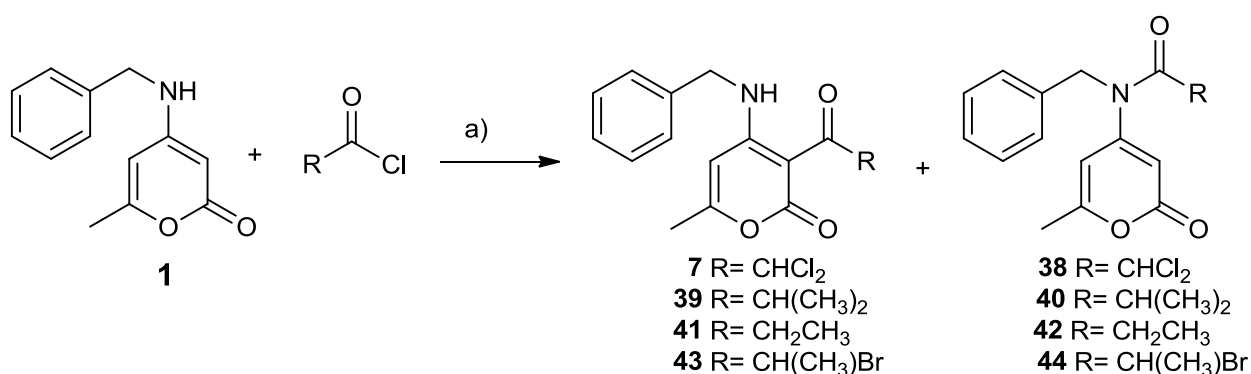
Figure 3.9. Imino-enamino tautomeric equilibrium for pyrone **1**

A selectivity has been observed in *N*, *C*-acylation by changing the base, the solvent and electrophile. The results have been discussed as reported below.

3.2.10.1. Synthesis and structural characterization of compounds 38-43

General procedure of synthesis

To a solution of compound **1** or **45** (0.02 mmol) dissolved in anhydrous CH_2Cl_2 (0.5 mL), suitable amine (0.05 mmol) was added and the solution cooled at 0°C for 30 minutes. Acyl chloride (0.04 mmol) was slowly added at this temperature. The mixture was stirred at room temperature for 18 hours monitoring by TLC (hexane / ethyl acetate = 6:4) (Scheme 3.4). After concentration *in vacuo*, the crude products were analyzed by $^1\text{H-NMR}$ spectra.



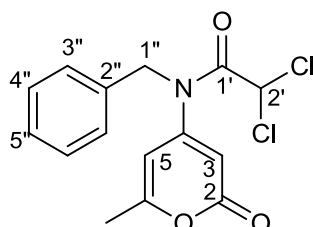
Scheme 3.4. Base effect on the selectivity of *N*, *C*-acylation of benzylpyrone **1**. *Reagents and conditions:* a) base, CH_2Cl_2 , $0^\circ\text{C} \rightarrow \text{r.t.}$, 18h, 78-90% yield.

3.2.10.2. Spectroscopic and mass spectrometric data

4-(Benzylamino)-3-(2,2-dichloroacetyl)-6-methyl-2H-pyran-2-one (7)

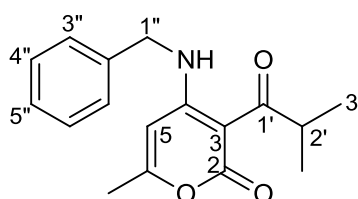
These data have been already reported in § 3.2.6.

N-Benzyl-2,2-dichloro-*N*-(6-methyl-2-oxo-2H-pyran-4-yl)acetamide (38)



Yield 82%. Oil. ^1H NMR (400 MHz, CDCl_3) δ (ppm): 7.34 (m, 3H, H-4'', H-5'' and H-6''), 7.20 (m, 2H, H-3'' and H-7''), 6.19 (s, 1H, H-2'), 5.93 (s, 1H, H-3), 5.88 (s, 1H, H-5) 4.90 (s, 2H, H-1''), 2.26 (s, 3H, CH_3 -C(6)). ^{13}C NMR (100 MHz, CDCl_3) δ (ppm): 171.53 (C-1'), 164.91 (C-2 and C-6) 154.72 (C-4), 134.63 (C-2''), 128.77 (C-4'', C-5'' and C-6''), 127.67 (C-3'' and C-7''), 108.61 (C-5), 103.19 (C-3), 63.32 (C-2'), 51.58 (C-1''), 20.62 (CH_3 -C(6)). ESI-MS (positive mode): 348 ($[\text{M} + \text{Na}]^+$). EI-MS m/z (%): 325 ($[\text{M}^+]$, 4), 214 (10), 91 (100); HR(EI)MS: 325.0267 \pm 0.0030 ($\text{C}_{15}\text{H}_{13}\text{Cl}_2\text{NO}_3$, calcd. 325.02725).

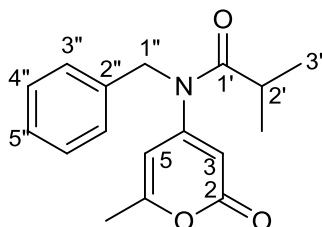
4-(Benzylamino)-3-isobutyryl-6-methyl-2H-pyran-2-one (39)



Yield 79%. Oil. ^1H NMR (400 MHz, CDCl_3) δ (ppm): 12.03 (br s, 1H, NH), 7.37 (m, 3H, H-4'', H-5'' and H-6''), 7.26 (m, 2H, H-3'' and H-7''), 5.81 (s, 1H, H-5), 4.50 (d, $J = 5.6$ Hz, 2H, H-1''), 2.16 (s, 3H, CH_3 -C(6)), 1.11 (d, $J = 6.7$ Hz, 6H, H-3'). ^{13}C NMR (100 MHz, CDCl_3) δ (ppm): 208.84 (C-1'), 165.53 and 165.11 (C-2 and C-6) 162.72 (C-4), 136.09 (C-2''), 128.56 and 128.02 (C-4'', C-5'' and C-6''), 127.42 (C-3'' and C-7''), 94.56 (C-5), 93.20 (C-3), 46.71 (C-1''), 37.78 (C-2'), 20.63 (CH_3 -C(6)), 18.58 (C-3'). ESI-MS (positive mode): m/z 286 ($[\text{M} + \text{H}]^+$), 308 ($[\text{M} + \text{Na}]^+$); MS/MS (286): m/z 268 ($[\text{M} + \text{H} - \text{H}_2\text{O}]^+$), 216 ($[\text{M} + \text{H} - \text{C}_4\text{H}_6\text{O}]^+$). EI-MS

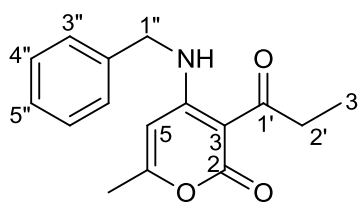
m/z (%): 285 ($[M^{+}]$, 9), 242 (63), 194 (42), 91 (100); HR(EI)MS: 285.13652 \pm 0.0030 ($C_{17}H_{19}NO_3$, calcd. 285.13649).

***N*-Benzyl-*N*-(6-methyl-2-oxo-2H-pyran-4-yl)isobutyramide (40)**



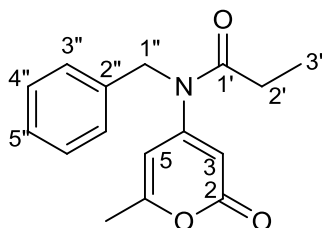
Yield 78 %. Oil . 1H NMR (400 MHz, $CDCl_3$) δ (ppm): 7.32 (m, 3H, H-4'', H-5'' and H-6''), 7.17 (m, 2H, H-3'' and H-7''), 5.99 (s, 1H, H-3), 5.77 (s, 1H, H-5), 4.85 (s, 2H, H-1''), 2.83 (septet, $J=6.6$ Hz, 1H, H-2'), 2.23 (s, 3H, CH_3 -C(6)), 1.15 (d, $J=6.6$ Hz, 6H, H-3'). ^{13}C NMR (100 MHz, $CDCl_3$) δ (ppm): 177.80 (C-1'), 162.76 (C-2 and C-6) 157.24 (C-4), 136.49 (C-2''), 128.48 (C-4'', C-5'' and C-6''), 127.07 (C-3'' and C-7''), 105.52 (C-5), 103.31 (C-3), 51.49 (C-1''), 32.08 (C-2'), 20.65 (CH_3 -C(6)), 19.07 (C-3'). ESI-MS (positive mode): m/z 286 ($[M+H]^+$), 308 ($[M+Na]^+$), 593($[2M+Na]^+$); MS/MS (286): m/z 216 ($[M+H-C_4H_6O]^+$). EI-MS m/z (%): 285 ($[M^{+}]$, 17), 214 (47), 91 (75), 43 (100); HR(EI)MS: 285.13607 \pm 0.0030 ($C_{17}H_{19}NO_3$, calcd. 285.13649).

4-(Benzylamino)-6-methyl-3-propionyl-2H-pyran-2-one (41)



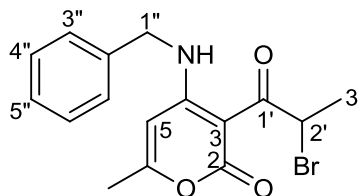
Yield 75%. Oil . 1H NMR (400 MHz, $CDCl_3$) δ (ppm): 11.97 (br s, 1H, NH), 7.36 (m, 3H, H-4'', H-5'' and H-6''), 7.26 (m, 2H, H-3'' and H-7''), 5.81 (s, 1H, H-5), 4.51 (d, $J=5.8$ Hz, 2H, H-1''), 3.07 (q, $J=7.2$ Hz, 2H, H-2'), 2.16 (s, 3H, CH_3 -C(6)), 1.10 (t, $J=6.7$ Hz, 3H, H-3'). ^{13}C NMR (100 MHz, $CDCl_3$) δ (ppm): 204.70 (C-1'), 165.56 (C-2 and C-6) 161.58 (C-4), 136.31 (C-2''), 128.51 (C-4'', C-5'' and C-6''), 127.11 (C-3'' and C-7''), 94.71 (C-5 and C-3), 45.22 (C-1''), 37.31 (C-2'), 20.70 (CH_3 -C(6)) 8.34 (C-3'). ESI-MS (positive mode): m/z 272 ($[M+H]^+$), 294 ($[M+Na]^+$), 564($[2M+Na]^+$); MS/MS (272): m/z 216 ($[M+H-C_3H_4O]^+$); MS^3 (216): m/z 138 ($[M+H-C_6H_6]^+$). EI-MS m/z (%): 271 ($[M^{+}]$, 33), 242 (71), 180 (21), 91 (100); HR(EI)MS: 271.12072 \pm 0.0030 ($C_{16}H_{17}NO_3$, calcd. 271.12084).

***N*-Benzyl-*N*-(6-methyl-2-oxo-2H-pyran-4-yl)propionamide (42)**



Yield 73%. Colorless oil. ^1H NMR (400 MHz, CDCl_3) δ (ppm): 7.32 (m, 3H, H-4'', H-5'' and H-6''), 7.16 (m, 2H, H-3'' and H-7''), 6.13 (s, 1H, H-3), 5.77 (s, 1H, H-5), 4.88 (s, 2H, H-1''), 2.43 (q, $J=7.4$ Hz, 2H, H-2'), 2.23 (s, 3H, $\text{CH}_3\text{-C}(6)$), 1.16 (t, $J=7.4$ Hz, 3H, H-3'). ^{13}C NMR (100 MHz, CDCl_3) δ (ppm): 174.11 (C-1'), 162.42 (C-2 and C-6) 157.21 (C-4), 136.16 (C-2''), 127.89 (C-4'', C-5'' and C-6''), 126.80 (C-3'' and C-7''), 103.28 (C-5), 58.32 (C-2'), 51.50 (C-1''), 20.61 ($\text{CH}_3\text{-C}(6)$), 18.14 (C-3'). ESI-MS (positive mode): m/z 272 ($[\text{M} + \text{H}]^+$), 294 ($[\text{M} + \text{Na}]^+$); MS/MS (272): m/z 216 ($[\text{M} + \text{H} - \text{C}_3\text{H}_4\text{O}]^+$). EI-MS m/z (%): 271 ($[\text{M}^+]$, 33), 242 (66), 180 (20), 91 (100); HR(EI)MS: 271.12064 \pm 0.0030 ($\text{C}_{16}\text{H}_{17}\text{NO}_3$, calcd. 271.12084).

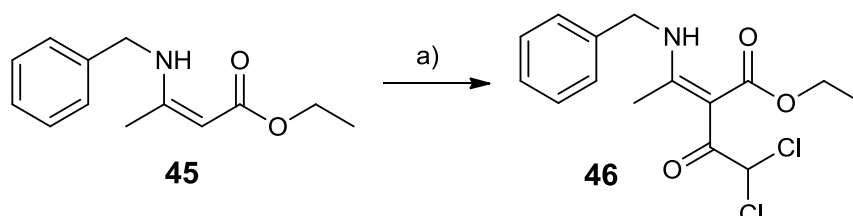
4-(Benzylamino)-3-(2-bromopropanoyl)-6-methyl-2H-pyran-2-one (43)



Yield 85%. Pale yellow oil. ^1H NMR (400 MHz, CDCl_3) δ (ppm): 11.69 (br s, 1H, NH), 7.38 (m, 3H, H-4'', H-5'' and H-6''), 7.27 (m, 2H, H-3'' and H-7''), 6.13 (q, $J=6.7$ Hz, 1H, H-2''), 5.87 (s, 1H, H-5), 4.53 (d, $J=5.7$ Hz, 2H, H-1''), 2.19 (s, 3H, $\text{CH}_3\text{-C}(6)$), 1.79 (d, $J=6.7$ Hz, 3H, H-3'). ^{13}C NMR (100 MHz, CDCl_3) δ (ppm): 197.25 (C-1'), 166.23 (C-2 and C-6) 162.92 (C-4), 135.61 (C-2''), 128.78 (C-4'', C-5'' and C-6''), 127.06 (C-3'' and C-7''), 94.97 (C-5), 91.81 (C-3), 47.75 (C-2'), 46.98 (C-1''), 20.87 ($\text{CH}_3\text{-C}(6)$), 20.49 (C-3'). ESI-MS (positive mode): m/z 350/352 ($[\text{M} + \text{H}]^+$), 372/374 ($[\text{M} + \text{Na}]^+$), 388/390 ($[\text{M} + \text{K}]^+$); MS/MS (252): m/z 270 ($[\text{M} + \text{H} - \text{H}^{81}\text{Br}]^+$), 180 ($[\text{M} + \text{H} - \text{H}^{81}\text{Br} - \text{C}_7\text{H}_6]^+$). EI-MS m/z (%): 349 ($[\text{M}^+]$, 1.5), 270 (51), 242 (27), 91 (100); HR(EI)MS: 349.02959 \pm 0.0030 ($\text{C}_{16}\text{H}_{16}^{79}\text{BrNO}_3$, calcd.349.03136).

3.2.10.3. Study of selectivity in enamino-ester **45** as a model compound

The enaminoester **45** has been selected as model compound. It was prepared according to the procedure reported (Brandt, 2004), and later subjected to reaction with suitable bases and dichloroacetyl chloride (Scheme 3.5).



Scheme 3.5. Acylation of enaminoester **45**. *Reagents and conditions:* a) different base (2.5 eq.) dichloroacetyl chloride (2.0 eq.), CH₂Cl₂, 0°C → r.t., 18h, 78-90% yield.

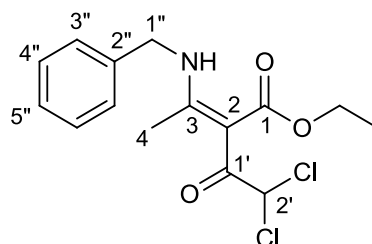
Synthesis and structural characterization of precursor **45**

A mixture of ethyl acetoacetate (0.5 mL, 3.9 mmol), benzylamine (0.43 mL, 3.9 mmol) and acetic acid (25 μ L, 0.44 mmol) was placed in an ultrasound bath at a temperature never exceeding 30°C, for 1 hour. Later ethanol (10 mL) was added, the resulting solution was dried on anhydrous Na₂SO₄, filtered and concentrated *in vacuo* to give pure product (850 mg, quantitative yield). Yellow oil. ¹H NMR (400 MHz, CDCl₃) δ (ppm): 8.94 (br s, 1H), 7.31-7.20 (m, 5H), 4.52 (s, 1H), 4.42 (d, *J*=6.4 Hz, 2H), 4.09 (q, *J*=7.0 Hz, 2H), 1.9 (s, 3H), 1.25 (t, *J*=7.0 Hz, 3H). The data are consistent with the ones reported by Brandt, 2004.

Synthesis and structural characterization of compound **46**

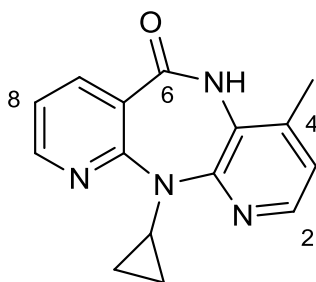
The adopted synthetic procedure was the same as reported for the preparation of compounds **38-43** (§ 3.2.19.1).

(*Z*)-Ethyl 3-(benzylamino)-2-(2,2-dichloroacetyl)but-2-enoate (**46**)



Yield 82%. Yellow oil. ^1H NMR (400 MHz, CDCl_3) δ (ppm): 12.65 (br s, 1H, NH), 7.40 (m, 3H, H-4'', H-5'' and H-6''), 7.27 (m, 2H, H-3'' and H-7''), 6.92 (s, 1H, H-2'), 4.57 (d, $J = 5.6$ Hz, 2H, H-1''), 4.25 (q, $J=7.1$ Hz, 2H, $-\text{OCH}_2-$), 2.29 (s, 3H, C-4), 1.34 (t, $J=7.1$ Hz, 3H, CH_3CH_2). ^{13}C NMR (100 MHz, CDCl_3) δ (ppm): 173.79 (C-1'), 171.37 (C-3), 168.26 (C-1), 135.32 (C-2''), 128.15 (C-4'', C-5'' and C-6''), 127.66 (C-3'' and C-7''), 98.89 (C-2), 71.75 (C-2'), 60.97 ($-\text{OCH}_2-$), 47.80 (C-1''), 17.95 (C-4), 13.89 (CH_3-). ESI-MS (positive mode): m/z 330 ($[\text{M} + \text{H}]^+$), 352 ($[\text{M} + \text{Na}]^+$); MS/MS (330): m/z 284 ($[\text{M} + \text{H} - \text{C}_2\text{H}_6\text{O}]^+$). EI-MS m/z (%): 329 ($[\text{M}^+]$, 2), 246 (55), 91 (100); HR(EI)MS: 329.05801 ± 0.0030 ($\text{C}_{15}\text{H}_{17}^{35}\text{Cl}_2\text{NO}_3$, calcd. 329.05855).

3.2.11. Purification and structural characterization of drug nevirapine isolated from Viramune[®] in tablets



One tablet of viramune[®] containing 200 mg of nevirapine (NVP), was grinded finely in a mortar. The powder was extracted repeatedly with CH_2Cl_2 . The extracts were evaporated *in vacuo* and the residue was passed through a pad of silica gel and eluted with CH_2Cl_2 / EtOH/ acetone= 1:1:1. The white residue (180 mg, 90 % recovery) obtained after *in vacuo* evaporation of the solvent was pure NVP. M.p. 243-245°C (Lit. 242-246°C; Hargrave 1991) ^1H NMR (400 MHz, CDCl_3) δ (ppm): 8.51 (d, $J = 3.2$ Hz, 2H), 8.14 (d, $J = 4.8$ Hz, 1H), 8.09 (d, $J = 7.5$ Hz, 1H), 7.04 (dd, $J = 7.4, 4.9$ Hz, 1H), 6.92 (d, $J = 4.8$ Hz, 1H), 3.74 (s, 1H), 2.37 (s, 3H), 0.97 (br s, 1H), 0.49 (dd, $J = 21.5, 10.5$ Hz, 1H). ^{13}C NMR (100 MHz, CDCl_3) δ (ppm): 168.81, 160.47, 153.97, 152.08, 143.96, 140.34, 139.37, 124.86, 121.93, 118.78, 29.35, 17.11, 8.62. EI-MS m/z (%): 265 ($[\text{M}^+]$, 94), 251 (100), 237 (34), 183 (12), 133(58) ; HR(EI)MS: 265.10802 ± 0.0030 ($\text{C}_{15}\text{H}_{13}\text{N}_4\text{O}$, calcd. 265.10894).

NMR data (Figure 3.10, 3.11 and 3.12) are consistent with the ones reported by Hannongbua, 2001.

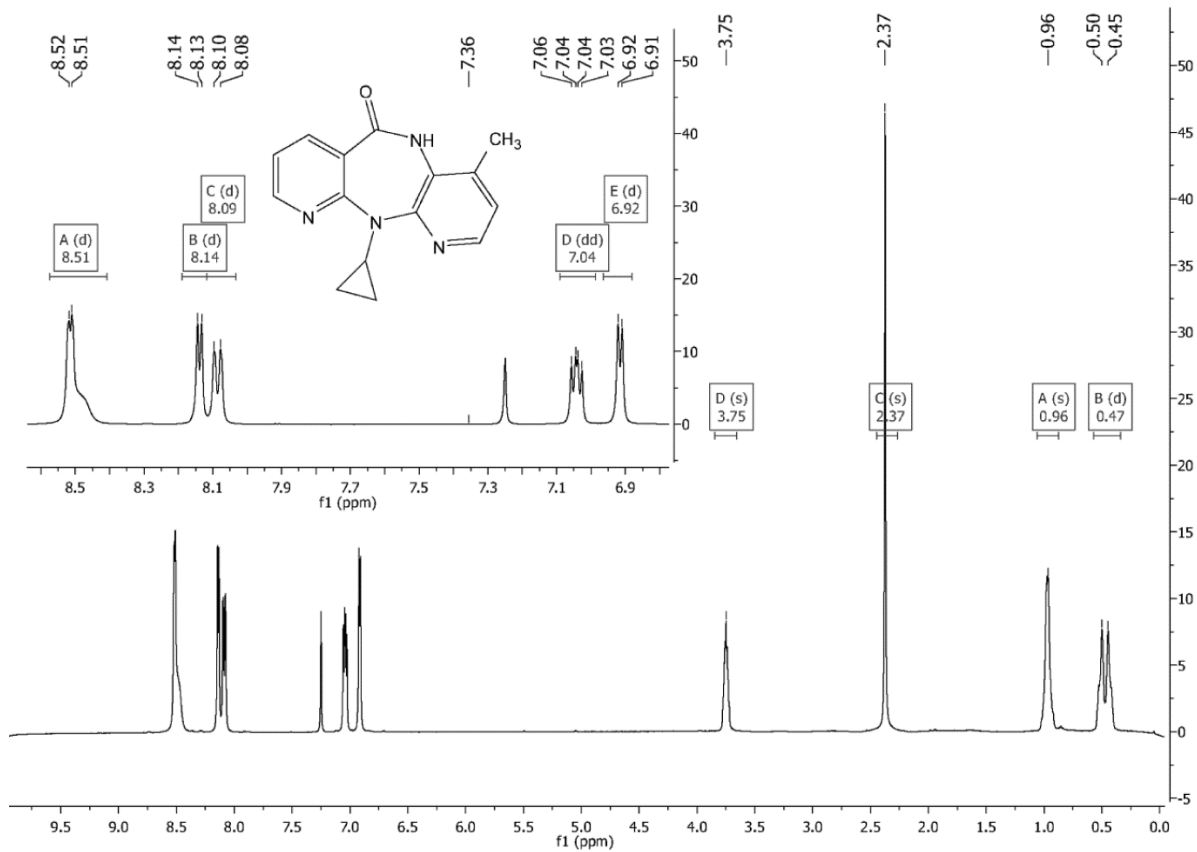


Figure 3.10. ^1H -NMR (400MHz) spectrum in CDCl_3 of nevirapine isolated from the drug

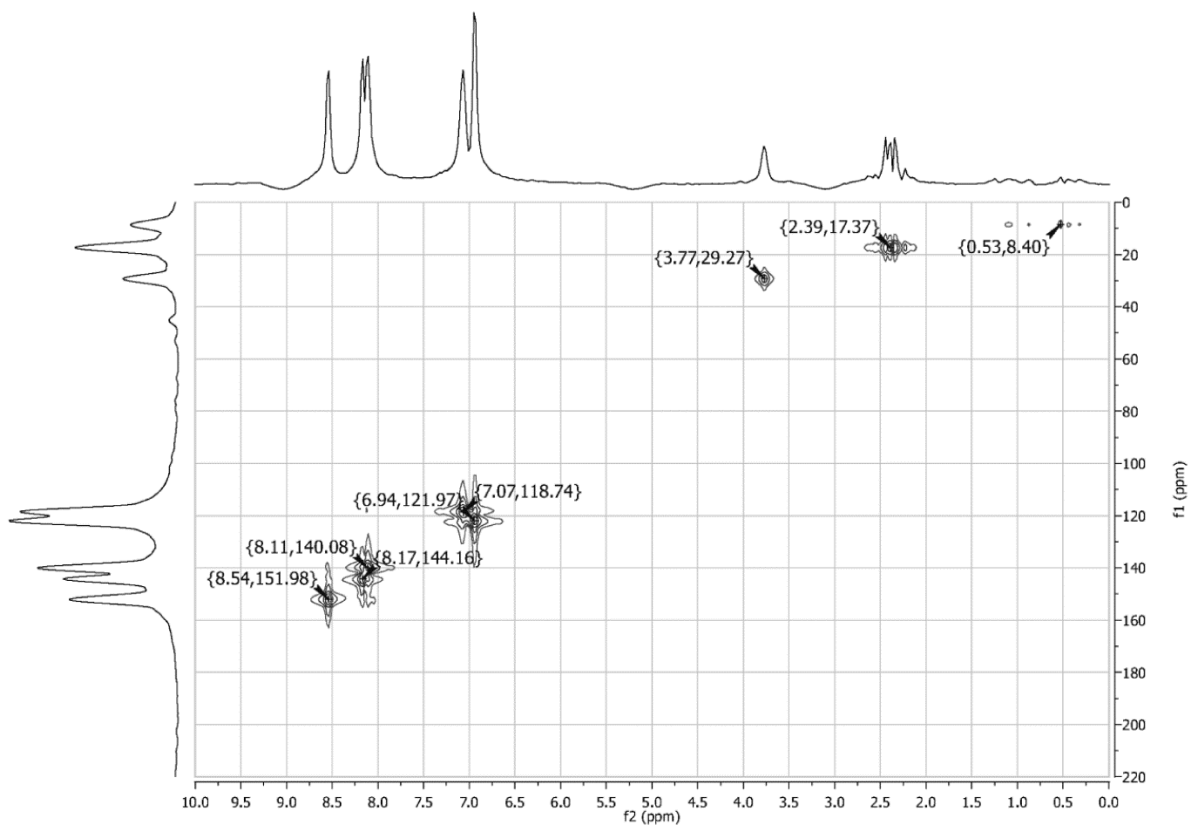


Figure 3.11. ^1H , ^{13}C NMR (HSQC) spectrum of nevirapine in CDCl_3

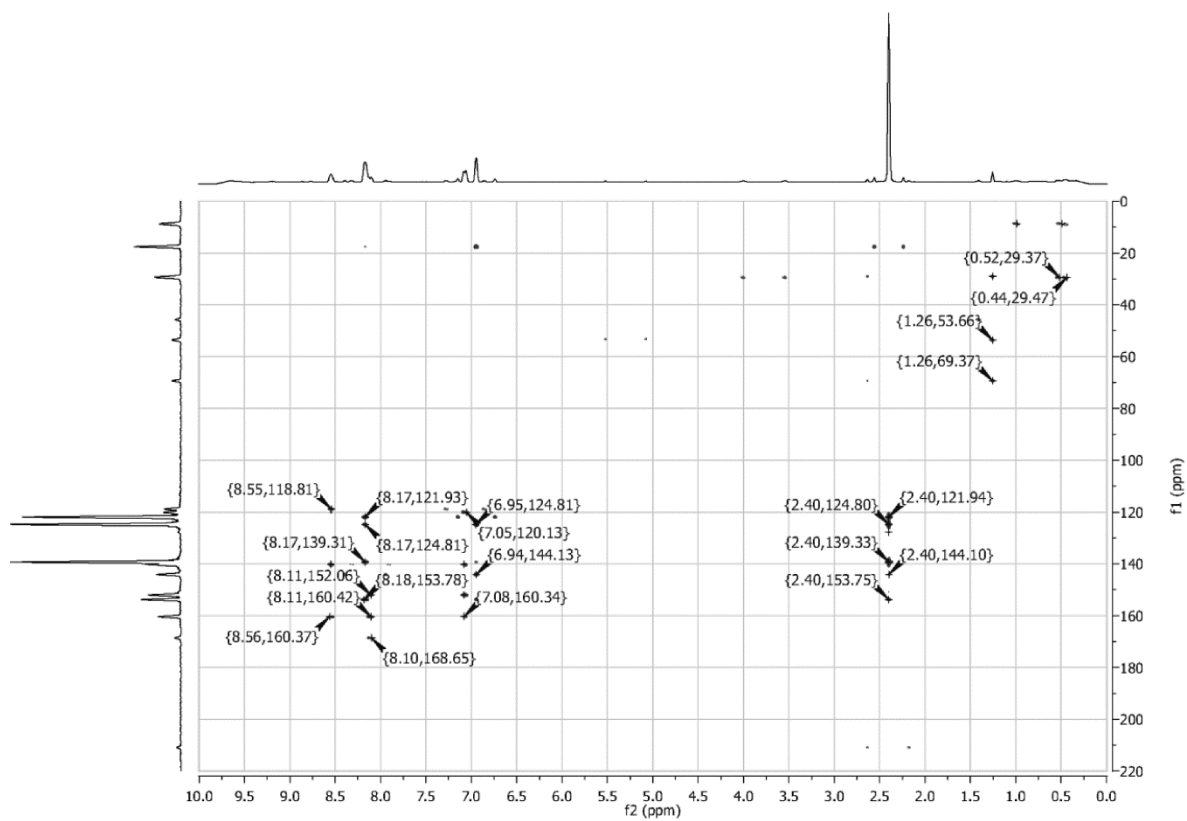


Figure 3.12. Long range ^1H , ^{13}C NMR (HMBC) spectrum of nevirapine in CDCl_3

3.3. Biological evaluation

3.3.1. ELISA enzymatic assay

A stock solution in DMSO of compounds **1-2** and **7-10a** was prepared by dissolving 0.5-1.5 mg of each compound in DMSO (0.5 mL) obtaining a concentration in the range 3.0 ÷ 6.0 mM and stored at -20°C until the use.

The HIV-RT inhibition assay was performed by using a RT assay kit (Roche), according to the procedure for assaying RT inhibition performed as described in the kit protocol (Figure 3.13).

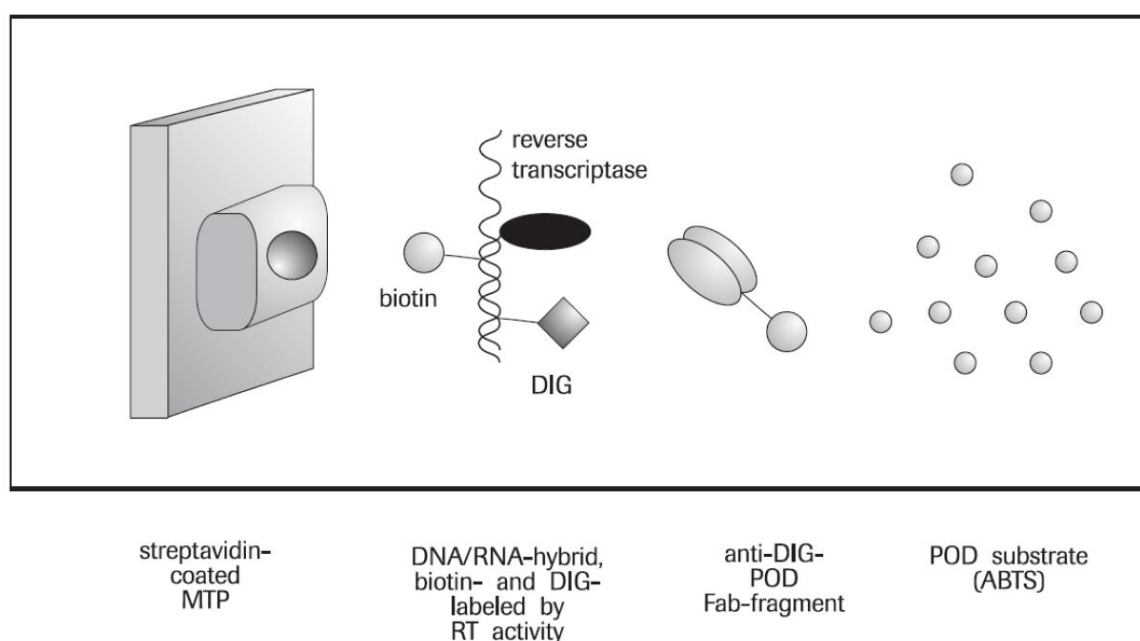


Figure 3.13. Schematic representation of working method for RT ELISA.

Briefly, the reaction mixture consists of template / primer complex, 2'-deoxy-nucleotide-5'-triphosphates (dNTP's) and reverse transcriptase (RT) enzyme in the lysis buffer without or with inhibitors at final concentration of 200 μ M. After 1 hour incubation at 37°C, the reaction mixture was transferred to streptavidine-coated microtitre plate (MTP). The biotin-labeled dNTPs that are incorporated in the template because of the activity of RT were bound to streptavidine. The unbound dNTPs were washed using wash buffer and anti-digoxigenin-peroxidase (DIG-POD) was added in MTP. The DIG-labeled dNTPs incorporated in the template was bound to anti-DIG-POD Antibody. The unbound anti-DIG-

POD was washed and the peroxide substrate (ABST) was added to the MTP. A colored reaction product was produced during the cleavage of the substrate catalyses by a peroxide enzyme. The absorbance (O.D.) of the samples were determined at λ 405 nm using microtiter plate ELISA reader. The resulting color intensity is directly proportional to the actual RT activity. The percentage inhibitory activity of RT inhibitors was calculated by comparing to a sample that does not contain an inhibitor. The percentage inhibition was calculated by the formula as given:

$$\% \text{ Inhibition} = 100 - \left[\frac{\text{O. D. 405nm with inhibitor}}{\text{O. D. 405nm without inhibitor}} \times 100 \right]$$

3.3.1.1. Validation of ELISA assay

The kit was validated using different concentration of nevirapine (NVP) and reading the absorbance of colored reaction product at different time. The results are summarized in table 3.4.

Table 3.4. Validation of ELISA enzymatic test (Roche)

Concentration of nevirapine (μ M)	Reading time (minutes)				
	10	15	20	30	40
	% RT inhibition \pm SD	% RT inhibition \pm SD	% RT inhibition \pm SD	% RT inhibition \pm SD	% RT inhibition \pm SD
1.0	32.1 \pm 1.1	-1.5 \pm 2.0	-6.5 \pm 5.9	-6.9 \pm 4.8	-11.4 \pm 4.9
2.5	29.9 \pm 4.8	10.2 \pm 0.5	10.1 \pm 0.1	2.47 \pm 1.2	-8.61 \pm 1.3
25	70.1 \pm 0.5	69.2 \pm 0.9	64.8 \pm 0.5	50.5 \pm 0.8	39.2 \pm 1.1

The kit contained only a small amount of reverse transcriptase, not enough to be used in all the microtiter plate and the other reagents contained in it, so that the inhibitory activity of nevirapine was studied on a different recombinant reverse transcriptase (Pierce Biotechnology) using all the other reagents present in the kit. Figure 3.14 reports the effect of nevirapine at 200 μ M of concentration on Pierce reverse transcriptase in pure water and in buffer phosphate at pH 7.4 added of 0.2% of BSA, in comparison with the original RT present in the kit.

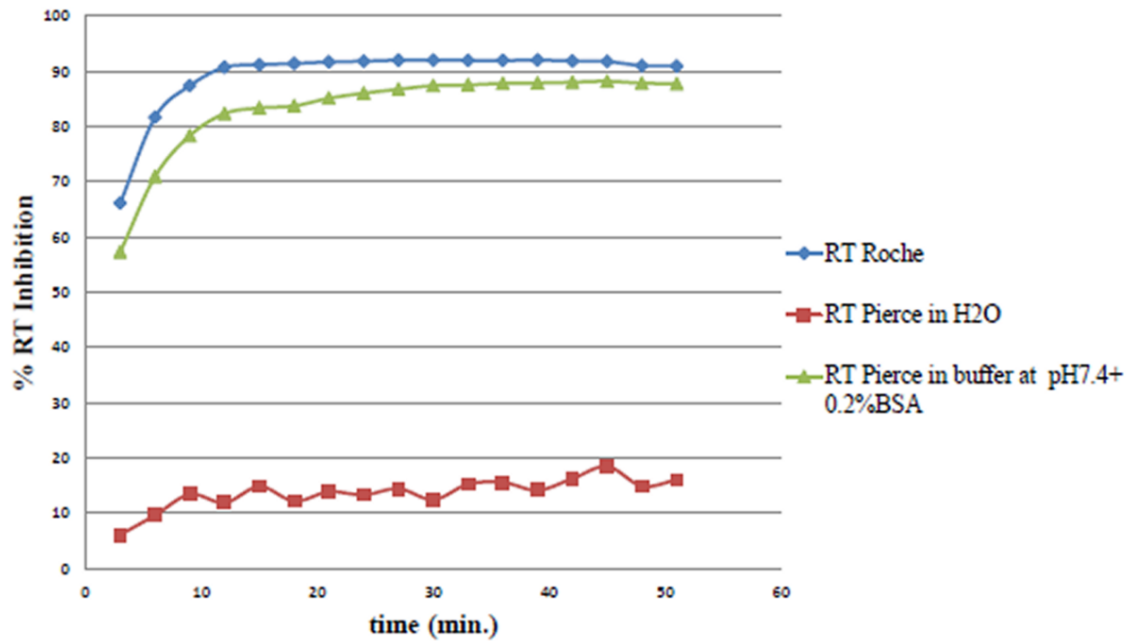


Figure 3.14. Comparison of percentage inhibition with different RT enzymes in the presence of nevirapine (200 μ M)

In order to test the stability of Pierce reverse transcriptase, using the same conditions adopted in the Roche kit, a cycle of freezing at -80°C and thawing at 0°C was applied on both reverse transcriptase samples. The results are shown in figure 3.15.

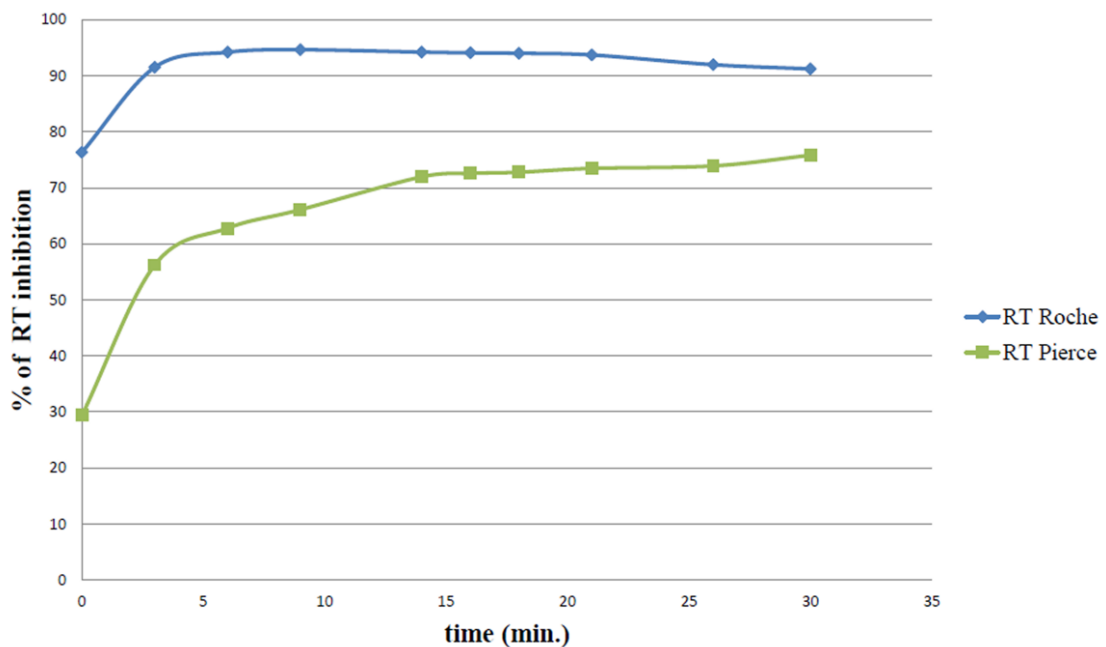


Figure 3.15. Comparison between Roche and Pierce RT inhibition after a cycle of freezing/thawing.

From these preliminary validation tests it was possible to establish that Pierce reverse transcriptase is not useful with the Roche kit and that the best time to read the plate at the microplate reader is 10 minutes after the addition of ABTS reagent.

3.3.1.2. Results of the assay

Stock solutions of compounds **1-2** and **7-10a** were diluted with lysis buffer at a final concentration of 200 μ M. Each compound was assayed three times and nevirapine was used as positive control test. The results are summarized in the table 3.5.

Table 3.5. Results of HIV-RT Kit Assay

Compound	% of RT inhibition ^{b)} \pm SD
1	4.92 \pm 0.07
2	66.5 \pm 0.8
8a	77.3 \pm 0.5
8b	30 \pm 7
9	20 \pm 1
10	32 \pm 2
NVP^{a)}	58.5 \pm 0.6

a) NVP = nevirapine

b) Results from three independent experiments

3.3.2. Anti-HIV activity assay

Inhibition of HIV-1(IIIB) and HIV-2(ROD)-induced cytopathicity in CEM cell cultures was measured in microtiter 96-well plates containing $\sim 3 \times 10^5$ CEM cells/mL, infected with 100 CCID₅₀ of HIV per mL and containing appropriate dilutions of the test compounds. After 4–5 days of incubation at 37 °C in a CO₂-controlled humidified atmosphere, CEM giant (syncytium) cell formation was examined microscopically. The EC₅₀ (50% effective concentration) was defined as the compound concentration required to inhibit HIV-induced giant cell formation by 50% (Table 3.6).

Table 3.6. Anti-HIV activity and cytotoxicity in CEM cells by testing the synthesized molecules

Compound	EC ₅₀ ^{a)} (μ M)		CC ₅₀ ^{b)} \pm SD (μ M)
	HIV-1	HIV-2	CEM
1	>250	>250	148 \pm 11
2	>10	>10	175 \pm 106
3	>10	>10	83 \pm 12
4	>10	>10	182 \pm 27
5	>10	>10	76 \pm 7
6	25 \pm 3.5	\geq 50	121 \pm 10
7	>2	>2	4.9 \pm 1.5
8a	>2	>2	5.4 \pm 3.6
8b	\geq 10	\geq 10	50 \pm 18
9	>50	>50	93 \pm 16
11	>10	>10	6.5 \pm 4.0
12	>2	>2	4.2 \pm 2.5
13	\geq 2	\geq 2	4.0 \pm 1.6
14	>10	>10	16 \pm 0
15	>10	>10	5.4 \pm 2.0
17	>2	>2	83 \pm 34
18	\geq 50	\geq 50	150 \pm 25
18a	>50	>50	25 \pm 4
19	>10	>10	214 \pm 52
20	>10	>10	\geq 250
21	>10	>10	2.2 \pm 1.6
22	>10 ^c	>10 ^c	> 250
23	>0.4	>0.4	4.4 \pm 2.3
24	>10	>10	41 \pm 18
25	>10	>10	77 \pm 9
26	>2	>2	68 \pm 21
NVP	0.11 ^d	10 ^d	>200 ^d

a) EC₅₀=effective concentration or concentration required to protect CEM cells against the cytopathogenicity of HIV by 50 %

b) Concentration required to reduce CEM cell viability by 50%.

c) Compound precipitation was detected at higher compound concentration.

d) Values obtained from: <http://pubchem.ncbi.nlm.nih.gov/assay/assay.cgi?cid=4463>

3.3.3. Antiviral activity

The antiviral assays were based on inhibition of virus-induced cytopathicity in HEL cell cultures for herpes simplex virus type 1 (HSV-1), HSV-2(G), vaccinia virus, vesicular stomatitis virus (Table 3.7) and varicella-zoster virus (VZV) (Table 3.8); in Vero cell cultures for parainfluenza- 3, reovirus-1, Sindbis, Coxsackie B4 and Punta Toro virus (Table 3.10); in HeLa cell cultures for vesicular stomatitis virus, Coxsackie virus B4 and respiratory syncytial virus (Table 3.9); in MDCK (Madin Darby canine kidney) cell cultures for influenza A (H1N1 and H3N1) and influenza B virus (Table 3.12) and in CrFK (Crandell-Rees Feline Kidney) cell cultures for feline herpes virus and feline corona virus (FIPV) (Table 3.11).

Confluent cell cultures in microtiter 96-well plates were inoculated with 100 cell culture inhibitory dose-50 (CCID₅₀) of virus (1 CCID₅₀ being the virus dose to infect 50% of the cell cultures) in the presence of varying concentrations of the test compounds. Viral cytopathicity was recorded as soon as it reached completion in the control virus infected cell cultures that were not treated with the test compounds.

For the anti-cytomegalovirus assay, confluent human embryonic lung (HEL) fibroblast cultures were grown in 96-well microtiter plates and infected with the human cytomegalovirus (HCMV) strains AD-169 and Davis at 100 PFU per well. After a 2 hour-incubation period, residual virus was removed and the infected cells were further incubated with medium containing different concentrations of the test compounds (in duplicate). After incubation for 7 days at 37 °C, virus-induced cytopathogenicity was monitored microscopically after ethanol fixation and staining with Giemsa.

Antiviral activity was expressed as the EC₅₀ or compound concentration required to reduce virus-induced cytopathogenicity by 50%. EC₅₀'s were calculated from graphic plots of the percentage of cytopathogenicity as a function of concentration of the tested compounds (Table 3.13)

Table 3.7. Anti-herpes simplex, vaccinia and vesicular stomatitis virus activity in HEL cell line cultures by testing the new synthetic molecules **1-26**

Compound	Minimum cytotoxic concentration ^{a)} (µM)	EC ₅₀ ^{b)} (µM)				
		Herpes simplex virus-1 (KOS)	Herpes simplex virus-2 (G)	Vaccinia virus	Vesicular stomatitis virus	Herpes simplex virus-1 TK ⁻ KOS ACV ^r
1	>100	>100	>100	>100	>100	>100
2	>100	>100	>100	>100	>100	>100
3	>100	>100	>100	>100	>100	>100
4	>100	>100	>100	>100	>100	>100
5	>100	>100	>100	>100	>100	>100
6	>100	>100	>100	>100	>100	>100
7	20	>4	>4	>4	>4	>4
8a	>100	>100	>100	>100	>100	>100
8b	>100	>100	>100	>100	>100	>100
9	>100	>100	>100	>100	>100	>100
11	≥4	>4	>4	>4	>4	>4
12	20	>4	>4	>4	>4	>4
13	>100	>100	>100	>100	>100	>100
14	>100	>100	>100	>100	>100	>100
15	20	>4	>4	>4	>4	>4
17	≥20	>20	>20	>20	>20	>20
18	>100	>100	>100	>100	>100	>100
18a	≥20	>20	>20	>20	>20	>20
19	>100	>100	>100	>100	>100	>100
20	>100	>100	>100	>100	>100	>100
21	20	>4	>4	>4	>4	>4
22	>100	>100	>100	>100	>100	>100
23	>100	>100	>100	>100	>100	>100
24	>100	>100	>100	>100	>100	>100
25	>100	>100	>100	>100	>100	>100
26	>100	>100	>100	>100	>100	>100
Reference compounds						
Brivudin	>250	0.04	250	10	>250	250
Cidofovir	>250	1	0.4	17	>250	0.4
Acyclovir	>250	0.2	0.1	>250	>250	50
Ganciclovir	>100	0.03	0.02	>100	>100	12

a) Required to cause a microscopically detectable alteration of normal cell morphology.

b) Required to reduce virus-induced cytopathogenicity by 50 %.

Table 3.8. Anti-varicella-zoster virus activity in HEL cell line cultures for the synthetic compounds 1-26

Compound	Antiviral activity EC ₅₀ (μM) ^{a)}		Cytotoxicity (μM)	
	TK ⁺ VZV strain OKA	TK ⁻ VZV strain 07-1.	Cell morphology (MCC) ^{b)}	Cell growth (CC ₅₀) ^{c)}
1	>100	>100	>100	
2	62	89	>100	100
3	>100	>100	>100	
4	100	>20	100	
5	>20	>20	100	
6	>100	>100	>100	
7	>20	>20	100	
8a	>4	>4	20	
8b	47	41	>100	39
9	>100	>100	>100	
11	>4	>4	20	
12	>4	>4	20	
13	8	9	100	2
14	>20	>20	100	
15	>20	>20	100	
17	13	>4	20	
18	>100	>100	>100	
18a	>20	9.6	100	>100
19	>20	>20	100	
20	>20	>20	100	
21	>100	>100	>100	
22	>20	>20	100	
23	>0.16	>0.16	0,8	
24	>4	>4	20	
25	>20	>20	100	
26	>20	20	100	
Reference compounds				
Acyclovir	3.5	131	>440	440
Brivudin	0,050	95	>300	260

a) Effective concentration required to reduce virus plaque formation by 50%. Virus input was 20 plaque forming units (PFU).

b) Minimum cytotoxic concentration that causes a microscopically detectable alteration of cell morphology.

c) Cytotoxic concentration required to reduce cell growth by 50%.

Table 3.9. Anti-vesicular stomatitis, Coxsackie and respiratory syncytial viruses activities in HeLa cell line cultures for the synthetic compounds **1-26**

Compound	Minimum cytotoxic concentration ^{a)} (µM)	EC ₅₀ ^{b)} (µM)		
		Vesicular stomatitis virus	Coxsackie virus B4	Respiratory syncytial virus
1	>100	>100	>100	>100
2	>100	>100	>100	>100
3	>100	>100	>100	>100
4	>100	>100	>100	>100
5	>100	>100	>100	>100
6	>100	>100	>100	>100
7	20	>4	>4	>4
8a	20	>4	>4	>4
8b	100	>20	>20	>20
9	>100	>100	>100	>100
11	20	>4	>4	>4
12	20	>4	>4	>4
13	>100	>100	>100	>100
14	>100	>100	>100	>100
15	≥20	>20	>20	>20
17	100	>20	>20	>20
18	>100	>100	>100	>100
18a	>100	>100	>100	>100
19	>100	>100	>100	>100
20	>100	>100	>100	>100
21	100	>20	>20	>20
22	>100	>100	>100	>100
23	4	>0.8	>0.8	>0.8
24	>100	>100	>100	>100
25	100	>20	>20	>20
26	100	>20	>20	>20
Reference compounds				
DS-5000 (µg/ml)	>100	20	>100	0.6
(S)-DHPA	>250	>250	>250	>250
Ribavirin	>250	10	112	2

a) Required to cause a microscopically detectable alteration of normal cell morphology.

b) Required to reduce virus-induced cytopathogenicity by 50 %.

Table 3.10. Anti-parainfluenza, reovirus-1, Sindbis, Coxsackie and Punta Toro viruses activities in VERO cell line cultures for the synthetic compounds **1-26**

Compound	Minimum cytotoxic concentration ^{a)} (µM)	EC ₅₀ ^{b)} (µM)				
		Para-influenza-3 virus	Reovirus-1	Sindbis virus	Coxsackie virus B4	Punta Toro virus
1	>100	>100	>100	>100	>100	>100
2	>100	>100	>100	>100	>100	>100
3	>100	>100	>100	>100	>100	>100
4	>100	>100	>100	>100	>100	>100
5	>100	>100	>100	>100	>100	>100
6	>100	>100	>100	>100	>100	>100
7	≥20	>20	>20	>20	>20	>20
8a	100	>20	>20	>20	>20	>20
8b	100	>20	>20	>20	>20	>20
9	>100	>100	>100	>100	>100	>100
11	≥4	>4	>4	>4	>4	>4
12	≥4	>4	>4	>4	>4	>4
13	>100	>100	>100	>100	>100	>100
14	≥100	>100	>100	>100	>100	>100
15	20	>4	>4	>4	>4	>4
17	≥20	>20	>20	>20	>20	>20
18	>100	>100	>100	>100	>100	>100
18a	≥20	>20	>20	>20	>20	>20
19	>100	>100	>100	>100	>100	>100
20	>100	>100	>100	>100	>100	>100
21	20	>4	>4	>4	>4	>4
22	>100	>100	>100	>100	>100	>100
23	≥100	>100	>100	>100	>100	>100
24	>100	>100	>100	>100	>100	>100
25	100	>20	>20	>20	>20	>20
26	≥20	>20	>20	>20	>20	>20
Reference compounds						
DS-5000 (µg/ml)	>100	>100	100	>100	100	>100
(S)-DHPA	>250	250	>250	>250	>250	>250
Ribavirin	>250	22	148	>250	>250	50

a) Required to cause a microscopically detectable alteration of normal cell morphology.

b) Required to reduce virus-induced cytopathogenicity by 50 %.

Table 3.11. Anti-feline corona virus and feline herpes virus activities in CRFK cell cultures for the synthetic compounds **1-26**

Compound	CC ₅₀ ^{a)} (μ M)	EC ₅₀ ^{b)} (μ M)	
		Feline Corona Virus (FIPV)	Feline Herpes Virus
1	>100	>100	>100
2	>100	>100	>100
3	>100	>100	>100
4	>100	>100	>100
5	>100	>100	>100
6	>100	>100	>100
7	6.5	>4	>4
8a	12.7	>4	>4
8b	84.9	>20	>20
9	>100	>100	>100
11	5.4	>4	>4
12	6.5	>4	>4
13	48.3	>20	>20
14	>100	>100	>100
15	5.4	>4	>4
17	9.5	>4	>4
18	>100	>100	>100
18a	>100	>100	>100
19	>100	>100	>100
20	>100	>100	>100
21	10.7	>4	>4
22	>100	>100	>100
23	13.2	>4	>4
24	>100	>100	>100
25	38.7	>20	>20
26	13.8	>4	>4
Reference compounds			
HHA (μg/ml)	>100	30.9	44.3
UDA (μg/ml)	46.3	9.3	3.1
Ganciclovir	>100	>100	2.2

a) 50% Cytotoxic concentration, as determined by measuring the cell viability with the colorimetric formazan- based MTS assay.

b) 50% Effective concentration, or concentration producing 50% inhibition of virus-induced cytopathic effect, as determined by measuring the cell viability with the colorimetric formazan-based MTS assay.

Table 3.12. Anti-influenza A and B activities in MDCK cell cultures by testing the synthetic compounds 1-26

Compound	Cytotoxicity		Antiviral EC ₅₀ ^{c)} (μM)					
	CC ₅₀ ^{a)} (μM)	Minimum cytotoxic conc. ^{b)} (μM)	Influenza A H1N1 subtype		Influenza A H3N2 subtype		Influenza B	
			visual CPE score	MTS	visual CPE score	MTS	visual CPE score	MTS
1	>100	>100	>100	>100	>100	>100	>100	>100
2	>100	≥100	>100	>100	>100	>100	>100	>100
3	47.0	100	>20	>20	>20	>20	>20	>20
4	41.2	≥20	>20	>20	>20	>20	>20	>20
5	33.1	≥20	>20	>20	>20	>20	>20	>20
6	33.5	≥20	>20	>20	>20	>20	>20	>20
7	9.6	20	>4	>4	>4	>4	>4	>4
8a	>100	4	>0.8	>0.8	>0.8	>0.8	>0.8	>0.8
8b	43.0	20	>4	>4	>4	>4	>4	>4
9	>100	≥100	>100	>100	>100	>100	>100	>100
11	1.8	4	>0.8	>0.8	>0.8	>0.8	>0.8	>0.8
12	2.0	4	>0.8	>0.8	>0.8	>0.8	>0.8	>0.8
13	2.3	4	>0.8	>0.8	>0.8	>0.8	>0.8	>0.8
14	>100	>100	>100	>100	>100	>100	>100	>100
15	1.9	4	>0.8	>0.8	>0.8	>0.8	>0.8	>0.8
17	8.9	20	>4	>4	>4	>4	>4	>4
18	>100	≥20	>20	>20	>20	>20	>20	>20
18a	>100	100	>20	>20	>20	>20	>20	>20
19	>100	>100	>100	>100	>100	>100	>100	>100
20	>100	>100	>100	>100	>100	>100	>100	>100
21	9.1	20	>4	>4	>4	>4	>4	>4
22	>100	>100	>100	>100	>100	>100	>100	>100
23	5.4	0.8	>0.16	>0.16	>0.16	>0.16	>0.16	>0.16
24	17.4	≥20	>20	>20	>20	>20	>20	>20
25	10.2	20	>4	>4	>4	>4	>4	>4
26	10.4	20	>4	>4	>4	>4	>4	>4
Reference compounds								
Oseltamivir carboxylate	>100	>100	3	8.2	0.8	0.6	100	>100
Ribavirin	>100	>100	7	11.3	4	3.3	2	1.0
Amantadine	>200	>200	89	51.8	0.7	0.6	>200	>200
Rimantadine	>200	>200	14	9.8	0.7	0.6	>200	>200

a) 50% Cytotoxic concentration, as determined by measuring the cell viability with the colorimetric formazan- based MTS assay.

b) Minimum compound concentration that causes a microscopically detectable alteration of normal cell morphology.

c) 50% Effective concentration, or concentration producing 50% inhibition of virus-induced cytopathic effect, as determined by visual scoring of the CPE, or by measuring the cell viability with the colorimetric formazan-based MTS assay.

Table 3.13. Anti- Cytomegalovirus activity in HEL cell cultures by testing for the synthetic compounds 1-26

Compound	Antiviral activity EC50 ^{a)} (μ M)		Cytotoxicity (μ M)	
	AD-169 strain	Davis strain	Cell morphology ^{b)} (MCC)	Cell growth ^{c)} (CC ₅₀)
1	>100	>100	>100	
2	54	66	>100	100
3	82	78	>100	>100
4	78	78	>100	>100
5	33	38	100	>100
6	>100	>100	>100	
7	>20	>20	100	
8a	>4	>4	20	
8b	38	33	>100	27
9	>100	>100	>100	
11	>4	>4	20	
12	>4	>4	20	
13	>20	>20	100	
14	>20	>20	100	
15	>20	>20	100	
17	>20	>4	20	
18	100	>100	>100	
18a	>100	>100	>100	
19	>20	>20	100	
20	>20	>20	100	
21	>20	>20	100	
22	>100	>100	>100	
23	>20	>20	100	
24	>20	>20	100	
25	20	20	100	
26	>20	>20	100	
Reference compounds				
Ganciclovir	9	9	>350	140
Cidofovir	0.9	1.6	>300	63

a) Effective concentration required to reduce virus plaque formation by 50%. Virus input was 100 plaque forming units (PFU).

b) Minimum cytotoxic concentration that causes a microscopically detectable alteration of cell morphology.

c) Cytotoxic concentration required to reduce cell growth by 50%.

3.3.4. Cytostatic activity

Murine leukaemia L1210, human T-lymphocyte CEM, human cervix carcinoma (HeLa) and human lung fibroblast (HEL) cells were suspended at 300,000-500,000 cells/mL of culture medium, and 100 μ L of a cell suspension was added to 100 μ L of an appropriate dilution of the test compounds in wells of 96-well microtiter plates. After incubation at 37°C for two (L1210) or three (CEM, HeLa, HEL) days, the cell number was determined using a Coulter counter. The IC₅₀ was defined as the compound concentration required to inhibit cell proliferation by 50% (Table 3.14).

Table 3.14. Cytostatic activity on murine leukemia, human T-lymphocyte and human cervix carcinoma activity by testing compounds **1-26**

Compound	IC ₅₀ ^{a)} \pm SD (μ M)		
	L1210	CEM	HeLa
1	135 \pm 1	148 \pm 11	108 \pm 1
2	98 \pm 25	175 \pm 106	105 \pm 1
3	89 \pm 19	83 \pm 12	96 \pm 10
4	125 \pm 41	182 \pm 27	167 \pm 83
5	42 \pm 0	76 \pm 7	30 \pm 3
6	106 \pm 5	121 \pm 10	23 \pm 2
7	2.5 \pm 0.4	4.9 \pm 1.5	3.1 \pm 0.2
8a	3.3 \pm 0.9	5.4 \pm 3.6	1.4 \pm 0.6
8b	32 \pm 4	50 \pm 18	28 \pm 3
9	93 \pm 9	93 \pm 16	92 \pm 19
11	2.3 \pm 0.2	6.5 \pm 4.0	1.4 \pm 0.4
12	3.0 \pm 0.2	4.2 \pm 2.5	1.6 \pm 0.4
13	2.9 \pm 0.9	4.0 \pm 1.6	2.8 \pm 0.4
14	122 \pm 13	214 \pm 52	89 \pm 27
15	21 \pm 14	77 \pm 9	14 \pm 10
17	0.95 \pm 0.07	2.2 \pm 1.6	2.9 \pm 0.6
18	141 \pm 6	150 \pm 25	173 \pm 81
18a	38 \pm 10	25 \pm 4	88 \pm 56
19	67 \pm 43	68 \pm 21	67 \pm 15
20	183 \pm 11	\geq 250	136 \pm 20
21	71 \pm 15	83 \pm 34	60 \pm 39
22	160 \pm 11	$>$ 250	191 \pm 10
23	4.9 \pm 3.5	4.4 \pm 2.3	4.5 \pm 0.3
24	94 \pm 21	41 \pm 18	30 \pm 12
25	32 \pm 16	16 \pm 0	20 \pm 1
26	3.6 \pm 0.1	5.4 \pm 2.0	4.6 \pm 0.2

a) 50% inhibitory concentration.

3.3.5. Antibacterial activity

Agar diffusion assay

Compounds were tested for biological activities against several target organisms including Gram-negative bacteria *Escherichia coli* ATCC 25922 and *Pseudomonas aeruginosa* ATCC 27853 as well as Gram-positive bacteria *Staphylococcus aureus* ATCC 25923, Methicillin-resistant *Staphylococcus aureus* (MRSA) ATCC 43300. Amoxicillin, penicillin, gentamycin, erythromycin and vancomycin were used as positive control tests.

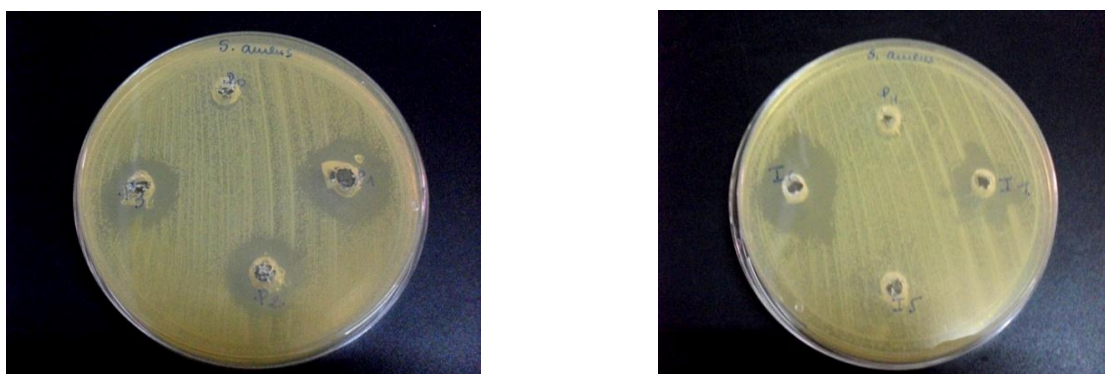


Figure 3.16. Antibacterial activity of compounds **1-4** (on the left) and **14, 18, 20, 22** (on the right) against *S. aureus* ATCC 29523

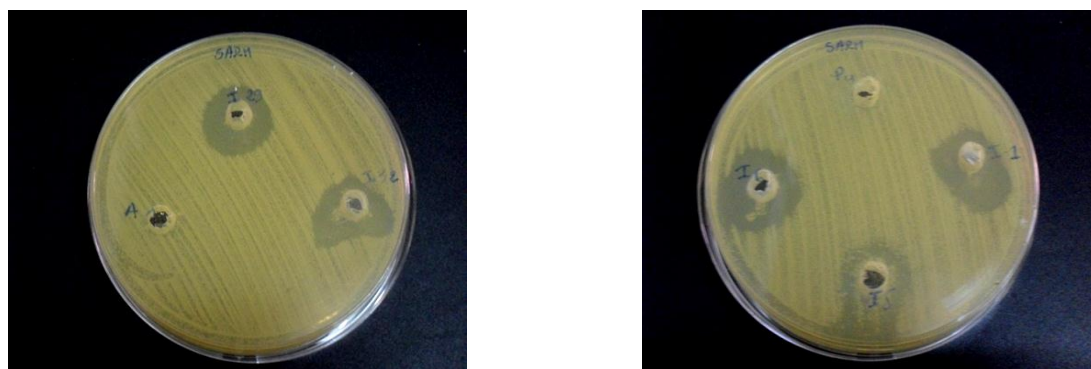


Figure 3.17. Antibacterial activity of **9, 18a** and **19** (on the left) and **14, 18, 20** and **22** (on the right) against *MRSA* ATCC 43300

Table 3.15. Antibacterial activity on *E. coli* (ATCC 25922), *P. aeruginosa* (ATCC 27853), *S. aureus* (ATCC 25923) and *MRSA* (ATCC 43300) strains. 100 µg of each new compound has been used. The strength of activity is presented as resistant (R, Ø < 13mm), intermediate (I, Ø =14÷16 mm) and susceptible (S, Ø > 17mm)

Compound (µmol)	Inhibition zone diameter ± SD (mm)							
	Gram (-)				Gram (+)			
	<i>E. coli</i> ATCC 25922	Activity strength	<i>P.</i> <i>aeruginosa</i> ATCC 27853	Activity strength	<i>S. aureus</i> ATCC 25923	Activity strength	<i>MRSA</i> ATCC 43300	Activity strength
1 (0.46)	8.42±0.16	R	8.33±0.2	R	0	R	0	R
2 (0.38)	7.83±0.25	R	0	R	21.34±0.39	S	19.42±0.26	S
3 (0.36)	8.60±0.14	R	9.87±0.22	R	18.16±0.1	S	0	R
4 (0.36)	7.34±0.22	R	7.42±0.19	R	17.77±0.18	S	0	R
9 (0.30)	11.73±0.28	R	13.05±0.14	R	10.81±0.12	R	10.66±0.21	R
14 (0.35)	0	R	0	R	20.18±0.38	S	19.45±0.14	S
18 (0.38)	8.35±0.12	R	0	R	12.82±0.19	R	17.92±0.13	S
18a (0.25)	13.88±0.03	R	0	R	0	R	15.27±0.35	I
19 (0.36)	0	R	0	R	11.07±0.36	R	20.19±0.21	S
20 (0.25)	9.79±0.57	R	0	R	0	R	16.52±0.6	I
Reference antibiotics								
Penicillin G (6 µg, 0.017)	-	-	-	-	27.84±0.26	S	-	-
Erythromycin (15 µg, 0.02)	-	-	-	-	25.03±0.24	S	14.63±0.27	I
Vancomycin (30 µg, 0.02)	-	-	-	-	18.65±0.19	S	-	-
Gentamicin (10 µg, 0.02)	23.37±0.5	S	18.11±0.61	S	22.02±0.45	S	-	-

Determination of the minimum inhibitory concentrations (MIC) for antibacterial activity

MIC values have been determined for some selected compounds. The data are reported in table 3.16.

Table 3.16. Minimum Inhibitory Concentration on *S. aureus* (ATCC 25923), *MRSA* (ATCC 43300) and *P. aeruginosa* (ATCC 27853) strains.

MIC ^{a)} (μM)						
Compound	<i>S. aureus</i> ATCC 25923	SI ^{b)}	<i>MRSA</i> ATCC 43300	SI ^{b)}	<i>P.</i> <i>aeruginosa</i> ATCC 27853	SI ^{b)}
2	120	1	120	1	-	-
3	29	3	-	-	58	2
4	< 7.2	>17	-	-	< 7.2	>17
14	<7.1	>16	<7.1	>16	-	-
18	-	-	< 7.5	>19	-	-
19	<7.1	>9	<7.1	>9	-	-
20	-	-	<5	>27	-	-
Reference antibiotic						
Vancomycin	-	-	< 1.4	-	-	-

a) MIC is the minimal inhibitory concentration

b) Selectivity Index, SI = IC₅₀/EC₅₀

4. Discussion

4.1. Drug design

In order to find novel molecules able to overcome the resistance of the clinically used non-nucleoside reverse transcriptase inhibitors (§ 1.5), this thesis has the aim to use a fragment based design of new potential anti-HIV agents, based on hybrid structures deriving from active molecules, both of synthetic and natural origin. Otherwise, natural products have always played a relevant role in medicine. The major advantage offered by using secondary metabolites as useful templates, is that they are *per se* highly bioactive and selective. Because they are produced by Nature to protect a particular organism, they have been subjected to evolutive pressure for several hundreds of millions of years and have been selected to reach optimal activity and to perform specialized functions, e.g. of defence or sexual mechanisms (Mancini, 2007).

(+)-Calanolide A is the most active anti-HIV-1 compound isolated from the rainforest tree *Calophyllum lanigerum* (Kashman, 1992). It inhibits laboratory strains of HIV-1 (EC_{50} 0.10–0.17 μ M) and HIV-1 reverse transcriptase, but it is inactive on HIV-2 reverse transcriptase or cell DNA polymerase (Currens, 1996). Synthetic molecules with unnatural structures have been also produced with the aim to be used as anti-HIV drugs. In this contest α -anilino-phenylacetamide (α -APA) has shown to inhibit reverse transcriptase by interaction with the allosteric pocket with IC_{50} 14 nM in CEM cells (Pauwels, 1993).

In details, the series of hybrid molecules under investigation derives from the benzyl-amino moiety, present in α -APA structure and the simplified pyranone unit, present in the structure of the natural product (+)-calanolide A (Figure 4.1). The choice is reinforced by the fact that the 2-pyrone fragment, present in many natural products, is associated to the exhibition of analgesic, fungicide and antibacterial activities (Novikov, 2002).

The R group in the pyranone moiety reported in the structures of figure 4.1 has been modified in order to modulate both steric and electronic effects by substitution of H-3 (in the subunit deriving from calanolide A structure) with halogen, nitro, alkyl or acyl groups. The lengthening of the chain between the X group and the aryl unit allows to increase the number of rotatable bonds, with the possibility to adapt better the ligand into the binding pocket of the enzyme.

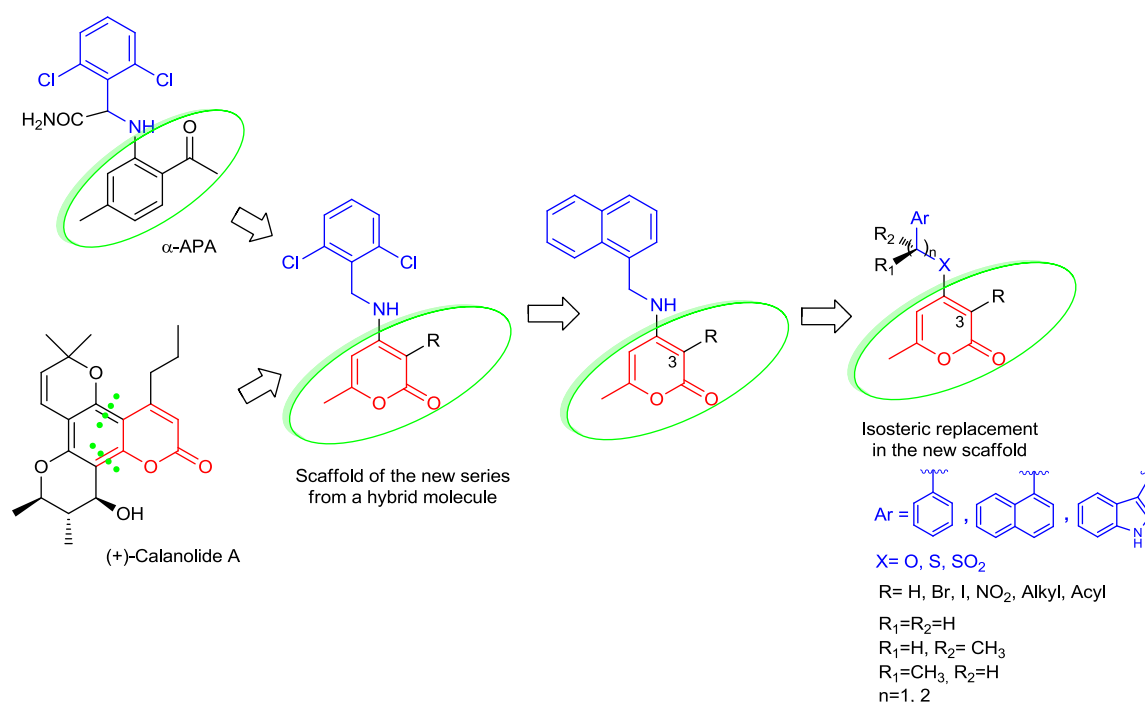


Figure 4.1. Drug design process to select the series of new molecules

Isosterism is a strategy used in medicinal chemistry for the rational design of new molecules able to modify the interactions with the binding pocket, both for the steric (size and shape) and electro-topological character (Kier, 2004), transferring the effect on the whole molecule. It is known that ether or thioether units are often present in NNRT molecules, as observed in the structures of (S)-4-isopropoxycarbonyl-6-methoxy-3-methylthiomethyl-3,4-dihydroquinoxalin-2(1H)-thione (HBY) and 3-[2-bromo-4-(1H-pyrazolo[3,4-c]pyridazin-3-ylmethyl)phenoxy]-5-methylbenzonitrile (PZ2) compounds (Figure 3.3). They have inspired a replacement of NH group with oxygen or sulfur atoms in the scaffold of the hybrid molecules under investigation in this thesis (Figure 4.1). The oxidation of thioether group yields the formation of sulfone unit, in which the S atom has a tetrahedral geometry able to induce a butterfly-like geometry of the molecules, as observed in many NNRTIs (e.g. 5-bromo-3-(pyrrolidin-1-ylsulfonyl)-1H-indole-2-carboxamide (MRX), Figure 3.3). This knowledge has suggested the substitution of NH group with –O– or –S– or –SO₂–units.

It has been reported that the introduction of a methyl group in a small molecule can boost 10-fold or greater its activity (Leung, 2012); for this reason and with the aim to increase the hydrophobic interaction in the RT pocket (rich in non-polar amino acids), a methyl group has been introduced at the benzylic carbon. Its presence allowed to create a stereogenic

center, producing enantiomeric molecules expected to give different diastereomeric interactions responsible for potential different inhibitor activity against reverse transcriptase.

From all the possible combinations, only the molecules following the Lipinsky rule, which is a useful guide to discriminate *a priori* structures with drug-like chemical-physical properties (§1.6.1; Lipinsky, 2000 and 2001) have been subjected to docking calculation. They are about 100 and the relative data are reported in Table 3.3 and Appendix A.

4.1.1. Docking validation

Molecular docking can help to select the molecules which are potential candidates to be synthesized and furtherly assayed for their biological activities. Recently, a study of docking validation on 780 ligand-receptor complexes, both with rigid and flexible treatment of ligands during the docking calculation, has shown that taking into account the ligand flexibility the binding energy increases, in contrast to rigid treatment in which the binding energy remains constant (Figure 4.2; Mukherjee, 2010). In particular the success of docking (average 75%) is obtained with fewer than seven rotatable bonds and it decreases at 55% for 8-15 rotatable bonds, down to 39% if the rotatable bonds are greater than 15.

In order to have trusted results, the docking process has been validated before to be used with the new designed molecules. For this purpose different X-ray crystal structures of reverse transcriptase, complexed with clinically used NNRTI ligands or promising NNRTIs, were downloaded from RCSB Protein Data Bank and the ligand of each structure has been docked both in the same original structure and in other structures for a process of cross-validation. The results of these calculations have shown that the molecules with a higher number of rotatable bonds have a better interaction energy (Table 3.2).

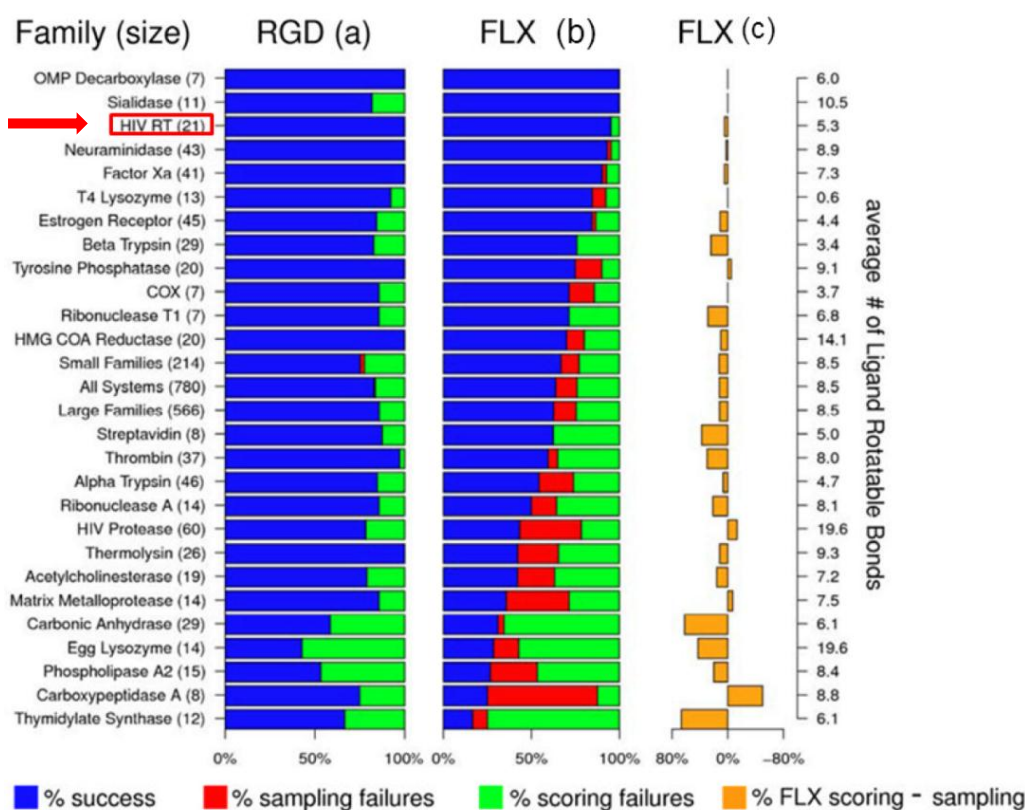


Figure 4.2. Success and failures of docking calculation on rigid and flexible ligands in different family of enzymes. Red arrow indicates the HIV-RT family; (a) rigid ligand (RGD), (b) flexible ligand (FLX). The left y-axis shows protein family and size and the right y-axis shows average number of ligand rotatable bonds (#RB). (c) (orange bars) shows difference in scoring - sampling failures for FLX (adapted from Mukherjee, 2010).

In details, rilpivirine, delavirdine, PZ2, MRX and HBY with a number of rotatable bonds of 5, 7, 4, 4 and 6 respectively show a binding energy of -12.99, -10.05, -12.58, -9.62 and -7.76 Kcal/mol, respectively. The lower value of the latter one is probably caused by a low resolution (3.00Å) of X-ray protein structure. Efavirenz and nevirapine have 3 and 0 rotatable bonds and their calculated binding energy is -8.68 and -8.50 Kcal/mol respectively. The visual inspection of the calculated and experimental X-ray structures of the different reverse transcriptase (Figure 3.4) shows that rilpivirine, efavirenz, nevirapine, PZ2 and MRX are well overlapped, whereas delavirdine is not well overlapped, likely due to the higher number of rotatable bonds. The cross-validation data are in agreement with the results obtained previously with "the bests" docking position in the same X-ray crystallographic structure. From the validation results a compromise has been here chosen for the docking calculation of the new molecules among the X-ray structure resolution, the R-factor, the number of rotatable bonds, the calculated binding energy and the position of ligand after docking

calculation in comparison with the original structure. 1FK9 resulted the appropriate structure to subject the new molecules at docking calculation.

4.1.2. Docking evaluation

Docking calculations have been carried out on a first series of molecules having as aryl (Ar) unit a substituted phenyl (C1-C6 compounds in Appendix A). The corresponding calculated binding energy values were between -9.04 and -9.56 Kcal/mol. A substitution of phenyl ring with a 2-benzimidazole moiety increased the binding energy at -10.51 Kcal/mol (compound C8). The same effect was observed changing the 2-benzimidazole with a naphthyl group, increasing the energy until a maximum of -13.14 Kcal/mol in the compound C28. This series of molecules could be obtained only by a long sequence of reaction because of the lacking of commercial synthetic precursors or starting materials. All the compounds reported in Appendix A are amides, therefore for extending the calculation at other isosters, the acyl group in tertiary amide was simplified by transferring it in position 3 of the pyranones ring and limiting it to acetyl (-COCH₃) or dichloroacetyl (-COCHCl₂) groups.

A substitution of amine with an oxygen or sulfur atom gave an ether or a thioether, respectively; the latter one is able to be easily oxidated to sulfone, in order to achieve a new series of compounds to be submitted to docking calculation. The results are summarized in table 3.3 showing, in some cases, lower binding energy in comparison with the amides reported in table I. However compounds **1-26** have a higher molecular diversity giving the possibility to obtain a potential structure-activity relationship after the biological assays.

As previously reported, a threshold of -7.00 Kcal/mol of binding energy is a straightforward value to distinguish potential active from inactive compounds (Chang, 2007). All the molecules reported in table 3.3 show comparable binding energy to drugs taken as reference compounds and have a value greater than -7.00 Kcal/mol. The higher value of energy for the new compounds is -13.32 kcal/mol calculated for the compound **18a**, although it is penalized by its too high partition coefficient (Log P). In order to obtain results closer to the biological environment, the flexibility of amino acid residues present in the NNBP have been taken into account during the process of docking calculation for reference compounds (efavirenz, nevirapine, rilpivirine, α -APA and (+)-calanolide A) and for the new compounds **1-26**. However the obtained data resulted to be not consistent, both for the too low interaction energy and for the right position in the pocket (data not reported). A further docking

calculation, using Molegro Virtual Docker software, has given results in agreement with AutoDock calculation, although Molegro uses a different ranking score and the direct comparison is not possible.

4.1.3. ADME and drug-like properties prediction

The drug-like properties and the calculations of Absorption, Distribution, Metabolism, and Excretion (ADME) on the new molecular structures, are important to select potential lead candidates during the process of drug design. In particular, the partition coefficient must be lower than 5 and all the molecules under investigation, with two exceptions (**10** and **18a**), have showed a Log P between 1.8 and 4.2. ADME calculations for the intestinal absorption carried out for all the designed compounds gave a good intestinal absorption (97-99%) whereas the binding plasma protein has resulted between 80 and 99%, in agreement with the potential drug-like values.

In summary, the results from docking calculations and ADME predictions have allowed to select compounds **1-26** as interesting molecules to be later synthesized and subjected to biological assays.

4.2. Chemical synthesis and structural characterization of the selected molecules

The production of compounds **1-21** was obtained through a convergent synthesis starting from the same commercial compound 4-hydroxy-6-methyl-2-pyrone (**27**). It was converted into tosylate **28** by the treatment with tosyl chloride in the presence of pyridine (Fairlamb, 2005) or triethylamine (Hansen, 2005). The latter base gave higher yields (90%) in comparison with the use of pyridine (68% yield). Similarly, tosylates **31**, **34** and **36** were synthesized.

Tosylate **28**, or **34** or **36**, has been put to react with the suitable amine in a polar solvent (*e.g.* ethanol) at room temperature for 60 hours in the presence of triethylamine as base (Scheme 3.1). The yields were not higher than 55 %, even if by using 2 molar equivalents of (aryl)alkyl amine. Amines acted both as nucleophiles and bases, giving the desired (aryl)alkyl-aminopyrone (**1-6**, **22** and **23**) and also the (aryl)alkyl-tosylamide, as resulted by:

i) molecular composition deduced by high resolution experiment in EI-MS spectrum ($m/z = 311.09795 \pm 0.0030$, calcd. 311.09800 for $C_{18}H_{17}NO_2S$), ESI(-)-MS/MS (Figure 4.3) and ii) 1H -NMR spectra (Figure 4.4), in the specific example of the by-product obtained in the reaction between tosylate **28** and 1-naphthylmethanamine.

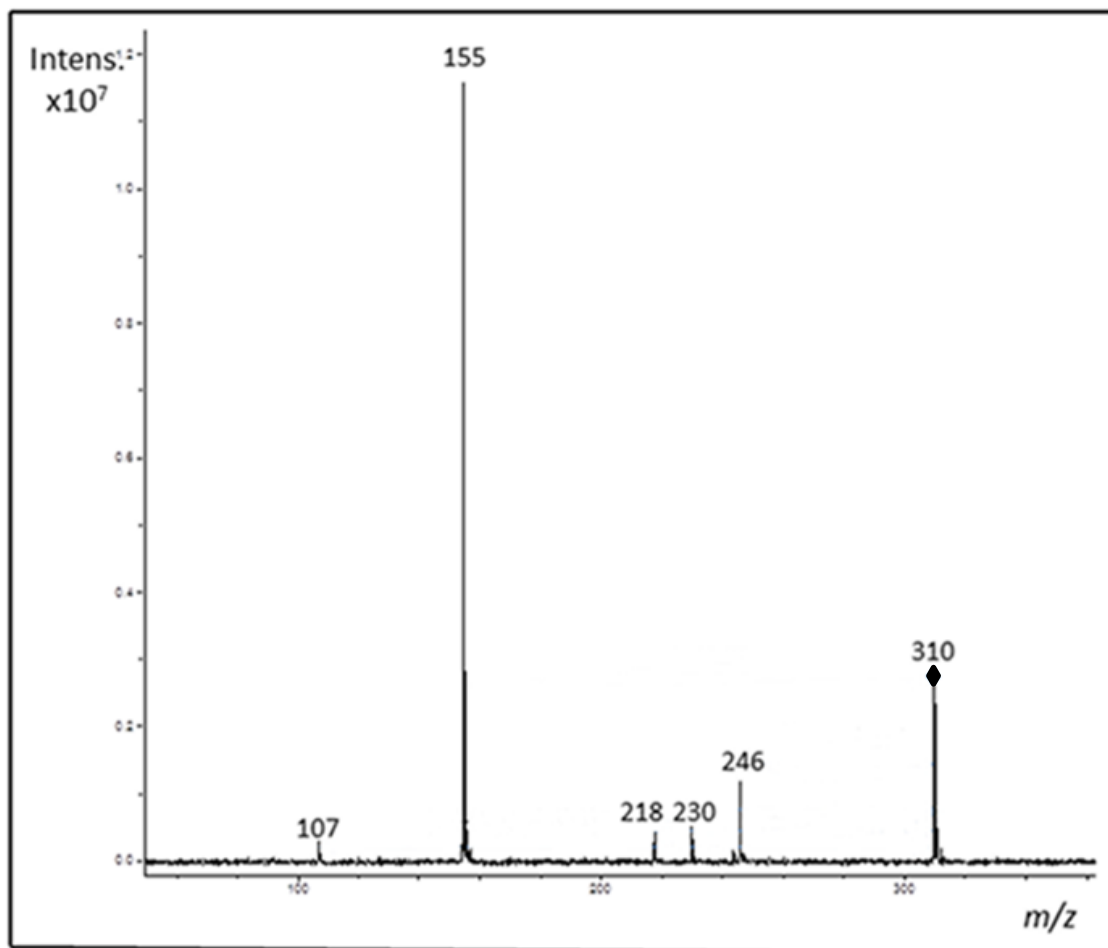


Figure 4.3. ESI(-)-MS/MS spectrum of $[M-H]^-$ ion at m/z 310 of the by-product from aminolyses of tosylate **28**. M is the by-product of aminolysis

In particular, 1H -NMR spectrum reported in Figure 4.3 shows the assignment for the protons present in the molecule and the most intense peak at m/z 155 in MS spectrum is more probably attributable to the negative $C_{11}H_9N$ ion.

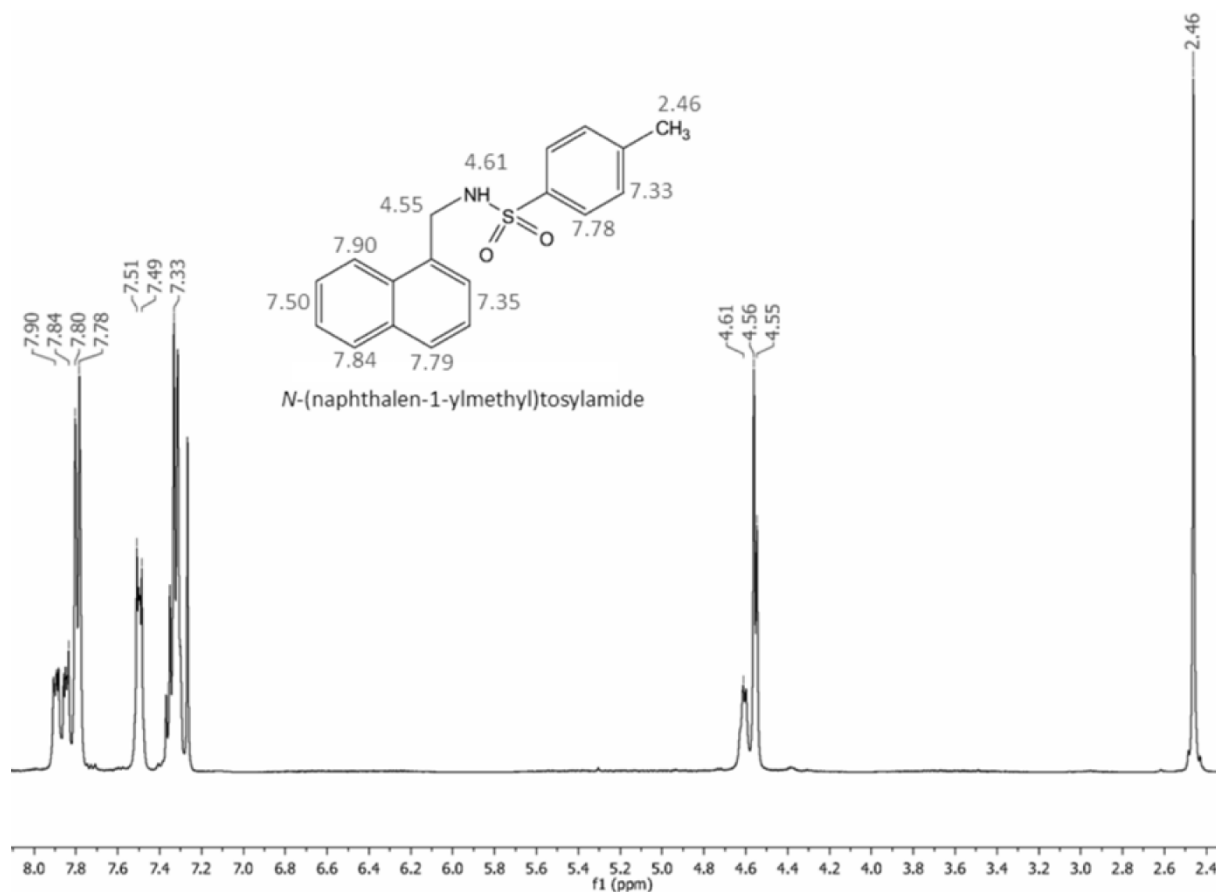
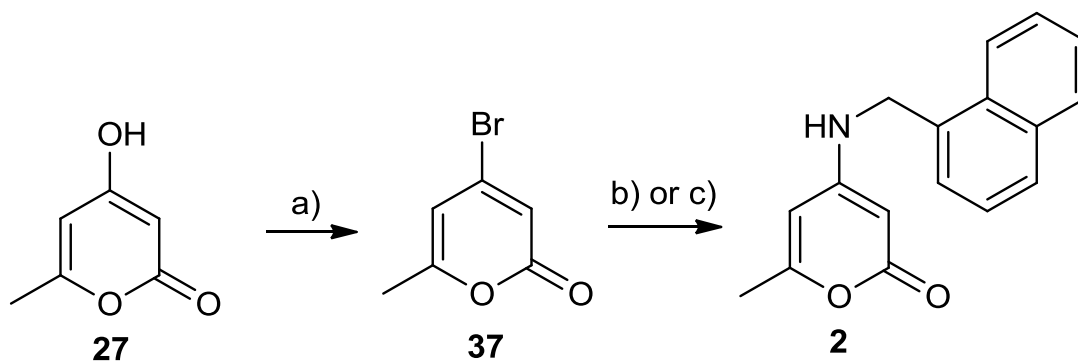


Figure 4.4. $^1\text{H-NMR}$ spectrum (400 MHz, in CDCl_3) and chemical structure of the by-product deriving from aminolysis of tosylate **28** with 1-naphthylmethanamine

Attempts to improve the yields have been carried out by replacing tosylate **28** with 4-bromo-6-methyl-2-pyrone (**37**), (prepared by heating **27** with tetra-*n*-butylammonium bromide and P_2O_5 in toluene at 100°C for 1 hour (Kato, 2001)), in the reaction with the amines in absolute ethanol at reflux for 20 hours (McLaughlin, 2002), also by microwave irradiation at the place of conventional heating (Scheme 4.1), but without finding positive effects.



Scheme 4.1. Synthesis of 4-bromo-6-methyl-2H-pyran-2-one. *Reagents and conditions:* a) $n\text{Bu}_4\text{N}^+\text{Br}^-/\text{P}_2\text{O}_5/\text{toluene}$, 100°C 1h, 82% yield; b) 1-naphthylmethanamine (1.5 eq)/ EtOH/ reflux 20h, 50% yield or c) 1-naphthylmethanamine (1.5 eq), MW, 100°C , 2h, 55% yield.

In order to obtain amides **8b**, **9** and **10**, amines **1-4** have been acylated by dichloroacetyl chloride and amine **2** with a series of acyl chlorides. The reaction carried out in the presence of Et₃N at room temperature gave the expected *N*-acyl products in mixture with the C(3)-acyl compounds. These results have allowed to obtain new molecules of interest for biological evaluation (**7**, **8a** and **11-13**). In addition they have suggested the opportunity to go insights into the study of *N*, *C*-acylation selectivity.

Nucleophilic substitution of tosylate **28** with sodium hydrosulfide hydrate in absolute ethanol has provided the unstable 4-mercapto-6-methyl-2H-pyran-2-one, which was directly alkylated with 1-(bromomethyl)naphthalene in chloroform / 1% NaOH aqueous solution under phase transfer catalysis (PTC) conditions (Majumdar, 2002), to produce compound **14** in 84% of yields. Otherwise, attempts to use the same experimental conditions to prepare compounds **16**, **25** and **32**, gave yields very low (< 10%). In order to have a higher product amount, PTC has been replaced by a system using an apolar solvent in homogeneous phase with 1,8-diazabicyclo[5.4.0]undec-7-ene (DBU) as base (Ono, 1980): in this case 40÷86% yields were obtained (Scheme 3.2 and 3.3).

The convergent synthesis has allowed to prepare the sulphones **15**, **17**, **21** and **26** in quantitative yields by a "green" oxidation of the corresponding thioethers with urea-hydrogen peroxide complex (UHP) in a THF/85% formic acid solution at room temperature (Schemes 3.2 and 3.3; Balicki, 1999).

Ethers **18-20** and **23** have been obtained in 40÷60% yields by refluxing the suitable 4-hydroxy-pyran-2-one (**27**, **29** and **35**) with an equimolar amount of 1-(bromomethyl)naphthalene or 1-(2-bromoethyl)naphthalene in acetone, in the presence of solid potassium carbonate and potassium iodide (Rabnawaz, 2010). In the case of ether **18**, the by-product **18a** was produced by a double O- and C(3)- alkylation of pyrone unit.

The precursor of sulfide **32**, 3-bromo-4-hydroxy-6-methyl-2H-pyran-2-one (**30**), has been obtained in 66% of yield by direct bromination of compound **27** with bromine in dichloromethane at room temperature in the darkness (Scheme 3.2; de March, 1985).

Attempts to synthesize 3-iodo-4-hydroxy-6-methyl-2H-pyran-2-one (**29**) using iodine in the presence of an oxidant as cerium(IV) ammonium nitrate (CAN) (Asakura, 1990; Das, 2007) or bis(tetra-n-butylammonium) peroxydisulfate in acetonitrile (Whang, 1997), both at room temperature or 80°C, gave a complex mixture difficult to be separated. Nevertheless, the iodination procedure used for methoxy-benzaldehydes (Hathaway, 2007) employing iodine and an equimolar amount of silver nitrate in methanol at room temperature in the darkness, has allowed to obtain the pure desired product in 85% yield (Scheme 3.2).

By reduction of 3-acetyl group of the commercial dehydroacetic acid (**33**) it was possible to synthesize 3-ethyl-4-hydroxy-6-methyl-2*H*-piran-2-one (**35**). For this purpose a simple and eco-friendly reaction has been carried out using zinc powder in acetic acid as solvent, in the presence of hydrochloric acid as catalyst (Kappe, 1995). However the reaction did not work effectively and the yields did not go beyond 5%. On the contrary, under the ionic reduction by using triethylsilane in trifluoroacetic acid in the presence of Lewis acid (Scheme 3.3), the reaction proceeded smoothly and in excellent yields (90%) (Lokot, 1999).

All the synthesized new compounds have been fully characterized by extensive NMR analysis including ^1H , ^{13}C - bidimensional experiments (HMBC, HSQC) which also allowed to deduce ^{13}C values. Their chemical composition has been obtained by high resolution experiments in electronic impact mass spectrometry (EI-MS), whereas fragmentation experiments gave additional structural indications. As an example, the characterization of the compound **23** is here reported. The ^1H -NMR spectrum shows a triplet at δ 1.00 ppm with a coupling constants $J = 7.5$ Hz corresponding to three protons on carbon C-2', a singlet at 2.23 ppm attributable to the methyl group at C-6, a quartet centered at 2.44 ppm with $J = 7.5$ Hz for the two protons on C-1'. The singlets at 5.56 and 6.13 ppm can be assigned to the two magnetically equivalent protons on C-1'' and one proton on the pyrone unit in C-5 position, respectively. The multiplet centered at 7.59 ppm corresponds to the two protons on the carbons C-3'' and C-4'' of the naphthyl moiety, whereas the multiplet centered at 7.56 ppm is attributable to the two protons in C-7'' and C-8''; finally the multiplet at 7.91 ppm corresponds to the three protons in C-5'', C-6'' and C-9'' (Figure 4.5).

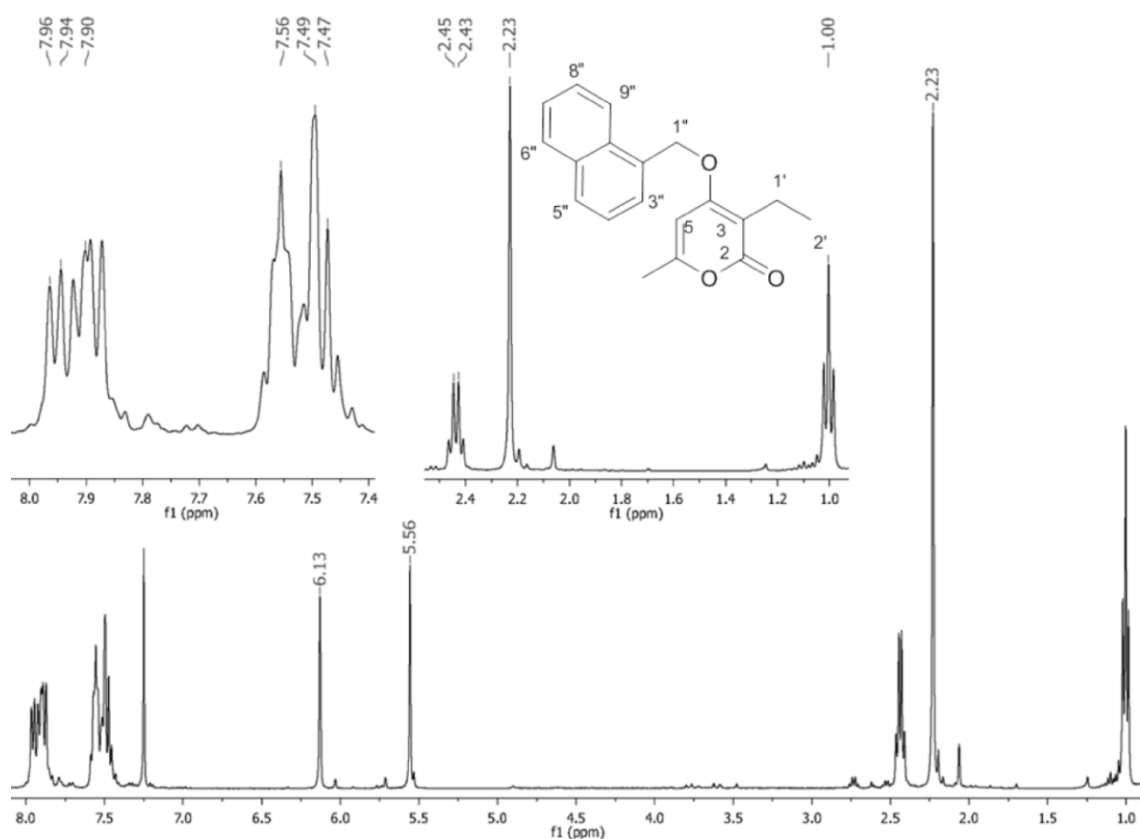


Figure 4.5. ^1H -NMR of compound **23** (400MHz, in CDCl_3)

From the bidimensional, Heteronuclear Single Quantum Coherence (HSQC) experiment, the chemical shifts of the carbons bearing at least one proton have been deduced (Figure 4.6). In particular, C-2' is at 11.74 and C-1' is at 16.23 ppm; the chemical shift of methyl group in 6-position of the pyrone is at $\delta(\text{C})$ 20.25 ppm and the methylene group attached to oxygen corresponds to $\delta(\text{C})$ 68.94 ppm, and the signal at 95.57 ppm corresponds to C-5 in the pyrone unit. The carbon atoms of the fused rings in naphthalene show the following chemical shifts: 129.04 ppm for C-6'', 126.21 ppm for C-7'' and C-8'', 125.81 ppm for C-3'' and C-4'' and 122.75 ppm for C-9''. For the quaternary carbon atoms with no attached protons, the chemical shifts were defined by long-range ^1H , ^{13}C hetero-correlation experiment (HMBC) (Figure 4.7 and Figure 4.8).

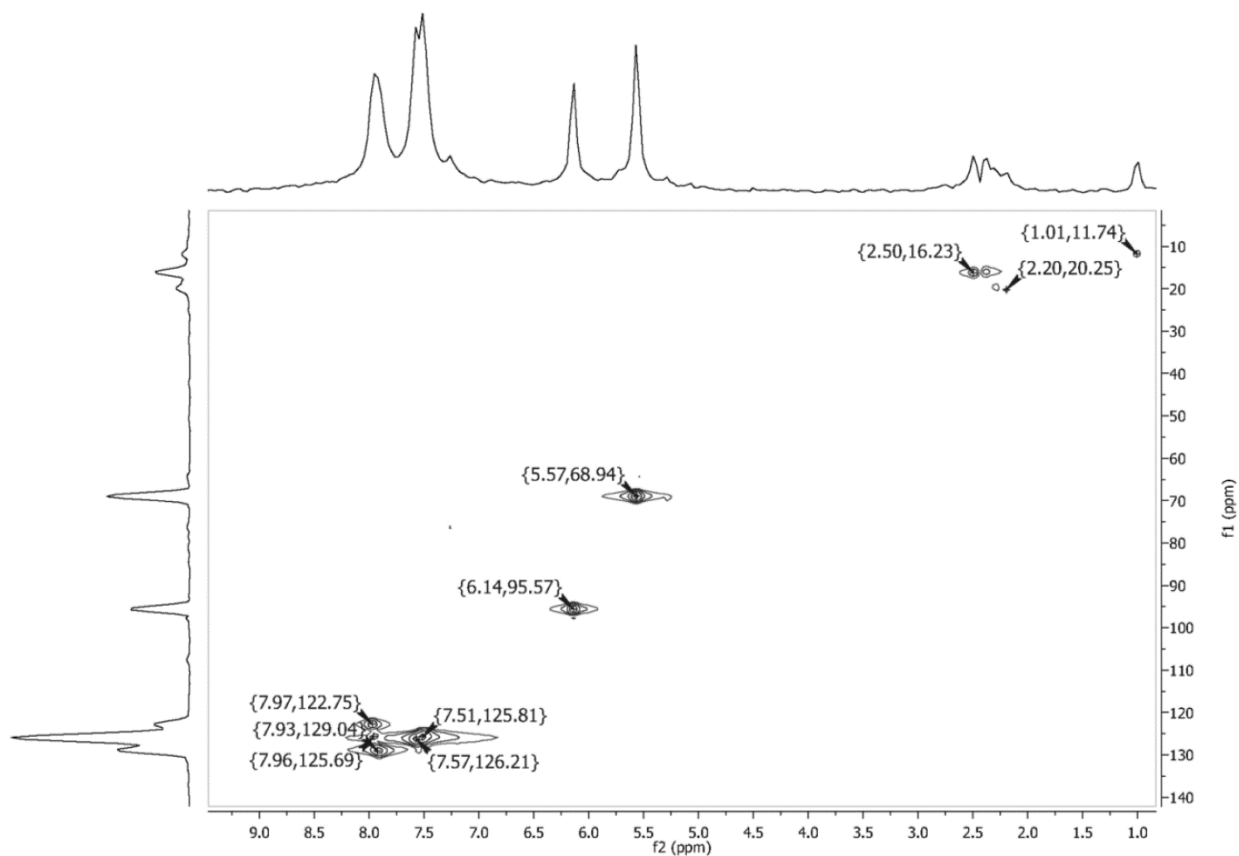


Figure 4.6. HSQC spectrum of compound **23** (400MHz, in CDCl₃)

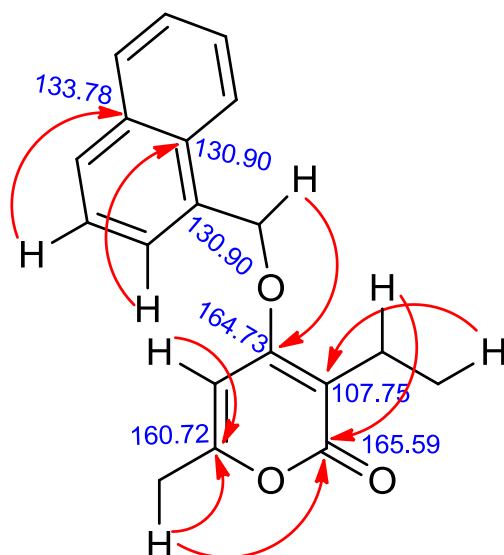


Figure 4.7. Relevant ¹H/ ¹³C long-range correlations deduced by HMBC experiment in CDCl₃ for the compound **23**

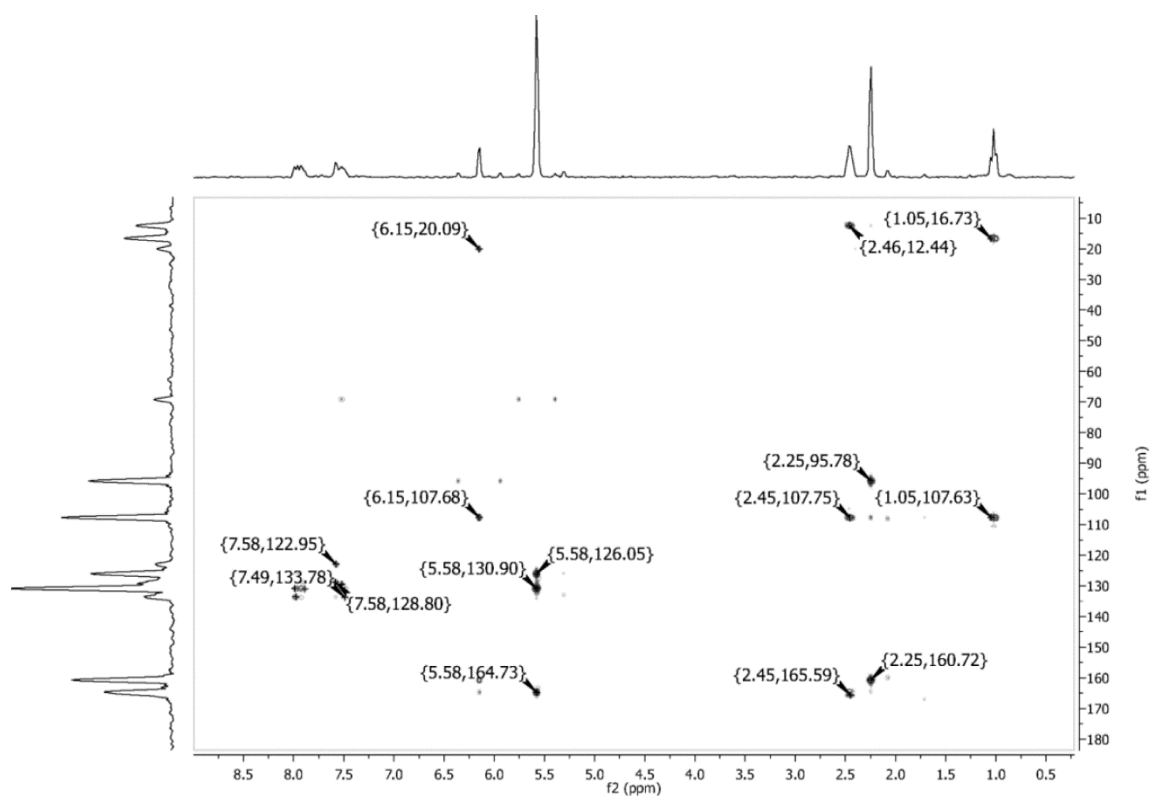


Figure 4.8. Long-range ^1H , ^{13}C NMR spectrum by HMBC experiment in CDCl_3 for compound **23**

From high resolution experiments in EI-MS analysis the molecular composition $\text{C}_{19}\text{H}_{18}\text{O}_3$ has been deduced, and the fragmentation at m/z 141 gave indication on the loss of the pyrone unit (Figure 4.9).

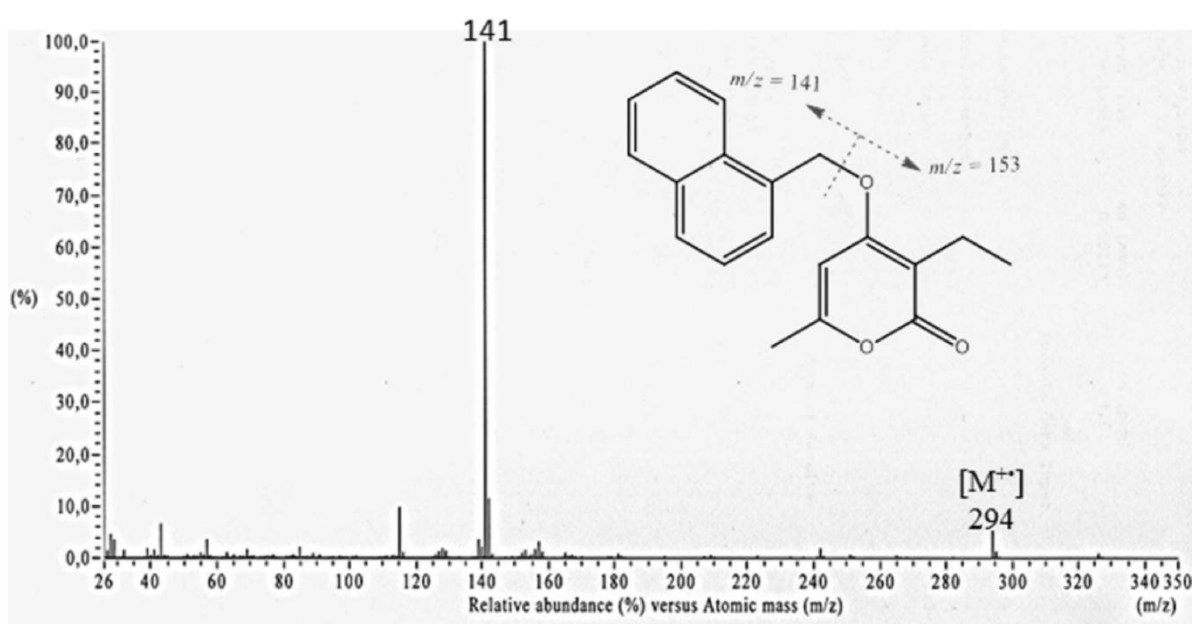


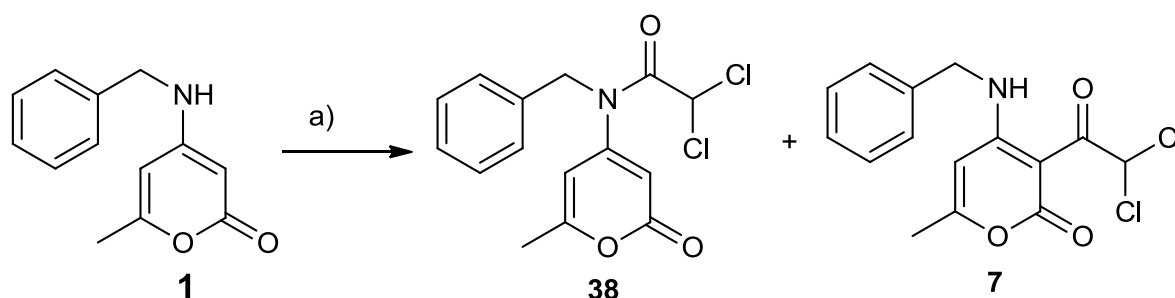
Figure 4.9. EI-MS spectrum of compound **23** with indication of the fragmentation pattern

4.3. Study of the selectivity in *N*, *C*-acylation of 4-benzylamino-pyrone

The designed compounds to be subjected to biological assays have been planned as deriving from acylation of aminopyrone **1**, for which the enamino form resulted the most stable tautomer by DFT calculation (Figure 3.9).

With the aim to obtain compound **38**, compound **1** has been treated with the suitable acyl chloride in the presence of triethylamine, the latter one working as a base for trapping HCl, as usually reported, in the reaction with amines to give amides (Montalbetti, 2005). It was reported that the reaction of primary or secondary amines with dichloroacetyl chloride in the presence of Et₃N gave dichloroacetamido derivatives in high yields, supposedly *via* dichloroketene Cl₂C=C=O, which reacts with the more nucleophilic nitrogen centre (Hazara, 1989). In addition it was known that the reaction between dichloroacetyl chloride and triethylamine gave dehydrohalogenation of acyl chloride, producing *in situ* the instable dichloroketene, whose formation was verified by trapping with cyclopentadiene (Ghosez, 1966). More recently, ketenes were studied in reactions with amines to give amides (Allen, 1999), and a mechanism involving enols of amides as intermediate has been proposed (Raspoet, 1998).

Unexpectedly, in our hands a mixture of products containing the desired amide **38** and **7** in 60:40 ratio was obtained. The products derived from both *N*- and *C*-acylations of aminopyrone **1** acting as a bidentate electrophile in the reaction with dichloroacetyl chloride are reported in Scheme 4.2.



Scheme 4.2. *N*, *C*-acylation of benzylpyrone **1**. *Reagents and conditions:* a) Et₃N (2.5 eq.) dichloroacetyl chloride (2.0 eq.), CH₂Cl₂, 0 °C → r.t., 18h, 88 % yield.

The structure of regioisomers **7** and **38** has been assigned by extensive NMR analysis (§ 3.2.3.2 and § 3.2.12.2, respectively). In addition infrared spectroscopy gives useful structural

informations, especially when the comparison with DFT calculated spectra can allow the assignments of the signals. In this studies, a good agreement between experimental and calculated IR spectra were observed for compounds **7** and **38** (Figures 4.10 and 4.11).

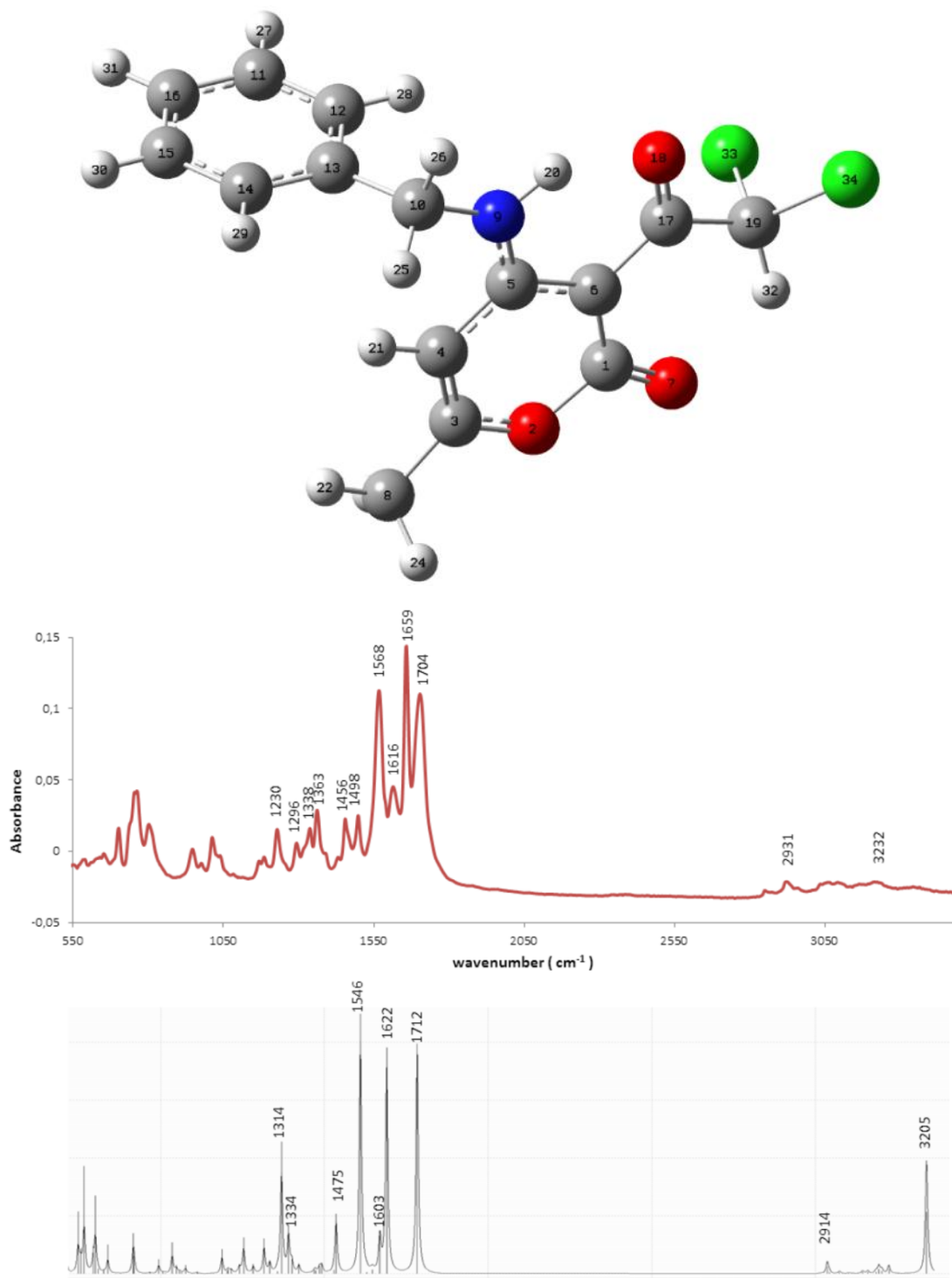


Figure 4.10. Energy minimized structure of compound **7** by DFT calculation (top); experimental (centre) and calculated (bottom) infrared spectra of compound **7**

In particular, for compound **7** the peak at 1704 cm^{-1} corresponds to $\text{C}(1)=\text{O}(7)$ stretching, the signal at 1659 cm^{-1} is attributable to the stretching of the double bond $\text{C}(3)=\text{C}(4)$, and the peaks at 1616 and 1568 cm^{-1} have been assigned to the vibrations of $\text{C}(17)=\text{O}(18)$ and $\text{C}(5)-\text{N}(9)$ respectively. In addition the signals with lower intensities in the region between 1230 - 1498 cm^{-1} are vibrations of the whole molecule, whereas intramolecular hydrogen bond between $\text{H}(20)\cdots\text{O}(18)$ can be attributed to the broad band at 3232 cm^{-1} (Figure 4.10).

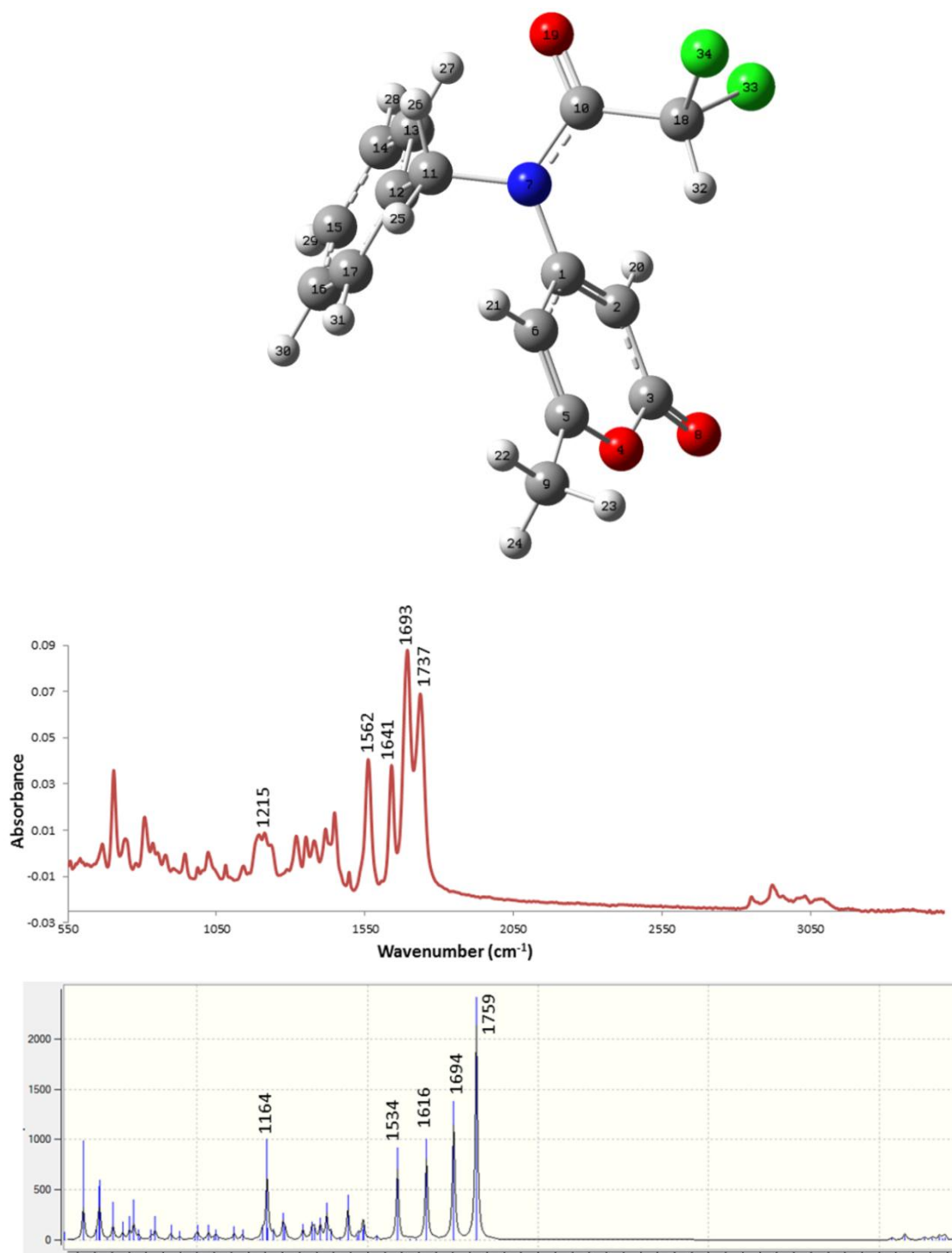


Figure 4.11. Energy minimized structure of compound **38** by DFT calculation (top); experimental (centre) and calculated (bottom) infrared spectra of compound **38**

Similarly, the comparison of experimental and simulated IR spectra for amide **38** has allowed to attribute the following vibrations: the peak at 1737 cm^{-1} to the stretching of $\text{C}(3)=\text{O}(8)$, the most intense signal at 1693 cm^{-1} to $\text{C}(10)=\text{O}(19)$ in the amide unit, the vibrations at 1641 and 1562 cm^{-1} to $\text{C}(5)=\text{C}(6)$ and $\text{C}(1)=\text{C}(2)$ stretchings in the pyrone ring, respectively (Figure 4.11).

Despite a recent growing interest in amino-pyrone chemistry as precursors in the synthesis of natural products (Wang, 2006; Sklenicka, 2002; McLaughlin, 2002; Hsung, 1999), to the best of our knowledge, only an old theoretical study on the *N*-basicity of these molecules has been reported (Menghezzi, 1983). It was a further reason in the investigation of the selectivity for the reaction involving aminopyrone **1**. The same reaction has been carried out without any bases (entry 15 in table 4.1) obtaining a complete regioselectivity in favour of C-acyl product. A plausible explanation for this reactivity can be found in the particular structure of the aminopyrone **1** for which the involvement of a zwitterionic resonance form is possible (Figure 4.12), where the charged C-nucleophile reacts with C-electrophile of the acylating agent. This is in line with the Klopman-Salem concept that hard-hard interactions are charge controlled (and soft-soft interactions are orbital controlled) (Mayr, 2011). In particular the presence of two electronegative atoms in dichloroacetyl chloride is able to increase the positive charge on the $\text{C}=\text{O}$ group.

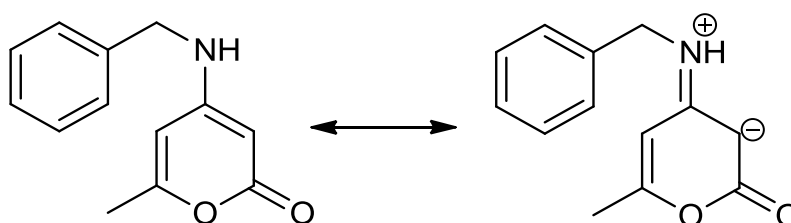
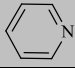
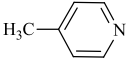
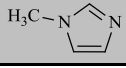
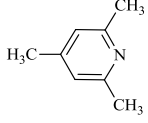
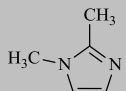
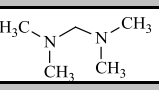
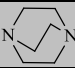
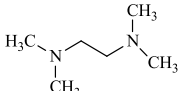
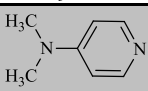
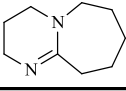


Figure 4.12. Two resonance forms of aminopyrone **1**

Later, aminopyrone **1** has been subjected to the same reaction conditions reported in scheme 4.2, in the presence of pyridine as base. The reaction gave again pure compound **7** as C-acylated product.

Further investigation with a series of organic base has given the results reported in table 4.1.

Table 4.1. Selectivity in *N*, *C*- dichloroacetylation of aminopyrone **1** by changing the base (in CH₂Cl₂ at 0°C for 18 hours, yield 89%), see scheme 3.4

Entry ^{a)}	Base	Chemical structure of base	pK _a	% C-acylated product 7 ^{b)}	% N-acylated product 38 ^{b)}
1	pyridine		5.37	100	0
2	4-methylpyridine		6.02	100	0
3	1-methylimidazole		6.95	100	0
4	2,4,6-trimethylpyridine		7.43	52	48
5	1,2-dimethylimidazole		7.64	100	0
6	TMDM		7.67	c)	c)
7	triethanolamine	(HOCH ₂ CH ₂) ₃ N	7.80	c)	c)
8	tributylphosphine	(<i>n</i> -C ₄ H ₉) ₃ P	8.30	100	0
9	DABCO		8.82	0	100
10	TMED		9.42	34	66
11	DMAP		9.87	100	0
12	triethylamine	Et ₃ N	10.8	40	60
13	DIPEA	(<i>i</i> -C ₃ H ₇) ₂ NEt	11.2	10	90
14	DBU		11.6 0	0	100
15	-	-	-	100	0

a) In sequence according to increasing pK_a of the base

b) The ratio of *N*- and *C*- acylations has been evaluated in the crude reaction mixture by the integrals of signals in ¹H-NMR spectrum recorded in CDCl₃, at δ=4.55 ppm (d, PhCH₂) in product **7** and δ=4.90 ppm (s, PhCH₂) in product **38**.

c) No products were obtained; starting aminopyrone **1** was practically recovered in quantitative amount.

In details, by replacing pyridine, with the aromatic bases 4-methylpyridine, 4-dimethylaminopyridine (DMAP), 1-methylimidazole and 1,2-dimethylimidazole, and tributylphosphine the reaction always gave pure **7**. An interesting completely reversed selectivity has been obtained by using DBU, DABCO and diisopropylethylamine (DIPEA), whereas a lack of selectivity was given by 2,4,6-trimethylpyridine, TMED and triethylamine.

In order to find a correlation in the selectivity, the acid-base property has been taken into account. For this reason the pK_a values of conjugated acid forms have been reported in table 4.1, but no correlation with the selectivity was observed.

In addition proton affinity, defined as the tendency of a base to accept a proton in gas phase and reported as the difference between the energy values for protonated (BH^+) form and free base ($B:$) (Jaramillo, 2007) has been regarded. The calculated results of some used amines are reported in table 4.2, from where no correlations are evident with the results of selectivity. It is noteworthy that carrying out the reaction reported in scheme 4.2 without triethyl amine and any other bases pure C-acylated compound **7** was produced.

Table 4.2. Calculated values for proton affinity of some bases used in the acylation reaction

Entry	Base	pK_a	Calculated proton affinity ^{a)}
1	pyridine	5.37	-965.08
2	4-methylpyridine	6.02	-984.50
3	1-methylimidazole	6.95	-995.58
4	2,4,6-trimethylpyridine	7.43	-1016.30
5	DABCO	8.82	-1000.21
6	TMED	9.42	-992.28
7	DMAP	9.87	-924.00
8	triethylamine	10.8	-1012.44
9	DBU	11.6	-1091.48

a) Calculations were performed at DFT B3LYP/ aug-ccpVDZ level of theory

The changing of base in dichloromethane has given the access to the pure expected product **38**, but also to the regioisomeric compound **7**. The evaluation of solvent effect has been also investigated in two cases of highly selective acylation: by using pyridine giving pure C-acyl product **7** and DBU giving N-acyl compound **38**. The change to solvents with a different polarity has not affected the selectivity. In particular, with DBU as the base the selectivity in N, C- acylation was lost in toluene or acetonitrile, whereas it was fully reversed in acetone (Table 4.3).

The opportunity of obtaining the C-acyl product **7** as pure regioselective compound, has been taken into account to expand the library of molecules accessible for biological evaluation. In details, compounds **8a**, **11**, **12** and **13** were obtained as pure C-acylated products by using pyridine, and **8b**, **9** and **10** as pure N-acyl products by DBU (Scheme 3.1).

Table 4.3. Selectivity in *N*, *C*- dichloroacetylation of aminopyrone **1** using pyridine or DBU by changing the solvent (at 0°C for 18 hours, yield 89%)

Entry	Solvent	% <i>C</i> -acyl product 7 ^{a)}	% <i>N</i> -acyl product 38 ^{a)}
pyridine			
1	dichloromethane	100	0
2	toluene	100	0
3	acetonitrile	100	0
4	acetone	100	0
DBU			
5	dichloromethane	0	100
6	toluene	40	60
7	acetonitrile	36	64
8	acetone	100	0

a)The ratio of *N*- and *C*- acylations has been evaluated in the crude reaction mixture by the integrals of signals in ¹H-NMR spectrum recorded in CDCl₃, at δ=4.55 ppm (d, PhCH₂) in product **7** and δ=4.90 ppm (s, PhCH₂) in product **38**.

For studying in depth, other acylating agents have been used in the reactions carried out in dichloromethane with pyridine or DBU, previously selected as the base giving fully reversed selectivity (Table 4.4).

Table 4.4. Selectivity in *N*, *C*- acylation of aminopyrone **1** using pyridine or DBU by changing the acyl halide (in CH₂Cl₂ at 0°C for 18 hours, yields 78-90%)

Entry	Acyl halide	% <i>C</i> -acyl product ^{a)}	% <i>N</i> -acyl product ^{a)}
pyridine			
1	dichloroacetyl chloride	100	0
2	propionyl chloride	93	7
3	isobutyryl chloride	100	0
4	2-bromopropionyl bromide	100	0
DBU			
6	dichloroacetyl chloride	0	100
7	propionyl chloride	12	88
8	isobutyryl chloride	0	100
9	2-bromopropionyl bromide	b)	b)

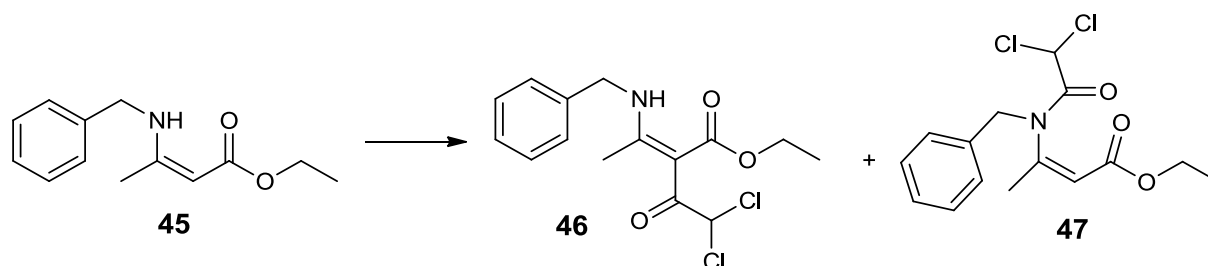
a)The ratio of *N*- and *C*- acylation has been evaluated in the crude reaction mixture by the integrals of signals of benzylic protons in ketones and amides in ¹H-NMR spectrum recorded in CDCl₃

b) No products were obtained, tars were recovered.

The results indicate that selectivity is not affected by the structure of electrophiles. It is noteworthy that 2-bromopropionyl bromide did not work with DBU, probably due to the formation of the highly instable bromoketene, which is reported to give polymerization in few minutes at -80°C (Staudinger, 1923).

4.3.1. Regioselectivity in a model enamino-ester

In order to expand the study reported above, (*Z*)-ethyl 3-(benzylamino)but-2-enoate (**45**, Scheme 4.4) has been treated with dichloroacetyl chloride in the same conditions used to obtain pure *N*- or *C*-acyl products starting from compound **1** (Scheme 4.3). The reaction gave only the *C*-acyl product in the presence of different bases (pyridine, DBU and triethylamine), (Table 4.5). This selectivity is imputable to: *i*) the *Z* configuration of enamino-ester **45**, secured by a stable six membered ring intramolecular hydrogen bond, as established by the presence of a broad singlet at 8.94 ppm in $^1\text{H-NMR}$ spectrum recorded for **45** in CDCl_3 (§ 3.2.10.3), *ii*) the presence of the benzyl moiety which does not allow *N*-acylation for steric hindrance (Eberlin, 1990). The same selectivity producing pure *C*-acylation has been observed also without using any base (Table 4.5).



Scheme 4.3. Base effect on the selectivity of *N*, *C*-acylation of enaminoester **45**. *Reagents and conditions:* a) different base (2.5 eq.) dichloroacetyl chloride (2.0 eq.), CH_2Cl_2 , $0^{\circ}\text{C} \rightarrow \text{r.t.}$, 18h, 78-90% yield.

Table 4.5. Selectivity in *N*, *C*-dichloroacetylation of enaminoester **45** by changing the base (in CH_2Cl_2 at 0°C for 18 hours, yield 85%), see scheme 3.5

Entry	Base	pK _a	% <i>C</i> -acyl product 46 ^{a)}	% <i>N</i> -acyl product 47 ^{b)}
1	pyridine	5.37	100	0
2	DBU	11.6	100	0
3	Et ₃ N	10.8	100	0
4	-	-	100	0

- a) The ratio of *N*- and *C*-acylations has been evaluated in the crude reaction mixture by the integrals of signals of benzylic protons in ketones in $^1\text{H-NMR}$ spectrum recorded in CDCl_3
- b) No signals of *N*-acylated product were detected in $^1\text{H-NMR}$ spectrum

4.4. Biological evaluation

4.4.1. ELISA enzymatic assay

Drug discovery is an iterative process in which drug design and chemical organic synthesis are driven from bioassays. Therefore, a first small series of new molecules, designed *in silico* from the fragments belonging to (+)-calanolide A and α -APA molecules (Figure 4.1), and synthesized in laboratory, has been subjected to a preliminary enzymatic ELISA test. These compounds have shown a reverse transcriptase inhibition range from 5% to 77% at concentration of 200 μ M. In particular, compounds **2** and **8a** have shown comparable inhibition values (77% and 66% respectively) with the clinically used drug nevirapine (59%) (Table 3.5). It is evident that the acylation of nitrogen is detrimental for the inhibition activity as shown for compounds **8b**, **9** and **10**, which have shown a RT inhibition of 30%, 20% and 32% respectively. Also the aromatic unit seems to play a relevant role in the interaction with the reverse transcriptase allosteric pocket as observed in compound **2**, bearing a naphthyl ring, in comparison with compound **1**, where the presence of the phenyl ring having a smaller surface, can be responsible of the not significant enzyme inhibition (5%). The results obtained in this assay has encouraged to synthesize a series of isosters and analogues to be furtherly assayed in enzymatic *in vitro* tests.

In order to optimize the time for reading the colorimetric results, the effect of the known reverse transcriptase inhibitor nevirapine has been tested at three different concentrations and at a different time of absorbance reading. The best result has been obtained using a concentration of 200 μ M of nevirapine and a time of 10 minutes after the addition of ABTS colorimetric reagent. Because of the small amounts of reverse transcriptase present in the enzymatic kit, not enough to allow the use of all the microplates present in the kit and due to the commercially unavailability of the only enzyme, we have bought a new sample of HIV-1 recombinant reverse transcriptase from Pierce Biotechnology (USA). Before using it with the Roche kit, the efficiency of the new reverse transcriptase has been tested in water solution and in phosphate buffer at pH 7.4 added of 0.2% of BSA, as reported in the composition of the reverse transcriptase present in the Roche kit. The results have shown that the reverse transcriptase by Pierce does not work properly in water (Figure 3.11), whereas in the presence of pH 7.4 buffer and bovine serum albumin the enzyme works only slightly less than the original one present in the Roche kit. A further investigation on the Pierce RT has been carried out analyzing the effect of one cycle of freezing and thawing. The result has

indicated that the activity of Pierce reverse transcriptase drastically decreases in comparison with the original Roche reverse transcriptase (Figure 3.12). From this data it is evident that it is not possible to use the Pierce RT in the enzymatic assay.

4.4.2. Anti-HIV activity

The series including 26 new molecules have been exposed to CEM cell cultures infected with wild-type HIV-1(III_B) and HIV-2(ROD) strain. The compounds have shown no inhibitory activities against HIV-infected CEM cell cultures, except compound **6** which was endowed with a modest anti-HIV activity (EC_{50} : 25-50 μ M). Its cytostatic activity (CC_{50}) was 121 μ M resulting in an anti-HIV selectivity of \sim 2.5 to 5. Some of the compounds have proved to be rather cytostatic against CEM cells (CC_{50} between 2 and 10 μ M for compounds **7**, **8a**, **11**, **12**, **13**, **15**, **21** and **23**).

For the development of a new potential therapeutical agent, cytotoxicity has to be evaluated, in order to establish the selectivity index (SI), defined as the ratio between cytotoxicity (CC_{50}) and EC_{50} . For anti-infective agents, it must reach values preferably as high as possible. In table 4.6 the cytostatic activity values for the molecules under investigation are reported. The only member of the series which has inhibited the virus replication at a no cytotoxic concentration was compound **6**. Anyway, it has shown a modest anti-HIV activity ($EC_{50} = 25 \mu$ M), associated to a low selectivity index: 5 for HIV-1 and 3 for HIV-2 .

Table 4.6. Anti-HIV activity, cytotoxicity and selectivity index in CEM cells for the synthetic compounds **1-26**

Compound	EC ₅₀ ^{a)} (μ M)		IC ₅₀ ^{b)} \pm SD (μ M)	Selectivity Index (SI) ^{c)}	
	HIV-1	HIV-2	CEM	HIV-1	HIV-2
1	>250	>250	148 \pm 11	-	-
2	>10	>10	175 \pm 106	<18	<18
3	>10	>10	83 \pm 12	<8	<8
4	>10	>10	182 \pm 27	<18	<18
5	>10	>10	76 \pm 7	<8	<8
6	25 \pm 3.5	\geq 50	121 \pm 10	5	3
7	>2	>2	4.9 \pm 1.5	<3	<3
8a	>2	>2	5.4 \pm 3.6	<3	<3
8b	\geq 10	\geq 10	50 \pm 18	<5	<5
9	>50	>50	93 \pm 16	<18	<18
11	>10	>10	6.5 \pm 4.0	<1	<1
12	>2	>2	4.2 \pm 2.5	<2	<2
13	\geq 2	\geq 2	4.0 \pm 1.6	<2	<2
14	>10	>10	16 \pm 0	<2	<2
15	>10	>10	5.4 \pm 2.0	-	-
17	>2	>2	83 \pm 34	<42	<42
18	\geq 50	\geq 50	150 \pm 25	<3	<3
18a	>50	>50	25 \pm 4	-	-
19	>10	>10	214 \pm 52	<22	<22
20	>10	>10	\geq 250	<25	<25
21	>10	>10	2.2 \pm 1.6	-	-
22	>10 ^d	>10	> 250	<25	<25
23	>0.4	>0.4	4.4 \pm 2.3	<10	<10
24	>10	>10	41 \pm 18	<4	<4
25	>10	>10	77 \pm 9	<8	<8
26	>2	>2	68 \pm 21	<34	<34
NVP	0.11 ^e	10 ^e	>200 ^e	>1820	>20

a) EC₅₀=effective concentration or concentration required to protect CEM cells against the cytopathogenicity of HIV by 50 %

b) Concentration required to reduce CEM cell viability by 50%.

c) SI= IC₅₀/EC₅₀

d) Compound precipitation was detected at higher compound concentration.

e) Values obtained from: <http://pubchem.ncbi.nlm.nih.gov/assay/assay.cgi?cid=4463>

The strength of molecular docking is in the prevision of molecules as potential bioactive agents, so that this approach addresses in the choice of the molecules to be produced for the biological evaluation. It is difficult to find the reason for the discrepancy between the promising docking studies and the disappointing biological results. Otherwise, the weakness

of this study can be attributed to the antiviral activity which is relevant if related to a low cytotoxicity, the latter one unpredictable by the computational approach.

The aims of this research activity have been obtained and the study on these molecules as potential anti-HIV agents can be considered over, however the results are not so good as expected. In addition, the biological evaluation has been expanded in order to including tests against other pathogenic viruses and bacterial strains, the latter ones for the molecules showing the lower cytotoxic effect.

4.4.3. Antiviral activity

The study of potential antiviral activity on the new molecules has been expanded to different types of viruses. In particular in herpes simplex virus 1 and 2, vaccinia and vesicular stomatitis virus all compounds are inactive at subtoxic concentrations (Table 3.7).

In the evaluation of inhibition on varicella zoster virus, EC_{50} values show a similar trend; only for compounds **2**, **8b**, **13** and **17** some activities were observed. Compound **13** has given a selectivity index of ~ 10 against VZV when toxicity is considered, but its cytotoxicity is higher than its antiviral activity. Compound **8b** has shown anti-CMV activity at cytostatic concentrations. Therefore, it is most likely that **13** and **8b** indirectly inhibit virus replication due to toxicity. No appreciable activities have been detected against any of the other viruses at subtoxic concentrations.

4.4.4. Cytostatic activity of some molecules

An issue in the development of new antiviral molecules is the study of cytotoxic effect in non-infected cells, in order to avoid that the drug interferes with the normal cell cycle. The cytostatic activity is not easily predictable, so it is important to evaluate their values for the concentration of 50% growth inhibition (IC_{50}) (Lemke, 2008). For this purpose an evaluation has been carried out by using a murine (L1210) and acute lymphoblastic (CEM) leukemia cell lines, and the cell line deriving from solid human cervical cancer (HeLa). The sensitivity resulted very similar with IC_{50} values in the range $0.9\div 200$ μM . Compounds **7**, **8a**, **11-13**, **17**, **23** and **26** (whose structures are reported in table 3.3) showed the higher cytotoxicity at micromolar concentration as observed for clinically used drugs, here selected in order to have molecules acting with different mechanism of action: 5-fluorouracil known to be a pyrimidine

analogue with an antimetabolite activity, nimustine and melphalan as alkylating agents and irinotecan as inhibitor of topoisomerase-I (Topo-I), (Table 4.7).

In detail, compounds **8a**, **11** and **12**, bearing the dichloroacetyl unit in the pyrone ring, showed activity paragonable to irinotecan in inhibiting HeLa cell line, in which this drug is the most active among the ones taken as references. In the case of leukemic CEM cell line, all the molecules under investigation have an activity like the alkylating drug melphalan but with a lower effect than Topo-I inhibitor irinotecan. Against murine leukemia L1210 cells sulfone **17** (Table 4.7) emerged as the compound with the highest activity, better than the one of the drugs selected as reference.

It is noteworthy that cytostatic activity was mainly observed for molecules bearing a dichloroacetyl group which may be regarded a masked α -ketoaldehyde, probably responsible of the reactivity as alkylating agent. The structures of these molecules showing cytotoxicity at micromolar concentration are worthy of attention for a future study as antitumoral agents.

Table 4.7. Cytostatic activity on murine leukemia, human T-lymphocyte and human cervix carcinoma activity for the compounds **1-26**

Compound	IC ₅₀ ^{a)} ± SD (μ M)		
	HeLa	CEM	L1210
7	3.1 ± 0.2	4.9 ± 1.5	2.5 ± 0.4
8a	1.4 ± 0.6	5.4 ± 3.6	3.3 ± 0.9
11	1.4 ± 0.4	6.5 ± 4.0	2.3 ± 0.2
12	1.6 ± 0.4	4.2 ± 2.5	3.0 ± 0.2
13	2.8 ± 0.4	4.0 ± 1.6	2.9 ± 0.9
17	2.9 ± 0.6	2.2 ± 1.6	0.95 ± 0.07
23	4.5 ± 0.3	4.4 ± 2.3	4.9 ± 3.5
26	4.6 ± 0.2	5.4 ± 2.0	3.6 ± 0.1
Clinically used drugs			
5-Fluorouracil	2.85±0.75 ^{b)}	14.9±0.46 ^{c)}	4 ^{g)}
Nimustine	6.07±2.85 ^{b)}	8 ^{d)}	27 ^{g)}
Melphalan	2.69±0.323 ^{b)}	2.5 ± 0.2 ^{e)}	2.1 ± 0.02 ^{e)}
Irinotecan	1.82±1.02 ^{b)}	0.01 ^{f)}	1200 ^{h)}

a)IC₅₀= 50 % inhibitory concentration (μ mol L⁻¹) required to inhibit tumor cell proliferation by 50 %.

b)Takara, 2002; c) Abdelwahab, 2011; d) Yamauchi, 2008; e) Karki, 2009;

f) <http://dtp.nci.nih.gov/dtpstandard/dwindex/index.jsp>; g) Yokoyama, 1988;

h) Srivastava, 2005

4.4.5. Antibacterial activity of some molecules

The compounds showing an IC_{50} value greater than 100 μM in cytotoxic assays (**1-4**, **9**, **14**, **18-20**) can be investigated for other bioactivity. The emergence of multiple-drug-resistant strains of bacteria due to the indiscriminate use of antibiotics and the increasing susceptibility in people with acquired immunodeficiency syndrome (AIDS) induce an urgent need for the development of new strategies to treat bacterial infections (Mancini, 2007).

Therefore, due to the structural similarity of these synthetic compounds with natural antibacterial products (Liu, 2011) and also recently isolated in our laboratory (I. Djinni, unpublished results), some of them have been investigated as inhibitors of pathogenic bacteria. The effects have been evaluated against Gram(+) and Gram(-) ATCC bacterial strains. In detail, a preliminary assay using agar diffusion method has allowed to select: *i*) **2-4** and **14** as compounds able to inhibit selectively Gram(+) *S. aureus*, *ii*) **2**, **14** and **19** as compounds inhibiting selectively MRSA (Table 3.15). The compounds resulting more promising have been furtherly investigated in order to define their MIC values. Taking into account their cytotoxicity (Table 3.14), the corresponding selectivity index (SI) has been calculated. Compound **20** has emerged as the most interesting, with a MIC value $< 5\mu\text{M}$ associated to a $SI > 27$ on MRSA strain (Table 3.16).

5. Conclusion

This study has focused on the design and chemical synthesis of new pyrone derivatives with potential anti-HIV activity. The strategy adopted in the design of these molecules has taken into account the fragment based approach, regarding structural peculiarities of the natural product (+)-calanolide A and the synthetic compound α -APA, both showing a potent and specific reverse transcriptase inhibitory activity. The hybrid structures were subjected to docking calculations (both by AutoDock and Molegro software), in order to select the molecules displaying a better interaction with the viral enzyme. With the aim of expanding the chemical space, the nitrogen atom present between the alkyl-aromatic and pyrone moieties was replaced by isosteric atoms as oxygen and sulfur, or by a sulfone group. A library containing more than 100 molecules was built, for which an ADME filter was applied, in order to only select the compounds having drug-like properties. A number of these compounds (26) was chosen to be synthesized based on a convergent synthetic strategy.

Therefore, adopting common precursors, these new compounds were obtained starting from the commercial available 4-hydroxy-6-methyl-2H-pyran-2-one (**27**) and dehydroacetic acid (**33**). Each product, purified by liquid chromatography or crystallization, was structurally characterized by extensive NMR analysis and mass spectrometry before being subjected to biological assays.

Attempts to obtain suitable amides (**8b**, **9** and **10**) by usual acylation employing acyl chloride in the presence of triethylamine, resulted in the expected products by *N*-acylation, but in mixture with *C*(3)-acyl compounds. These results have suggested that we should look further into the study of *N,C*-acylation selectivity for the ambidentate amino-pyrone, whose reactivity is poorly known. Regioselectivity was investigated by replacing triethylamine with other organic bases, changing the solvent and the acylating agents also for an enamino-ester taken as a model compound.

Based on the usually iterative process adopted in drug discovery, the first compounds (six) to be synthesized were subjected to enzymatic assay using an ELISA kit. Two of them (**2** and **8a**) showed significant reverse transcriptase inhibitory effects, with values comparable to the activity of nevirapine taken as a reference drug. The whole library of molecules was later synthesized and subjected to assays against HIV-1 and

HIV-2 virus strains. No activities against HIV-infected CEM cell cultures were observed, except for compound **6** which showed a modest but promising value (EC_{50} : 25-50 μ M). In order to be a potential candidate for therapeutic applications, its antiviral activity must be related to a low cytotoxic effect, which cannot be easily predicted neither by the chemical structure, nor by a computational approach. Unfortunately, high cytostatic activities were obtained for the compounds showing promising NNRTI effect. No antiviral activities at subtoxic concentrations were also observed against herpes simplex virus 1 and 2, vaccinia, vesicular stomatitis virus, varicella zoster virus, cytomegalovirus and other viruses. For these reasons the study on these molecules as potential antiviral agents can be considered over.

It is noteworthy that molecules bearing the dichloroacetyl unit in the pyrone ring (**8a**, **11** and **12**) showed the highest cytostatic activity, comparable to irinotecan in inhibiting HeLa cell line, whereas the compound containing sulfone group gave an activity at sub-micromolar concentration against murine leukemia L1210 cells. These molecular structures are worthy of future study with the aim of developing new antitumor agents. It could be a further example of serendipity, which in several cases has worked in scientific research, and specifically in medicinal chemistry.

In addition, for compounds showing low cytostatic activity (>100 μ M) the investigation was expanded to the study of antibacterial activity, due to the similarity of these compounds with antibacterial natural pyrones. A selectivity has been observed for some compounds against Gram(+) bacteria, and one of them (compound **20**) has resulted interesting for its activity against *MRSA*, associated to a favourable selectivity index.

In conclusion, the results deriving from this multidisciplinary study show that new molecular structures selected by docking calculations according to favourable enzyme-ligand interactions are not an obvious requirement for good experimental bioactivities. In addition, in the case of antiviral agents which were the topic of this research, detailed NNRTI activity must be associated to a low cytotoxicity which is hardly predictable.

6. References

- Abdelwahab S.I., Abdul A.B., Mohan S., Taha M.M.E., Syam S., Ibrahim M.Y., Mariod A.A. **2011**. Zerumbone induces apoptosis in T-acute lymphoblastic leukemia cells. *Leukemia Research*, *35*, 268-271
- Allen A.D., Tidwell T.T. **1999**. Amination of ketenes: kinetic and mechanistic studies. *Journal of Organic Chemistry*, *64*, 266-271
- Asakura J., Robins M.J. **1990**. Cerium(IV)-mediated halogenation at C-5 of uracil derivatives. *Journal of Organic Chemistry*, *55*, 4928-4933
- Auwerx J., Rodríguez-Barrios F., Ceccherini-Silberstein F., San-Félix A., Velázquez S., De Clercq E., Camarasa M-J, Perno C.F., Gago F., Balzarini J. **2005**. The role of thr139 in the human immunodeficiency virus type 1 reverse transcriptase sensitivity to (+)-calanolide A. *Molecular Pharmacology*, *68*, 652-659
- Balicki, R. **1999**. An efficient method for oxidation of organic sulfides to sulfones. *Journal für Praktische Chemie*, *342*, 184-185
- Barre-Sinoussi F., Chermann J.C., Rey F., Nugeyre M.T., Chamaret S., Gruest J., Dautet C., Axler-Blin C., Vezinet-Brun F., Rouzioux C., Rozenbaum W., Montagnier L. **1983**. Isolation of a T-lymphotropic retrovirus from a patient at risk for acquired immune deficiency syndrome (AIDS). *Science*, *220*, 868-871
- Becke A.D. **1993**. Density-functional thermochemistry III. The role of exact exchange. *Journal of Chemical Physics*, *98*, 5648-5652
- Beresford A.P., Selick H.E., Tarbit M.H. **2002**. The emerging importance of predictive ADME simulation in drug discovery. *Drug Discovery Today*, *7*, 109-116
- Bottegoni G. **2011**. Protein-ligand docking. *Frontiers in Bioscience*, *16*, 2289-2306.
- Brandt C.A., da Silva A.C.M.P., Pancote C.G., Brito C.L., da Silveira M.A.B. **2004**. Efficient synthesis method for β -enamino esters using ultrasound. *Synthesis*, *2004*, 10, 1557-1559
- Broder S. **2010**. The development of antiretroviral therapy and its impact on the HIV-1/AIDS pandemic. *Antiviral Research*, *85*, 1-18
- Chang M. W., Lindstrom W., Olson A. J., Belew R. K. **2007**. Analysis of HIV wild-type and mutant structures via in silico docking against diverse ligand libraries. *Journal of Chemical Information and Modeling*, *47*, 1258-1262
- Chinen J., Shearer W. T. **2002**. Molecular virology and immunology of HIV infection. *Journal of Allergy and Clinical Immunology*, *110*, 189-198

Clavel, F., Guetard, D., Brun-Vezinet, F., Chamaret, S., Rey, M.A., Santos-Ferreira, M.O., Laurent, A.G., Daughet, C., Katlama, C., Rouzioux, C., Klatzmann, D., Champalimaud, J.L., Montagnier, L. **1986**. Isolation of a new human retrovirus from West African patients with AIDS. *Science*, 233, 343–346

Cocuzza A. J., Chidester D.R., Cordova B.C., Jeffrey S., Parsons R.L., Bachelier L.T., Erickson-Viitanen S., Trainor G.L., Ko S.S. **2001**. Synthesis and evaluation of efavirenz (SustivaTM) analogues as HIV-1 reverse transcriptase inhibitors: replacement of the cyclopropylacetylene side chain. *Bioorganic & Medicinal Chemistry Letters*, 11, 1177–1179

Coffin, J.M. **1995**. HIV population dynamics in vivo: implications for genetic variation, pathogenesis, and therapy. *Science*, 267, 483–489

Cole J.C., Murray C.W., Nissink J.W.M., Taylor R. D., Taylor R. **2005**. Comparing protein-ligand docking programs is difficult. *Proteins: Structure, Function and Bioinformatics*. 60, 325-332

Currens M. J., Gulakowski R. J., Mariner J. M., Moran R. A., Buckheit R. W., Gustafson K. R., McMahon J. B., Boyd M. R. **1996**. Antiviral activity and mechanism of action of calanolide A against the human immunodeficiency virus type-1. *Journal of Pharmacology and Experimental Therapeutics*, 279, 645–651.

Currens M. J., Mariner J. M., McMahon J. B., Boyd M. R. **1996**. Kinetic analysis of inhibition of human immunodeficiency virus type-1 reverse transcriptase by calanolide A. *Journal of Pharmacology and Experimental Therapeutics*, 279, 652–661

Das B., Krishnaiah, Venkateswarlu K., Reddy, V.S. **2007**. A mild and simple regioselective iodination of activated aromatics with iodine and catalytic ceric ammonium nitrate. *Tetrahedron Letters*, 48,81-83

Das K., Lewi P.J., Hughes S.H., Arnold E. **2005**. Crystallography and the design of anti-AIDS drugs: conformational flexibility and positional adaptability are important in the design of non-nucleoside HIV-1 reverse transcriptase inhibitors. *Progress in Biophysics and Molecular Biology*, 88, 209–231

De Clercq, E. **1998**. The role of non-nucleoside reverse transcriptase inhibitors (NNRTIs) in the therapy of HIV-1 infection. *Antiviral Research*, 38, 153–179

De Clercq E. **2009**. Anti-HIV drugs: 25 compounds approved within 25 years after the discovery of HIV. *International Journal of Antimicrobial Agents*, 33, 307–320

De March, P.; Moreno-Manas, M.; Pi, R.; Ripoll, I.; Sanchez-Ferrando, F. **1985**. Brominated derivatives of 4-hydroxy- and 4-methoxy-6-methyl-2H-pyran-2-ones. *Journal of Heterocyclic Chemistry*, 22, 1537-1542

Ding J., Das K., Tantillo C., Zhang W., Clark A.D., Jessen Jr, S., Lu X., Hsiou Y., Jacobo-Molina A., Andries K., Pauwels R., Moereels H., Koymans L., Janssen P.A.J., Smith R.H., Jr, Kroeger Koepke M., Michejda C.J., Hughes S.H., Arnold E. **1995**. Structure of HIV-1 reverse transcriptase in a complex with the non-nucleoside inhibitor α -APA R 95845 at 2.8 Å resolution. *Structure*, 3, 365-379

Di Marzo Veronese F., Copeland T.D., De Vico A.L., Rahman R., Oroszlan S., Gallo R.C., Sarngadharan M.G. **1986**. Characterization of highly immunogenic p66/p51 as the reverse transcriptase of HTLV-III/LAV. *Science*, *231*, 1289–1291

Djakovitch L., Rollet P. **2004**. Sonogashira Cross-Coupling Reactions Catalysed by Copper-Free Palladium Zeolites. *Advanced Synthesis & Catalysis*, *346*, 1782 – 1792.

Eberlin M.N., Takahata Y., Kascheres C. **1990**. Experimental and theoretical study of the reactivity of primary and secondary enamines toward diphenylketene. A comparison of AM1 and HAM/3 semiempirical methods. *Journal of Organic Chemistry*, *55*, 5150-5155

Esnouf R., Ren J., Ross C., Jones Y., Stammers D., Stuart D. **1995**. Mechanism of inhibition of HIV-1 reverse transcriptase by nonnucleoside inhibitors. *Nature Structural & Molecular Biology*, *2*, 303-308

Esté J. A., Cihlar T. **2010**. Current status and challenges of antiretroviral research and therapy. *Antiviral Research*, *85*, 25–33

Fairlamb I.J.S., Marrison L.R., Dickinson J.M., Lu F-J., Schmidt J.P. **2004**. 2-Pyrones possessing antimicrobial and cytotoxic activities. *Bioorganic and Medicinal Chemistry*, *12*, 4285–4299

Fairlamb I.J.S., Lee A.F., Loe-Mie F.E.M., Niemelä E.H., O'Brien C.T., Whitwood A.C. **2005**. Halogenated-2-pyrones in Sonogashira cross-coupling: limitations, optimisation and consequences for GC analysis of Pd-mediated reactions. *Tetrahedron*, *61*, 9827–9838

Frisch MJ, Trucks GW, Schlegel HB, Scuseria GE, Robb MA, Cheeseman JR, Montgomery JA, Vreven T Jr, Kudin K N, Burant JC, Millam JM, Iyengar SS, Tomasi J, Barone V, Mennucci B, Cossi M, Scalmani G, Rega N, Petersson GA, Nakatsuji H, Hada M, Ehara M, Toyota K, Fukuda R, Hasegawa J, Ishida M, Nakajima T, Honda Y, Kitao O, Nakai H, Klene M, Li X, Knox JE, Hratchian HP, Cross JB, Adamo C, Jaramillo J, Gomperts R, Stratmann RE, Yazyev O, Austin AJ, Cammi R, Pomelli C, Ochterski JW, Ayala PY, Morokuma K, Voth GA, Salvador P, Dannenberg JJ, Zakrzewski VG, Dapprich S, Daniels AD, Strain MC, Farkas O, Malick DK, Rabuck AD, Raghavachari K, Foresman JB, Ortiz JV, Cui Q, Baboul AG, Clifford S, Cioslowski J, Stefanov BB, Liu G, Liashenko A, Piskorz P, Komaromi I, Martin RL, Fox DJ, Keith T, Al-Laham MA, Peng CY, Nanayakkara A, Challacombe M, Gill PMW, Johnson B, Chen W, Wong MW, Gonzalez C, Pople JA (**2004**) *Gaussian, revision E.01* Inc, Wallingford, CT

Ghosez L., Montaigne R., Mollet P. **1966**. Cycloadditions with dichloroketene. *Tetrahedron Letters*, 135-139

Gilbert M.T., Rambaut A., Wlasiuk G, Spira T.J., Pitchenik A.E., Worobey M. **2007**. The emergence of HIV/AIDS in the Americas and beyond. *Proceedings of the National Academy of Sciences (PNAS)*, *104*, 18566–18570

Goff S.P. **1990**. Retroviral reverse transcriptase: synthesis, structure, and function. *Journal of Acquired Immune Deficiency Syndromes*, *3*, 817–831

Gohlke H., Klebe G. **2002**. Approaches to the Description and Prediction of the Binding Affinity of Small-Molecule Ligands to Macromolecular Receptors. *Angewandte Chemie International Edition*, *41*, 2644-2676

Grobler J.A., Dornadula G., Rice M.R., Simcoe A.L., Hazuda D.J., Miller M.D. **2007**. HIV-1 reverse transcriptase plus-strand initiation exhibits preferential sensitivity to non-nucleoside reverse transcriptase inhibitors in vitro. *Journal of Biological Chemistry*, *282*, 8005–8010

Hang, J.Q., Li, Y., Yang, Y., Cammack, N., Mirzadegan, T., Klumpp, K. **2007**. Substrate-dependent inhibition or stimulation of HIV RNase H activity by non-nucleoside reverse transcriptase inhibitors. *Biochemical Biophysical Research Communications*, *12*, 341–350

Hannongbua S., Prasithichokekul S., Pungpo P. **2001**. Conformational analysis of nevirapine, a non-nucleoside HIV-1 reverse transcriptase inhibitor, based on quantum mechanical calculations. *Journal of Computer-Aided Molecular Design*, *15*, 997–1004

Hansen A.L., Skrydstrup T. **2005**. Regioselective heck couplings of α,β -unsaturated tosylates and mesylates with electron-rich olefins. *Organic Letters*, *7*, 5585–5587

Hargrave K. D., Proudfoot J. R., Grozinger K. G., Cullen E., Kapadia S. R., Patel U. R., Fuchs V. U., Mauldin S. C., Vitous J. **1991**. Novel non-nucleoside inhibitors of HIV-1 reverse transcriptase. 1. Tricyclic pyridobenzo- and dipyridodiazepinones. *Journal of Medicinal Chemistry*, *34*, 2231–2241

Hasiou J.C., Ding J., Das K., Clark jr. A.D., Hughes S.H., Arnold E. **1996**. Structure of unliganded HIV-1 reverse transcriptase at 2.7 Å resolution: Implications of conformational changes for polymerization and inhibition mechanism. *Structure*, *4*, 853-860

Hathaway B.A., White K.L., M.E. McGill. **2007**. Comparison of iodination of methoxylated benzaldehydes and related compounds using iodine/silver nitrate and iodine/periodic acid. *Synthetic Communications*, *37*, 3855–3860

Hazra B.G., Pore V.S., Maybhate S. P., **1989**. An improved procedure for the dichloroacetylation of primary and secondary amines. *Organic Preparations and Procedures International*, *21*, 355-358

Ho, D.D., Neumann, A.U., Perelson, A.S., Chen, W., Leonard, J.M., Markowitz, M. **1995**. Rapid turnover of plasmavirions and CD4 lymphocytes in HIV-1 infection. *Nature*, *373*, 123–126

Hoptkins A.L., Groom C.R., Alex A. **2004**. Ligand efficiency: a useful metric for lead selection. *Drug Discovery Today*, *9*, 430-431

Hsung R.P., Wei L., Sklenicka H.M., Douglas C.J. McLaughlin M.J. Mulder J.A., Yao L.J. **1999**. Formal cycloaddition reactions of vinylogous amides with α,β -unsaturated iminiums. a strategy for constructing piperidiny heterocycles. *Organic Letters*, *1*, 509-512

Hu DJ, Buve A, Baggs J, van der Groen G, Dondero TJ. **1999**. What role does HIV-1 subtype plays in transmission and pathogenesis? An epidemiological perspective. *AIDS*, *13*, 873-881

- Hu R., Barbault F., Delamar M., Zhang R. **2009**. Receptor and ligand-based 3D-QSAR study for a series of non-nucleoside HIV-1 reverse transcriptase inhibitors. *Bioorganic and Medicinal Chemistry*, *17*, 2400–2409
- Huang D., Caflish A. **2009**. Library screening by fragment-based docking. *Journal of Molecular Recognition*, *23*, 183-193
- Jaramillo P., Pérez P., Fuentealba P., **2007**. Relationship between basicity and nucleophilicity. *Journal of Physical Organic Chemistry*, *20*, 1050-1057
- Jorgensen W. L. **2009**. Efficient Drug Lead Discovery and Optimization. *Accounts of Chemical Research*, *42*, 724–733
- Kallings L.O. **2008**. The first postmodern pandemic: 25 years of HIV/AIDS. *Journal of Internal Medicine*, *263*, 218–243
- Kappe T., Aigner A., Roshger P., Schnell B., Stadlbauer W. **1995**. A simple and effective method for the reduction of acyl substituted heterocyclic 1,3-dicarbonyl compounds to alkyl derivatives by zinc- acetic acid- hydrochloric acid. *Tetrahedron*, *51*, 12923-12928
- Karki S.S., Hazare R., Kumar S., Bhadauria V.S., Balzarini J., De Clercq E. **2009**. Synthesis, anticancer and cytostatic activity of some 6H-indolo[2,3-b]quinoxalines. *Acta Pharmaceutica*, *59*, 431-440
- Kashman Y., Gustafson K. R., Fuller R. W., Cardellina J. H., McMahon J. B., Currens M. J., Buckheit R. W., Hughes S. H., Cragg G. M., Boyd M. R. J. **1992**. HIV inhibitory natural products. Part 7. The calanolides, a novel HIV-inhibitory class of coumarin derivatives from the tropical rainforest tree, *Calophyllum lanigerum*. *Journal of Medicinal Chemistry*, *35*, 2735–2743
- Kato Y., Okada S., Tomimoto K., Mase T. **2001**. A facile bromination of hydroxyheteroarenes *Tetrahedron Letters*, *42*, 4849-4851
- Kati W.M., Johnson K.A., Jerva L.F., Anderson K.S. **1992**. Mechanism and fidelity of HIV reverse transcriptase. *Journal of Biological Chemistry*, *267*, 25988–25997
- Kier L.B., Hall L.H. **2004**. Bioisosterism: quantitation of structure and property effect. *Chemistry and Biodiversity*, *1*, 138-151
- Kohlstaedt, L.A., Wang J., Friedman J.M., Rice P.A., Steitz T.A. **1992**. Crystal structure at 3.5 Å resolution of HIV-1 reverse transcriptase complexed with an inhibitor. *Science*, *256*(5065), 1783-1790
- Kuntz, I. D., Blaney, J. M., Oatley, S. J., Langridge, R. & Ferrin, T. E. **1982**. A geometric approach to macromolecule–ligand interactions. *Journal of Molecular Biology*, *161*, 269–288
- Kuntz I.D., Chen K., Sharp K.A., Kollman P.A. **1999**. The maximal affinity of ligands. *Proceedings of the National Academy of Sciences (PNAS)*, *96*, 9997-10002
- Lee C., Yang W., Parr R.G. **1988**. Development of the Colle-Salvetti correlation-energy formula into a functional of the electron density. *Physical Review B*, *37*, 785–789

- Lei X., Gao L., Ding Q., Peng Y., Wu J. **2011**. Generation of diverse 2-pyrone derivatives via palladium-catalyzed site-selective Suzuki-Miyaura couplings of 3-bromo-4-tosyloxy-2-pyrone. *Organic and Biomolecular Chemistry*, *9*, 6265–6270
- Lemke T.L., Williams D.A., Roche V.F., Zito S.W. **2008**. *Foye's Principles of Medicinal Chemistry* sixth edition. Lippincott Williams & Wilkins, Philadelphia. ISBN: 978-0-7817-6879-6885
- Leung C.S., Leung S.S.F., Tirado-Rives J, Jorgensen W.L., **2012**. Methyl effects on protein-ligand binding. *Journal of Medicinal Chemistry*, *55*, 4489-4499
- Liu D., Li X-M, Meng L., Li C-S., Gao S-S., Shang Z., Proksh P., Huang C-G, Wang B-G., **2011**. Nigerapyrone A-H, α -pyrone derivatives from marine mangrove-derived endophytic fungus *Aspergillus niger* MA-132. *Journal of Natural Products*, *74*, 1787-1791
- Liu J., Wright E.R., Winkler H. **2010**. 3D visualization of HIV virions by cryoelectron tomography. *Methods in Enzymology*, *483*, 267–290
- Lipinski C. A. **2000**. Drug-like properties and the causes of poor solubility and poor permeability. *Journal of Pharmacological and Toxicological Methods*, *44* 235- 249
- Lipinski C. A., Lombardo F., Dominy B. W., Feeney P. **2001**. J. Experimental and computational approaches to estimate solubility and permeability in drug discovery and development settings. *Advanced Drug Delivery Reviews*, *46*, 3–26
- Lokot I.P., Pashkovsky F.S., Lakhvich F.A. **1999**. A new approach to the synthesis of 3,6- and 3,5-dialkyl derivatives of 4-hydroxy-2-pyrone. Synthesis of *rac*-germicidin. *Tetrahedron*, *55*, 4783-4792
- Lowe DM, Aitken A, Bradley C, Bradley C., Darby G. K., Larder B. A., Powell K. L., Purifoy D. J. M., Tisdale M., Stammers D. K. **1988**. HIV-1 reverse transcriptase: crystallization and analysis of domain structure by limited proteolysis. *Biochemistry*, *27*, 8884–8889
- Majumdar K. C., Kundu U. K., Ghosh S. **2002**. Studies on triacetic acid lactone-annulated heterocycles: synthesis of 3-aryloxyacetyl-6-methyl-2,3-dihydrothieno-[3,2-*c*]pyran-4-ones by tandem cyclization. *Tetrahedron*, *58*, 10309–10313
- Mancini I., Defant A., Guella G. **2007**. Recent synthesis of marine natural products with antibacterial activities. *Anti-Infective Agents in Medicinal Chemistry*, *6*, 17-48
- Mayr H., Breugst M., Ofial A.R., **2011**. Farewell to the HSAB treatment of ambident reactivity. *Angewandte Chemie, International Edition*, *50*, 6470-6505
- McLaughlin M. J., Hsung R. P., Cole K. P., Hahn J. M., Wang J. **2002**. A Novel and Highly Stereoselective Approach to Aza-Spirocycles. A Short Total Synthesis of 2-epi-(±)-Perhydrohistrionicotoxin and an Unprecedented Decarboxylation of 2-Pyrone. *Organic Letters*, *4*, 2017–2020

- Mehellou Y., De Clercq E. **2010**. Twenty-six years of anti-hiv drug discovery: where do we stand and where do we go? *Journal of Medicinal Chemistry* 53, 521-538
- Menghezzi H, Boucekkine A, Kolli B., Hamdi M. **1983**. Protonation of aminopyrone: a four centers problem, CNDO/2 versus MNDO study. *International Journal of Quantum Chemistry*, XXIV, 425-428
- Meréndez-Arias L. **2010**. Molecular basis of human immunodeficiency virus drug resistance: an update. *Antiviral Research*, 85, 210-231
- Merrick J.P., Moran D., Radom L. **2007**. An evaluation of harmonic vibrational frequency scale factors. *Journal of Physical Chemistry A*, 111, 11683-11700
- Mishima Y, Steitz JA. **1995**. Site-specific crosslinking of 4-thiouridine-modified human tRNA (3Lys) to reverse transcriptase from human immunodeficiency virus type I. *The EMBO Journal*, 14, 2679-2687
- Montagnier L. **2010**. 25 years after HIV discovery: Prospects for cure and vaccine, *Virology*, 397, 248-254
- Montalbetti C.A.G.N., Falque V. **2005**. Amide bond formation and peptide coupling, *Tetrahedron* 61, 10827-10852
- Mordant C. , Schmitt B., Pasquier E. , Demestre C., Queguiner L., Masungi C., Peeters A., Smeulders L., Bettens E., Hertogs K., Heeres J., Lewi P., Guillemont J. **2007**. Synthesis of novel diarylpyrimidine analogues of TMC278 and their antiviral activity against HIV-1 wild-type and mutant strains. *European Journal of Medicinal Chemistry*, 42, 567-579
- Morris G. M., Goodsell D. S., R. S. Halliday, R. Huey, W. E. Hart, Belew R. K., Olson A.J. **1998**. Automated docking using a lamarckian genetic algorithm and an empirical binding free energy function. *Journal of Computational Chemistry*, 19, 1639-1662
- Mukherjee S., Balias T. E., Rizzo R. C. **2010**. Docking Validation Resources: Protein Family and Ligand Flexibility Experiments. *Journal of Chemical Information and Modeling*, 50, 1986-2000
- Muyembe J.-J., Kabongo J.-M. M., Kalengayi R. M., Van Marck E., Gilbert M. T. P., Wolinsky S. M. **2008**. Direct evidence of extensive diversity of HIV-1 in Kinshasa by 1960. *Nature*, 455 (7213), 661-664
- Nisachon K., Nitirat C., Arunee T., Patchreenart S., Kiattawee C, Pornpan P., Supa H., Supanna T. **2009**. Dipyrrodoiazepinone derivatives; synthesis and anti HIV-1 activity. *Beilstein Journal of Organic Chemistry*, 5, No. 36. doi:10.3762/bjoc.5.36
- Novikov D.V., Yakovlev I.P., Zakhs V.E., Prep'yalov A.V. **2002**. Synthesis, properties and biological activity of 4-hydroxy-2H-pyran-2-ones and their derivatives. *Russian Journal of General Chemistry*, 72, 1701-1714
- Ono N., Miyake H., Saito T., Kaji A. **1980**. A convenient synthesis of sulfides, formaldehyde dithioacetals and chloromethyl sulfides. *Synthesis*, 952-953

Patel M., McHugh R.J., Cordova B.C., Klabe R. M., Erickson-Viitanem S., Trainor G. L., Ko S.S. **1999**. Synthesis and evaluation of benzoxazinones as HIV-1 reverse transcriptase inhibitors. Analogues of efavirenz. *Bioorganic & Medicinal Chemistry Letters*, *9*, 3221-3224

Pauwels R., Andries K., Debyser Z. , Van Daele P., Schols D., Stoffels P., De Vreese K., Woestenborghsi R., Vandamme A-M., Janssent C.G.M., Anne J., Cauwenberghi G., Desmyter J., Heykants J., Janssent M.A.C., De Clercq E., Janssen P. A.J. **1993**. Potent and highly selective human immunodeficiency virus type 1 (HIV-1) inhibition by a series of anilinophenylacetamide derivatives targeted at HIV-1 reverse transcriptase. *Proceedings of the National Academy of Sciences (PNAS)*, *90*, 1711-1715

Pink R., Hudson A., Mouriès M-A., Bendig M. **2005**. Opportunities and challenges in antiparasitic drug discovery. *Nature Reviews Drug Discovery*, *4*, 727-740

Quan Y., Liang C., Inouye P., Wainberg M.A. **1998**. Enhanced impairment of chain elongation by inhibitors of HIV reverse transcriptase in cell-free reactions yielding longer DNA products. *Nucleic Acids Research*, *15*, 5692– 5698

Quan Y., Rong L., Liang C., Wainberg M.A. **1999**. Reverse transcriptase inhibitors can selectively block the synthesis of differently sized viral DNA transcripts in cells acutely infected with human immunodeficiency virus type1. *Journal of Virology*, *73*, 6700–6707

Rabnavaz M., Benson S.D., Khan B., Shah M.R. **2010**. Ethyl 2-(3-acetyl-6-methyl-2-oxo-2H-pyran-4-yloxy)acetate. *Acta Crystallographica Section E*, *E66*, o397

Radzio J., Sluis-Cremer, N. **2008**. Efavirenz accelerates HIV-1 reverse transcriptase ribonuclease H cleavage, leading to diminished zidovudine excision. *Molecular Pharmacology*, *73*, 601–606

Raspoet G., Nguyen M.T., Kelly S.,Hegarty A.F.**1998**. Amination of ketenes: evidence for a mechanism involving enols of amides as intermediates. *Journal of Organic Chemistry*, *63*, 9669-9677

Reeves J. D., Doms R. W. **2002**. Human immunodeficiency virus type 2. *Journal of General Virology*, *83*, 1253–1265

Reynolds C.H., Bembenek S.D., Tounge B.A.B. **2007**. The role of molecular size in ligand efficiency. *Medicinal Chemistry Letters*, *17*, 4258-4261

Rodgers D.W., Gamblin S.J., Harris B.A., Ray S., Culp J.S., Hellmig B., Woolf D.J., Debouck C., Harrison S.C. **1995**. The structure of unliganded reverse transcriptase from the human immunodeficiency virus type 1. *Proceedings of the National Academy of Sciences (PNAS)*, *92*, 1222–1226

Schäfer W, Friebe WG, Leinert H, Mertens A, Poll T, von der Saal W, Zilch H, Nuber B, Ziegler ML. **1993**. Non-nucleoside inhibitors of HIV-1 reverse transcriptase: molecular modeling and X-ray structure investigations. *Journal of Medicinal Chemistry*, *36*, 726-732

Sepkowitz K.A. **2001**. AIDS-the first 20 years. *The New England Journal of Medicine*, *344*, 1764–1772

Shaw-Reid C.A., Feuston B., Munshi V., Getty K., Krueger J., Hazuda D.J., Parniak M.A., Miller M.D., Lewis D. **2005**. Dissecting the effects of DNA polymerase and ribonuclease H inhibitor combinations on HIV-1 reverse transcriptase activities. *Biochemistry*, *8*, 1595–1606

Shoichet B. K., McGovern S. L., Wei B., Irwin J. J. **2002**. Lead discovery using molecular docking. *Current Opinion in Chemical Biology*, *6*, 439–446

Sklenicka H.M., Hsung R.P., McLaughlin M.J. Wei L., Gerasyuto A.I., Brennessel W.B. **2002**. Stereoselective Formal [3 + 3] Cycloaddition Approach to cis-1-Azadecalins and Synthesis of (-)-4a,8a-diepi-Pumiliotoxin C. Evidence for the First Highly Stereoselective 6π -Electron Electrocyclic Ring Closures of 1-Azatrienes. *Journal of the American Chemical Society*, *124*, 10435-10442

Sluis-Cremer N., Tachedjian G. **2008**. Mechanisms of inhibition of HIV replication by non-nucleoside reverse transcriptase inhibitors. *Virus Research*, *134*, 147–156

Solis F.J. Wets., R.J.-B. **1981**. Minimization by random search techniques. *Mathematical Operations Research*, *6*, 19-30

Sousa S. F., Fernandes P. A., Ramos M. J. **2006**. Protein–Ligand Docking: Current Status and Future Challenges. *PROTEINS: Structure, Function, and Bioinformatics*, *65*, 15–26

Srivastava V., Negi A.S., Kumar J.K., Gupta M.M., Khanuja S.P.S. **2005**. Plant-based anticancer molecules: A chemical and biological profile of some important leads. *Bioorganic and Medicinal Chemistry*, *13*, 5892–5908

Staudinger H., Schneider H. **1923**. Über ketene: XLIV. Mitteilung. Über unorganisch substituierte ketene. *Helvetica Chimica Acta*, *6*, 304-315

Takara K., Sakaed T., Yagami T., Kobayashi H., Ohmoto N., Horinouchi M., Nishiguchi K., Okumura K. **2002**. Cytotoxic Effects of 27 Anticancer Drugs in HeLa and MDR1-Overexpressing Derivative Cell Lines. *Biological and Pharmaceutical Bulletin*, *25*, 771-778

UNAIDS, WHO (December 2011). 2010 AIDS epidemic update. www.unaids.org

Viegas-Junior C., Danuello A., da Silva Bolzani V., Barreiro E.J., Fraga C.A. **2007**. Molecular hybridization: a useful tool in the design of new drug prototypes. *Current Medicinal Chemistry*, *14*, 1829-1852

Wang J., Swidorski, J.J. Sydorenko N., Hsung R.P., Coverdale H.A., Kuyava J.M., Liu J. **2006**. Aza-[3+3] annulations. Part 6. Total syntheses of putative (-)-lepadiformine and (-)-cylindricine C. *Heterocycles*, *70*, 423-459

Weiss R.A. **1993**. How does HIV cause AIDS? *Science*, *260* (5112), 1273–1279

Whang J.P., Yang S.G., Kim Y.H. **1997**. Novel α -iodination of functionalized ketones with iodine mediated by bis(tetra-*n*-butylammonium) peroxydisulfate. *Chemical Communications*, 1355-1356

Wijesundara D. K., Jackson R. J., Ramshaw I. A., Ranasinghe C. **2011**. Human immunodeficiency virus-1 vaccine design: where do we go now? *Immunology and Cell Biology*, 89, 367-374

Worobey M., Gemmel M., Teuwen D. E., Haselkorn T., Kunstman K., Bunce M. **2008**. Direct evidence of extensive diversity of HIV-1 in Kinshasa by 1960. *Nature*, 455(7213), 661-664

Xu Z.Q., Flavin M.T., Jenta T.R. **2000**. Calanolides, the naturally occurring anti-HIV agents. *Current opinion in drug discovery & development*, 3, 155-166

Yamauchi T., Ogawa M., Ueda T. **2008**. Carmustine-resistant cancer cells are sensitized to temozolomide as a result of enhanced mismatch repair during the development of carmustine resistance. *Molecular Pharmacology*, 74, 82-91

Yee S. **1997**. In vitro permeability across Caco-2 cells (colonic) can predict in vivo (small intestinal) absorption in man- fact or myth. *Pharmaceutical Research*, 14, 763-766

Yokoyama Y., Ohmori I., Kohoda K., Kawazoe Y. **1988**. Potentiation of cytotoxic activity of anti-cancer drugs against cultured L1210 cells by *bacillus thuringiensis* subsp. *israelensis* toxin. *Chemical and Pharmaceutical Bulletin*, 36, 4499-4504

Zhan P., Chen X., Li D., Fang Z., De Clercq E., Liu X. **2011**. HIV-1NNRTIs: Structural Diversity, Pharmacophore Similarity, and Implications for Drug Design. *Medicinal research reviews*, Epub ahead of print, DOI 10.1002/med.20241

Zhao Y. H., Le J., Abraham M.H., Hersey A., Eddershaw P. J., Luscombe C. N., Boutina D., Beck G., Sherborne B., Cooper I., Platts J. A. **2001**. Evaluation of human intestinal absorption data and subsequent derivation of a quantitative structure-activity relationship (qsar) with the abraham descriptors. *Journal of Pharmaceutical Sciences*, 90, 749-784

Acknowledgments

I would like to thank Prof. Jan Balzarini at Rega Institute, University of Leuven Belgium, for his kind collaboration in doing anti-HIV assays; Prof. R. Snoeck and Prof. G. Andrei at the same institute for their supervision in other antiviral assays.

My gratitude goes to Dr. Rossella Tomazzolli, Faculty of Science at the University of Trento, for her precious help in performing the enzymatic test and to Dr. Ibtissam Djinni, doctoral student at the University A. Mira of Bejaia, Algeria, for doing antibacterial test.

I am grateful to Mr. A. Sterni and Mr. D. Avi, university of Trento for recording mass and FT-IR spectra, respectively.

Appendix A

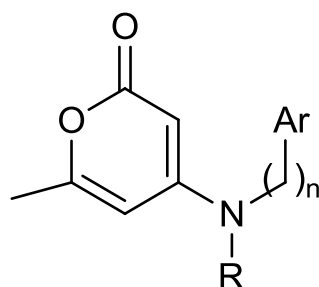
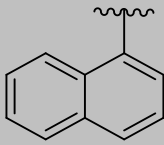
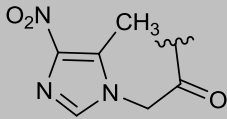
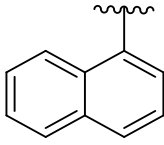
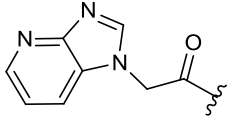
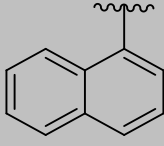
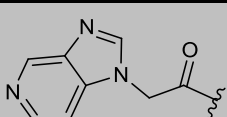
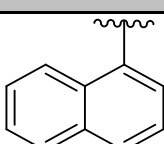
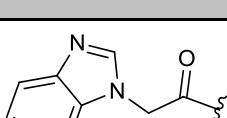
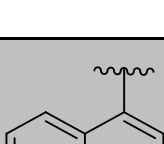
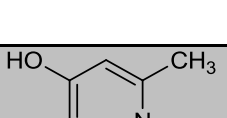
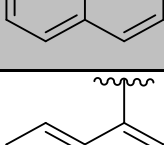
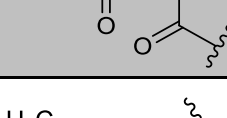
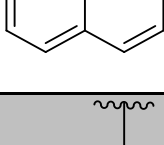
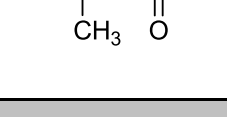
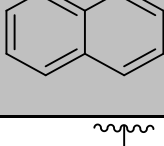
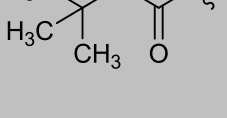
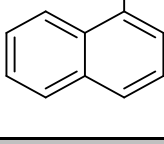
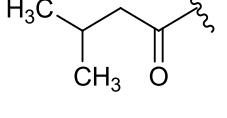
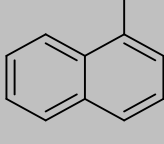
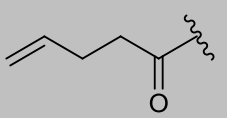
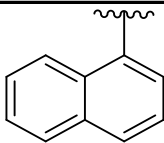
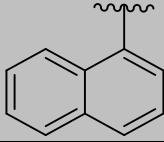
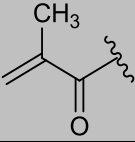
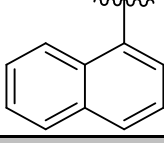
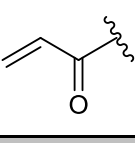
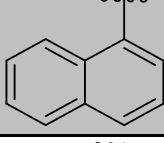
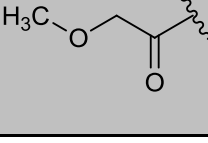
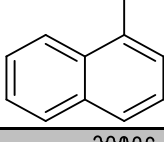
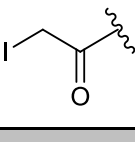
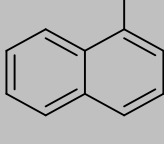
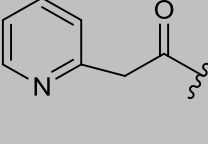
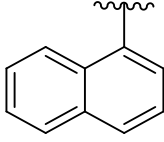
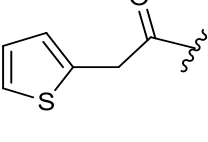
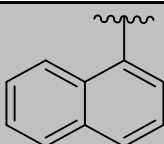
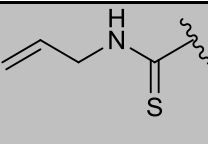
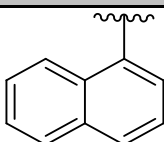
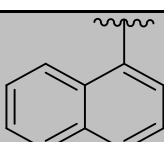
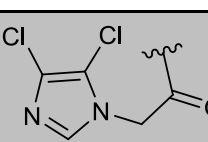
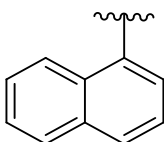
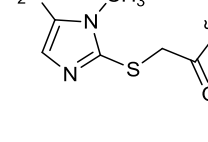


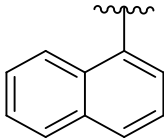
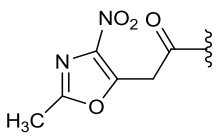
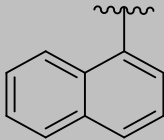
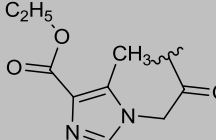
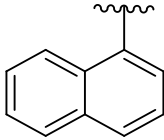
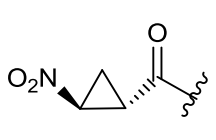
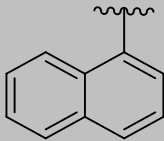
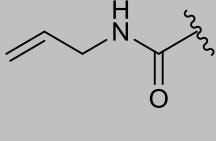
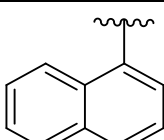
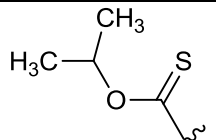
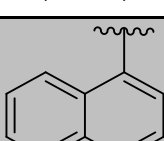
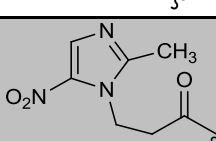
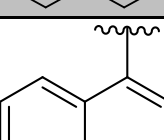
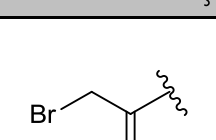
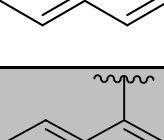
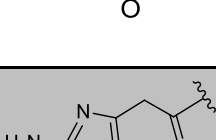
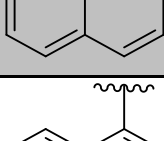
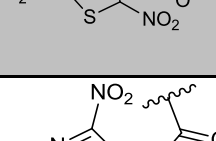
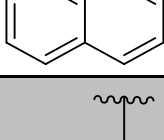
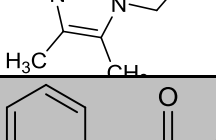
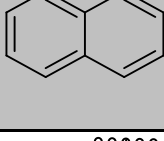
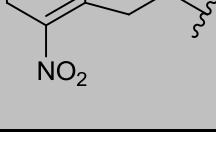
Table. Results from docking calculations on a theoretical library of molecules

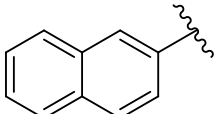
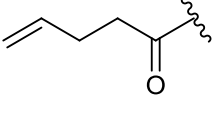
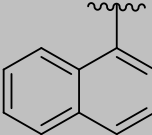
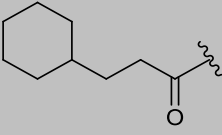
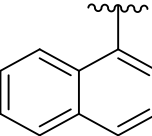
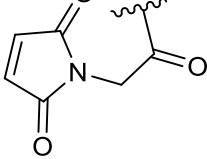
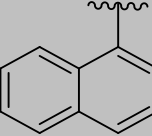
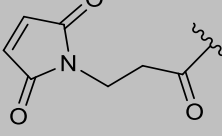
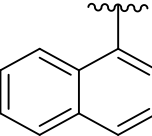
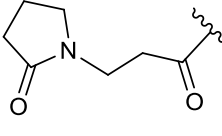
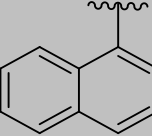
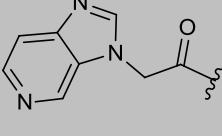
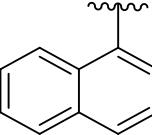
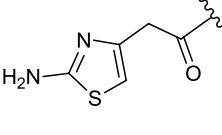
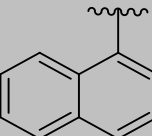
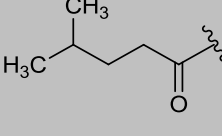
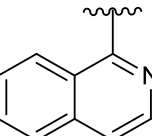
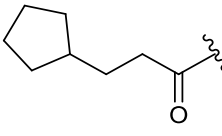
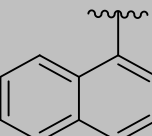
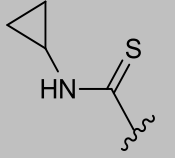
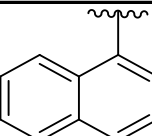
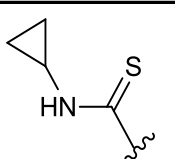
Compound	Ar	n	R	Calculated Log P	M.W. ^a	E _{Dock} (Kcal/mol)
C1		1		2.81±0.4	317.79	-9.04
C2		1		2.98±0.3	362.24	-9.56
C3		1		2.98±0.3	362.24	-9.52
C4		1		2.69±0.3	297.38	-9.34
C5		1		2.29±0.4	313.38	-9.12
C6		1		2.15±0.4	328.35	-9.27
C7		1		2.31±0.6	357.82	-9.71

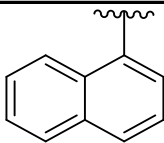
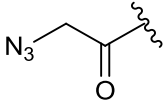
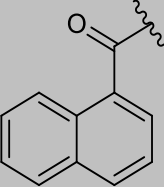
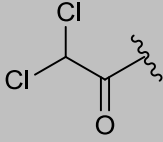
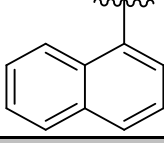
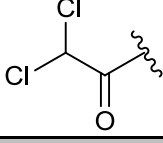
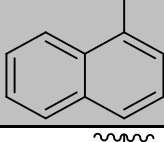
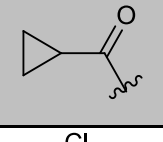
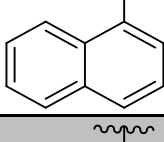
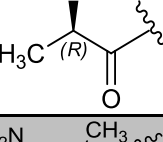
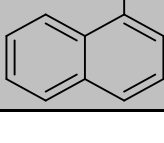
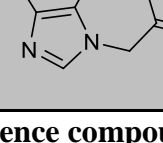
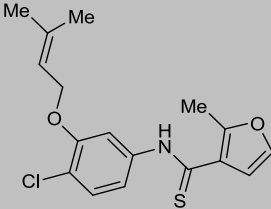
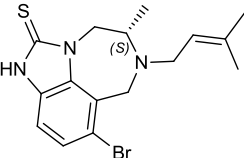
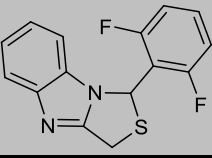
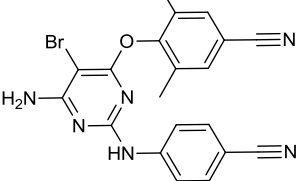
Compound	Ar	n	R	Calculated Log P	M.W. ^a	E _{Dock} (Kcal/mol)
C9		1		2.10±0.6	456.88	-10.15
C8		2		2.42±0.8	371.85	-10.51
C10		1		3.42±0.3	333.41	-10.31
C11		1		3.58±0.3	355.84	-10.66
C12		1		3.58±0.3	355.84	-10.34
C13		1		3.76±0.5	400.29	-10.70
C14		1		3.76±0.5	400.29	-11.12
C15		1		3.26±0.4	321.40	-10.59
C16		1		3.57±0.43	333.41	-10.69
C17		1		3.28±0.5	353.47	-10.46
C18		1		2.94±0.5	432.42	-12.12

Compound	Ar	n	R	Calculated Log P	M.W. ^a	E _{Dock} (Kcal/mol)
C19		1		3.12±0.5	432.47	-12.85
C20		1		3.15±0.5	424.49	-13.14
C21		1		2.87±0.3	424.49	-12.80
C22		1		3.14±0.5	424.49	-12.89
C23		1		2.86±0.9	430.49	-11.59
C24		1		3.96±0.4	347.44	-10.74
C25		1		4.41±0.5	363.49	-11.24
C26		1		4.01±0.4	349.46	-10.88
C27		1		3.83±0.3	346.44	-10.94
C28		1		2.76±0.4	431.48	-13.20

Compound	Ar	n	R	Calculated Log P	M.W. ^a	E _{Dock} (Kcal/mol)
C29		1	CH ₃ SO ₂	2.37±1.0	343.43	-10.04
C31		1		3.57±0.4	333.41	-10.88
C32		1		3.18±0.4	319.38	-10.54
C33		1		2.52±0.4	337.40	-10.01
C34		1		3.54±0.4	433.26	-10.55
C35		1		3.30±0.5	384.46	-11.37
C36		1		4.08±0.4	389.50	-11.71
C37		1		3.74±0.5	364.50	-10.27
C38		1	C ₂ H ₅ SO ₂	2.77±0.9	357.46	-10.47
C39		1		3.97±0.6	442.33	-12.59
C40		1		3.47±0.4	464.54	-11.14

Compound	Ar	n	R	Calculated Log P	M.W. ^a	E _{Dock} (Kcal/mol)
C41		1		3.23±0.5	433.45	-11.62
C42		1		3.37±0.4	459.54	-7.66
C43		1		2.84±0.5	378.41	-9.00
C44		1		3.24±0.4	348.43	-10.57
C45		1		4.46±0.3	367.50	-10.87
C46		1		3.02±0.6	446.50	-11.29
C47		1		3.44±0.5	386.26	-10.99
C48		1		3.07±0.45	450.51	-12.49
C49		1		3.49±0.4	446.50	-11.70
C50		1		4.23±0.4	428.47	-10.20
C51		1		2.24±0.7	389.45	-9.52

Compound	Ar	n	R	Calculated Log P	M.W. ^a	E _{Dock} (Kcal/mol)
C52		1		3.86±0.4	347.44	-10.53
C53		1		5.46±0.6	403.56	-7.59
C54		1		2.30±0.3	402.43	-11.51
C55		1		2.25±0.5	416.46	-11.12
C56		1		3.25±0.4	390.52	-10.74
C57		1		2.86±0.3	424.49	-11.34
C58		1		3.07±0.4	405.51	-11.22
C59		1		4.42±0.5	363.49	-9.08
C60		1		4.03±0.5	390.52	-9.68
C61		1		3.72±0.4	364.51	-10.39
C62		2		4.06±0.4	378.53	-10.24

Compound	Ar	n	R	Calculated Log P	M.W. ^a	E _{Dock} (Kcal/mol)
C63		2		2.94±0.9	362.42	-8.62
C64		1		3.44±0.4	404.27	-10.34
C65		2		4.09±0.4	390.29	-10.85
C66		2		3.77±0.3	347.44	-10.65
C67		2		3.92±0.3	369.87	-10.86
C68		2		3.40±0.4	446.50	-11.87
Reference compounds						
UC781				4.77±0.8	355.8 8	-10.11
TIBO-Br				3.86±0.8	366.3 6	-8.75
TBZ				3.83±0.7	288.3 4	-8.16
TMC125				4.22±0.8	435.3 1	-10.28

a) M.W. = molecular weight

Appendix B

Presentation of preliminary results at XIII International Workshop on Complex Systems. Andalo (Trento-Italy), 18-22 March 2012

<http://ds.science.unitn.it/wiki/index.php?n=Main.Andalo>

Abstract of the poster contribution

**Numeric simulation on biological macromolecules applied to drug design:
molecular docking in the study of new potential anti-HIV agents**

Andrea Defant and Ines Mancini

Laboratorio di Chimica Bioorganica, Dipartimento di Fisica, Università di Trento,

via Sommarive 14, I-38123 Povo Trento, Italy.

Computational approach is widely recognized as the starting phase in recent drug development, in order to predict biological properties of a series of molecules, from which selecting the best candidates to be synthesized and later tested in bioassays. Many computational tools have been developed for studying the interactions involved between a ligand (drug) and enzymes or DNA. One of most used approaches is molecular docking, which allows to find favorable orientations of potential ligands into the active or allosteric site of the macromolecules and evaluates the interaction energy score derived from empirical force field.

In our recent activity on drug design of potential anti-HIV agents solving the problem of resistance observed with the known therapeutic molecules, we have focused our attention on non-nucleoside inhibitors of reverse transcriptase. It is a crucial enzyme for the virus replication and represents an optimal candidate to fight the viral infection. Based on X-ray crystallographic structures of reverse transcriptase interacting with clinical drugs, AutoDock and Molegro softwares have been applied for the docking calculations on a wide series of new molecules in comparison with clinical agents. This approach provides a selection of novel molecules showing a more favorable interaction energy than the one observed with commercial drugs. This study has indicated a reduced number of molecules, to be synthesized and further subjected to bioassays.

Numeric Simulation on Biological Macromolecules Applied to Drug Design: Molecular Docking in the Study of New Potential Anti-HIV Agents



Andrea Defant and Ines Mancini

Laboratorio di Chimica Bioorganica, Dipartimento di Fisica, Università di Trento, Povo-Trento, Italy

1. Introduction

Molecular docking approach is widely applied in the development of new drugs. It allows to find favorable orientations of these molecules as potential ligands into the active or allosteric site of the macromolecules (enzymes or DNA) and evaluates the interaction energy score derived from empirical force field.

In our recent activity on drug design of potential anti-HIV agents solving the problem of resistance observed with the known drugs, we have studied non-nucleoside inhibitors of reverse transcriptase (NNRTI). It is a crucial enzyme for the virus replication and represents an optimal candidate to fight the viral infection (Figure 1).

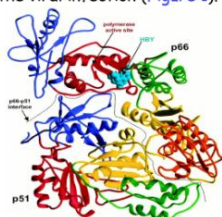


Figure 1. Structure of enzyme HIV-1 reverse transcriptase binding an inhibitor (HBY)

2. Drug Design of New Potential RT-Inhibitors

NNRTI can have heterogeneous structures. A pharmacophoric model is reported in Figure 2.

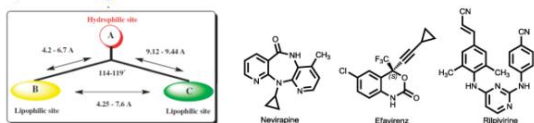


Figure 2. Schematic representation of NNRTI pharmacophoric distance map (left) and structures of clinically used drugs (right)

According to this model, we have designed a series of novel molecules to be submitted to docking calculations (Figure 3).

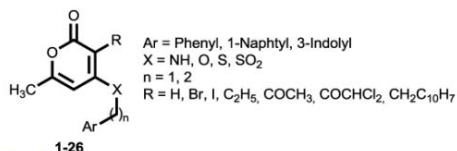


Figure 3. General molecular structure of new potential NNRTI (compounds 1-26)

3. Docking calculation

Docking calculation was carried out with AutoDock software. It is the most used software and gives straightforward results, as reported for true and false protease inhibitors (Figure 4).¹

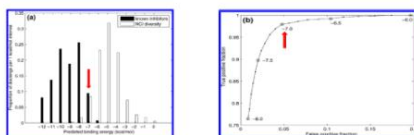


Figure 4. (a) Comparison of the distribution of binding energies for known inhibitors with National Cancer Institute (NCI) Diversity Set Compounds; (b) ROC curve showing a sensitivity/specificity tradeoff for threshold values from -8 to -6 Kcal/mol.

By these results it is evident that:

- a threshold of -7.0 Kcal/mol works well to discriminate between putative specific and nonspecific binding with protease.
- This general approach is broadly applicable to other enzyme systems.

We have applied these data for the calculation on our molecules.

L.Chang M.W., et al., J. Chem. Inf. Model. 2007, 47, 1258

4. Computational details with AutoDock 4.0

- Energy-minimized structures were optimized by Gaussian 03 (DFT level of theory, B3-LYP/6-31G(d,p)).
- Efavirenz was removed from X-Ray structure (PDB code: 1FK9) of RT, replaced by each new molecule and calculations were carried out.
- Grid box size of 60x60x60 points centred on the binding pocket of RT using a 0.375 Å grid spacing was set.
- 100 Runs were used (by Lamarckian genetic algorithm with default settings).

5. Validation Method

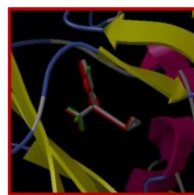


Figure 5. Structure of docked efavirenz (in red lines) superimposed on X-Ray structure of RT/efavirenz complex

In order to validate the goodness of this method, the drug efavirenz, removed from X-Ray structure of RT, was docked and its new position compared with the original one. (Figure 5)

6. Results

In the whole series of novel molecules (168) submitted to docking calculation we selected 26 molecules with comparable or higher docking score than drugs in clinical use. A comparison between AutoDock and Molegro docking scores gave similar results. In particular, compound 20 has shown the best affinity with RT enzyme.

Table: Results by docking calculation carried out with AutoDock 4.0 and Molegro Virtual Docker

Compound	E _{docking} AutoDock (Kcal/mol)	E _{docking} Molegro Score (Rerank Score)	Compound	E _{docking} AutoDock (Kcal/mol)	E _{docking} Molegro Score (Rerank Score)
1	-9.40	-119 (-97)	16	-10.36	-133 (-105)
2	-7.72	-97 (-82)	17	-10.95	-143 (-114)
3	-9.70	-131 (-103)	18	-10.96	-145 (-102)
4	-9.39	-123 (-101)	19	-11.48	-143 (-98)
5	-9.94	-127 (-104)	20	-13.32	-167 (-116)
6	-10.52	-130 (-104)	21	-10.66	-142 (-115)
7	-10.03	-122 (-102)	22	-9.23	-119 (-92)
8	-9.52	-137 (-108)	23	-11.67	-140 (-104)
9	-9.64	-124 (-102)	24	-11.16	-152 (-113)
10	-9.79	-129 (-103)	25	-10.94	-160 (-117)
11	-10.30	-130 (-109)	26	-10.31	-160 (-116)
12	-10.47	-133 (-106)	Drugs as Reference Molecules		
13	-9.93	-124 (-102)	Nevirapine	-8.25	104 (-80)
14	-10.08	-136 (-110)	Efavirenz	-8.61	-139 (-119)
15	-9.70	-132 (-100)	Rilpivirine	-10.39	-151 (-74)

Compound 20 and efavirenz give a different interaction mode with RT: a π - π interaction between the naphthyl unit of 20 and Tyr 188, whereas a H-bridge between N of efavirenz and Lys 101 in RT are obtained (Figure 6 a,b).

A good overlapping between molecule 20 and efavirenz is observed taking into account shape, electrostatic potential, lipophilicity and molecular refractivity (Figure 6c).

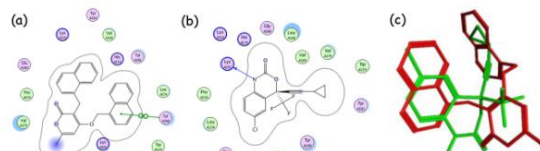


Figure 6. 2D representation of interactions for RT allosteric site and molecule 20 (a) or efavirenz (b). (c) Superimposition of molecular structures for efavirenz (green) and molecule 20 (red)

7. Conclusions

These calculations have allowed to select the most promising molecules as candidates to be synthesized and later subjected to bioassays.

Appendix C

Contribution at the 16th International Electronic Conference on Synthetic Organic Chemistry. 1-30 November 2012

Abstract of the E-conference contribution

A study on the regioselectivity in *N*, *C*-acylation of β -enamino esters.

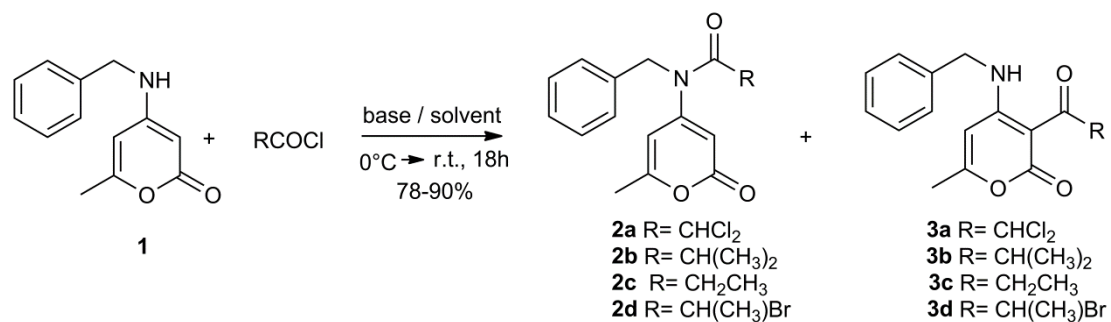
Andrea Defant¹ and Ines Mancini¹

¹⁾ *Università di Trento, Dipartimento di Fisica, Laboratorio di Chimica Bioorganica, via Sommarive 14, I-38123 Povo Trento, Italy.*

In our recent synthesis of potential antiviral agents, we have been interested in the acylation products from 4-(benzylamino)-6-methyl-2H-pyran-2-one (**1**). With the aim to obtain amides **2a-2d**, **1** has been treated with the suitable acyl chloride in the presence of triethylamine. An unexpected mixture of *N*- and *C*-acyl products, **2a-2d** and **3a-3d** respectively were obtained (Scheme). It was observed that the selectivity was not affected by the structure of acyl chlorides. All the products were fully characterized by extensive NMR and mass spectrometric analyses, as well as by comparison of experimental IR spectra with the simulated ones by density functional theory (DFT) calculations for the regioisomeric products.

Despite a recent growing interest in amino-pyrone chemistry as precursors in the synthesis of natural products, only few studies have been reported. That was a further reason in the investigation of the selectivity for the reaction involving amino-pyrone **1**. The same reaction was carried out without any bases, obtaining a complete regioselectivity in favour of *C*-acyl product (**3a-3d**), or replacing triethylamine with a series including 13 organic bases. In particular a fully reversed selectivity was observed, in favour of *N*-acyl product (**2a-2d**). These data have been supported by a plausible explanation in terms of the molecular structure of amino-pyrone. The evaluation of solvent effect was also investigated in two cases of highly selective acylation, observing that the presence of solvents with a different polarity did not affect the selectivity. Finally the investigation included the reactivity of a (*Z*)-acyclic β -enamino-ester [(*Z*)-ethyl 3-(benzylamino)but-2-enoate], selected as a model

compound: only *C*-acyl products were obtained under the same conditions previously adopted for amino-pyrone **1**. An explanation will be furnished for this high regioselectivity.



Scheme. *N,C*-acylation of amino-pyrone **1**.

Appendix D

Additional research activity

In addition to the study regarding this thesis, other activities were carried out on some topics investigated in the Bioorganic Chemistry Laboratory. In particular, the results of these studies have produced the following papers:

1) V. F. Tamboli, N. Re, C. Coletti, **A. Defant**, I. Mancini, P. Tosi, "A joint experimental and theoretical investigation on the oxidative coupling of resveratrol induced by copper and iron ions", *International Journal of Mass Spectrometry*, **2012**, 319-320, 55-63

Abstract

Currently, a mounting interest exists on the biological activity of polyphenolic compounds, which have been suggested to exert positive effects on the human health. In this paper we report the first electrospray ionization mass spectrometry (ESI-MS) study on the gas-phase production of isomeric δ -viniferin and ϵ -viniferin dimers in racemic form, starting from acetonitrile/water solutions containing resveratrol and CuSO_4 or FeCl_3 , respectively. Interestingly, the formation of racemic δ -viniferin dehydrodimer is observed in ESI-MS experiments carried out on resveratrol-copper mixtures, while the analogous resveratrol-iron reaction affords the racemic ϵ -viniferin dehydrodimer. The use of gas-phase techniques and of ab initio calculations, at BHandHLYP/LACV3P + ** level of theory, allowed us to elucidate some important aspects of these reaction mechanisms. In particular, a different stability for the resveratrol radicals involved in the oxidative coupling has been obtained in the presence of copper ion, favoring the formation of δ -viniferin, as proposed for the in vivo mechanism where copper is able to switch the resveratrol from an antioxidant to a prooxidant agent. Finally, the structure-reactivity relationship has been investigated for synthetic analogues of resveratrol, showing the crucial role of the OH group in para position.

2) G. Cazzolli, S. Caponi, **A. Defant**, C. M. C. Gambi, S. Marchetti, M. Mattarelli, M. Montagna, B. Rossi, F. Rossia and G. Vilianni, "Aggregation processes in micellar solutions: a Raman study", *Journal of Raman Spectroscopy*, DOI 10.1002/jrs.4120

Abstract

Ionic surfactants such as sodium dodecyl sulfate (SDS) belong to the amphiphile family: they possess a long hydrophobic hydrocarbon chain and a polar hydrophilic headgroup. In a polar solvent and over the critical micellar concentration these molecules join to form micelles. The micellar solutions, in turn, if doped with various ligands tend to aggregate.

Solid SDS, micelles of SDS in water and micelles of SDS doped with two types of macrocyclic ligands, Kryptofix 2.2.2 (K222) and crown ether 18-Crown-6 (18C6), at different concentrations are studied by Raman scattering, that represents a new approach to such systems. The experimental Raman spectrum, obtained on crystalline powders of SDS, is compared with the ab initio computed spectrum in order to assign the vibrational bands. After discriminating sensitive peaks by comparing the crystalline powders of the single components and their water solutions, the aggregation process and the action of the ligands are analyzed following the evolution of the intensity and wavenumber of these characteristic Raman peaks. This shows that Raman spectroscopy is sensitive to the aggregation dynamics and to the effects induced by the hydration layer on the molecules in solutions. A saturation effect in the aggregation process with the increase of the ligand concentration is observed.

3) L. Chiari, A. Zecca, S. Girardi, **A. Defant**, F. Wang, X. G. Ma, M. V. Perkins, and M. J. Brunger, "Positron scattering from chiral enantiomers", *Physical Review A*, **2012**, 85, 052711

Abstract

We report on total cross section measurements for positron scattering from the chiral enantiomers (+)-methyl (*R*)-2-chloropropionate and (–)-methyl (*S*)-2-chloropropionate. The energy range of the present study was 0.1–50 eV, while the energy resolution of our incident positron beam was ~0.25 eV (FWHM). As positrons emanating from β decay in radioactive nuclei have a high degree of spin polarization, which persists after moderation, we were particularly interested in probing whether the positron helicity differentiates between the measured total cross sections of the two enantiomers. No major differences were, however, observed. Finally, quantum chemical calculations, using the density functional theory based B3LYP-DGTZVP model within the GAUSSIAN 09 package, were performed as a part of this work in order to assist us in interpreting some aspects of our data.

4) A. Zovko , M. Vaukner Gabric , K. Sepcic , F. Pohleven , D. Jaklic, N. Gunde-Cimerman , Z. Lu , R.A. Edrada-Ebel , W. E. Housen , I. Mancini, **A. Defant** , M. Jaspars, T. Turk, "Antifungal and antibacterial activity of 3-alkylpyridinium polymeric analogs of marine toxins", *International Biodeterioration & Biodegradation*, **2012**, 68, 71-77

Abstract

Analogues of marine sponge-derived 3-alkylpyridinium compounds (3-APS) were synthesized and screened for possible antibacterial and antifungal activities. They were found to exhibit moderate antibacterial activity. Antifungal potential was tested on pathogenic fungus *Candida albicans*, baker's yeast *Saccharomyces cerevisiae* and hypersaline species *Wallemia sebi*. *S. cerevisiae* was the most susceptible to the action of selected 3-APS. Inhibitory effects on fungal growth were also studied on two wood-rotting fungi, brown-rot fungus *Gloeophyllum trabeum* and a white-rot fungus *Trametes versicolor*. The former showed a higher susceptibility to the action

of 3-APS. The highest antifungal potential was observed with the poly-1,3-dodecyl pyridinium chloride (APS12-3, 7), while a complete loss of activity was noticed with the poly-1,3-butyl pyridinium chloride (APS3, 1), suggesting that this activity may closely correlate to the length of their alkyl chains. Based on our results, synthetic APS12-3 is a good candidate to be used as biocide or wood preservative against wood-rotting fungi.

5) **A. Defant**, I. Mancini, L.Raspor, G. Guella, T. Tom. K.Sepcic, "New Structural Insights into Saraines A, B, and C, Macrocyclic Alkaloids from the Mediterranean Sponge *Reniera (Haliclona) sarai*", *European Journal of Organic Chemistry*, **2011**, 2011, 3761-3767

Abstract

The structural peculiarity of saraines A, B and C, wherein a zwitterionic-like form is present due to the coordination of a nitrogen atom to the C-2 aldehyde by a strong proximity effect, has been further extended by experimental and theoretical evidences. They include the detection of $[2M + H]^+$ clusters in electrospray ionization mass spectrometry in the positive ion mode of a water/acetonitrile solution, whereas only signals corresponding to $[M + H]^+$ ions are detectable after addition of trifluoroacetic acid to the same solution. The zwitterionic form can be trapped to give O-methyl derivatives only by reaction with a strong alkylating agent such as Meerwein's reagent. DFT calculations carried out on the core structural model suggest that the nucleophilic N-1 atom in the minimized conformation is at a suitable distance from the carbonyl group and also defines an approach angle in good agreement with the Bürgi–Dunitz model. Antibacterial and hemolytic activities and inhibition of acetylcholinesterase (AChE) assays have been evaluated for saraines A–C in comparison to those of saraines 1–3 and isosaraine 1, all the metabolites isolated from the sponge *Reniera (Haliclona) sarai* collected in the Northern Adriatic sea.

6) I.Mancini, **A.Defant**, T.Mesaric, F. Potocnik, U.Batista, G.Guella, T.Turk, K.Sepcic, "Fatty acid composition of common barbel (*Barbus barbus*) roe and evaluation of its haemolytic and cytotoxic activities", *Toxicon*, **2011**, 57(7-8), 1017-1022

Abstract

Eggs of the common barbel (*Barbus barbus*) cause intoxication in humans after ingestion. In this work, the chemical composition of the haemolytically active fraction from methanolic barbel roe extract was analyzed. Compounds showing haemolytic activity and cytotoxicity towards normal and transformed cell lines were isolated and identified as polyunsaturated fatty acids, using online liquid chromatography–electrospray ionization mass spectrometry through tandem fragmentation experiments (HPLC–MS/MS). Arachidonic acid (C20:4), docosahexaenoic acid (C22:6) and eicosapentaenoic acid (C20:5) proved to be the three most abundant members of a complex series of free fatty acids ranging from C14:0 to C24:5.

7) V. Tamboli, **A. Defant**, I. Mancini, P. Tosi, "A study of resveratrol-copper complexes by electrospray ionization mass spectrometry and density functional theory calculations ", *Rapid Communications in Mass Spectrometry*, **2011**, 25(4), 526-532

Abstract

Resveratrol is a polyphenolic compound found in plants and human foods which has shown biological activities including chemoprevention, acting through a mechanism which involves the reduction of Cu(II) species. By electrospray ionization (ESI) mass spectrometry we have produced and detected the resveratrol-copper complexes $[\text{Resv}+\text{Cu}]^+$, $[\text{Resv}+\text{CuRH}_2\text{O}]^+$ and $[2\text{Resv}+\text{Cu}]^+$ by using a resveratrol/ CuSO_4 solution in $\text{CH}_3\text{CN}/\text{H}_2\text{O}$. The most stable structures of the detected complexes have been calculated at the B3LYP/6-311G(d) level of theory. Resveratrol interacts with the copper ion through nucleophilic carbon atoms on the aromatic ring and the alkenyl group. The fact that only singly charged ions were observed implies that Cu(II) is reduced to Cu(I) in the ESI process. For investigating the structure-reactivity correlation, we have carried out a similar study on the synthetic analogue dihydroresveratrol (DHResv). For the latter only the $[\text{DHResv}+\text{Cu}]^+$ complex has been detected.

8) **A. Defant**, I. Mancini, C. Torri, D. Malferrari, D. Fabbri, "An efficient route towards a new branched tetrahydrofuran δ -sugar amino acid from a pyrolysis product of cellulose", *Amino Acids*, **2011**, 40(2), 633-640.

Abstract

(1R,5S)-1-Hydroxy-3,6-dioxo-bicyclo[3.2.1]octan-2-one, is a bicyclic lactone obtained in gram-scale by catalytic pyrolysis of the renewable source cellulose. Now it has been used as a chiral building block in the preparation of the new δ -sugar amino acid, (3R,5S)-5-(aminoethyl)-3-hydroxytetrahydrofuran-3-carboxylic acid, by an efficient synthesis in five steps with a 67% overall yield. The structure of this tetrahydrofuran amino acid, isolated in protonated form, was assigned by extensive mono- and bidimensional ^1H - and ^{13}C -NMR analysis and mass spectrometry, including measurements by electrospray and matrix-assisted laser desorption ionization techniques, the latter one for high-resolution experiments. This amino acid is an isoster of dipeptide glycine-alanine (H-Gly-Ala-OH), with a potential use in the access of new peptidomimetics with conformationally restricted structures due to the presence of tetrahydrofuran ring. As a preliminary study in order to disclose this effect, density functional theory calculation performed in water using polar continuum model was applied to the new amino acid and H-Gly-Ala-OH dipeptide, so that to evaluate and compare the relative torsional angles for the energy-minimized structures.

9) **A. Defant**, B. Rossi, G. Viliani, G. Guella and I.Mancini, "Metal-assisted regioselectivity in nucleophilic substitutions: a study by Raman spectroscopy and density functional theory calculations", *Journal of Raman Spectroscopy*, **2010**, *41*, (12), 1398–1403.

Abstract

A series of complexes(Fe^{II} , Cu^{II} and Ni^{II})of the N,O bidentate ligand 6,7-dichloroquinoline-5,8-dione in water was investigated by using Raman spectroscopy, and the experimental peaks were assigned with the help of computed spectra by density functional theory (DFT) calculations. A strong shift to lower wavenumbers was observed for the vibration of the CO group involved in chelation, depending on the type of metal ion. When each complex was used in the substitution reaction by the nucleophilic reagent piperidine, two products having the same molecular composition but showing the substituent in different regions of the molecule were obtained, and moreover their regioselective formation was in agreement with the size of the Raman shifts previously observed for the complexes. This example confirms the potential of the approach involving Raman spectroscopy combined with DFT calculations in the characterization of metal complexes as key intermediates in organic reactions, with the possibility of predicting the metal system capable to achieve the highest selectivity.

In addition, my contribution to write a chapter book on invitation to I.Mancini:

I. Mancini and **A.Defant**, *Bioactive poly(arsenic) compounds*, contribution after invite to I.M. for the "Progress in Molecular and Subcellular Biology "book series, editor H. C. Schröder, Springer Verlag, 2012, in press

Appendix E

ACADEMIC CV

Personal Data

Name and Surname	Andrea Defant
Contact details	Via Sommarive 14 – 38123 Povo-Trento (Italy) Phone: +39 0461-281548 defant@science.unitn.it
Nationality	Italian
Birth date and city	November 16 th 1962, Trento

Positions held

Since 2009 **PhD student** of the International Doctoral School in Biomolecular Sciences (XXV cycle), University of Trento, Dept. of Physics, Bioorganic Chemistry Laboratory

Sciences faculty, University of Trento, Italy

2012-2008 **Laboratory assistant** in Organic Chemistry (40 hours each academic year)

Provincia Autonoma of Trento, Italy

2009-1990 **Teacher** of Chemistry in the high school

Sciences faculty, University of Trento, Italy

2009-1997 **MD Collaborator** in the Bioorganic Chemistry Laboratory, Department of Physics, University of Trento, Povo-Trento, Italy, under supervision of prof. Ines Mancini

Engineering faculty, University of Trento, Italy

1995-1992 **Teaching assistant** for General Chemistry (40 hours each academic year)

University of Milan, Italy

1989-1988 **Research collaborator** for the Glaxo S.p.A.

Polytechnic of Milan, Italy

1988-1987 **R&D collaborator** for Pierrel S.p.A.

Accademic training

1999-2000 **Qualification** in “**Chemistry and Chemical Technologies**” for high school teaching

1998-1997 **Diploma of specialization** in “**Education and Multimedial Communication**” at University of Ferrara.

1997-1996 **Diploma of specialization** in “**General and Experimental Teaching**” at University of Ferrara.

1989- 1987 **Diploma of Specialization in Chemical Synthesis** at Polytechnic of Milan. Supervisor : prof. L. Merlini.: Thesis title “A new synthesis of 4,5,6,7-tetrahydro-furo-[2,3-c]-piridina and furo[2,3-c]-pirrolidine”.

1988 **Habilitation in Pharmacy**

1987-1982 **University degree in Chemistry and Pharmaceutical Technology** at University of Pavia. Score degree 110/110 *cum laude*. Supervisor: prof. G. Pagani. Thesis title: “Preparation and antibacterial activity of some derivatives of 1-ethyl-1,4-dihydro-4-oxo-quinolin-3-carboxylic acid”.

1982-1977 **Scientific high school diploma** at Liceo Scientifico “L. da Vinci” – Trento

Publications

Research papers

V. F. Tamboli, N. Re, C. Coletti, **A. Defant**, I. Mancini, P. Tosi, “A joint experimental and theoretical investigation on the oxidative coupling of resveratrol induced by copper and iron ions”, *International Journal of Mass Spectrometry*, **2012**, 319-320, 55-63

G. Cazzolli, S. Caponi, **A. Defant**, C. M. C. Gambi, S. Marchetti, M. Mattarelli, M. Montagna, B. Rossi, F. Rossia and G. Vilianni, "Aggregation processes in micellar solutions: a Raman study", *Journal of Raman Spectroscopy*, DOI 10.1002/jrs.4120

L. Chiari, A. Zecca, S. Girardi, **A. Defant**, F. Wang, X. G. Ma, M. V. Perkins, and M. J. Brunger, "Positron scattering from chiral enantiomers", *Physical Review A*, **2012**, *85*, 052711

A. Zovko, M. Vaukner Gabric, K. Sepcic, F. Pohleven, D. Jaklic, N. Gunde-Cimerman, Z. Lu, R.A. Edrada-Ebel, W. E. Houssen, I. Mancini, **A. Defant**, M. Jaspars, T. Turk, "Antifungal and antibacterial activity of 3-alkylpyridinium polymeric analogs of marine toxins", *International Biodeterioration & Biodegradation*, **2012**, *68*, 71-77

A. Defant, I. Mancini, L. Raspor, G. Guella, T. Tom. K. Sepcic, "New Structural Insights into Saraines A, B, and C, Macrocyclic Alkaloids from the Mediterranean Sponge *Reniera (Haliciona) sarai*", *European Journal of Organic Chemistry*, **2011**, *2011*, 3761-3767

I. Mancini, **A. Defant**, T. Mesarić, F. Potocnik, U. Batista, G. Guella, T. Turk, K. Sepcic, "Fatty acid composition of common barbel (*Barbus barbus*) roe and evaluation of its haemolytic and cytotoxic activities", *Toxicon*, **2011**, *57*(7-8), 1017-1022

V. Tamboli, **A. Defant**, I. Mancini, P. Tosi, "A study of resveratrol-copper complexes by electrospray ionization mass spectrometry and density functional theory calculations", *Rapid Communications in Mass Spectrometry*, **2011**, *25*(4), 526-532

A. Defant, I. Mancini, C. Torri, D. Malferrari, D. Fabbri, "An efficient route towards a new branched tetrahydrofuran δ -sugar amino acid from a pyrolysis product of cellulose", *Amino Acids*, **2011**, *40*(2), 633-640.

A. Defant, B. Rossi, G. Vilianni, G. Guella and I. Mancini, "Metal-assisted regioselectivity in nucleophilic substitutions: a study by Raman spectroscopy and density functional theory calculations", *Journal of Raman Spectroscopy*, **2010**, *41*, (12), 1398-1403.

A. Defant, G. Guella, I. Mancini, "Synthesis and In-Vitro Cytotoxicity Evaluation of Novel Naphthindolizinedione Derivatives, Part II: Improved Activity for Aza-Analogues", *Archive der Pharmazie*, **2009**, *342*, 80-86.

A. Defant, G. Guella, I. Mancini, "Microwave-assisted multi-component synthesis of aza- and diaza-, benzo- and dibenzofluorenedione derivatives", *Synthetic Communications*, **2008**, *38*(17), 3003-3016.

A. Defant, G. Guella, I. Mancini, "Synthesis and in vitro cytotoxicity evaluation of novel naphthindolizinedione derivatives", *Archive der Pharmazie*, **2007**, *340*, 147-153.

A. Defant, G. Guella, I. Mancini, "Regioselectivity in the multi-component synthesis of indolizinoquinoline-5,12-dione derivatives", *European Journal of Organic Chemistry*, **2006**, *2006*, 4201-4210

I. Mancini, G. Guella, **A. Defant**, M. Candenas, C. Armesto, D. Depentori, F. Pietra, "Polar metabolites of the tropical green seaweed *Caulerpa taxifolia* which is spreading in the Mediterranean Sea. Glycoglycerolipids and stable enols (alpha-keto esters) ", *Helvetica Chimica Acta*, **1998**, *81*, 1681-1691.

Reviews

I. Mancini, G. Guella, **A. Defant**, "Synthesis of marine natural products with antimalarial activity", *Mini-Reviews in Medicinal Chemistry*, **2008**, *8* (12), 1265-1284.

I. Mancini, **A. Defant**, G. Guella, "Recent synthesis of marine natural products with antibacterial activities", *Anti-infective Agents in Medicinal Chemistry*, **2007**, *6*, 17-48.

Book Chapter

I. Mancini and **A. Defant**, *Bioactive poly(arsenic) compounds*, contribution after invite to I.M. for the "Progress in Molecular and Subcellular Biology "book series, editor H. C. Schröder, Springer Verlag, 2012, in press

Posters and oral presentations

Andrea Defant and Ines Mancini" A study on the regioselectivity in N, C-acylation of β -enamino esters" 16th International Electronic Conference on Synthetic Organic Chemistry. 1-30 November 2012. Accepted.

Andrea Defant and Ines Mancini "Numeric Simulation on Biological Macromolecules Applied to Drug Design: Molecular Docking in the Study of New Potential Anti-HIV Agents". Andalo (Trento), Italy, , March 18th - 22nd 2012.

Andrea Defant, Ines Mancini, Lucija Raspor, Graziano Guella, Tom Turk, Kristina Sepčić "New structural insights into saraines A, B and C, macrocyclic alkaloids from the Mediterranean sponge *Reniera (Haliclona) sarai*". Lecce, Italy, September, 11th-16th 2011.

Vajir Fakirsab Tamboli, Ines Mancini, **Andrea Defant**, Paolo Tosi. "An ESI-MS/MS study on metal ion-catalyzed oxidative dimerization of resveratrol and its synthetic analogues". Fiera di Primiero, Trento (Italy), May 15th - 19th 2011.

V. Tamboli, I. Mancini, **A. Defant**, P.Tosi, *An ESI-MS/MS study on copper complexes of resveratrol and its dihydrofuran dimer*. Workshop" La Spettrometria di massa nello studio delle biomolecole", Bari, Italy, November 26th, 2010

A. Poli, **A. Defant**, G. Guella, I. Mancini, *DNA Interaction with antitumoral molecules: a study by UV-spectroscopy, circular dichroism and docking calculations*. XII International Workshop on Complex Systems, Andalo-Trento, Italy, March 15-18,2010.

A. Defant, A. Poli, I. Mancini, *New antitumoral molecules and DNA interactions: a study by docking calculations supporting spectroscopic evidences and biological activities*. E-WiSPOC- European Winter School on Physical Organic Chemistry 2010, Bressanone, Italy, January 31- February 5, 2010. The poster contribution was selected as one of the 12 posters, in order to present the topic in an additional oral communication.

D. Malferrari, **A. Defant**, D. Fabbri, I. Mancini, C. Torri. *A novel chiral synthone from biomass. Production of an anhydro isosaccharino- δ -lactone from catalytic pyrolysis of cellulose and its application to the synthesis of bio-mimetic molecules*; 8th Green Chemistry Conference, Zaragoza, Spain, September 9-11, 2009.

Ines Mancini, **Andrea Defant**, Lucija Raspor, Graziano Guella, Tom Turk, Kristina Sepčić *New Structural Evidences for Saraines A-C, Macroyclic Alkaloids from the Mediterranean Sponge Reniera (Haliclona)sarai*. 6th European Conference on Marine Natural Products, Porto(Potogallo), July 19-23, 2009.

Andrea Defant, Ines Mancini, Barbara Rossi, and Gabriele Viliani, *Raman Spectroscopy and DFT Calculations of Transition Metal Complexes Involved in Regioselective Reactions*. XXI CONGRESSO GNSR 2009, Milano, 10-13 febbraio 2009.

Defant A., Mancini I, Rossi B., Viliani G., *Spectroscopy and DFT calculations of transition metal complexes inducing regioselectivity in organic synthesis*. 11th International workshop on complex systems, Andalo (Trento), March 17-20 2008.

Mancini I., **Defant A.**, Guella G., *Sintesi altamente selettiva di entrambi i regioisomeri di derivati Indolizino-5,12-dionici*, SCI 2006: XXII congresso nazionale della Società Chimica Italiana, Firenze, 10-15 settembre 2006 ; ORG-P064.

Mancini I., **Defant A.**, Guella G., *Investigation of the regioselective one-pot synthesis of Indolizino-quinoline-5,12-dione derivatives*. First Austrian-German-Italian Meeting of Organic Chemistry, Vienna, April 1-2 2005, p. 17.

Workshop participation.

XIII International Workshop on Complex Systems, Andalo (TN) March from 18th to 22nd 2012.

Computationally Driven Drug Discovery Meeting, L'Aquila November from 21st to 23th 2011.

XXIV Congresso Nazionale della Società Chimica Italiana (SCI 2011), Lecce September from 11th to 16th 2011.

29th Informal meeting on Mass Spectrometry, Fiera di Primiero-Trento (Italy) from 15th to 19th May 2011.

12th International Workshop on Complex Systems, Andalo-Trento, Italy, March 15-18, 2010.

E-WiSPOC- European Winter School on Physical Organic Chemistry 2010, Bressanone, Italy, 31 January-5 February 2010.

11th International Workshop on Complex Systems", Andalo (Trento), March 17-20 2008.

3rd Meeting of Italian Chemical Society "Chimica e Sicurezza nei Laboratori"; Milano, November 27 1998.

References.

Prof. Graziano Guella, Laboratory of Bioorganic Chemistry, Dept. Physics, University of Trento. Via Sommarive 14, I-38123 Povo Trento, Italy.

Prof. Ines Mancini, Laboratory of Bioorganic Chemistry, Dept. Physics, University of Trento. Via Sommarive 14, I-38123 Povo Trento, Italy.

Prof. Paolo Tosi, Dept. of Physics University of Trento. Via Sommarive 14, I-38123 Povo Trento, Italy

Additional Informations

General English Intensive Course at Alpha College of English in Dublin, (03 - 14 August 2009).

PET certificate of Cambridge University.

Scientific Collaborations:

Jan Balzarini, Rega Institute - Department of Microbiology and Immunology Laboratory of Virology and Chemotherapy, Leuven (Belgium)

Tom Turk and Kristina Sepcic K., Dept of Biology, University of Ljubljana, Slovenia.

Marcel Jaspars and Rod Scott, College of Medical Sciences, University of Aberdeen, Scotland, U.K.

National Cancer Institute (NCI), Chemotherapeutic Agents Repository, Rockville, MD 20852, USA

M. Luz Cadenas, Cristina P. Armesto, Instituto de Investigaciones Químicas Isla de la Cartuja, CSIC, Americo Vespucio s/n, Isla de La Cartuja, Sevilla, Spain

Marco Faimali, CNR, ISMAR – Istituto di Scienze Marine, Genova, Italy

Daniele Fabbri, Università di Bologna, Centro Interdipartimentale di Scienze Ambientali, sede di Ravenna, Italy

Rosanna Matucci, Dipartimento di Farmacologia , Universita' di Firenze, Italy

Barbara Gatto, Dipartimento di Scienze Farmaceutiche, University of Padova, Italy

Paolo Tosi Department of Physics, University of Trento, Italy

Trento, October 16th, 2012